

https://dspace.org/

Optimization of synthesis and separation performance of nanotube-infused polysulfone membrane with polyvinyl alcohol layer to separate oil-containing wastewater

Makumba, Aliki John

2016

http://hdl.handle.net/10539/20614

Downloaded from a DSpace repository. https://dspace.org/



OPTIMIZATION OF SYNTHESIS AND SEPARATION PERFORMANCE OF NANOTUBE-INFUSED POLYSULFONE MEMBRANE WITH POLYVINYL ALCOHOL LAYER TO SEPARATE OIL-CONTAINING WASTEWATER

Aliki John Makumba

A research report submitted to the Faculty of Engineering and the Built Environment, University of the Witwatersrand, Johannesburg, in fulfilment of the requirements for the degree of Masters of Science in Engineering.

Johannesburg, 2015

DECLARATION

I, Aliki Makumba, declare that this research report is my own unaided work under the supervision of Dr. Jean Mulopo, Dr. Diakanua Nkazi and Professor Sunny Iyuke. It is being submitted to the degree of Master of Science to the University of the Witwatersrand. It has not been submitted before for any degree or examination to any other university.

Signed……..

Aliki Makumba

On this..... Day of …….. Year ……

EXECUTIVE SUMMARY

Wastewater is one of the major problems to human life because it contains contaminants (such as viruses, worms, bacteria, etc.) which pollute the environment and causes various diseases (like cholera, dehydration, skin disease, eye disease, etc.) that are dangerous to human being. Various industries generate high volumes of concentrated oil-water emulsion containing wastewater on a daily basis. Therefore, it is important to reduce the concentration of oil in the oil-containing wastewater to an acceptable discharge limit before its disposal in order to avoid environmental pollution. In view of this, this project was aimed at optimising the synthesis and operational performance of the nanotube-infused polysulfone (PS) membrane with a polyvinyl alcohol layer to separate oil-containing wastewater.

To achieve the afore-mentioned goal, first the carbon nanotubes (CNTs) were produced and infused into the membranes in order to increase their mechanical stabilities. The CNTs were produced using a vertical swirled fluid chemical vapour deposition (VSFCCVD) method at the temperature of 850^{o}C. Ferrocene was used as both a catalyst and a source of carbon, nitrogen gas was run through the equipment in order to make sure that there were no gas leaks and that the contaminants (other unidentified/unknown gases) are removed from the system, and argon gas was used as a carrier. The CNTs were also functionalised and purified using various acids in order to increase their hydrophilic capability and to further enhance the mechanical stability of the membranes. The CNTs were characterised using the transmission electron microscope (TEM), thermogravimetric analysis (TGA), X-ray diffraction spectroscopy (XRD), Raman spectroscopy and many other characterisation methods. The as-produced and the purified CNTs were blended in 20% polysulfone solution. Seven membranes were synthesised using the phase immersion inversion method. A polyvinyl alcohol layer was used to further improve the hydrophilicity and the mechanical stability of the membrane. The improved mechanical stability and hydrophilicity of the membrane, minimises fouling and concentration polarisation on the membrane. The membranes were characterised using the Fourier transform infrared spectroscopy (FTIR), contact angle, Braunner-Emmet-Teller (BET) and the scanning electron microscope (SEM). The separation performance of the membrane was tested using real industrial oil-containing wastewater.

It is known that ferrocene can be used as both a catalyst and source of carbon as it has produced multi-walled CNTs with the lengths that are between 450-850 nm long. The

mixture of nitric acid and sulphuric acid in a ratio of 1:3 was able to remove about 59% of the ferrocene catalyst particles during functionalization of CNTs. Hydrofluoric acid, hydrochloric acid together with the oxidation process removed about 99% of the contaminated impurity catalyst particles during the purification of CNTs. The use of 20% PS solution improved the quality but reduced the porosity which in turn reduced the membrane's flux but maintained the separation performance of the membrane since all membranes have rejected the concentration of oil in the retentate of over 82%. BET gave the average pore sizes that ranged between 11 and 24 nm which are capable of rejecting oil droplets of the industrial oil-containing wastewater with diameter that ranges between 0.02-0.2 µm.

During the separation performance evaluation using the oil-containing wastewater, all the membranes tested gave excellent results with high throughput and oil rejections that ranged between 82 and 95%. This was due to the polyvinyl alcohol (PVA) hydrophilic layer that all membranes possessed. These rejections were consistent with those obtained when the synthetic oil-containing wastewater was used. However, unlike when the synthetic oil-water was used, all membranes did not meet the acceptable discharge limit as they showed the concentration of oil in the permeate that ranged between 16 and 64 mg/L at flow rates ranging between 46.8 and 52.2 L/h. The best performing membrane using the as-produced CNTs was 5% CNTs with the rejection of oil in the retentate that ranged between 18 and 52 mg/L at the afore-mentioned flow rates. The as-produced infused membranes were those membranes that their separation performance was first tested using the synthetic oil-containing wastewater. This indicated that the performance of the membrane increases with a decrease in the concentration of the as-produced CNTs as well as the membrane's flux. The overall best performing membrane was p7.5% CNTs (membrane infused with 7.5% of purified CNTs) with oil rejections ranging between 94.9 and 95.7%. The permeate showed the oil concentration that ranged between 16 and 19 mg/L at the mentioned flow rates. This was due to the purified CNTs which further increased the hydrophilicity of the membranes. These results showed that the performance of the polysulfone is directly related to the concentration of oil in the permeate and inversely related to the increase of the concentration of oil in the permeate, the flow rate as well as the membrane's flux.

The utilisation of the purified CNTs increases the hydrophilicity which in turn improves the fouling resistance and enhances the mechanical stability of the membrane.

Thus the separation performance of the PS membrane with the PVA layer and the purified CNTs is greater than that with the infused as-produced/non-purified CNTs.

Keywords: Ferrocene catalyst, source of carbon, as-produced CNTs, functionalised, purified, polysulfone membrane, polyvinyl alcohol, hydrophilicity, Industrial oil-containing wastewater, permeate concentration, rejected concentration of oil, flux, separation, performance.

DEDICATION

This research report is dedicated to:-

- The Lord God almighty Jesus Christ, Who Was, still Is and Will always be there for me. He whispers sweet peace to me.
- My mother and siblings for their continuous support.

ACKNOWLEDGEMENTS

I would like to thank my supervisors, Dr Jean Mupolo, Dr Diakanua Nkazi and Prof. Sunny Iyuke for their continuous support and making sure that I finish this project.

I also like to thank all people who were involved in this project for their unconditional assistance. At the School of Chemical and Metallurgical Engineering I would like to thank: Dr. Daramola, Dr. Geoffrey Simate, Ms Palesa Hlanyane, Mr. Bruce Mothibeli, Mr. Phatu, Mr. Rod, Ms Sibongile, Ms Modiba, Mr. Omalanga, Mr. Doctor Mbense, Mr. Tshepo Motaung, Sbusiso Makonjwa, Lerato Shakoane, Tendai Kadudu, Kwame and Alain Mufolo.

I also like to thank the following people at the School of Chemistry for their assistance: Tumelo Phaahlamohlaka, Neo Phao and everyone at the XRD unit. I also like to thank Rudolph at the School of Physics for his assistance with the Raman Spectroscopy.

I would like to thank CHIETA and Wits University for the financial assistance.

Finally I thank the Lord Jesus Christ for advising me that patience is the key, God's time is the best time. Good Morning (all the time) !!!

CONTENTS

DECLARATION i

EXECUTIVE SUMMARY ii

DEDICATION v

ACKNOWLEDGEMENTS vi

CONTENTS vii

LIST OF FIGURES xi

LIST OF TABLES xiv

LIST OF ABREVIATIONS xv

CHAPTER 1: INTRODUCTION 1

1.1 Background and Motivation 1

1.2 Aim and objectives 3

1.3 Research questions 3

1.4 Hypothesis 4

1.5 Justification of study 4

1.6 Scope of the project 5

1.7 Expected contribution to knowledge 5

1.8 Report project outline 6

CHAPTER 2: LITERATURE REVIEW 7

2.1 Introduction 7

2.2 Previous and current methods used to separate oil containing wastewater 7

2.2.1 American Petroleum Institute (API) separator 7

2.2.2 Flotation Method 8

2.2.3 Coagulation Method 8

2.2.4 Centrifugal oil-water separator 9
2.2.5 Filtration method 11
2.2.6 Surface (membrane) filtration 12
2.2.7 Summary of oil-containing wastewater separation methods. 19
2.3 Fouling and concentration polarization 22
2.3.1 Concentration polarization 22
2.3.2 Fouling 22
2.4 Polysulfone polymer 24
2.5 Polysulfone membrane 26
2.6 The use of polyvinyl alcohol polymer 27
2.7 CNT membranes 29
2.8 The phase inversion method 34
CHAPTER 3: EXPERIMENTAL 38
3.1 Introduction 38
3.2 Materials and methods 38
3.3 Experimental Procedure 42
3.3.1 Synthesis of CNTs 42
3.3.2 Functionalization of the CNTs 43
3.3.3 Purification of the CNTs 43
3.3.4 Characterisation of the CNTs 45
3.3.5 Synthesis of the polysulfone (PS) membrane with the CNTs and PVA layer 51
3.3.6 Characterisation of the PS membranes 52
3.3.7 The size of the pores and the porosity measurements 54
3.3.8 The separation performance of the PS membrane 56
CHAPTER 4: RESULTS AND DISCUSSION 61
4.0 Introduction 61

4.1 The CNTs **61**
4.1.1 TEM analysis **61**
4.1.2 TGA analysis **64**
4.1.3 Raman spectroscopy analysis **67**
4.1.4 Energy Dispersive X-ray Spectroscopy analysis **69**
4.1.5 Fourier transform infrared (FTIR) spectroscopy analysis **71**
4.1.6 XRD spectroscopy analysis **73**
4.2 The PS membrane analysis: characterisation and assessment **77**
4.2.1 SEM analysis of the PS membrane **78**
4.2.2 BET analysis **86**
4.2.3 Contact angle analysis **88**
4.2.4 FTIR analysis **89**
4.3 Application of the synthesised membranes for the treatment of oil-containing wastewater **92**
4.3.1 Determination of the concentration of the permeate (Cp) **93**
4.3.2 The percentage of the removed oil concentration (R%) **95**
4.3.3 Membrane flux (MF) **97**
4.3.4 The relative flux **101**
4.3.5 The decrease in flux, DF (The flux decline) **102**
CHAPTER 5: CONCLUSIONS AND RECOMMENDATIONS 105
5.1 Conclusions **105**
5.2 Recommendations **107**
REFERENCES 109
APPENDIX A 132
A.1 Raman spectroscopy data **132**
A.2 Fourier transform infrared (FTIR) spectroscopy for the CNTss **135**
A.3 X-ray diffraction (XRD) analysis **137**

A.4 CNTs functionalization equipment 140

APPENDIX B 142

B.1 Brunauer-emmet-teller (BET) data 142

B.1.1 BET data for the 0 PVA PS membrane 142

B.1.2 BET data for the 5% PS membrane 145

B.1.3 BET data for 2.5% CNTs PS membrane 150

B.1.4 BET data for 7.5% CNTs PS membrane 153

B.1.5 BET data for p7.5% CNTs PS membrane 156

B.1.6 BET data for 10% CNTs PS membrane 159

B.2 FTIR data for the PS membranes 162

B.3 Separation performance data 168

LIST OF FIGURES

Figure 2.1: Pictures of the centrifugal oil-containing wastewater separator, (a) Vertical and (b) horizontal. 10
Figure 2.2: Formation of polysulfone from diphenol and bis(4 – chlorophenyl)sulfone 25
Figure 2.3: Picture of polysulfone membrane 27
Figure 2.4: Schematic drawing of the reaction for the synthesis of polyvinyl alcohol. 28
Figure 2.5: Picture of a CNT-infused polysulfone membrane. 32
Figure 3.1: Picture of a vertical swirled fluid bed catalytic chemical vapour deposition 40
Figure 3.2: A schematic drawing of SFCCVD 41
Figure 3.4: A horizontal CVD for the oxidation of CNTs 44
Figure 3.5: Picture of a Transmission electron microscope. 46
Figure 3.6: Picture of a thermogravimetric analyzer 47
Figure 3.7: Picture of an energy dispersive spectroscopy. 48
Figure 3.8: Picture of a Fourier Transform Infrared 49
Figure 3.9: Picture of an X-ray diffraction 50
Figure 3.10: Schematic diagram of PS membrane casting 51
Figure 3.11: Picture of Micromeritics Tristar 3000 for the BET analysis. 53
Figure 3.12: Picture of the cross flow filtration system used to separate oil-containing wastewater system. 57
Figure 3.13: The schematic drawing of the setup of separation performance experiment. 58
Figure 3.14: UV-Vis spectrophotometer. 59
Figure 4.1: TEM micrographs of the produced CNTs: (a) as-produced CNTs, (b) fCNTs, and (c) pCNTs. 63
Figure 4.2: The TGA spectra for the as-produced CNTs, fCNTs and the pCNTs. 65
Figure 4.3: The derivative weight percentage graphs of the CNTs, fCNTs and the pCNTs. 66
Figure 4.4: The Raman shift for the CNTs, fCNTs and the pCNTs 68
Figure 4.5: EDS spectra for the CNTs. 70
Figure 4.6: IR spectra of the CNTs, fCNTs and pCNTs. 72
Figure 4.7: XRD spectra a) as-produced CNTs, b) fCNTs and c) pCNTs. 76
Figure 4.8: SEM images of the seven PS membranes. 83
Figure 4.9: Contact angle plot for the PS membranes. 88
Figure 4.10: Infrared (IR) spectra for 6 PS membranes without PVA layer. 90

Figure 4.11: IR for the PS membrane with 0% CNTs. 91
Figure 4.12: IR for the p7.5% CNTs (7.5 % of the pCNTs) PS membrane. 91
Figure 4.13: IR for p7.5% CNTs PS membrane with the PVA layer. 92
Figure 4.15: Variation of Cp of the PS membrane with different CNT concentrations at the flow rates of 46.8, 50.4 and 52.2 L/h. 94
Figure 4.16: The rejected concentration of oil in the retentate, R (%), by the PS membrane with different CNT concentrations. 96
Figure 4.17: Variation of the membrane flux changes with the flow rates and membranes with different concentrations of the CNTs. 98
Figure 4.18: The flux of the membrane as a function of time. 100
Figure 4.19: Relative flux as a function of time. 101
Figure 4.20: Variation of DF with PS membranes containing different concentration of CNTs. 103
Figure A.1: Raman Shift of the CNTs at 850^{o}C. 132
Figure A.2: Raman shift of the fCNTs at 850^{o}C. 133
Figure A.3: Raman shift of the pCNTs at 850^{o}C. 134
Figure A.4: Raman shift for the CNTs, fCNTs and pCNTs. 135
Figure A.5: IR spectrum for the CNTs. 136
Figure A.6: IR spectrum for the fCNTs. 136
Figure A.7: IR for the pCNTs. 137
Figure A.8: The IR spectra for the CNTs, fCNTs and the pCNTs. 137
Figure A.9: XRD Spectrum for the as-produced CNTs. 138
Figure A.10: XRD spectrum for the fCNTs. 139
Figure A.11: XRD spectrum for the pCNTs. 140
Figure A.13: Schematic setup drawing of the functionalization of the CNTs. 141
Figure B.1: The BET Isotherm linear plot for the adsorption of 0PVA PS membrane. 143
Figure B.2: BET surface area plot for the 0 PVA PS membrane. 144
Figure B.3: The Langmuir surface area plot for the 0 PVA membrane. 145
Figure B.4: BET surface area plot for PS membrane with 5% CNTs 146
Figure B.5: BET linear isotherm plot for the adsorption of 5% CNTs PS membrane. 147
Figure B.6: The Langmuir surface area plot for the 5% CNTs PS membrane. 149
Figure B.7: BET linear isotherm plot for the adsorption of 2.5% CNTs PS membrane. 150
Figure B.8: BET surface area plot for 2.5% CNTs PS membrane. 151
Figure B.9: Langmuir surface area plot for 2.5% CNTs PS membrane. 152

Figure B.10: BET linear isotherm plot for the adsorption of 7.5% CNTs PS membrane. 154
Figure B.11: BET surface area plot for 7.5% CNTs PS membrane. 155
Figure B.12: Langmuir surface area plot for 7.5% CNTs PS membrane. 156
Figure B.13: BET linear isotherm plot for the adsorption of p7.5% CNTs PS membrane. ..157
Figure B.14: BET surface area plot for p7.5% CNTs PS membrane. 158
Figure B.15: Langmuir surface area plot for p7.5% CNTs PS membrane. 159
Figure B.16: BET linear isotherm plot for the adsorption of 10% CNTs PS membrane. 160
Figure B.17: BET surface area plot for 10% CNTs PS membrane. 161
Figure B.18: Langmuir surface area plot for 10% CNTs PS membrane. 162
Figure B.19: The IR spectrum for the 0% CNTs PS membrane.....163
Figure B.20: The IR spectrum for the 5% CNTs PS membrane.....163
Figure B.21: The IR spectrum for the 2.5% CNTs PS membrane.....164
Figure B.22: The IR spectrum for the 7.5% CNTs PS membrane.....165
Figure B.23: The IR spectrum for the 10% CNTs PS membrane.....166
Figure B.24: The IR spectrum for the p7.5% CNTs PS membrane.....167
Figure B.25: The IR spectra of all the PS membranes.....168
Figure B.26: A calibration curve for the determination of the unknown concentration of the oil-containing wastewater permeates (Cp), at the flow rates of 46.8, 50.4 (840 ml/min) and 52.2 L/h. 169

LIST OF TABLES

Table 1: Comparison between different oil-containing wastewater separation methods: (a) industrial, and (b) filtration methods. 20
Table 2: BET analysis showing the pore size, pore volume and the surface area of the PS membranes 86
Table B3: Isotherm linear report for the adsorption of 0 PVA PS membrane. 142
Table B.4: BET surface area report data 143
Table B.5: Langmuir surface area report data 144
Table B.6: BET surface area report data 146
Table B.7: BET linear isotherm report data 147
Table B.8: Langmuir Surface Area Report data 148
Table B.9: Langmuir surface area report data 148
Table B.10: BET linear isotherm data for the adsorption of 2.5% CNTs PS membrane 150
Table B.11: BET surface area data for 2.5% CNTs PS membrane. 151
Table B.12: Langmuir surface area data for 2.5% CNTs PS membrane. 152
Table B.13: BET linear isotherm data for the adsorption of 7.5% CNTs PS membrane. 153
Table B.14: BET surface area data for 7.5% CNTs PS membrane. 154
Table B.15: Langmuir surface area data for 7.5% CNTs PS membrane. 155
Table B.16: BET linear isotherm data for the adsorption of p7.5% CNTs PS membrane. 156
Table B.17: BET surface area data for p7.5% CNTs PS membrane. 157
Table B.18: Langmuir surface area data for p7.5% CNTs PS membrane. 158
Table B.19: BET linear isotherm data for the adsorption of 10% CNTs PS membrane. 159
Table B.20: BET surface area data for 10% CNTs PS membrane. 160
Table B.21: Langmuir surface area data for 10% CNTs PS membrane. 161
Table B.22: Concentration of oil in the permeate (Cp), in mg/L; at the flow rates of 46.8, 50.4 and 52.2 L/h. 169
Table B.23: Rejection of oil concentration, R (%) in the retentate data 170
Table B.24: Data for the separation performance. 170

LIST OF ABREVIATIONS

A	The effective area of the membrane
ACE	Associated Chemical Enterprises
AFROX	African Oxygen (Ltd)
Ar	Argon
BET	Brunauer Emmett Teller
C_f	Oil concentration in the feed
CNTs	Carbon nanotubes
Cp	Oil concentration in the permeate
CPO	Centrifugal pump organisation
DMF	Dimethylformamide
EDS	Energy dispersive spectroscopy
EPA	Environmental Protection Agency
fCNTs	Functionalised carbon nanotubes
FTIR	Fourier transform infrared spectroscopy
HPLC	High performance liquid chromatography
I_D	The intensity of the D-band
I_G	The intensity of the G-band
IUPAC	International Union of Pure and Applied Science
MA	Maleic acid
MF	Membrane flux
MMU	Microscopy and Microanalysis Unit

P	Pressure in mmHg
P/Po	Relative pressure
p7.5%	Purified 7.5 % concentration of CNTs
pCNTs	Purified carbon nanotubes
Po	Initial pressure in mmHg
PS	Polysulfone
PVA	Polyvinyl alcohol
Q	Quantity adsorbed in cm^3/g STP
R	The removed concentration of oil
SEM	Scanning electron microscope
S_F	The flux of the membrane at start
t''	The time it took to get the permeate
TEM	Transmission electron microscope
T_F	Time flux
TGA	Thermogravimetric analysis
UHF	Ultra high purity
V	The resulting permeate volume after separation
VSFCCVD	Vertical swirled fluid catalytic chemical vapour deposition
XRD	X-ray diffraction

CHAPTER 1: INTRODUCTION

1.1 Background and Motivation

Oil-containing wastewater is a serious environmental pollution problem which is usually an aftermath of oil production, refinery or other oil industrial processing. It remains one of the major environmental pollution to human life and ecosystems because it contains toxic contaminants if not reduced, and can weave into water sources and have long term consequences, which include destruction of eco-systems and endangering human health. Oil fields, petrochemicals (e.g., refineries), food and beverages, pharmaceuticals and others are some of the industrial examples that generate oil-containing wastewater (Siriverdin and Dallbauman, 2004). These industries generate huge volumes of oil-water emulsion with typical concentrations of oil that ranges between 500-1000 mg/L daily (Chakrabarty et al., 2008). Before disposing or discharging oil-containing wastewater into the sea/rivers, the oil concentration in the wastewater should be reduced to acceptable discharge limit of 10-15 mg/L range (Bevis, 1992; Environmental Protection Agency, 2008). Therefore, the removal of oil from the oil-containing wastewater is necessary before its disposal.

In order to reduce or remove the concentration of oil from water, different membrane-based techniques such as microfiltration (MF) (Abadi et al, 2011), ultrafiltration (UF) (Chakrabarty et al., 2010), nanofiltration (NF) and reverse osmosis (RO) (Ramli et al., 2012; Mondal & Wickramasinghe, 2008) have been generally adopted as remediation treatment methods to solve the challenges posed by the oil containing wastewater. The main advantages of membrane filtration technologies is that they can separate particles with smaller diameters because of their pore sizes that are less than 10 μm (Baker, 2012), they use less energy during separation and are easy to make (Sauvetgoichon, 2007).

Performance of these membrane techniques, however, is affected by fouling and concentration polarization (Gekas & Hallstrom, 1990). During fouling, the surface and/or pores of the membranes are blocked by an organic or inorganic substance, thereby lowering the membrane flux (Lee et al., 2011). According to Wijmans (2000) and Parker (2003), during concentration polarization the concentration gradient (a change in the concentration of substances in a solution) occurs which is caused by the concentration of the feed flow

becoming less than that of the solute particles attached to the boundary layer, thereby decreasing the membrane flux (the performance of the membrane during separation). To prevent fouling, hydrophilicity of the membrane material should be increased. Hydrophilicity is the ability of a molecule or a substance to dissolve in water (McNaught and Wilkinson, 1997). Hence a hydrophilic membrane is a membrane that only permits substances that dissolve in water. Concentration polarization can be minimised by increasing the speed at which the feed is flowing (McNaught and Wilkinson, 1997). Control of fouling and minimization of concentration polarization improves the performance of the membrane and prolongs the lifespan of the membrane (Wakeman & Williams, 2002). To clean fouled membranes, chemical enhanced backwash (CEB) and chemical-in-place (CIP) (Choi, 2005) are used. The use of these chemicals increases the operating costs and may also introduce unwanted chemicals in the stream to be disposed off.

Recently a new hydrophilic polymer composite membrane containing CNT/polysulfone and polyvinyl alcohol (PVA), a water-soluble biodegradable polymer, was recently synthesized and tested on synthetic (laboratory prepared) oil-containing wastewater with the view of solving the above mentioned problem of concentration polarisation, fouling and subsequent cleaning with chemicals during treatment of oil-containing wastewater. The performance of the membrane was excellent with high throughput and oil injection of more than 95% (Maphutha et al., 2013). The permeate through the membrane showed the oil concentration below 10 mg/L. However, the performance of this new hydrophilic polymer composite membrane using the real industrial oil-containing wastewater has not yet been assessed.

In view of this, this project was aimed a) to optimise the synthesis of the polymer composite membrane containing CNT/polysulfone and polyvinyl alcohol (PVA) by using pCNTs and optimizing the amount of the PS (polysulfone) solution used b) to assess the separation performance of the new synthesized membrane on the industrial oil-containing wastewater with the goal of gathering data for the potential future implementation of the technology at industrial scale. The mechanical stability of PS and the CNTs increases the overall mechanical and hydrophilicity of the membrane colloidal or fine particles.

1.2 Aim and objectives

The aim of this project was to optimise the synthesis and operational performance of the CNT-infused polysulfone (PS) membrane with a polyvinyl alcohol layer to separate oil-containing wastewater.

The following objectives were formulated to achieve the aim:

- To synthesize the CNTs using ferrocene as a catalyst and a source of carbon, using nitrogen gas to make sure that there were no gas leaks in the system and that the contaminants (other unidentified gases) are removed and using argon gas as a carrier.
- To purify the synthesized CNTs using hydrofluoric acid, hydrochloric acid, sulphuric acid and the nitric acid.
- To synthesize seven PS membranes (two with no addition of CNTs but one, among these two, with the PVA layer; four infused with different loadings of the as-produced CNTs as well as the PVA layer; and one containing the pCNTs with the PVA layer).
- To assess the separation performance of the synthesized PS membranes using the real industrial oil-containing wastewater.

1.3 Research questions

The following questions are to be answered while trying to achieve the above-mentioned aim and objectives:

- Can the separation performance of the as-produced CNTs PS membranes meet the acceptable discharge limit of 10-15 mg/L when the real industrial oil-containing wastewater is used?
- Will the use of the purified CNTs as well as the PVA layer improve the fouling resistance of the membrane?
- Could the use of the purified CNTs as well as 20% (see section 1.5) PS solution instead of 10% (which reduce the size of the pores of the membrane), optimize the synthesis and the separation performance of the membrane?
- Will the separation performance of the PS membrane with the PVA layer and the purified nanotubes be greater than those using the as-produced CNTs?

1.4 Hypothesis

The use of 20% PS solution and the purified CNTs will optimize the synthesis and the separation performance of the nanotube-infused PS membrane with the PVA layer to separate the oil-containing wastewater. The optimised synthesis could result to an improved separation performance and hence reduce the concentration of oil in wastewater to an acceptable discharge limit before its disposal.

1.5 Justification of study

Many research studies have been reported on the separation of the synthetic oil-containing wastewater using membrane technology, but very few on the industrial oil-containing wastewater. The permeate through the membrane synthesised by Maphutha et al. (2013) showed oil concentration below 10 mg/L and oil rejection of over 95% in the retentate when using the synthetic oil-containing wastewater. The performance of this promising membrane using the real industrial oil-containing wastewater, however, has not been assessed. Hence the performance of this membrane using the real industrial oil-containing wastewater will be assessed in this project.

(i) Justification for the use of 20% PS solution

Before synthesizing the membranes, the diameter of the oil droplets in the oily water should be measured so that the pore sizes of the membrane should be adjusted to suitable sizes that would enable the membrane to successfully filter the liquid. The diameters of oil droplets in the industrial oil-containing wastewater used were between 0.02 and 0.2 μm. This means that this oil could only be rejected by a membrane with pore sizes less than 0.02 μm. In-depth literature has shown that using higher amount (e.g. 20%) of the PS solution instead of the previously used 10% could reduce the porosity of the membrane and hence increase its separation performance (Huang & Yang, 2006). The use of 10 % PS solution to synthesise a membrane results in pore sizes greater than 0.02 μm (Maphutha et al., 2013). The utilisation of 15% results to porosity of more than 55% (Huang and Yang, 2006). A 19% PS solution gives a membrane with pore sizes slightly higher than 0.02 μm. The 20% PS solution gives membrane with pore sizes less than 0.02 μm which results to optimal rejection and flux balances as well as the improvement of the membrane's fouling resistance (hydrophilicity). Those membranes prepared with PS solution of more than 20%, e.g., 30%, however, would

results in very low fluxes and extremely high rejections than required, due to the decrease in pore size as the amount of PS solution is increasing. Therefore, 20% PS solution was used to investigate its effect on the synthesis and the separation performance of the membrane.

1.6 Scope of the project

In order to achieve possible optimisation of synthesis and separation performance of the membrane, this project will be conducted in four stages:

(i) Assessment of the separation performance of the membrane synthesised by Maphutha et al. (2013).
(ii) Production of purified and non-purified CNTs.
(iii) Utilisation of the purified CNTs and 20% PS solution to produce the optimised membrane.
(iv) Assessment of the separation performance of the optimised membrane and comparing it to (i).

1.7 Expected contribution to knowledge

This project which aims to optimise the synthesis and the separation performance of the nanotube-infused polysulfone membrane with PVA layer to separate oil-containing wastewater is projected to offer:

- Information on the separation performance of the membrane produced by Maphutha et al. (2013) using the real industrial oil-containing wastewater.
- Evidence on the use of the pCNTs on a PS membrane.
- Knowledge on the separation performance of the composite PS membrane with PVA layer containing purified and non-purified CNTs.
- Facts on the difference between the PS membrane with pCNTs (optimised) and the membrane produced by Maphutha et al. (2013).

1.8 Report project outline

Chapter 1

The background and motivation of this project are described in this chapter. The aim, objectives, research questions, hypothesis, justification of study, the scope of the project and the expected contribution to knowledge are also discussed.

Chapter 2

This chapter briefly reviews the literature on previous methods used to separate oil-containing wastewater and the PS membrane and its components, i.e., the PVA layer, maleic acid (MA), pCNTs and non-purified CNTs; as well as the phase inversion method which was used to synthesise the PS membranes.

Chapter 3

This chapter describes the materials and methods used to synthesize and characterise the CNTs and the PS membranes. The analytical methods as well as the procedures used to test the separation performance of the membranes are also described.

Chapter 4

The results from the experiments are presented and discussed in this chapter.

Chapter 5

This chapter contains the conclusions and the recommendations drawn from this project.

CHAPTER 2: LITERATURE REVIEW

2.1 Introduction

In this chapter the appropriate literature review is discussed in details. This literature review is described in two sections; the first part discusses the previous methods used to separate oil-containing wastewater including the current most widely used membrane filtration-based techniques (as introduced in chapter 1), and the second part discuss the phase inversion method used to produce the PS membrane in this project, as well as the components of this membrane, i.e., polysulfone, polysulfone membrane, PVA and CNTs.

2.2 Previous and current methods used to separate oil containing wastewater

There are several methods that have been used in the treatment of oil-containing wastewater, these include American Petroleum Institute (API) separator, floatation, coagulation and membrane filtration technologies.

2.2.1 American Petroleum Institute (API) separator

In the API separator, large amounts of oil, solids and other contaminants are separated from wastewater (Beychok, 1967). This method is commonly used in oil fields and petrochemical industries. The API separator is widely used because it is easy to manufacture, cheaper (compared to separators like floatation), easy to maintain, no addition of chemicals and is not easily blocked by solids (API, 1969). According to API (1990), this method is capable of separating particles with diameters larger than 150 μm. The API separator usually separates particles depending on their size and densities. It serves as a 'pre-filter' to separators like dissolved air floatation (DAF) (Edzwald, 1995). It has been reported to remove 90-95% of free oil, with the permeate showing the free oil concentration between 15-20mg/L range, it also separates between 80-95% of the suspended solids with 20-30 mg/L showing in the permeate (Klein Wolterink et al., 2004).

However, it cannot separate emulsified oil-water and droplets of oil with diameter less than 150µm (Mercer, 2012). The contaminants can easily be absorbed on its surface, thereby affecting its separation performance.

2.2.2 Flotation Method

Another method that is commonly used for separating oil-containing wastewater is flotation method. This method is used because it can remove oil particles with diameters in the range between 35-50 µm compared to API separators (Colic et al., 2001). Types of flotation include dissolved air flotation (DAF) and induced air flotation (IAF). In DAF, free oil and other suspended contaminated solid particles are separated from wastewater (Wang et al., 2004). Here according to Kiuru et al. (2000) and Beychock (1967), air is dissolved in the wastewater, in a tank at a certain pressure, producing smaller air bubbles which attaches to the oil droplets thereby suspending/floating them to the surface of wastewater. The free oil is then released to the atmosphere by the atmospheric pressure (Smith & Cox, 2010). The lighter the density of oil droplets, the faster they move to the surface. DAF is reported to separate 95-98% of free and emulsified oil, as well as suspended solids, with the permeate showing the oil and suspended solid concentration between 5-10 mg/L (Parker & Monteith, 1996). According to Beychock (1967) IAF is similar to DAF except air is injected/induced into the wastewater instead of being dissolved. Air bubbles are bigger which implies lesser separation performance compared to DAF. IAF is capable of separating between 80-90 % of free oil and suspended solids; however, it cannot separate the emulsified oil (Wang, 2007; Zhu and Zhang, 2002).

Both flotation methods, however, require the use of chemicals during their separation performance and they also have high operating costs compared to API separator (Shammas et al., 2010).

2.2.3 Coagulation Method

In coagulation process, colloids, solid particles and other contaminants present in wastewater combine into larger particles in order to be separated by filtration or any other separation method (Casellas-Salha et al., 1981). This method is used normally when these wastewater

constituents (colloids, solids, emulsified oil, organic substances, etc.) are not able to be separated by a physical separation method unless they are combined because of nature of colloids (Lee, 2000). Even larger particles than colloids are removed through this method. Zhang et al (2006) using a $Ca(OH)_2$ coagulant with a concentration of 900 mg/L, were able to remove 99.8% of oils and 97% chemical oxygen demand (COD), this also increased the phosphate removal from 46.4% to 99.6%. The use of composite Cellulose Acetate halide (CAX, where X is a halide) coagulant showed oil rejection of more than 98% with COD of 80% (Lin & Wen, 2003). This shows that this method is excellent when it comes to separation of oil-containing wastewater.

However, this method requires the use of chemicals, which contributes to the operational costs. It can only be used at a specific/ limited pH, is easily affected by fouling, and cannot be used at very low temperatures. Moreover, all these processes mentioned above are not able to remove emulsified oil-water when oil droplets are less than 30 μm (Luthy, 1978).

2.2.4 Centrifugal oil-water separator

This is a type of centrifuge that separates oil-containing wastewater which operates by using an electric motor to spin an object using a centrifugal force that is normal to the axis (Sammons and Fox Jr, 1979). There are several types of this kind of this device, which includes horizontal and vertical cone-shaped centrifugal oil-containing wastewater separators, both shown in Figure 2.1.

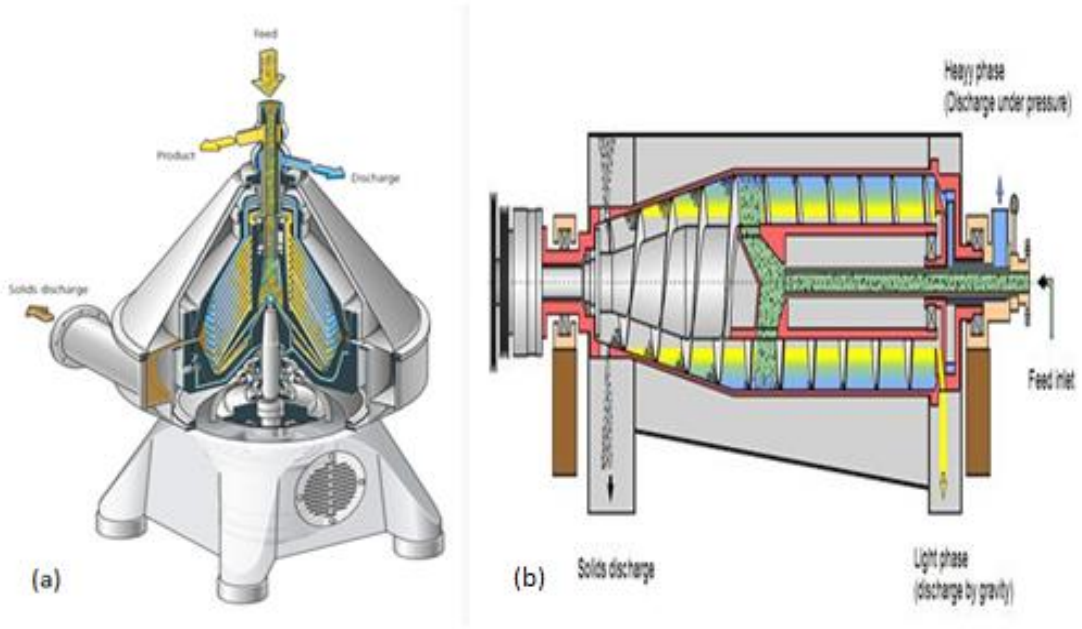


Figure 2.1: Pictures of the centrifugal oil-containing wastewater separator, (a) Vertical (GEA Westflia separator, 2014), and (b) horizontal (Flottweg Separation technology, 2014).

The vertical centrifuge is superior to its horizontal counter part because of its separation performance. The horizontal centrifuge removes about 10 - 30% of the emulsified oil-containing wastewater, whereas the vertical one removes about 40-80% (Klein Wolterink, 2004). The vertical centrifuge is also very stable at higher temperature and pressure as compared to its limited horizontal version (CPO, 2015). Sammons and Fox Jr (1979) used a vertical centrifugal oil-water separator to separate oil-containing wastewater with the aim of the oil concentration. The device had a small round container, with openings in the lower part, spinning inside a larger immobile container. The feed is vertically fed into the mouth of the smaller revolving container on the central upper surface of the device. The small inner container contains pores on its surface in which the filtrate passes through from the inside into the space or "gut" of the larger container, the solids remains in the smaller container which are trapped and then removed as the container keeps spinning. The trapped solids are then removed from the surface of the small container into the larger one where they are washed and dewatered. The combination of the greater rotating speed (produced by the electric motor) and the size of the larger container results into a centrifugal force which dewaters the solid particles (Pieralisi group, 2014; Sutherland, 2007). After dewatering, the

solids are then taken out of the container manually. This happens when the device is stopped or slowed down (Sutherland, 2007).

Separation of solids from liquids occurs on the surface of the smaller container. As the container spins, the particles move in the "same" direction parallel to the axis until they are disposed into the collecting ring outside the small container. Since the centrifugal force is so high, washing and drying processes occurs very fast. Baffles, in the outer larger container, prevent the oil from mixing with the washing liquids. Centrifugal force causes wastewater particles spinning inside the larger container of the vertical centrifuge to move perpendicularly up and out of the centrifuge (Webster, 2015). The wastewater is discharged in the outlet on the right side – upper surface of the container as shown in the Figure 2.1.

The separated oil is removed as a product on the left hand side of the upper surface. Any solid particles contained, are removed at the waist of the device. However, the vertical centrifuge is inferior to its horizontal counterpart. This is because the horizontal centrifuge is less costly to use since it can be operated at low temperature and no pressure is required during its operation (Records and Sutherland, 2001).

In the horizontal centrifuge, the feed enters the device horizontally on a side; wastewater, the oil and the solid particles exit from the device individually and perpendicular to the feed. The advantages of the centrifugal oil-containing separator device are that; it is made up of a solid material; its disc cleans itself, is used for purification and separation processes and is manufactured sterilized (GEA Westflia separator, 2014). The horizontal one can separate a mixture of two different liquids and a solid particle at the same time.

However, this device uses built in clean-in-place (CIP) system to clean after fouling (Pieralisi, 2014). This makes this device more expensive to use (Sutherland, 2007), it requires very high maintenance and uses more energy to operate (Olive oil source, 2014).

2.2.5 Filtration method

Filtration is a physical separation of fluids (liquid or gas) from solid substances through a permeable membrane (Sutherland, 2007*)*. There are two types of filtration for transportation of particles during separation performances: Cross-flow and dead end filtration.

Dead end filtration

In the dead end filtration, the filtrate (the permeate together with the retentate) flows away from and at 90^{o} to the surface in the same direction as the flow of feed (Seadler & Henley, 2006; MSU, 2014)).

Advantage of dead end filtration:

- It is cheaper and easy to make (Iritani et al., 1995).

Disadvantage of dead end filtration:

- It is easily affected by fouling and concentration polarization (Modise et al., 2005; Fr, 2014).

Cross flow filtration

Here the permeate flows away from the surface, perpendicular to the flow of feed where is to be collected; while the retentate (the rejected component) flows in the same direction as and away from the flow of feed (Koros et al., 1996), (Perry & Green, 2007)

Advantages of cross flow filtration:

- Less fouling due to hydrophilicity and shear rates of the passing flow (Bertera et al., 1984).

Disadvantage of cross flow filtration:

- It is more expensive compared to dead end filtration (Iritani et al., 1995).

2.2.6 Surface (membrane) filtration

Membrane filtration is a filtration method that is generally used in both laboratory and industrial applications for separation currently. They are commonly used because they are cheap and easy to make, saves energy since no heat is required during separation, and uses low quantity of chemicals to clean after fouling. Membrane filtration method was developed in the 1930's, as an alternative to the most probable number, MPN, and depth filters (DP),

became commercially available during World War II in the 1940's for its use in cleaning contaminated water for safe drinking (Kesting, 1972).

Membrane filtration was not only used for water treatment, but was also used for other analysis. Radioisotope technology increased the use of membrane filtration in the 1950's. During hybridisation studies, membrane filtration was used to form polymer acids such as DNA and RNA as well as agents for the electrophoresis in the field of biochemistry in the 1970's (Everett, 1988).

In the 1980's membrane filtration was used for water treatment at low temperature and pressure. One of its advantages is that, this method can also use less energy during operation with no heat addition (Hamlyn, 1990). It is also easy to manufacture the equipment which requires low cost of maintenance. It is the most used and trusted method to date. However, this method is negatively affected by concentration polarization and fouling which decreases the separation performance of the overall membrane flux (Shakaib, 2008).

Studies have shown that hydrophilicity increases the separation performance of the membrane. Hence membrane techniques with hydrophilic components have enhanced separation performance than those without them. Wu et al. (2008) reported that his polyvinyl alcohol layer ultrafiltration membrane was able to reject more than 95 % concentration of oil. Ultrafiltration by polysulfone membrane with polyvinylpyrrolidone (PVP) and polyethylene glycol (PEG) rejected more than 90 % of oil (Chakrabarty et al., 2008). The presence of a fouling resistance membrane and/or modification of the existing ones will be a good approach to overcome this problem (Al-Amoudi et al., 2007). A technique was recently developed for treating oil-containing wastewater, which was able to reject more than 95% and the permeate showed less than 10mg/L of oil concentration (Maphutha et al., 2013). However, this membrane only tested on laboratory synthetic wastewater. Membrane filters have pore sizes less than 10 µm (Baker, 2012). Their circular small sized pores are used to analyse samples and the larger ones are used for process filtration. They can be used to filter volumes up to 400 litres, more than this, cartilage filters are usually used. However, membrane filtration is sensitive to fouling (Westner et al., 1992).

Membrane filtration is used for different applications in the field of science and engineering. In the treatment of oil-water emulsion for the removal of wastewater, the concentration of oil is reduced to an acceptance level before the wastewater is being discharged. Wastewater can also be purified using membrane filtration so that it can be used all over again (Baker, 2012).

As technology increased and the number of industries developed, the more advanced membrane filtration techniques were established to cater for the needs of these industries. Advancement in technology improved the industrial use of the membrane filtration in the past couple of years. There are several different types of membrane filters all with the aim of separation in order to protect the environment and make life easier around them. These membranes can be either homogeneous or non-homogeneous.

There are four main types of membrane filtration that uses pressure during their separation performances and are also classified according to their pore sizes and the molecular weight cut off: (i) Microfiltration (MF), (ii) Ultrafiltration (UF), (iii) Nanofiltration (NF) and (iv) reverse osmosis (RO). These techniques are becoming more and more popular in treatment of oil-containing wastewater, and they are described below.

(i) Microfiltration (MF)

MF is a membrane filtration technique that is used to separate particles. This kind of membrane has larger pore sizes compared to other membrane filters.

It has pore sizes ranging from 0.1-10 µm (Abadi et al, 2011; Baker, 2012). They are mainly used to separate particles with diameters greater than 10 µm from a liquid phase, as well as large bacteria and protein particles (Crittenden et al., 2012). This technique works partially the same as the conventional filtration. It is a combination of both cross flow and dead-end filtration methods. During separation process it uses pressure to minimize the blockage of the surface and pores of the membrane by rejected particles. It normally operates at pressures between ranges of 0.5-2 bar, temperature of 32.5^{o}C and velocities ranging between 2-3 m/s perpendicular to the flow of the feed in the tubular shape (Abadi et al., 2011; Perry & Green, 2007). MF also functions as a pre-filter to the other membrane filtration techniques with pores less than 0.1 µm. Vacuum filtration is sometimes used during its separation performance, where pressure change is measured using a pressure gauge (Baker, 2012). It is capable of rejecting 90-98% of oil and other particles (Abadi et al., 2011; Kenna & Zander, 2000).

Some of MF disadvantages are that: the flow is aided by pumping a liquid into the surface to allow permeate through to the other side. It is affected by fouling and concentration polarisation where chemicals have to be used to clean after fouling.

(ii) Ultrafiltration (UF)

These are polymer-made membrane filters with pore sizes that range between 0.01-0.1 µm (Chakrabarty et al., 2010). UF is partially the same as MF, except that it is a physical separation of macromolecules instead of particles. UF is situated between MF and nanofiltration. It separates smaller particulates than MF. It is capable of rejecting molecules with diameters greater than 0.1 µm, such as proteins, colloids and other macromolecules. These molecules have molecular masses in the range between 1000 and 100,000 g/mol (Cheryan, 1998). Only viruses and small organic molecules will be absorbed at the surface and the pores of the membrane. It is also a type of both cross flow and dead end filtrations. As the pore sizes become narrower, the pressure increases. UF normally operates at pressure range of 1-10 bar (Farahbakhsh et al., 2003). It is usually used to separate permeates from MF and rejects the undissolved substances as retentates.

The uses of UF include:

- Removal of bacteria and purification of water for drinking purposes (Clever et al., 2000).
- Concentration of protein, e.g. Filtration of milk when cheese is made, in the dairy industry (Cheryan, 1998).
- It is also used in industries such as oil fields and petrochemicals to separate oil-containing wastewater.

Chakrabarty et al. (2010) used a polysulfone membrane to separate a stable oil-water emulsion containing wastewater. The results were good with oil rejection of more than 90% of the laboratory based oil-containing wastewater, and the permeate showing oil concentration below 10mg/L; and the industrial oil concentration was rejected up to 80%. This was largely due to polyvinylpyrrolidone (PVP) and polyethelene glycol (PEG) molecular weights, as well as the parameters used. Lafreniere et al. (1987) also studied the effect of PVP on the polyester-sulfone membrane.

Poly (vinyl alcohol) (PVA) membrane showed good separation performance when it was employed during the oily water separation (Wu et al., 2008). The membrane rejected more than 95% of oil which showed good fouling resistance character by the PVA membrane.

Addition of hydrophilic groups were demonstrated again to be effective as polyvinylidene fluoride (PVF) membrane was used in the separation of oil-containing wastewater (Yu et al.,

2006). The membrane separated oil particles with diameters below 2 µm, and the permeate showed oil concentration less than 1 mg/L. This was due to the enhanced hydrophilicity by the PVF which increased the fouling resistance of the overall membrane.

Ebrahimi et al. (2009) reported that UF with pore size 0.05 µm could remove oil less than 99% and total organic hydrocarbon (TOC) less than 39%, at cross flow velocity range between 0.6-1.3 m/s.

(iii) Nanofiltration (NF)

Nanofilters are the most advanced and improved membrane based filters currently. The relationship between MF and UF is the same as the one between UF and NF, i.e., UF serves as a pre-filter to NF, except that the nanofiltration technique separate smaller particles than UF. The pore sizes of NF ranges between 0.001-0.01 µm (Letterman, 1999). Accurate measurement of these pore sizes cannot be achieved since they are relatively small. It is capable of rejecting components of diameters more than 0.01 µm, such as viruses and valence ions (Rahimpour et al., 2010). This technique is used for its low maintenance and operational costs. It is a cross flow filtration that has circular pores with the same size as a nanometre. Their separation performance is based on the molecular weight of the component to be rejected, since they have the molecular weight cut off that ranges between 100 – 1000 Dalton (Schafer, 2005), they are capable of removing particles with molecular weight greater than 1000 Dalton. NF operates at pressure ranges between 4-18 bar (Seadler & Henley, 2006). Usually it rejects about 31% of oil concentration at a temperature of about 25^{o}C during its separation performance (Mondal & Wickramasinghe, 2008). New logic (2015) conducted a case study using produced water to analyse the performance of NF membrane. The membrane showed oil recovery of more than 90%.

Uses of NF include:

- Softening of water (Rahimpour et al., 2010).
- Retaining of a solvent without the use of heat, in the pharmaceutical industry, and retaining of metals from wastewater (Letterman, 1999).
- Filtration of permeates from MF and UF.
- Rejection of valence ions (Baker et al., 2006).
- Food and beverage industries to concentrate milk and juice.

- Purification of municipal wastewaters.

Water flow rates that are produced by NF are lower than that of UF. Rahimpour et al. (2011) applied both self-manufactured and commercial NF membranes for the removal of chemical oxygen demand (COD) and electrical conductivity (EC). Commercial NF showed 84 % of COD removal and 88% of EC, whereas the self-manufactured showed 79% of COD and 93% of EC. This is a good 10 times decrease. NF can also reject about 90% of salt particles (Mondal & Wickramasinghe, 2008). Orecki & Tomaszewska (2007) treated oil-containing wastewater using NF method, the membrane gave the retentate of over 75% oil concentration for the cations investigated and more than 95% of the sulphates analysed.

It also has problems of fouling and concentration polarization (Hong & Elimelech, 1997).

(iv) Reverse osmosis (RO)

Osmosis is a movement of molecules from a low concentration region to a higher concentration region, without the use of energy, until equilibrium is reached (Haynie, 2001). RO is the opposite of osmosis; it involves the use of energy. RO has pore sizes that are less than 0.001µm (Mondal & Wickramasinghe, 2008). They are commonly used to separate salt from water (sea water), of which they can reject more than 95% concentration of salt. They have molecular weight cut off of less than 100 Da, their structure does not contain pores. During separation performance, ionic species diffuse through the ionic permeable channels of the membrane, i.e., water travels by osmosis through the membrane and salt is rejected as a retentate. It is capable of rejecting smaller viruses and small organic molecules with diameters greater than 0.001 µm. NF is usually a pre-filter to RO.

Just like all other membrane filtration techniques, it also uses pressure during separation of particles. RO operates at pressure range 10-80 bar (Malki, 2008). It is capable of rejecting 95-98 % of salt-water retentates. It could also reject 85% of oil (Franks et al., 2009). Al-Jeshi & Neville (2008) conducted an investigation to separate oil-containing wastewater. The result obtained was that 99% of oil was rejected from the feed of oil-containing wastewater that had 30% oil. This was a good separation performance by R.O.

Some of RO disadvantages include:

- Because of its narrow pores, RO rejects healthy minerals as retentates during the treatment of water (Sauvetgoichon, 2007)
- Fouling and concentration polarization.

Other uses of membrane filtration are:

- Separation of oil-containing wastewater (Abadi et al., 2011)
- Municipal water treatment (no addition of chemicals) (Baker, 2000).
- Separation of bacteria from its medium, in the field of microbiology (Clever et al., 2000).
- Discovery of cancer in animal and human cell. Making of artificial kidneys and lungs for physiological and breathing, respectively; in the field of Medicine (Ullrich et al., 1999).
- Sterilisation of liquids and making of antibiotics, in the pharmaceutical industry (Veolia, 2013)
- Purification and production of molecules in the biotechnology field.
- Purification of water for drinking purposes (Clever et al., 2000).
- Concentration of fruit juices, in the food industry (Cheryan, 1998)
- Removal of salt from the sea water (Rahimpour et al., 2010).
- Treatment of wastewater for reuse purposes.
- Making of ultraclean fluids in the electronic industry.
- Increasing of the efficiency of evaporator when concentrating vegetable and fruit juices, in the food and beverage industry (Cheryan, 1998)
- Synthesise ethanol from renewable resources.
- Sterilisation, in pharmaceuticals and food and beverages (Veolia, 2013)
- Gas particulates separation during refining process in petrochemical industries (Baker, 2012)
- Make diary ingredients and separate major components of milk in the dairy industry.

Advantages of membrane filtration:

- Can filter any size of a sample. Hence membrane filtration is sensitive.

- More precise, it depends on the density on a particle.
- It is easy to manufacture.
- Gives the results within 24 hours.
- It is selective.
- Can filter particles less than 0.7 µm
- Can analyse more samples at the same time without the addition of extra help.
- Can be used to analyse toxic substances
- The filter is easy to handle and be transported (Sauvetgoichon, 2007)
- It is not easy to block by substances.
- Can be bought sterilised.
- It is stable to temperature less than 130^{o}C (Gitis et al., 2010)
- It rejects particles on the surface of the membrane, which could be used for analysis purposes.
- Saves energy since no heat is required during separation.
- Depends on the sample used.

All the membrane techniques above are used in many fields of science and engineering, as well as in the industries for separation of particles. Life without them would be diminished as separation techniques are more in demand now than ever.

However, the main disadvantage is that the performance of these techniques is affected by fouling and concentration polarization. They are also more expensive.

2.2.7 Summary of oil-containing wastewater separation methods.

The table on the next page shows the summary of how oil-containing wastewater separation methods differ/similar.

Table 1: Comparison between different oil-containing wastewater separation methods: (a) industrial, and (b) filtration methods.

(a) Industrial oil containing wastewater treatment methods								
Method	Advantages	Disadvantages	Operating principle	Diameter of oil-droplet separated (µm)	Separation efficiency (%)	Cost (US $)	Free oil/Emulsified oil/suspended solids	References
API separator	Does not use additional chemicals	Cannot separate the emulsified oil.	Gravity	> 150*	80-95	N/A	Free oil and Suspended solids	(Klein Wolterink, 2004; *Mercer, 2002)
Dissolved air floatation	Can withstand any oil-containing wastewater. Can separate the emulsified oil.	Addition of chemicals increases the cost.	Flotation	> 35[y]	95-98	[1]3000-170000/set	Emulsified oil	([1]Alibaba, 2015; [y]Ital traco, 2015; Klein Wolterink, 2004)
Induced air floatation	Easier to maintain and operate.	Cannot separate the produced water at higher temperatures[6]	Flotation	> 25**	80-90	[1]3000-60000 (10m3/h)	Free oil	([1]Alibaba, 2015; [6]Igunnu and Chen, 2012; **Frankiewicz, 2001; Klein Wolterink, 2004)
Hydro cyclone	low consumption of energy	Inflexible[5] during operations and easily blocked by suspended solids***	Centrifugation	**10-15	80-95	[1]10-60,000/set	Free oil and suspended solids	([1]Alibaba, 2015; **Frankiewicz, 2001; Klein Wolterink, 2004; [5]Marthinussen, 2011; ***Miranda, 2013)
Vertical centrifugal oil-water separator	Can separate free oil and suspended solids as well as emulsified oil	It uses the addition of chemicals	Centrifugation	> 2**	*40-80	[1]28,000-38,900/set	Emulsified oil	([1]Alibaba, 2015; **Frankiewicz, 2001; Klein Wolterink, 2004)

(b) Pressure driven membrane filtration methods									
Method	Pressure (bar)	Pore size (µm)	Diameter of oil-droplet separated (µm)	Separation efficiency (%)	Cost (US $)	Free oil/Emulsified oil/suspended solids	Advantages	Disadvantages	References
Microfiltration	0.5-2	0.1-10	> 10	90-98	212-2000[c]	Free and ***suspended solids	Non-permeable to: Large proteins, bacteria, suspended solids and other microorganisms.	Permeable to: Sugar multivalent ions, smaller proteins, salt water	(Abadi et al., 2011; [c]AMI membranes, 2015; Crittendon et al., 2012; Environmental technology centre, 2015; ***Miranda, 2013; Kenna & Zander, 2000)
Ultrafiltration	1-10	0.01-0.1	> 0.1	> 80	160-3600[b]	Emulsified oil	Non-permeable to: proteins, colloids and other macromolecules.	Permeable to: Sugar multivalent ions and salt water	(Chakrabarty et al., 2010; Cheryan, 1998; Environmental technology centre, 2015; [b]Purchase advantage, 2015)
Nanofiltration	4-18	0.001-0.01	> 0.01	> 90[#]	250-750[b]	Free oil	Non-permeable to: viruses and sugar multivalent ions	Permeable to salt water	(Environmental technology centre, 2015; Letterman, 1999; [#]New logic, 2015; [b]Purchase advantage, 2015; Rahimpour et al., 2010)
Reverse osmosis	10-80	< 0.001	> 0.001	> 99	66-220[c]	Free oil	Water purification. Non-permeable to: salt, microorganisms and other chemicals in water.	Easily affected by fouling and concentration polarisation. Sample containing larger metals and solids requires pre-filtration	([c]AMI membranes, 2015; Larry, 2011; Mondal & Wickramasinghe, 2008)

2.3 Fouling and concentration polarization

Control of fouling and minimization of concentration polarization may improve the membrane performance and prolongs the lifespan of the membrane.

2.3.1 Concentration polarization

Concentration polarization is a process that affects the flow transfer of the rejected component, i.e., it is a decrease or an increase of the concentration of the solute on the boundary layer because of the selective ability of the membrane (Parker, 2003). For example, the rejected component attaches itself on the surface of the membrane, thereby increasing its concentration as the feed continues to be reduced. The higher concentration of the rejected component on the boundary layer causes the concentration gradient and thereby decreasing the membrane flux.

Example of concentration polarization is biofouling. Biofouling is caused by the attachment of bacteria on the surface of the membrane. It usually occurs when a gel layer is formed by the attachment of bacteria on the surface of the membrane (Flemming et al., 1997). This layer reduces the flow rate thereby resulting in low yield of permeate. This layer can cause unequal flow of fluids thereby resulting in possible concentration polarization (Baker, 1998).

The reversible concentration polarization can be minimised by:

- Decreasing the differential pressure (Transmembrane pressure, TMP) (Probstein, 1994)
- Decreasing the solute concentration (Rubinstein and Zaltzman, 2000)
- Preventing the build-up of the concentration gradient by making the fluid flow passage thin (Kim et al., 2010)
- Using a cross flow filtration.

2.3.2 Fouling

Fouling is one of the major problems that reduce the performance of the membrane during separation process. It is both a physical and chemical process. Fouling is usually caused by blockage of pores and/or the surface of the membrane by the organic or inorganic substance

(Baker, 2004). Some example of these substances may be metal oxides, soluble salts, humic acids, clay, colloidal minerals and bacterial growth that usually attach themselves on the membrane. Fouling can be noticed by a decreased flow rate of both rejected component and permeate (Mo and Huanga, 2003*).*

Fouling can be organic or colloidal. In colloidal fouling, colloids attach themselves on the surface of the membrane, thereby decreasing the membrane flux (Quintanilla, (2005). In organic fouling, organic molecules attach themselves instead of colloids (Lee et al., 2005).

The irreversible fouling can be controlled by:

- Using chemical enhanced backwash (CEB) and chemical in place (CIP) to clean the membrane (Choi et al., 2005).
- Causing the pressure to flow the solutes in reverse (back pressuring), e.g., as in RO (Weisner et al., 1992)
- Remove the material from the membrane by using the balls made up of a sponge (Aoustin et al., 2001)
- Use enzymes to clean fouling that were caused by proteins (Makdissy et al., 2003)

However, the use of chemicals such as CEB and CIP to control fouling and minimize concentration polarization contribute immensely to the operating cost for the treatment of the wastewater. It is very costly to buy a membrane filter alone, so to buy a chemical as well is much more expensive.

This led to manufacture of a CNT-infused polysulfone membrane with polyvinyl alcohol layer for treating oil-containing wastewater (Maphutha et al. 2013). This is a membrane that controls fouling and minimize the concentration polarization without the use of chemicals (Maphutha et al. 2013). The membrane was used to treat oil-containing wastewater. Currently this membrane is only available for the laboratory use. It could reduce all cost of buying both membrane and chemicals if it is commercially available.

This membrane is a water-soluble biodegradable polymer and is highly hydrophilic. Polyvinyl alcohol (PVA) is a water-soluble polymer that enhanced the hydrophilicity of the overall membrane material. The enhanced hydrophilicity of the membrane makes it more resistance to organic fouling (Van der Bruggen et al., 2008), enhancing therefore the

separation performance of the membrane during the separation of oil-containing wastewater. In addition, the presence of the CNTs enhanced the mechanical and thermal stability of the membrane when compared to the mechanical and thermal stability of the existing pure polymeric membranes.

This membrane was fabricated and tested during separation of oil-containing wastewater. The performance of the membrane was excellent. The permeate through the membrane showed oil concentration below 10 mg/L and oil rejection of more than 95%. This is a proof of concept for the developed membrane material. However, to develop this promising membrane material from laboratory scale to commercial scale, optimization and scale-up studies are necessary. In view of this, this project aims to optimize the synthesis and operational performance of this membrane with a goal of developing the membrane for commercialization.

2.4 Polysulfone polymer

The morphology and properties of the membrane also depends on the choice of a polymer to be used (Laila et al., 2013). Polysulfone (PS) is one of the most widely used polymer for the synthesis of a membrane using the phase inversion method (Doménech-Carbó and Aura-Castro, 1999; Lalia et al., 2013). This is because PS is a thermoplastic polymer which is tough and stable at very high temperatures. In 1965 Union Carbide established PS as one of the first thermoplastic class/ family at the temperature of 149^{o}C (RTP Company, 2014). Its stiffness, high tensile strength and clearness enable the polymer to retain its possessions between the temperature ranges of 173 to 423 K (Parker et al., 2002). Outside this range, the polymer becomes ‘denatured’, i.e., its structure becomes damaged.

The typical structure of the PS is made up of the monomer units of diphenol and bis(4 – chlorophenyl)sulfone, of which the sulfone functional group bonds these phenyls together and defies this polymer (Figure 2.2):

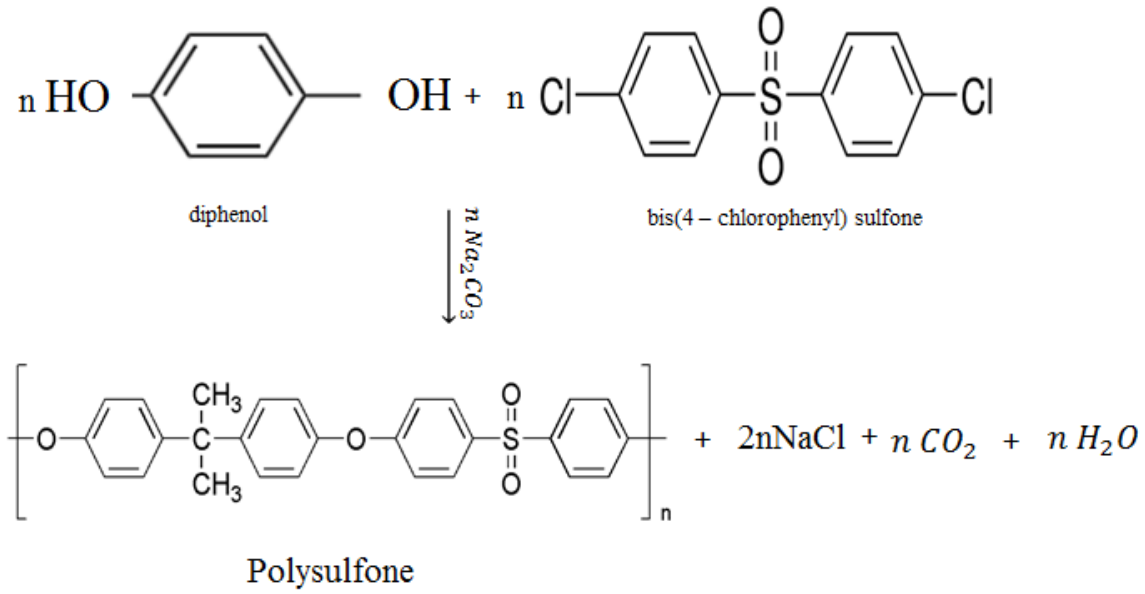


Figure 2.2: Formation of polysulfone from diphenol and bis(4 – chlorophenyl)sulfone (Parker, 2003; Calvero, 2006; Sigma Aldrich, 2014; Neuroticker, 2007).

According to Parker et al. (2002), these monomers must be highly purified in order obtain high molar mass of the product.

One of the properties of PS is that it has a melting point and glass transition temperature between the range of 453 and 463 K, above and below this temperature range its physical properties changes. At this temperature range, the polymer behaves as a rubber and sometimes it becomes rigid.

Some of the advantages of PS are that, it can only react with alkali metals and inorganic acids with pH that is less than 2 and more than 13. It cannot react with oils and surfactants. PS is highly resistance to heat, it is a self-extinguisher. The only hydrocarbons I can react with are aromatic, ketones and chlorine-containing hydrocarbons. It can be used at high pressures and temperatures because of its mechanical stability. PS is also resistant to alcohol. It has excellent chemical rejection, excellent characteristics of electricity and cannot dissolve electrolytes (Parker et al., 2002).

PS is mostly used to synthesize membranes. It is also used in medical industry for autoclaving and to sanitize the steam since it is hydrolytically stable. Sometimes it is used as

an alternative to polycarbonate in electronic and motor industries because of its low cost of production. Polysulfone increases the mechanical stability (it triples the Young's modulus and doubles the tensile strength) of a material when it is strengthened with a glass fiber. PS also extends the life of a membrane material when it is used as a copolymer (Hickner et al., 2004; Borup et al., 2007). The clothing worn by Neil Armstrong in 1969 trip to the moon contained a film of which its component was made up of a polysulfone (NASA, 2010). Polysulfone is also much cheaper compared to polyethersulfone which has lower protein rejection (Tisch Scientific, 2014). PS is chosen because it enhances the mechanical stability and produces membranes with asymmetric pores.

2.5 Polysulfone membrane

Because of its properties, polysulfone polymer synthesizes membranes with pores that could be controlled to desired sizes very easily (Tisch Scientific, 2014). The smaller the size of the pores, the higher the separation performance. The morphology of a PS membrane may be asymmetric, this qualifiers the membrane to serve as a pre-filter and to ensures maximum separation performance (Pacific membranes, 2014). The membrane produced by the phase inversion method has two sides and both of them could be utilised; one is hydrophilic and the other is hydrophilic (repulsive to water). The hydrophilic side is more flexible than the hydrophobic one. The size of the pores on this different surface is also not the same. The unequal pore sizes results in high separation performance. Those membranes that have a very low thickness are normally used at low pressures. PS membranes can be sterilised to about 50 times without losing their properties (Tisch Scientific, 2014).

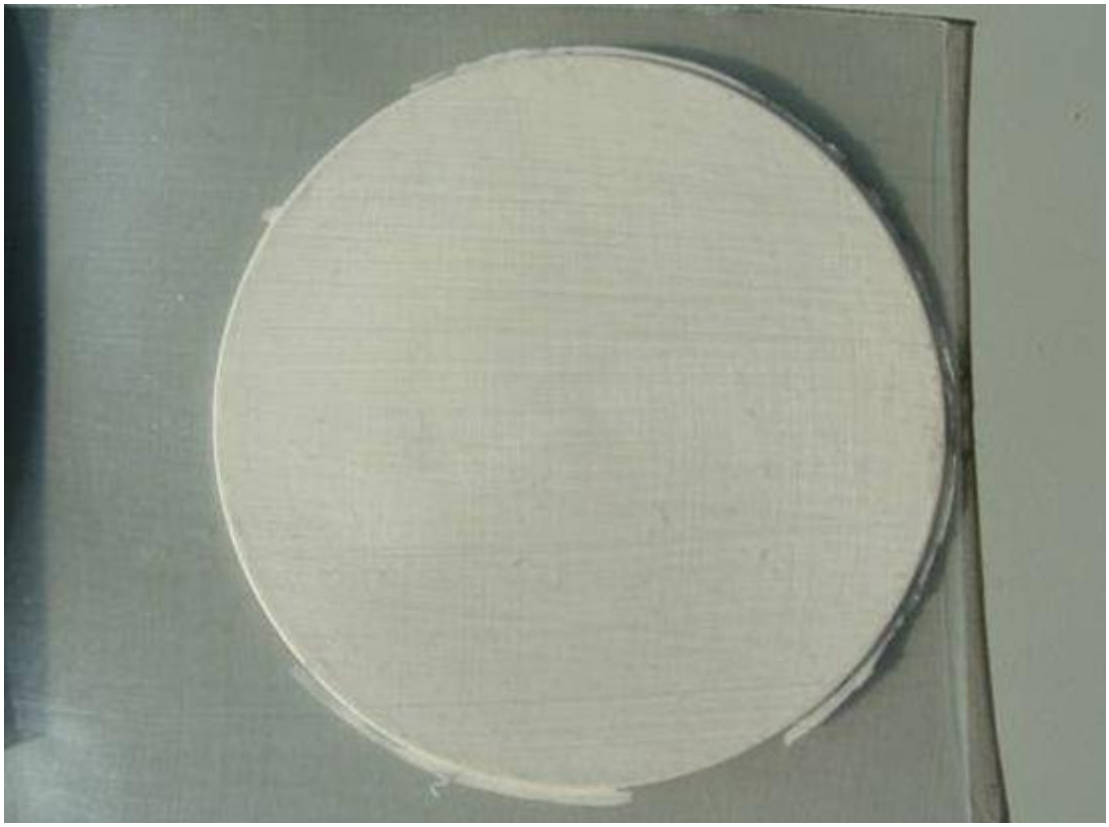


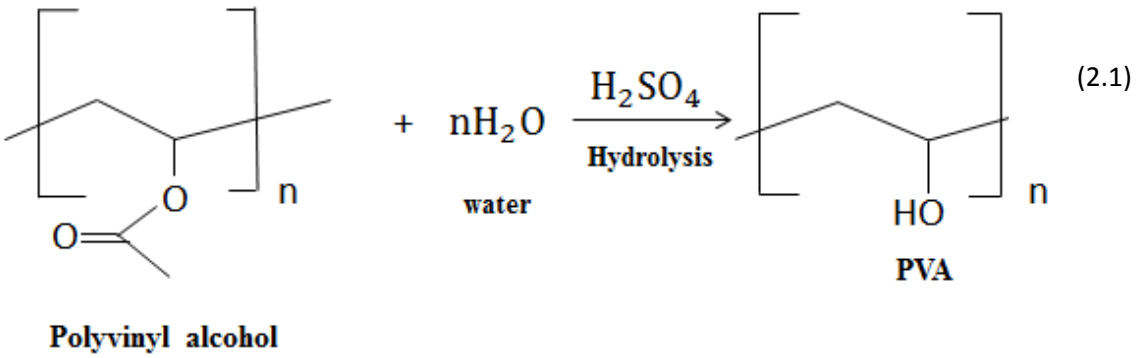
Figure 2.3: Picture of polysulfone membrane (Supercritical group, 2014).

Blended composite polysulfone membranes have increased mechanical stability; these membranes may be used at higher pressures. Chakrabarty et al., (2010) used a polysulfone membrane to separate a stable oil-water emulsion containing wastewater. The results were good with the oil rejection of more than 90% of the laboratory based oil-containing wastewater, and the permeate showing oil concentration below 10mg/L; and the industrial oil concentration was rejected up to 80%. This was largely due to polyvinyl pyrrolidone (PVP) and polyethylene glycol (PEG) molecular weights, as well as the parameters used. Javiya et al. (2008) used PEG to study the porometry of the PS membrane. Polysulfone membrane showed excellent separation performance when it rejected oil concentration of 99.16% with the permeate showing oil concentration of 0.67 mg/L (Zhang et al., 2009). PS membrane in this study was used to separate oil-containing wastewater.

2.6 The use of polyvinyl alcohol polymer

Polyvinyl alcohol (PVA) is one of the biodegradable polymers which are widely used in medical field. Biodegradable polymers are those polymers that are soluble in water (Swift,

1994) and provide the mechanical stability when they are used in tissue approximation (Pietrzak et al., 1997; Fromageau et al., 2003). PVA is formed by the reaction between the reaction between polyvinyl acetate and the repeating units of the monomers of water with the sulphuric acid as a catalyst according to the reaction (Haweel and Ammar, 2008):



(2.1)

Figure 2.4: Schematic drawing of the reaction for the synthesis of polyvinyl alcohol.

Where n is the number of the repeating units of the monomer. One of the good properties of PVA is that the completely hydrolysed grade melts at 503 K and the less hydrolysed grade melts between 453 and 463 K. This makes it possible to be used to separate oil-containing wastewater with temperatures less than 200^{o}C (Fromageu et al., 2003).

PVA has so many uses in different fields, lately has been used in the membrane technology industry for the separation of wastewater. A membrane containing PVA showed a good performance when it was employed during the oily water separation (Wu et al., 2008). The membrane rejected more than 95% of oil which showed good fouling resistance character by the PVA membrane.

Addition of hydrophilic groups were demonstrated again to be effective as polyvinylidene fluoride (PVF) membrane was used in the separation of oil-containing wastewater (Yu et al., 2006). The membrane separated oil particles with diameters below 2 µm, and the permeate showed oil concentration less than 1 mg/L. This was due to the enhanced hydrophilicity by the PVF which increased the fouling resistance of the overall membrane. Gohil and Ray (2009) were able to separate about 83% of salt water using a polysulfone membrane with a PVA layer.

In this project, PVA is used as a layer to enhance the hydrophilicity of the PS membrane during the separation of oil-containing wastewater. Maleic acid is to be as a cross linker to link the PVA with the PS.

2.7 CNT membranes

The CNTs are becoming more and more widely used nowadays because of their multi-purposes. The CNTs are the tube-shaped modified forms of carbon (Gullapalli and Wong, 2011; McNaught et al., 1997). The forms of carbon include graphite, amorphous carbon and diamond. The CNTs were 'discovered' by Iijima during the production of fullerene (Iijima, 1991). Since then, they have been of the rise in the field of science and engineering.

Generally there are three types of CNTs; this includes single-walled CNTs (SWCNTs), double-walled CNTs (DWCNTs) and multi-walled CNTs (MWCNTs) (Marulanda, 2010; Government Science, 2014). These are classified according to the number of layers (walls) they contain. The most widely used CNTs are SWCNTs and MWCNTs. This is because it is easy to synthesize them. SWCNTs are those CNTs composed of a single layer with diameters that ranges between 1.2-1.4 nm (Iyuke and Simate, 2011; Journet and Bernier, 1998). On the other hand, DWCNTs are composed two single-layer CNTs (Shen et al., 2011) and have a thickness of about 50 nm (Jia et al., 2007). It is very difficult to synthesize DWCNTs. MWCNTs are those with the external diameter that ranges between 25.6-33 nm and the internal diameter that ranges from 5.8-8nm (Phao et al., 2013; Maphutha et al., 2013), they also have carbon tops on each end (Shie, 2011).

Multiple functions of the CNTs enables them to be utilized in various industrial and laboratory applications, e.g., they could be used as reinforced materials, adsorption agents, etc. (De Volver et al., 2013; Cao and Rogers 2009; Hu et al., 2010; Schnorr and Swager, 2011). As the reinforced materials they are infused in polymer membranes to enhance the mechanical stability and prolong membrane's lifespan.

A CNT membrane is a membrane that is infused with CNT. The CNTs may be blended into the membranes either as they are produced, functionalised or purified in order to enhance the mechanical stability of the membrane. Mechanical stability is brought by, in general, the sp^2 carbon-carbon bond (Shie, 2011). The CNTs infused in the membrane are aligned at an angle

of 90º to the surface of the membrane, in other words, they lie parallel to the passage of water movement into the permeate and are held tangent to the flow of oil into the retentate. Because wastewater is polar and the CNTs are non-polar; when separating oil-containing wastewater, for example, wastewater easily passes through the CNTs into the permeate by repulsive forces without being stopped. A good analysis of water passing through the CNTs is the molecular dynamic simulations (Hummer et al., 2001; Sholl and Johnson, 2006). MWCNT-infused single-hole polystyrene membrane is believed to be the first membrane to assess how the mass of aqueous solutions passes through the CNTs (Sun and Crooks, 2000). Ion exchange membranes infused with SWCNTs electrodes showed very high efficiency in the treatment of salt water. The membrane was able to separate 97% of salt from water (Li and Zou, 2011). Kar et al. (2013) synthesized and evaluated the performance of a polysulfone membrane blended with SWCNTs during the treatment of bacteria *(E. Coli*). The membrane indicated a greater reduction to fouling compared to the ordinary (non-CNT blended) polysulfone membrane. The CNTs demonstrated to enhance the mechanical stability as well as the selective performance of a polyethersulfone membrane when the membrane attained the selectivity of more than 23, during the purification of the biogas, for CO_2/CH_4 (Kusworo et al., 2012). Alpatova et al. (2015) synthesized a ferric oxide (Fe_2O_3) nanoparticle and CNT-infused polyvinylidene fluoride composite membrane and utilised it to remove organic pollutants. The results obtained indicated that the mixture of the nanoparticles and the MWCNTs influenced the development of pores and enhanced the permeability of the membrane. The membrane, with the addition of the hydrogen peroxide (H_2O_2), was able to remove about 48% and about 53% of cyclohexanecarboxylic and humic acid, respectively. The membrane removed about 28% of the humic acid without the addition of the hydrogen peroxide. Ultrathin polymer photothermal-responsive hybrid membranes infused with SWCNTs indicated excellent performance with very good separation efficiency of more than 99.99% and flux of up to 35 m^2/h.bar during the separation of oil-in- water (Hu et al., 2015). Dumee et al. (2011) fabricated a bucky paper membrane blended with CNTs and evaluated its performance using the salt water. The membrane was able to reject the salt concentration of more than 99 % using a feed that contained the concentration of about 35 g/L of NaCl solution. A nanoporous anodic alumina composite MWCNT membrane was synthesised and used its transportation properties were assessed. The membrane contained controllable surface chemistry and nanotube dimensions. It was found that the membrane was selective and that the dimensions as well as the surface chemistry can control the membrane flux of the molecules (Alsawat et al., 2015). Han et al. (2015) used a graphene nanofiltration membrane

infused with the multi-walled CNTs to investigate its separation performance. It was found that the membrane flux was twice more than that of the ordinary graphene nanofiltration membrane without the MWCNTs. This MWCNT-containing membrane was able to reject more than 96% of methyl orange dye as well as more than 50% of NaCl. This was largely due to the MWCNTs. A dual polymer layer nanocomposite hollow-fiber membrane blended with MWCNTs was synthesized and its separation performance was assessed during the reverse osmosis pre-treatment of the industrial oil-containing wastewater. The membrane showed very good fouling resistance capacity and was able to reject 90% of protein and over 98% of extracellular polymeric substances from the refinery oil-containing wastewater (Liu et al., 2015). Janas et al. (2014) produced what is termed out to be the first self-heating nickel catalyst-CNT membrane in order to steam reform the alcohols. The membranes were able to synthesize hydrogen gas using various alcohols, they also indicated steam reforming at micro-scale level as well as other chemical changes that needs enough heating circumstances. An epoxy resin polymer membrane infused with the vertically arranged CNTs was assessed for its performance during the purification of water. The separation performance of the membrane was great with very high resistance to fouling and flux through the membrane greater than that of the commercial ultrafiltration membrane by almost the magnitude of three (Baek et al., 2014). The CNTs that were coated in platinum were used in the proton exchange membrane fuel cell as electrodes. It was found that there was a 21 % increase in platinum catalyst loading in comparison to the commercially available catalyst. This was largely due to the vertically aligned CNTs (Shen et al., 2014). The performance of a synthesized polypropylene membrane infused with the MWCNTs was assessed during the removal of salt from the industrial and the synthetic oil-containing wastewater. The membrane was able to reject salt concentration of more than 99.9%. This indicates 58% increase due to the MWCNTs (Okiel et al., 2015). Ultrathin free standing SWCNT-infused polymer membranes were used to treat oil/water. It was found that the membranes can separate both surfactant and non-surfactant stabilized oil/water emulsions up to nanometer in size, with membrane flux thrice faster than the commercially available separation membranes (Shi et al., 2013). Sae-Khow and Mitra (2010) used hollow fiber membranes to separate the volatile organic material from water. The CNTs demonstrated their enhancement ability when they were doped with nitrogen in a polyethersulfone membrane during the treatment of water (Phao et al., 2013).

Gu et al. (2014) used Janus hybrid polymer membranes infused with CNTs to separate oil-containing wastewater. The membrane was highly selective and it had two sides, one side is hydrophilic and the other is hydrophobic. The hydrophilic side was only permeable to water, whereas the hydrophobic side was only permeable to oil. Chen et al. (2012) demonstrated how the fluids passes through the passages of the ceramic pores of the yttria-stabilized zirconia membrane infused with CNTs during the separation of oil from the water. Maphutha et al. (2013) synthesized the CNT-infused polysulfone membrane. The membrane rejected over 95% concentration of oil in the retentate and showed oil concentration in the permeate on less than 10 mg/L. Figure 2.5 below shows a CNT-infused polysulfone membrane.

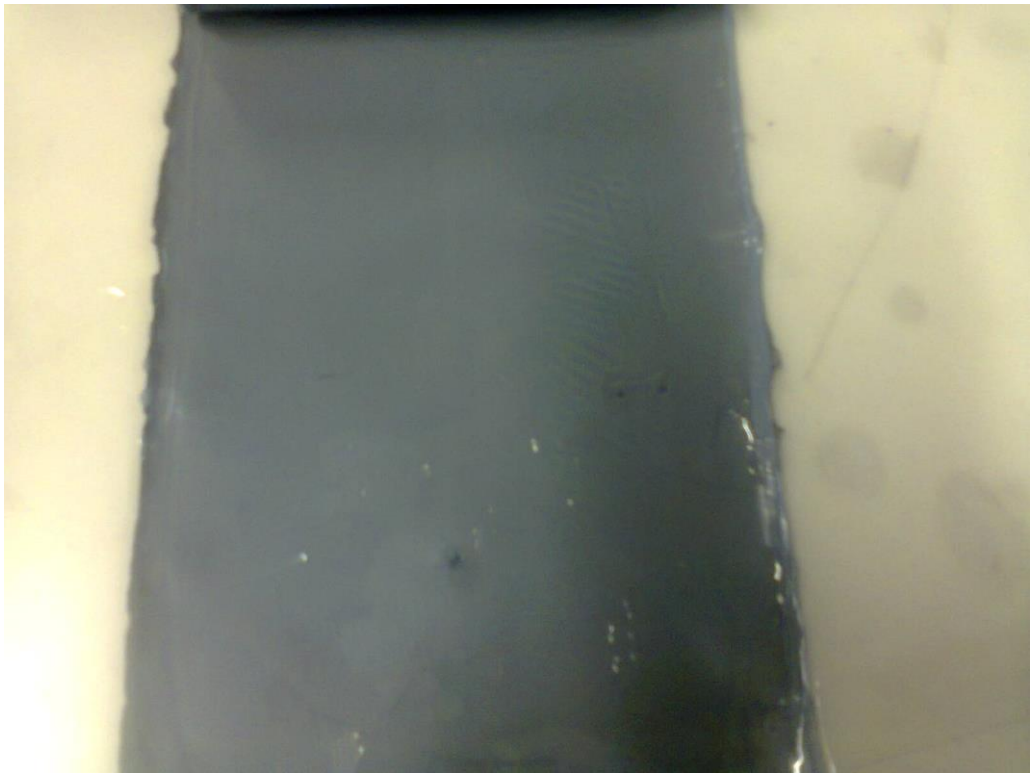


Figure 2.5: Picture of a CNT-infused polysulfone membrane (Maphutha et al., 2013).

In-depth literature review has shown that using pCNTs in the membrane synthesis could further enhance the mechanical properties of the membranes (Yesil and Bayram, 2011). The enhanced mechanical properties could improve fouling-resistance of the membrane, thereby improving the separation performance of the membrane. Khan et al. (2011) used the functionalised MWCNTs to separate a gas. Shah and Murthy (2013) synthesized a polysulfone membrane with controlled porosity and functionalized MWCNTs in order to separate metals from water. The membrane was able to reject more than 94% concentration of chromium (VI) and more than 78% of Cadmium (II). This was largely due to the improved

hydrophilicity which in turn enhanced the thermal stability of the membrane by the act of functionalized MWCNTs. A super-hydrophobic polyvinyl acetate composite porous membrane infused with the functionalized MWCNTs was fabricated to remove salt from water. The membrane was able to remove more than 99 % of the concentration of salt, with the flux through the membrane being above 20 Kg/m^2h (Zhang et al., 2014). Daraei et al. (2013) synthesized a polyethersulfone membrane infused with the functionalized MWCNTs in order to treat the contaminated water. The performance of the membrane was great, with improved fouling resistance and flux recovery of about 95%. A super-hydrophobic membrane material containing fCNTs was used to treat oil-water emulsion. The membrane showed steady super-hydrophobicity and great separation productivity in extreme circumstances (Gu et al., 2015). Kausar (2014) prepared amino-modified nanocomposite polystyrene membranes infused with functionalized MWCNTs in order to purify polluted water. The membranes indicated enhanced tensile strengths, increased content of water as well as good membrane flux and water recovery. Kim et al. (2013) synthesized two nanocomposite polymer membranes infused with acid modified MWCNTs during the treatment of oil-containing wastewater. These membranes were compared with the other two containing no MWCNTs. It was found that the acid modified MWCNTs enhanced the hydrophilicity of the membranes which in turn improved the rejection capacity and the resistance to fouling. In this project, different pre-treatment techniques will be investigated to obtain purified CNT that will be used in the synthesis of the membrane. In addition, Influence of synthesis variables such as composition of CNT and mixing speed will also be investigated.

There are different methods being used currently for the production of the CNTs, these includes laser ablation, arc discharge and chemical vapour deposition methods (Iyuke and Simate, 2011; Robertson, 2004; Agboola et al., 2007). Laser ablation method is a method in which a method in which a liquid is removed from the surface of a graphite by ablation (vaporization) using a laser beam (Journet & Bernier, 1998; Paradise & Goswami, 2007; Iyuke & Simate, 2011). Some of its disadvantages is that the components of the vapourised material are usually different to the original sample (Naes, 2009). This method is also very costly to use because of the lasers that uses very high powers (Iyuke and Simate, 2011). Arc discharge method; in this method, a method in which CNTs are synthesized from two electrodes of graphite which experienced an applied electric arc discharge, the electrodes may also be used without a catalyst (Iyuke and Simate, 2011; Journet et al., 1997; Lee et al., 2002; Agboola et al., 2007). This method is also quite expensive to use as it utilises very high

temperatures, e.g., the maximum temperature is 1773 K. In chemical vapour deposition method, CNTs, fullerenes and other nanomaterials are synthesized from sources of energy such as the reactor furnace and the inductively coupled plasma (Iyuke and Simate, 2011). There are two types of this method, the horizontal and vertical chemical vapour deposition.

Currently, a vertical chemical vapour deposition or swirled fluid bed catalytic chemical vapour deposition (SFCCVD) through the decomposition of hydrocarbons is used in producing both CNTs and CNFs (Iyuke et al., 2009). This method requires low reaction temperature with the potential for a low cost and large-scale production (Mionic et al., 2008). It can produce the CNTs continuously relying on the source of carbon (Yah et al., 2011b). This method is superior to the horizontal or fixed-bed CVD (Iyuke et al., 2009; Yah et al., 2011b). Unlike its horizontal counterpart, this method also uses cheaper catalysts such as only ferrocene (as both a catalyst and a source of carbon (Yah et al., 2011)), which in this project, is used to synthesise the CNTs. In a horizontal CVD, ferrocene is coupled with another supporting material to prepare a catalyst (Mionic et al., 2008). The mechanical stability of PS and the CNTs increases the overall mechanical stability and the hydrophilicity of the membrane.

2.8 The phase inversion method

There are so many methods that are used to synthesize a polymer membrane. These include interfacial polymerisation, track-etching, stretching, electron-spinning and the phase inversion method (Lalia et al., 2013). This section reveals why the phase inversion method was utilised to synthesize the membranes in this project.

Interfacial polymerisation method is an asymmetric polymerisation method in which a polymer is formed at the interface of two incompatible liquids (Morgan and Kwolek, 1959; Odian, 2004). The advantage of this method is that the reaction does not take long hours to polymerize, there is no need to use a stirrer and balanced equation ratio is not required to obtain high molar mass of a product polymer (Morgan and Kwolek, 1959; Odian, 2004). However, this method does not polymerize a reaction between two different phases (solid and liquid) and it is also very costly to use.

In track-etching method, is a template method in which symmetric membranes with the controllable dispersal of size of the pores, densities and the shapes are synthesized (Apel, 2001; Baker, 2004). The weakness of this method is that, it is very difficult to remove a template from the already synthesized solid membrane since that might damage the infused nanomaterial (Charcosset, 2007).

One of the latest methods for fabricating a membrane is the electron spinning method. In this method, nanofibers with morphology which is controllable are synthesized (Ahmed et al., 2015). However, this method uses high voltages and consequently high energy to synthesis nanofibers that will be infused into the membranes (Feng et al., 2010).

Stretching method is a method in which the internal connections between the pores of the membrane are promoted. This method also enhances the permeability of the membrane (Saffar et al., 2014). This method, however, requires that the polymer fibers be functionalized or purified since only this type of material have an effect on the pores of the membrane (Laila et al., 2013). This might increase the costs of operation and hence making this method very expensive to use.

Phase inversion method is an asymmetric method which is used to control the conversion of a polymer solution from liquid phase to a solid phase (Doménech-Carbó and Aura-Castro, 1999). This is the less costly, most effective and simplest method to fabricate a polymer membrane among the afore-mentioned methods. The polymer solution, in this case, can be dissolved at the room temperature or at relatively lower temperatures (hence less energy is used). This method also synthesizes the controllable size of the pores, density and the shape. The conversion can be achieved via immersion evaporation, solution casting, thermal-induced phase separation as well as the vapour-induced methods (Laila et al., 2013).

The shape of the membrane is mostly controlled by the choice of a polymer, non-solvent, solvent and other factors in the phase inversion immersion method. (Kim et al., 1996; Lalia et al., 2013; Strathmann et al., 1975; Zheng et al., 2006). In this project the distilled water is used as a non-solvent in the water bath in this project, this is because the distilled water opens up the pores of the membrane wider and helps to remove the solvent. In this method, the polysulfone solution (the dissolved mixture of a polymer and the solvent dimethylformamide (DMF)) is casted on a glass plate or a solid support and then immersed in a water bath containing the distilled water (This is because if any solvent other than water is used, the reaction between the polymer solution and that solvent will take place which might evaporate

the solution or thickens the layer of the membrane). The solvent then start to evaporate immediately after being immersed in the water, in other words, the solvent dissolves in the water and the evaporation takes place leaving behind a solid polymer membrane. After 24 hours, the membrane will have opened pores. The distribution of pores is controlled by the amount of polymer solution dissolved in the solvent (Doménech-Carbó, 1999). The membrane is dried after this 24 hours (Maphutha et al., 2013; Gohil and Ray, 2009; Lalia et al., 2013; Bossou et al., 2006).

In solution casting phase inversion method, the polymer solution is casted on a glass plate and then left for a day to evaporate the solvent and to dry in the air after casting the polysulfone solution on a glass plate. The pores of the membrane synthesized from this method are very less compared to the one above.

Thermally-induced phase inversion method depends on a change in temperature. In this method, i.e., when the temperature increases, the quality of the solvent (e.g., DMF) also increases and the dissolution becomes faster (Laila et al., 2013). The polymer solution is solidified by freezing process. The solvent can also be evaporated or extracted off the membrane to obtain a solid membrane. The average size of the pores in this case are very much less compared to those in solution casting method

In vapour-induced method, a polymer is dissolved in the distilled water to achieve a solution. After casting the solution, water is then removed by exposing the solution in the air in order to obtain a solid product (membrane). The membrane will be a little thicker and will have less number of pores (Doménech-Carbó, 1999) compared to those above.

Hence the phase inversion immersion method synthesised membranes with higher number of pores than all the above-mentioned phase inversion methods. Thus, in this project the phase immersion inversion method will be used to synthesis the polysulfone membranes, together with CNTs and the PVA layer, that have controlled pore sizes, enhanced mechanical stability as well as increased hydrophilicity to minimise fouling and maximise the separation performance. DMF is chosen as a suitable solvent to dissolve the solid polymer during the phase inversion immersion method because of lower boiling point (BP), of 153^{o}C, compared to others, such as dimethylacetamide (DMAc, BP = 165^{o}C), dimethylsulfoxide (DMSO, BP = 189^{o}C), N-Methylpyrrolidone (NMP, BP = 202^{o}C) and formylpiperidine (FP, BP = 222.5^{o}C). It also evaporate quicker the moment is immersed into the distilled water and it synthesizes

membranes that contains with greater porosity (Lalia et al., 2013; Pinnau and Freeman, 2000).

CHAPTER 3: EXPERIMENTAL

3.1 Introduction

The materials and experimental procedures used to synthesize CNTs, functionalised CNTs (fCNTs), pCNTs and PS membranes are described in this chapter. This chapter is made up of two sections, the first part is the materials and methods part (3.2), and the second one is the experimental procedure (3.3). This chapter also explains the procedures and methods used to characterise and synthesize both the CNTs and the membranes, as well as the procedure used to test the separation performance of the membranes. The first experiment performed was the synthesis of CNTs, followed by their functionalization and then purification of the functionalised CNTs. In between these was characterisation. The CNTs were then blended in the PS solution to synthesize the membranes. After characterisation of the membranes, the test for separation performance was then conducted.

The CNTs were functionalised in order to prepare them for blending with the PS solution. Because of the hydrophobicity of the CNTs produced by the chemical vapour deposition (CVD) method, purification was necessary. The pCNTs increase the mechanical properties of the membrane which in turn improves the fouling resistance of the membrane (in other words, they further increase the hydrophilicity of the membrane as later discovered). The use of 20% PS solution rather than 10% reduces the porosity and increases the quality factor which improves the separation performance of the membrane (Huang & Yang, 2006). Quality factor is a parameter used to analyze /study the performance of a membrane. It depends on the amount of a polymer solution added, amongst other factors. Increasing or enlarging a polymer solution, increases the quality factor and hence the separation performance of a membrane (Hinds, 1998; Huang & Yang, 2006; Wang et al., 2008).

3.2 Materials and methods

Ferrocene (98%, F408; from Aldrich, South Africa), argon and nitrogen gases (both UHF, 99%+; from AFROX, South Africa): were all used for the production of CNTs. The as grown CNTs were later crushed into a fine powder using a mortar to prepare them for characterisation and blending into a membrane solution. For the functionalization and

purification of the CNTs, the following materials were used: pH litmus papers, dry air (UHF, 99%+; from AFROX, South Africa), 55% nitric acid, 40% hydrofluoric acid, 37% hydrochloric acid, and 95% sulphuric acid (from Associated Chemical Enterprises (Pty) Ltd (ACE), South Africa). The purified CNTs were also characterised and blended into the membrane solution. Polysulfone pellets (average molecular weight 35, 000 Da), polyvinyl alcohol (99%+, average molecular weight 30,000 – 70,000 Da), Maleic acid (MA) (Reagent plus, R; 99% or more, molecular weight 116.07 g/mol); were all obtained from Sigma Aldrich, South Africa, N, N-Dimethylformamide (DMF) (99%; was obtained from ACE, South Africa), Millipore and distilled water: were all used to synthesize the membranes. All gases, chemicals and solvents used in this experiment did not need any further purification since they were all analytical grades.

A vertical swirled fluid bed catalytic chemical vapour deposition (VSFCCVD) method (Iyuke et al., 2009; Yah et al., 2011), Figure 3.1, from the nanotechnology group at the school of chemical and metallurgical engineering, was used to synthesize the CNTs.



Figure 3.1: Picture of a vertical swirled fluid bed catalytic chemical vapour deposition (VSFCCVD)

This VSFCCVD method is superior over its horizontal counterpart because it is less costly to use it. This is due to the amount of CNTs synthesised and the catalyst used by these methods. The rate of production of MWCNTs was found to be about 333 mg/min, when the horizontal CVD was used (Gulino et al., 2005), whereas Iyuke et al. (2009) reported the mass rate of about 700mg/min using the VSFCCVD. A cheaper metallic compound, such as a ferrocene, is usually alone used as a catalyst in the VSFCCVD. However in a horizontal CVD, ferrocene (or any metallic compound) is coupled with another supporting material in order to prepare a catalyst (Boncel et al., 2014; Gulino et al., 2005; Mionic et al., 2008). This increases the operational costs of the horizontal CVD. Figure 3.2 shows the schematic of the experimental setup for the synthesis of the CNTs.

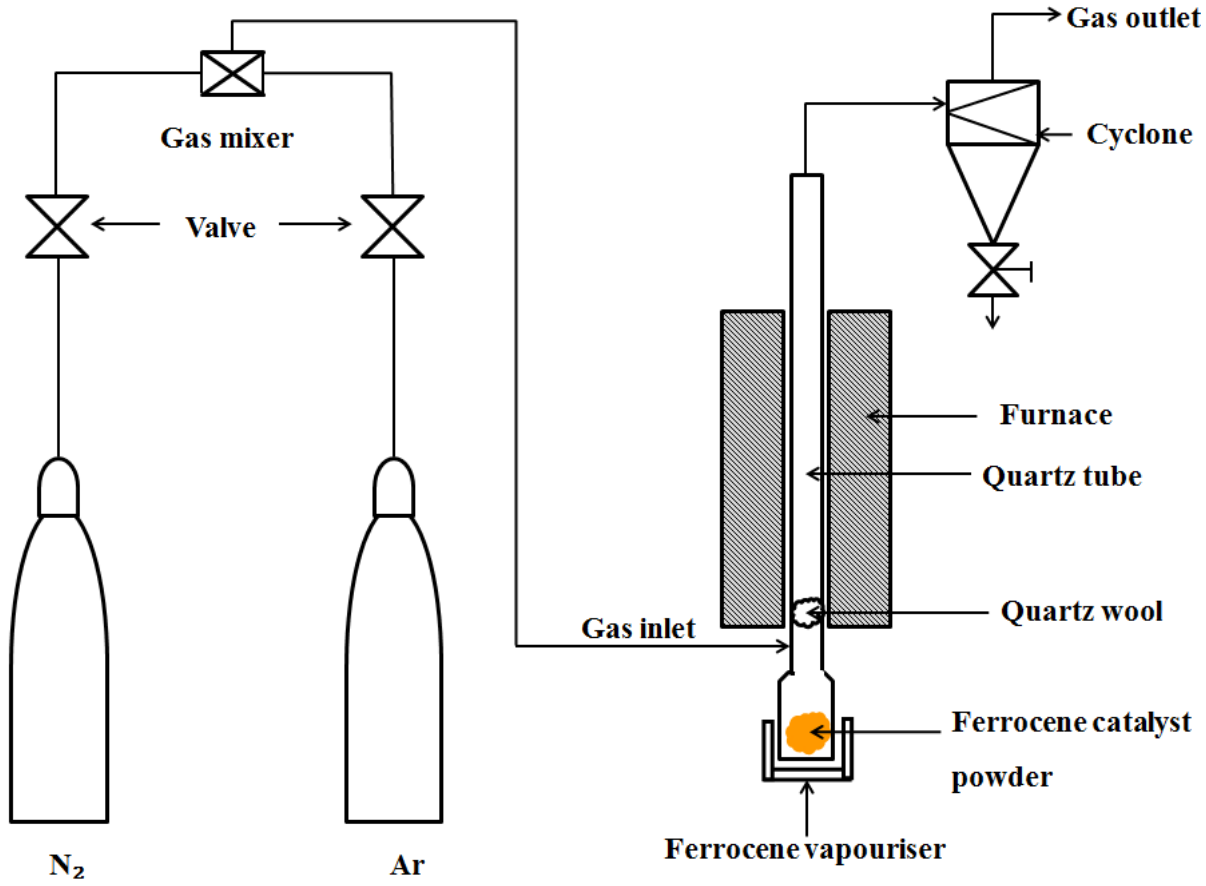


Figure 3.2: A schematic drawing of SFCCVD (Yah et al., 2011).

Ferrocene was used as a catalyst and a source for carbon. The valves were used to control gasses and the rotameters were used to control flow rates. The temperature was raised at a rate of 10^{o}C/min before reaching the desired temperature of 850^{o}C. As in figure 3.2, the VSFCCVD equipment contains a vertically aligned quartz reactor (the tube inside the furnace) with a length and the diameter of 105 and 5 cm, respectively. The tube was filled with a quartz wool layer almost 30 cm lowermost in order to prevent the catalyst from flowing uncontrollably without undergoing a reaction in the furnace and also to allow some of the product to fall on (Iyuke et al., 2009; Yah et al., 2011) its surface. The furnace which was used to heat the quartz reactor to a desired temperature has a maximum temperature of 1200^{o}C.

Upon opening the valves and adjusting the rotameters, gases (in this case nitrogen and argon) flow into quartz reactor through a gas mixer and ferrocene vapouriser. From the reactor, gases flow into the cyclone (which is located at the top and is connected to the quartz reactor through a pipe) and out through the gas outlet. The products (CNTs) are collected from the

cyclone, pipes connected to the cyclone, the surface of the quartz wool and on the walls of the quartz reactor.

Ferrocene is a powdered solid which might crystallize at lower temperatures; to prevent this, a higher temperature was maintained by wrapping a heating cord around the uncovered parts of the ferrocene vapouriser. The connections were airtight using high vacuum grease in order to prevent gas leakages. Nitrogen gas was run through the equipment in order to make sure that there were no leaks and that the contaminants (such as unidentified gases that might be present) are removed, for at least 21 minutes (Iyuke et al., 2009; Yah et al, 2011). Argon as a carrier gas was used to carry the ferrocene into the reactor and was also used to remove foreign gases at higher temperatures (Iyuke et al., 2009).

A horizontal CVD was used during the oxidation step of purification of CNTs to remove the metals. A phase inversion method (Gohil & Ray, 2009), a method of converting a polymer solution from liquid phase to a solid phase was used to synthesise the PS membranes. Characterisation of the CNTs and the membranes were carried out using the methods described in this section on the next pages.

3.3 Experimental Procedure

3.3.1 Synthesis of CNTs

A vertical catalytic chemical vapour deposition (SFCCVD) method (Iyuke et al., 2009) was used to synthesise CNTs at 850^{o}C.

After the connections were completed as shown in figure 3.2, the inlet to the nitrogen gas was opened for at least 18 minutes (to make sure that there were no leaks and that unidentified gases are removed from the equipment (Iyuke et al., 2009; Yah et al., 2011)), before switching the furnace and the ferrocene vapouriser on (nitrogen cannot be heated at higher temperatures because it can ignite fire), for the gas to go through the pipelines in order to remove contaminants from the system and to make sure that there are no gas leaks in between the pipe connections. The gas was then closed by first closing the main valve on the nitrogen gas cylinder. While nitrogen was draining from the system, the temperature of the furnace was switched on to the desired 850^{o}C at a heating rate of 10^{o}C/min. After nitrogen gas was

completely drained from the system (at this moment there was no gas flowing out through the gas outlet pipe), its controlling valve was closed and the inlet to the argon gas was opened while the temperature was increasing. This was to allow argon to provide inert surroundings to the system and to remove any foreign gas that contaminates the system (such as oxygen which could cause oxidation in the system and alter the results). Once the desired temperature of 850^{o}C was reached, the heating tape and the ferrocene vapouriser were switched on (Yah et al., 2011) and heated to a combined temperature of 500^{o}C. When the temperature of 500^{o}C was reached, all powder was completely vapourized and taken into the reactor by the argon gas. After the vapourization process has completed, the system was turned off by first switching off the furnace, heating tape, the ferrocene vapouriser, closing the main valve from the argon cylinder, letting the remaining gas in the pipes to be purged and then closing all other valves on the system. The system was left to cool down to a room temperature before collecting the CNTs. The CNTs were then characterised using the characterisation methods in section 3.3.4, functionalised, purified and blended in the PS membranes.

3.3.2 Functionalization of the CNTs

A 150 ml mixture of 55% nitric acid together with 95% concentration of sulphuric acid, in a ratio of 1:3 respectively, was reacted with 1.5 g of the as produced CNTs in a 250 ml round bottom flask topped by a condenser (Ngoy, 2010; Tsai et al., 2013). The schematic setup diagram of this experiment is shown Figure A.13.

This mixture was refluxed for a day (24 hours) at 50^{o}C. It was then allowed to cool for 8 hours at room temperature. The resulting product was then washed with distilled water until its pH was 7. The neutral solution was then dried at 40^{o}C for 12 hours. The functionalized CNTs where then purified and characterised using the methods in section 3.3.4.

3.3.3 Purification of the CNTs

Amorphous carbon was removed by reacting 1.0 g of the functionalised CNTs (fCNTs) from 3.3.2 was reacted with 26 ml of 55% hydrofluoric acid and 75 ml of distilled water, in a plastic container, under constant stirring for 18 hours (Yao et al., 2008). Hydrofluoric acid and water in the mixture were then removed by centrifugation process. Further purification of

the CNTs was undertaken in two oxidation steps in order to remove metal particles and other impurities still left in the CNTs (Chiang et al., 2001; Yao et al., 2008; Zheng et al., 2002):

(i) Using a horizontal CVD setup (Figure 3.4), a solid CNT sample was subjected to heat for 60 minutes (1h) at a vapouriser temperature of 400^{o}C in a flowing rate of 15/85 ml/min (air/argon) mixture (Yao et al., 2008; Zheng et al., 2002; Chiang et al., 2001). The sample was then rinsed with 75 ml of 32% HCl for about 20 minutes using a bath sonication.

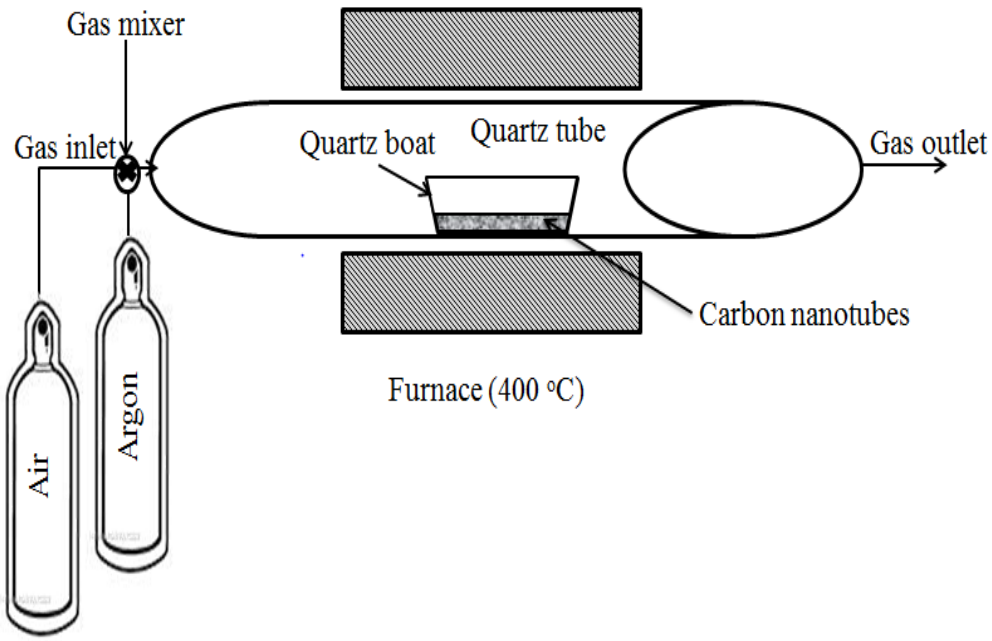


Figure 3.3: A horizontal CVD for the oxidation of CNTs [1*]

(ii) Step (i) was repeated at the temperature of 450^{o}C, to further burn the carbon impurities on the catalyst which exposes these impurities to an attack by the acid and leaves the CNT structure undestroyed because of the enhances stability compared to non-purified CNTs.

The mixture was then washed with distilled water until its pH was 7 and then filtered to achieve a solid product. The product was dried in the oven overnight at a temperature of 40^{o}C. Mass loss and the % yield were then calculated in order to know the final amount of the purified CNT sample.

[1*] http://ipn2.epfl.ch/CHBU/NTproduction1.htm

3.3.4 Characterisation of the CNTs

The as-produced CNTs, functionalised CNTs (fCNTs) and purified CNTs (pCNTs) were characterised using: (i) transmission electron microscope (TEM) to check their internal morphology in 2D, (ii) thermogravimetric analysis (TGA) to analyse the purification and the weight loss with change in temperature of the CNTs, (iii) Raman spectroscopy to analyse the structure of the CNTs and discover any CNT formed from the ferrocene which acts a source of carbon, (iv) Energy dispersive spectroscopy (EDS) to investigate the elements and to confirm the purity of the CNTs, (v) Fourier Transform Infrared (FTIR) spectroscopy to study the functional groups on the CNTs and (vi) X-ray diffraction analysis (XRD) to identify the chemical composition of the CNTs.

(i) TEM analysis procedure

TEM (model JOEL 100S FEI spirit 120 kV), originated from FEI Corporate USA, Figure 3.5, was used to characterise the CNTs in order to observe the internal morphological crystal arrangements of the sheets. About 0.5 mg of the CNT sample was dispersed in a small amount of ethanol solvent inside a plastic cap for about 60 seconds using a sonic bath. The solution was dropped one time in a copper grid supported by a filter paper. The solution on the grid was dried in the air by evaporating the ethanol before the analyses were made. The copper grid was then uploaded into the TEM chamber for samples to observe the results. After magnifications and adjustments, the pictures were taken.

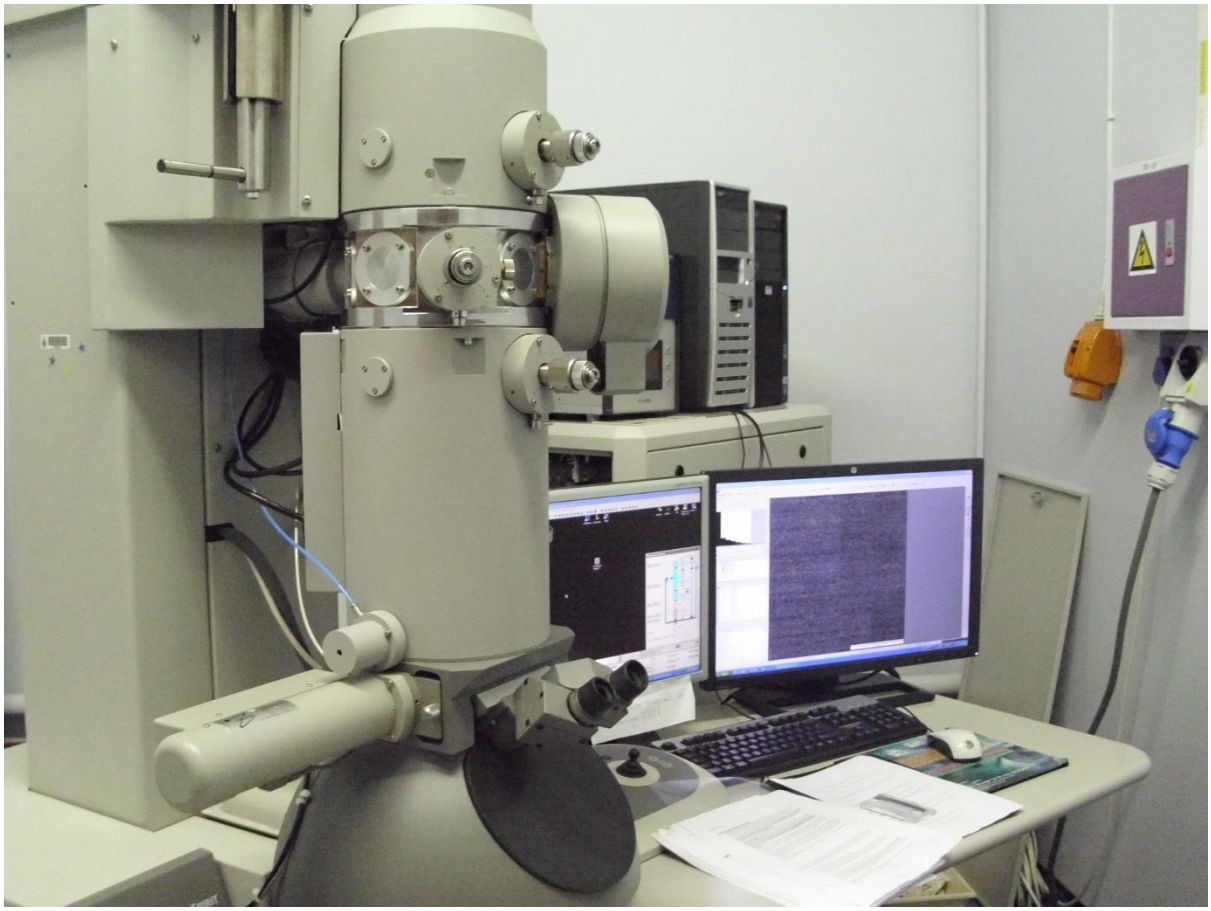


Figure 3.4: Picture of a Transmission electron microscope, TEM (model JOEL 100S FEI spirit 120 kV); FEI Corporate USA (MMU Wits, 2014).

(ii) TGA analysis procedure

To analyse the purification and the weight loss with change in temperature of the CNTs, TGA (model Perkin Elmer STA 6000); originated from PerkinElmer Inc. USA; figure 3.6, was used. About 0.055 g of the CNTs was placed inside a crucible which was mounted on a stage. The sample was then taken to the furnace. The temperature of the furnace ranged between 25 and 850^{o}C, and it was increasing at a rate of 10^{o}C/min. Nitrogen gas, at a flow rate of 20 ml/min, was used (as an inert gas) to provide an inert atmosphere to the system and to purge the contaminants (unidentified/unknown gases) from the system/device; then, the temperature of the CNT sample was raised to 850^{o}C under oxidative atmosphere (in air) at a flow rate of 50 ml/min. Weight percentage, gained or lost, was recorded as a function of a change in temperature.

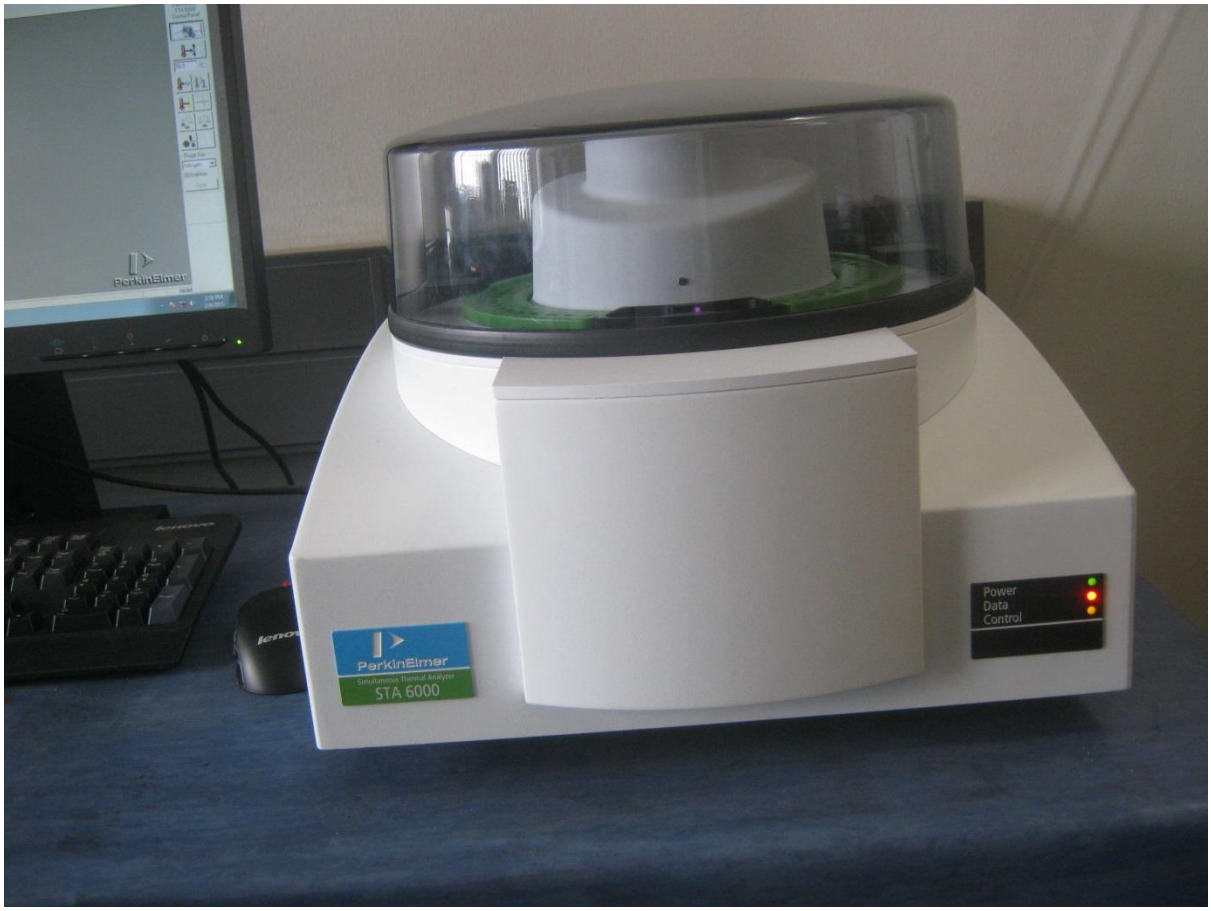


Figure 3.5: Picture of a thermogravimetric analyzer, TGA (model Perkin Elmer STA 6000); PerkinElmer Inc., USA. **(**Wits, School of Chemistry).

(iii) Procedure for the Raman spectroscopy analysis

Raman (model Jobin-Yvon LabRAM HR) spectrometer, originated from Horiba Japan, equipped with an Olympus BX41 microscope attachment was used to examine the vibrating, rotating modes (Gardiner, 1989), as well as the quality of the CNTs. About 5 mg of the CNT powder was inserted in an approximately 1.5 μm diameter of the equipment's sample chamber with the power set to 1.2 MW in order to minimise the heat. The extinction wavelength that came from the line of argon ion laser was 514.5 nm.

(iv) Procedure for EDS analysis

To identify the elements and to confirm the purity of the CNTs, Energy dispersive spectroscopy, EDS (model Carl Zeiss Sigma**)** analysis, originated from Germany, Figure 3.7, was conducted. The spectra that showed the elements in the respective CNT samples were then recorded.



Figure 3.6: Picture of an energy dispersive spectroscopy, EDS (model Carl Zeiss Sigma), Germany (Wits, School of Chemical and Metallurgical Engineering).

(v) Procedure for FTIR analysis

FTIR (model Bruker Tensor 27) spectroscopy, originated from Bruker Germany, figure 3.8, was used to obtain an infrared spectrum (IR) spectrum which was used to detect the functional groups in the CNTs. The spectra were recorded in the range of 600-4000 cm^{-1}.



Figure 3.7: Picture of a Fourier Transform Infrared, FTIR (model Bruker Tensor 27) Spectroscopy; Bruker Germany, (Wits, School of Chemistry).

(vi) Procedure for XRD analysis

XRD (model Bruker D2 Phaser); originated from Bruker Germany**,** Figure 3.9, was used to investigate changes in the structure of CNTs, determine the size and the shape of the unit cell as well as observing the presence and absence of the elements before and after purification. A voltage of 30 kV and the current of 10 mA for a Cu – Kα radiation were used in this procedure. About 0.001 g on CNTs was inserted in the sample chamber of the XRD device. It took about 10 minutes for the equipment to read the sample and 30 seconds for the spectrum to appear. The spectra were recorded in the range of $10° < 2\theta < 90°$.



Figure 3.8: Picture of an X-ray diffraction, XRD (model Bruker D2 Phaser) analysis; Bruker Germany. (Wits, School of Chemistry)

3.3.5 Synthesis of the polysulfone (PS) membrane with the CNTs and PVA layer

The membrane was synthesised using a phase inversion immersion method (Gohil & Ray, 2009). Two membranes were synthesized without CNTs; one with only just the solvent and PS pellets and the other with PVA layer. Five other membranes were synthesised with the CNTs, including one with the purified CNTs.

Different CNT concentrations (0, 2.5, 5, 7.5 and 10% w/v of both as-produced and purified CNTs) were dissolved in a 300 ml conical flask containing 25 ml of dimethylformamide (DMF) until the solution was homogeneous using a magnetic stirrer. The CNTs were added in order to investigate the thermal and mechanical stability which enhances the fouling resistance of the membrane. Polysulfone pellets (5g) were then added to the CNT/DMF solution and the mixture was stirred for 24 hours. The bubbles that formed were removed using the ultrasonic agitator for 20 minutes and the ultrasonicator at the amplitude of 60% in 1 cycle for 11 minutes. Casting blade was then used to cast the solution on a glass plate (see Figure 3.10 below)

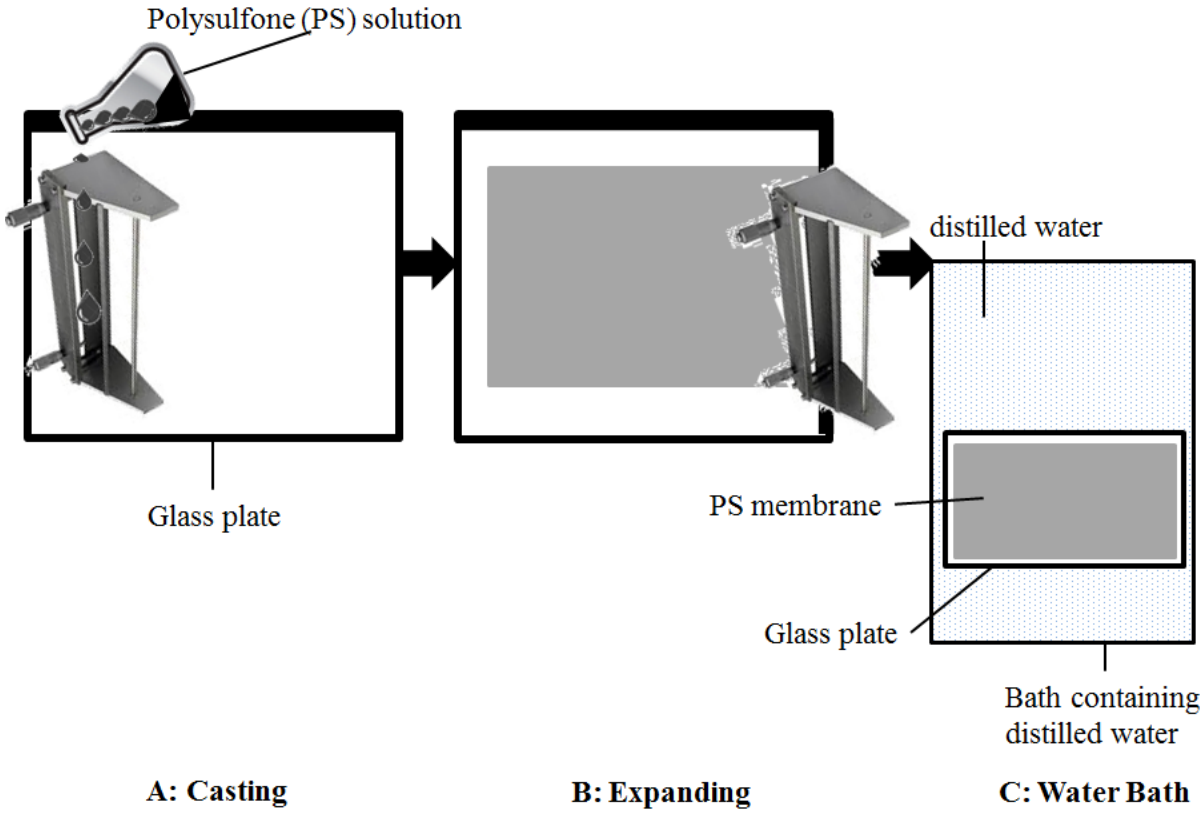


Figure 3.9: Schematic diagram of PS membrane casting (Javiya et al., 2008).

The casted solution, still on a glass plate, was left for 11 seconds (this was done to confirm/make sure that the bubbles are completely removed, to initiate solvent evaporation, to make sure that the solution is well mixed and stays homogeneous (Chung et al, 2005)) at room temperature and then placed 24 hours in the distilled water to remove the solvent (DMF). The casted solutions immediately turned into solid PS membranes after being placed into the distilled water. The membranes had a thickness of about 5 mm.

0.25 g of PVA powder was dissolved in 25 ml of Millipore water to obtain an aqueous solution. This aqueous solution was then poured over the membrane (which was placed on a glass plate) as a covering layer (in order to increase the hydrophilicity of the membrane). The PS membranes with PVA aqueous solution were left at room temperature for 3 minutes in contact (Gohil & Ray, 2009; Maphutha et al., 2013) and then the excess aqueous solution was removed from the membrane. 1% (w/v) Maleic acid aqueous solution (also prepared the same way as PVA using Millipore water) was then poured over the PVA layer as a cross linker. It was also left in contact for 3 minutes, to cross link (Gohil & Ray, 2009), of which the excess solution was removed. The membranes were then dried for 16 minutes at the temperature of 398 K using an oven. The PS membranes were then characterised and tested using the methods below.

3.3.6 Characterisation of the PS membranes

(i) Brunauer Emmett Teller (BET) studies was used to examine the pore size data, (ii) Contact angle was used to investigate the hydrophilicity of the membranes, (iii) Scanning electron microscope (SEM) was used to observe of the arrangement of the components making the PS membrane on the external and the cross sectional surfaces, and (iv) the FTIR to identify the functional groups on the membranes.

(i) BET analysis procedure

To examine the pore size data and to confirm the information on the surface area (Brunauer et al., 1938) of the membranes, Micromeritics Tristar 3000 surface area and porosity analyser (originated from Micromeritics USA), Figure 3.11, was used to conduct the BET analysis for those examination and confirmation purposes. 0.2 g of the PS membrane sample was cut into

smaller pieces and used to conduct the BET analysis. The moisture that was still in the sample was first removed by degassing the membranes in a nitrogen gas which was flowing at a rate of 40 ml/min at a temperature of 100^{o}C for 12 hours.



Figure 3.10: Picture of Micromeritics Tristar 3000 for the BET analysis, Micromeritics USA (Wits, School of Chemistry).

(ii) Contact angle procedure

Contact angle determines the hydrophilicity of the membrane. The CNTs increase the mechanical stability which in turn enhances the fouling resistance of the membrane, and hence the hydrophilicity. Different concentrations (0 – 2.5 g/ml) of the CNTs that were infused in the PS membrane were measured as functions of contact angles. The CNT–infused polysulfone membranes were investigated using a contact angle analyser (model FTA 200), originated from First Ten Angstrom USA. A droplet of water was dropped between on the membrane surface using a medicine dropper and the contact angle between the droplet and the surface was measured. The process was repeated 6 times and an average value was reported. The average of 6 measured data gave the value of the reported contact angle.

(iii) SEM procedure for PS membranes

To observe the arrangement of the components making the PS membrane on the external surface and the cross sectional area, SEM (model Carl Zeiss Sigma**)**, originated from Germany, was used. The membranes were first mounted on the SEM specimen stages and then sputter coated with gold coater for a few minutes to make them conductive. They (membranes) were then dried in the air for about three minutes at room temperature of 303 K before being sprayed with a sputter coater to form a layer. The membranes were then uploaded on the stage of SEM. Adjustment were done, picture were taken and saved.

(iv) FTIR Procedure

As with the CNTs, FTIR was also used to identify the functional groups on the membranes. The method used is the same as that in 3.3.4.5.

3.3.7 The size of the pores and the porosity measurements

(i) Porosity measurements

After drying the membranes in the oven (for 15 minutes at 398 K), a circular piece of the membrane with a 5 cm diameter was cut and its weight was measured as M_1. The same 5 cm diameter piece of membrane was soaked into the distilled water (for 24 hours) and then

measured again as M_2. The membrane was soaked in order to determine how much weight is gained (a difference in weight of wet and dry membrane pieces) during the porosity measurement (Zhang et al., 2009).

The following equation was used to calculate the porosity, Pr, of the PS membrane (Zhang et al., 2009):

$$Pr\ (\%) = \frac{M_2 - M_1}{\rho A d} \times 100\% \qquad (1)$$

Where M_1 and M_2 explained above; A is the area of the circular membrane given by πr^2, r is the half of the diameter 5 cm, ρ is the density of water, and d is the thickness of the membrane (5 mm).

(ii) Pore size measurements

The performance of the membrane also depends on the size of the pores of the membrane. The smaller the pore sizes of the membrane, the greater the permeable selectivity and hence good separation performance. The pore size of the membrane was measured by the pore radius, r_p, of the membrane which was measured through the following equation (Zhang et al., 2009):

$$r_p = 0.68 - \frac{32.33}{\Delta T} \qquad (2)$$

where ΔT is the change in temperature of the melting point depression in degree Celsius (^oC). Pore size = pore diameter = $2r_p$. The transition thermal potential from liquid to gas, W, in J/g, is given by:

$$W = -1.55\Delta T^2 - 11.38\Delta T - 332 \qquad (3)$$

Thermoporometry may also be used to determine the pore radius of the PS membrane and is measured by the differential thermal analysis (DTA). After tabulating the membrane data, pore radius was calculated using equation (2).

3.3.8 The separation performance of the PS membrane

A container filled with industrial oil-water emulsion containing wastewater (obtained from a company called Oil skip (South Africa) with oil concentration of approximately 372 mg/L. Inductively coupled plasma (ICP) for the liquids was used to analyse the components present in the oil-containing wastewater; whereas High performance liquid chromatography (HPLC) was used to determine the amount of each component present in the oil-water, before and after the separation performance. Initially the concentration of the oil-water emulsion containing wastewater, together with the dissolved substances and the solid particles, was about 5000 mg/L. After the removal of the thick emulsion and the solid particles, the concentration was 372 mg/L. This was done to obtain a homogeneous mixture of oil-water and to prevent unnecessary fouling and the concentration polarisation. The pH of this mixture was between 8 and 9. Flow rates of 46.8, 50.4 and 52.2 L/h were used during the separation process. Throughout the experiment, the mixture was stirred and heated in order to make sure it was well mixed and kept homogeneous, it is easier to remove oil from water when the temperature is raised a little higher (Klein Wolterink, 2004). The contents of the container were finally pumped into the membrane, using the Schleicher and Schuell cross flow separation device shown in figure 3.12.

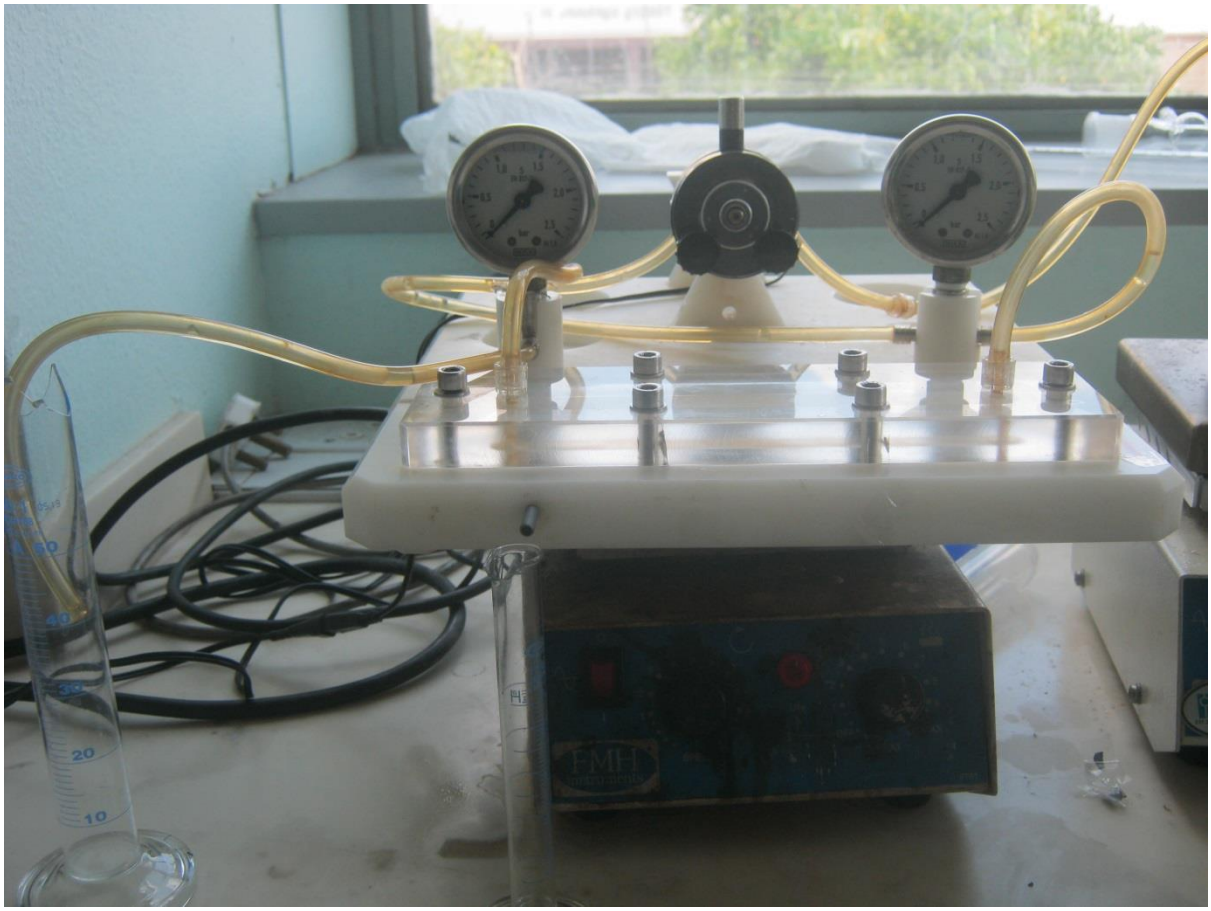


Figure 3.11: Picture of the cross flow filtration system used to separate oil-containing wastewater system.

The set-up of the experiment is shown in figure 3.13.

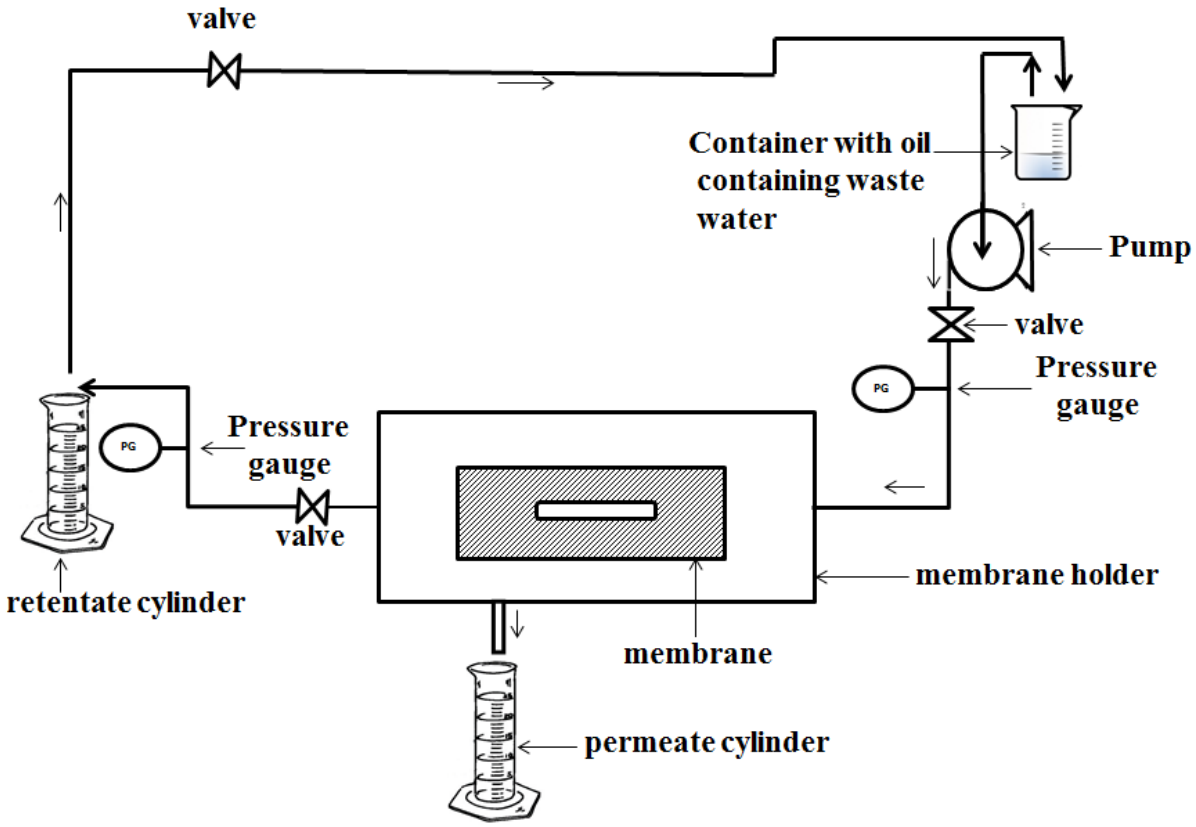


Figure 3.12: The schematic drawing of the setup of separation performance experiment.

About 20 mm operating diameter of the membrane with the rectangular area of 22.4 cm^2 (that gave an effective area of 24 cm^2) as well as the flow rates of 46.8, 50.4, and 52.2 L/h, were used for the evaluation of the separation performance in the cross flow system at room temperature as well as at the temperature of 308 K (An industrial operations temperature is around 305-311 K (Arthur et al., 2005)) for 8 hours (It took 8 hours to analyze the separation performance of a single membrane). All membranes had different pore sizes. After the experiment, only the concentrations of oil in the feed and permeate were evaluated using the UV-Vis spectrophotometer (model biochrom Libra S4), Figure 3.14.



Figure 3.13: UV-Vis spectrophotometer (model biochrom Libra S4); Biochrom Ltd UK.

The following equation was used to calculate the percentage of the removed oil concentration, R(%), in the retentate by the PS membrane (Maphutha et al., 2013):

$$\mathrm{R}(\%) = \left(1 - \frac{C_p}{C_f}\right) \times 100\ \% \qquad (4)$$

Where Cp is the oil concentration in the permeate and C_f is the feed oil concentration (both in mg/L. The value of C_f used for filtering was 372 mg/L, as mentioned.

The membrane flux (MF), which was used to evaluate the performance of the membranes, was determined using the following equation (Gohil & Ray, 2009):

$$MF = \frac{V}{At''} \qquad (5)$$

Where V is the permeate volume in litres (L) of the membrane at the time t'' in hours, A is the effective area of the membrane in m^2.

The following equation was used to investigate how the relative flux, RF, changes with time:

$$RF = \frac{T_F}{S_F} \qquad (6)$$

Where T_F is the time flux and S_F is the flux of the membrane at the beginning stages. Equation (6) leads to a decrease in flux, DF, which is given by (Chakrabarty et al., 2008):

$$\mathrm{DF}(\%) = \left(1 - \frac{T_F}{S_F}\right) \times 100\ \% \qquad (7)$$

All symbols in equation (7) have already been explained above.

CHAPTER 4: RESULTS AND DISCUSSION

4.0 Introduction

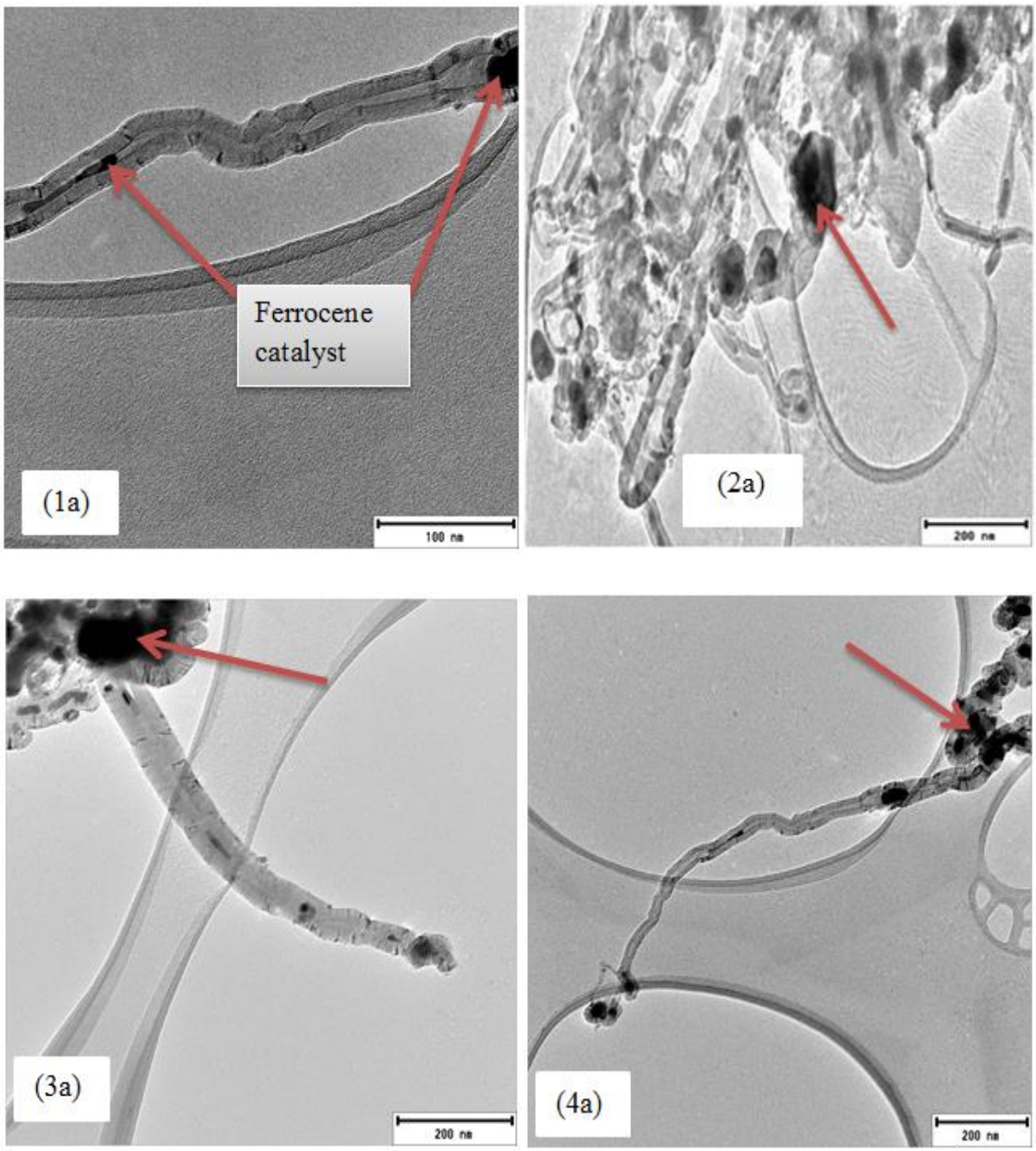
The results obtained from the experiment in chapter 3 are presented and discussed in this chapter. This chapter is divided into three sections: a) the characterisation results from the CNT synthesis, b) the polysulfone membrane results and finally c) the results from the separation performance of the membranes.

4.1 The CNTs

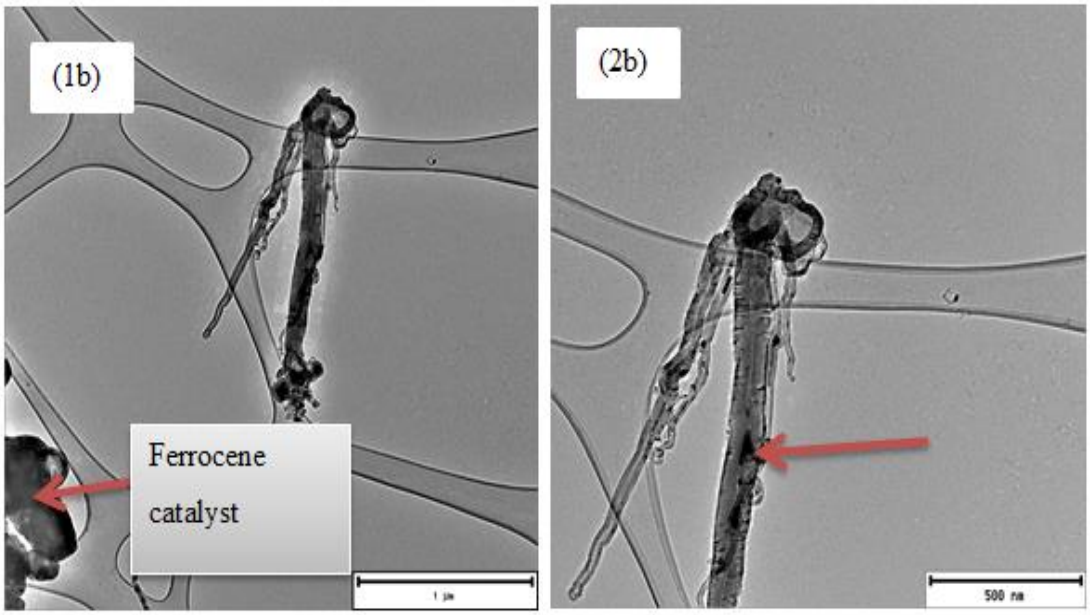
The CNTs were synthesized at the temperature of 850^{o}C and were characterised using the methods in section 3.3.4. This section presents experimental results for the as-produced CNTs, fCNTs and the pCNTs.

4.1.1 TEM analysis

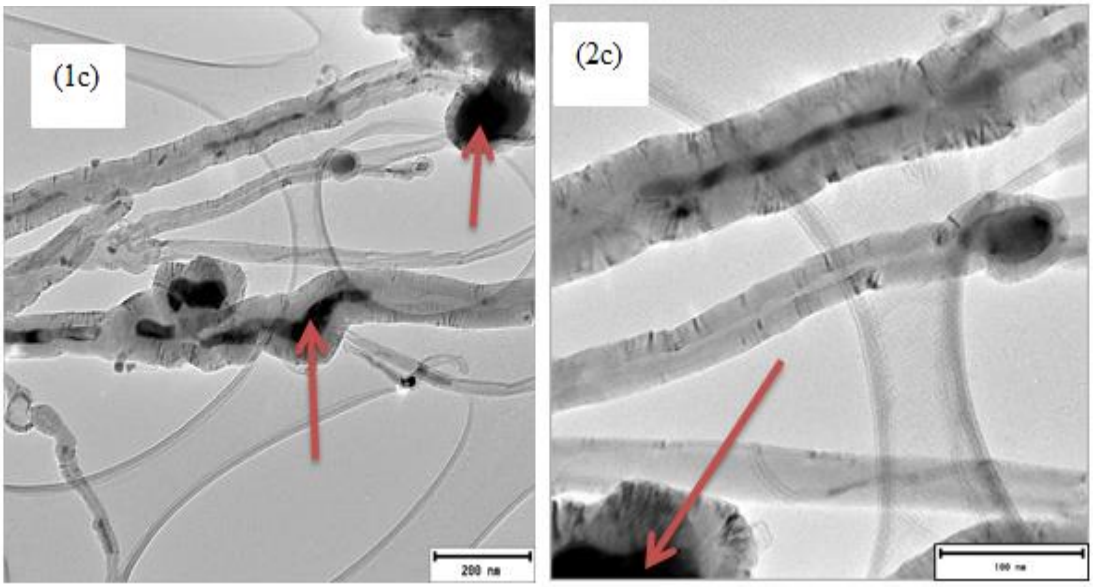
The transmission electron microscope, TEM (model JOEL 100S FEI spirit 120 kV), Figure 3.5, was used to look at the internal morphology of the CNTs in 2D. Figure 4.1 shows the TEM images of the as-produced CNTs, fCNTs and the pCNTs. From this figure, it is evident that the produced CNTs are multi-walled as they contain both the inner and outer diameter. They have the length ranging from 600 to 950 nm.



(a) TEM micrographs of the as-produced CNTs: micrograph (1a) depicts a high magnification of 850 nm long CNT, (2a) the clusters of the CNTs, (3a) low magnification of 700 nm long CNT, and (4a) low magnification of micrograph (1a).



(b) TEM micrographs of the fCNTs at low (1b) and high (2b) magnifications



(c) TEM micrographs of the pCNTs at (1c) low and (2c) high magnifications

Figure 4.1: TEM micrographs of the produced CNTs: (a) as-produced CNTs, (b) fCNTs, and (c) pCNTs.

Figure 4.1(a) depicts the as-produced CNTs. A CNT which is around 850 nm long is shown in (3a). (1a) is a higher magnification of (3a). About 700 nm long CNT can be seen in (2a). These CNTs have internal diameters that range between 5.8 and 8 nm, with the external diameters ranging between 25.6 to 33 nm. The black spots in the inner diameter of the CNTs,

pointed with a red arrow, are the particles of ferrocene catalyst (Yah et al., 2011). They can also be observed at the tips, the twisted and the concentrated areas on the tube.

In figures 4.1(b) and (c), the impurity ferrocene catalyst (black spots) still remains, however, is in small amounts compared to figure 4.1(a) as it can be seen, as it was mostly removed. It can be seen in figure 4.1(c) that the catalyst is found mostly at the tips and the twisted areas of the nanotubes. This is where the acids were not able to penetrate because of the "hidden" complex tubes. The use of the acids caused the diameter to contract a little in both the fCNTs and the pCNTs; this is due to the graphitic nature of these CNTs (Motchelaho et al., 2011; Phao et al., 2013). The carrier argon gas as well as the nitrogen gas did not have any effect on the structure of nanotubes, except what has already been explained. The remaining ferrocene in the fCNTs and the pCNTs shows how defected this type of CNTs are, the acids used could not penetrate the multiple walls and the twisted as well as the highly concentrated are of those nanotubes.

Ferrocene was successfully used to produce the CNTs as a source of carbon and a catalyst. This is because ferrocene is a volatile organic-transition metal compound which is composed of two reactive aromatic rings and an iron atom connected in a coordination number of two. This makes it possible for the ferrocene to start vapourizing at lower temperatures of about 115^{o}C within 5 minutes after turning on the vapouriser. These results are comparable to the literature (Barreiro et al., 2006; Maphutha et al., 2013; Phao et al., 2013; Yah et al., 2011; Yao et al., 2008).

4.1.2 TGA analysis

Thermogravimetric analysis (TGA) was used to analyse the purification and the weight as a function of the change in temperature (thermal stability) of the CNTs.

Figure 4.2 shows the TGA plots for the as-produced CNTs, fCNTs and the pCNTs. As it can be seen, the CNTs (shown by the blue line) contained a lot of impurities and disorders before they were functionalised and purified. The CNTs decomposed first followed by the fCNTs and then the pCNTs. The as-produced CNTs started to show a slight loss of weight (0.3%) at the temperature of 88^{o}C (the slight loss indicates the presence of the 0.3% amorphous carbon, this was later removed by the acid treatment as it can be seen on the fCNTs and the pCNTs), and then seemed to be stable as the temperature increases up until they started to show the

4% weight loss at the temperature of 444-516^{o}C. This occurred because the CNTs still contained large amount of the impurity ferrocene catalyst. From there, the material then lost about 59% of the weight until it become stable at a temperature of 660^{o}C; this means that 41% of the remaining mass was composed of the ferrocene catalyst and other impurities, whereas this 59% content was carbon. This type of behaviour shown by the as-produced CNTs confirms the fact that multi-walled CNTs have been produced (Motchelaho et al., 2011; Bom et al., 2002).

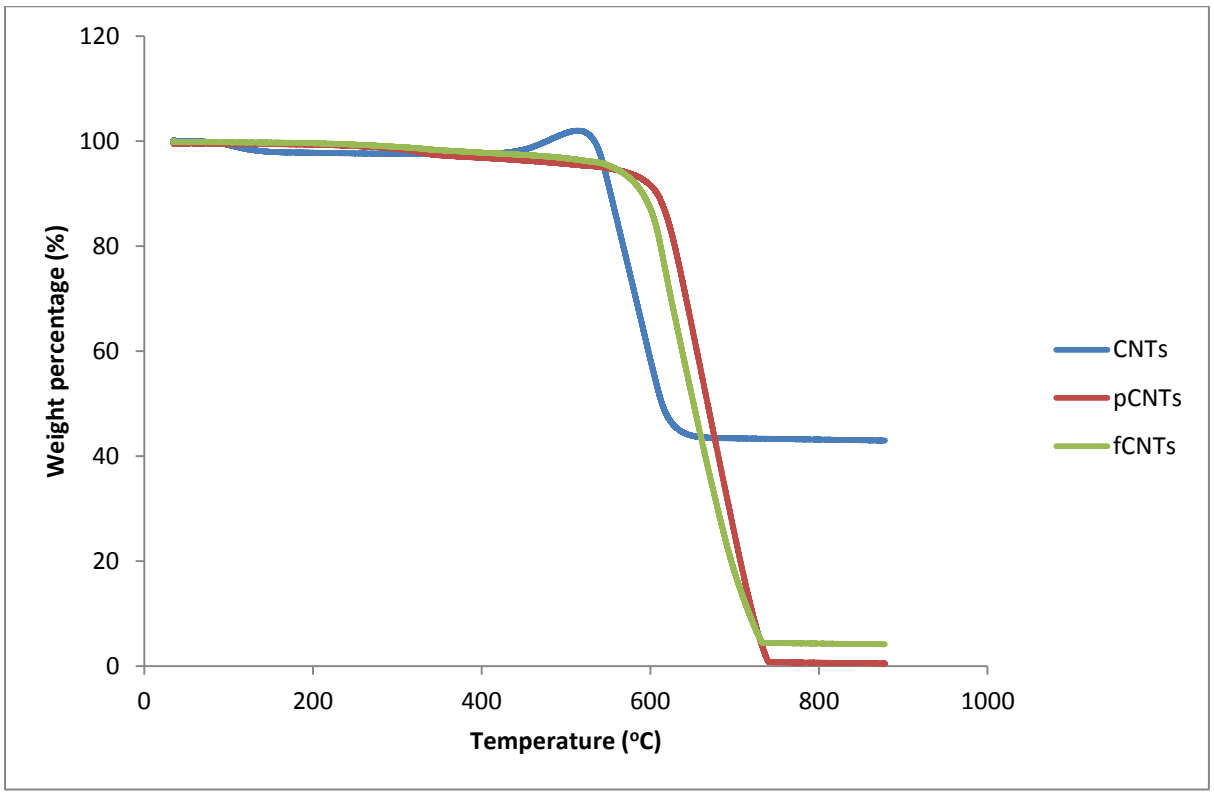


Figure 4.2: The TGA plots for the as-produced CNTs, fCNTs and the pCNTs.

The thermal stability of both the fCNTs and the pCNTs before 544^{o}C temperature indicates that most of the catalyst impurities and contaminants have been removed. The major decomposition for both fCNTs and the pCNTs initialised at the temperature of about 544^{o}C. The fCNTs then loses about 96 percent of its mass until it became stable at a temperature of 740^{o}C. This shows that after functionalization, only 4% of the impurities remained in the CNTs. The pCNTs shows the greatest thermal stability compared to the as produced CNTs and the fCNTs. Just like the fCNTs it indicates no sign of weight loss before the temperature of 276^{o}C, this implies that the structure of the CNTs was not destroyed with the use of the acids and hence they are suitable for blending into the membranes. The pCNTs lost about 99.4% of the mass. Hence the CNTs were only 0.6 % contaminated, after purification. This

indicates how pure they are, i.e., most of the contaminants and impurities have been removed as compared to the as-produced CNTs and the fCNTs. This result confirms the TEM results above, and they are also comparable to the literature (Phao et al., 2013).

Figure 4.3 depicts the derivatives of the curves in figure 4.2. It shows how pure the CNT materials are. The plot consists of three single peaks at the temperature of 509-749^{o}C. The CNTs were the first to oxidise, followed by the fCNTs and then the pCNTs (just like in figure 4.2 above). These peaks show the rate at which carbon is oxidising. The highest rate occurs at the peak of the pCNTs. Again this confirms the production of multi-walled CNTs, because this is how these kinds of CNTs behave (Motchelaho et al., 2011). The two small peaks pointed with an arrow, at temperatures less than 400^{o}C, indicates that initially there was a presence of an amorphous carbon, but as the temperature was increasing and the CNTs were functionalised and purified, the CNTs became more and more graphitised (Tam et al., 2008; Motchelaho et al., 2011). The peak pointed with a black arrow, shows increase in disorder of the contents of the as-produced CNTs.

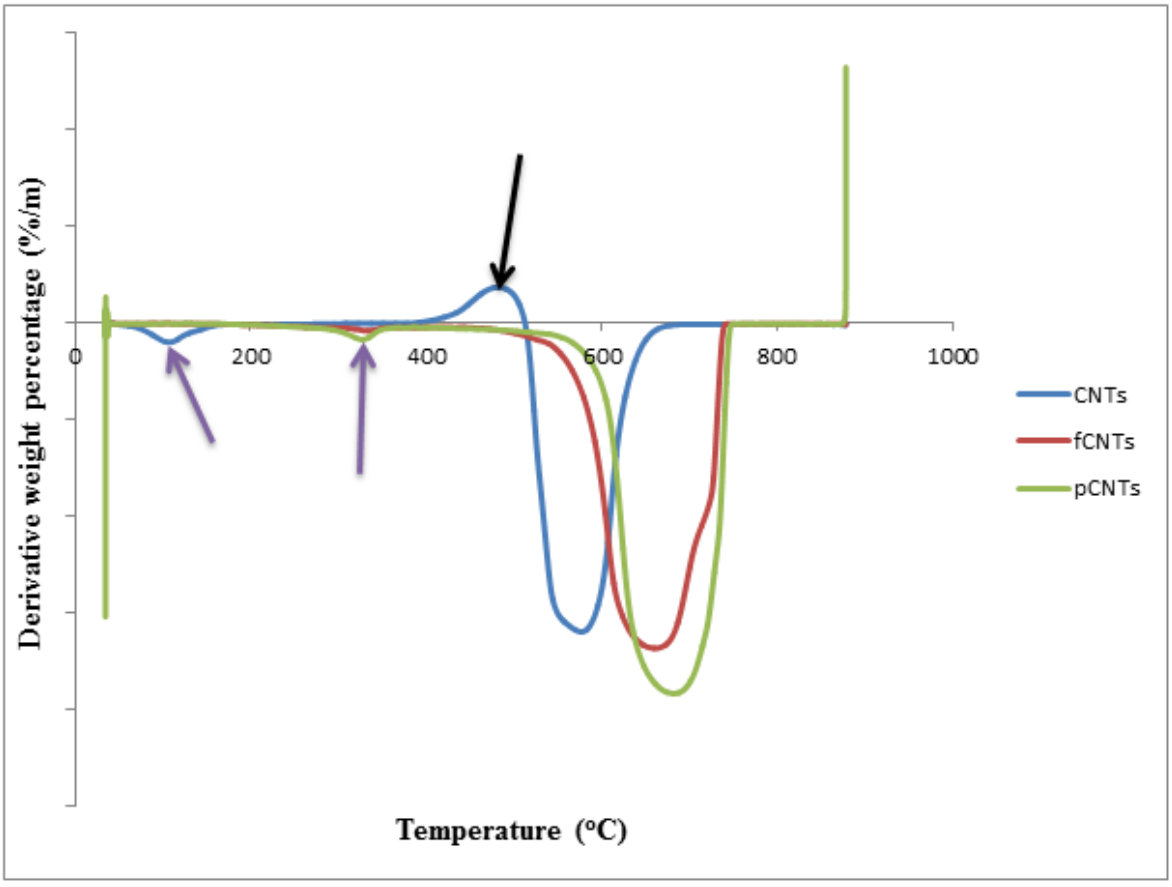


Figure 4.3: The derivative weight percentage graphs of the CNTs, fCNTs and the pCNTs.

From the figure, the rate at which carbon is oxidised increased from 580^{o}C for the as-produced CNTs, to 640^{o}C for fCNTs and the highest decomposition is at 688^{o}C of the pCNTs. This increase in temperature shows that the structure of the CNTs was not damaged by the acids used. This also improved the thermal stability of the CNTs. This is consistent with the TEM results and with the literature (Motchelaho et al., 2011).

4.1.3 Raman spectroscopy analysis

Raman spectroscopy was used to analyse the structure of the CNTs and to ascertain any other form of carbon formed during the synthesis of the CNTs. Figure 4.4 depicts the Raman shifts for the as-produced CNTs, fCNTs and the pCNTs using 514.5 nm excitation lines as mentioned in section 3.3.4. The Raman shift for the three spectra is the same. This similarity indicates that all three different CNTs materials have the same properties. In other words, this shows that the structure of the CNT is the same, i.e., it has not been damaged by the use of nitric acid and sulphuric acid during functionalization, and the use of hydrochloric and hydrofluoric acids during the purification. Hence this confirms the information in TEM and TGA analysis. The CNTs synthesised from ferrocene as a source of carbon and catalyst are generally not coiled and grouped together. Such CNTs are suitable for blending, CNT based transistors, etc. (Yah et al., 2011).

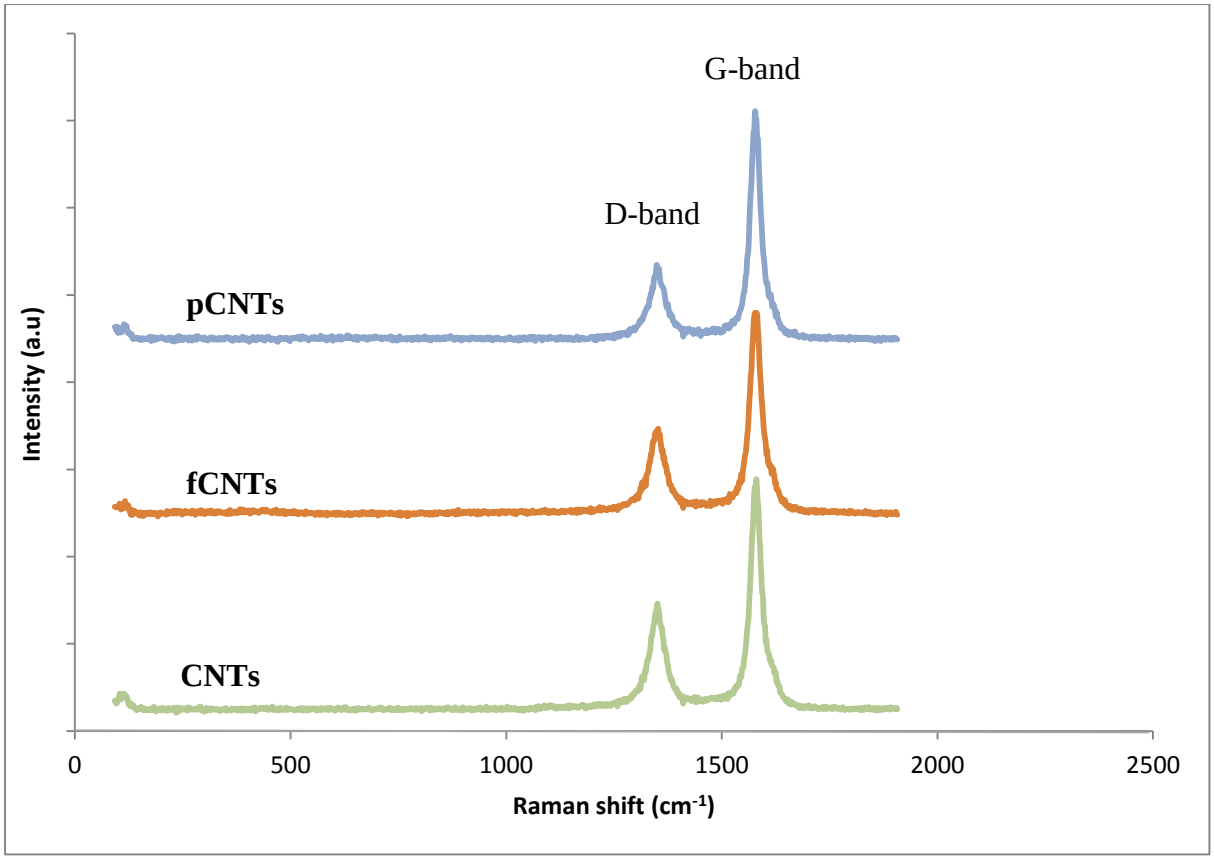


Figure 4.4: The Raman shift for the CNTs, fCNTs and the pCNTs

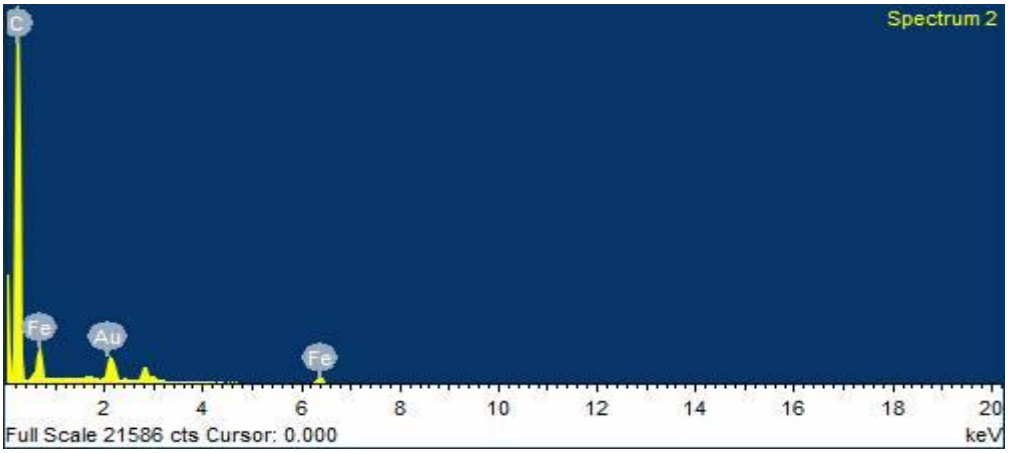
The two peaks; one at a Raman shift of approximately 1350 cm^{-1} and the other at 1580 cm^{-1} corresponds to the disorderly band (D-band) and the tangential graphite (G-band) mode, respectively. The G-band is also known as the E_2g graphitic mode (Schwan et al., 1996). These two peaks indicate that the CNTs have been synthesized (Iyuke et al., 2009), with the strongly-observed sharp G-band peak suggesting the MWCNTs (Yah et al., 2011). No radical breathing mode observed, hence no single-walled CNTs. The D-band indicates the presence of some discorded graphite hexagonal components (Lou et al., 2003) in the CNTs while the G-band showed the ordered components (Tuinstra & Koenig, 1970; Yah et al., 2011). As the G-band increases, going from CNTs to pCNTs, D-band decreases.

The intensity of the G-band is higher than that of the D-band, suggesting that the CNTs are composed of strong vibrations of carbon-carbon (C-C) bond, which is highly sp^2 hybridised. The I_D/I_G intensity ratio (measures the defects and purity) decreases from the CNTs (I_D/I_G = 0.47), fCNTs (0.41) to pCNTs (0.37) as the CNTs were functionalised and purified. These I_D/I_G ratios confirm the synthesis of MWCNTs and indicate that there are defects (Mhlanga and Coville, 2008; Moothi, 2009, Yah et al., 2011) in the hexagonal lattice graphite structure

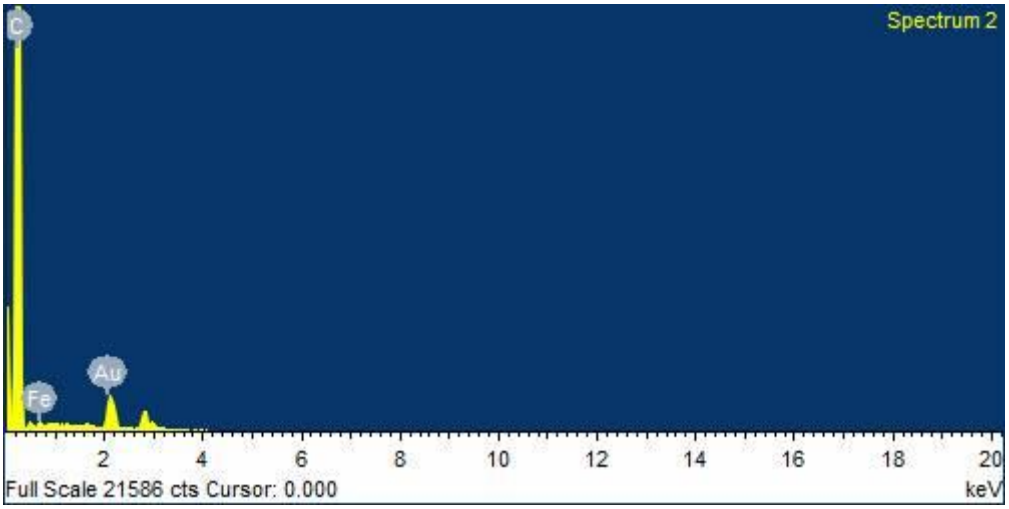
of the CNTs. The observed decrease in I_D/I_G ratios (from CNTs to fCNTs, then to pCNTs) indicates the decreased defects and high graphitisation degree (Afolabi et al., 2011; Wang et al., 2004a). The decrease in the D-band resulted in the increase of the G-band as the CNT materials were treated with acids. The lowest I_D/I_G ratio in the pCNTs shows that most impurities have been removed and the defects have been decreased (Liu et al., 2008; Yah et al., 2011), the pi bonds have been broken without any damage to the structure of the CNTs. These results are consistent with the literature (Yah et al., 2011; Tsai et al., 2013), and they confirm the TEM results in section 4.1.1. The individual spectra for the CNTs, fCNTs and the pCNTs are in the Appendix A. This also reconfirms that the use of ferrocene, at higher temperatures e.g., 850^{o}C, alone is good enough to synthesize the MWCNTs (Iyuke & Simate, 2011).

4.1.4 Energy Dispersive X-ray Spectroscopy analysis

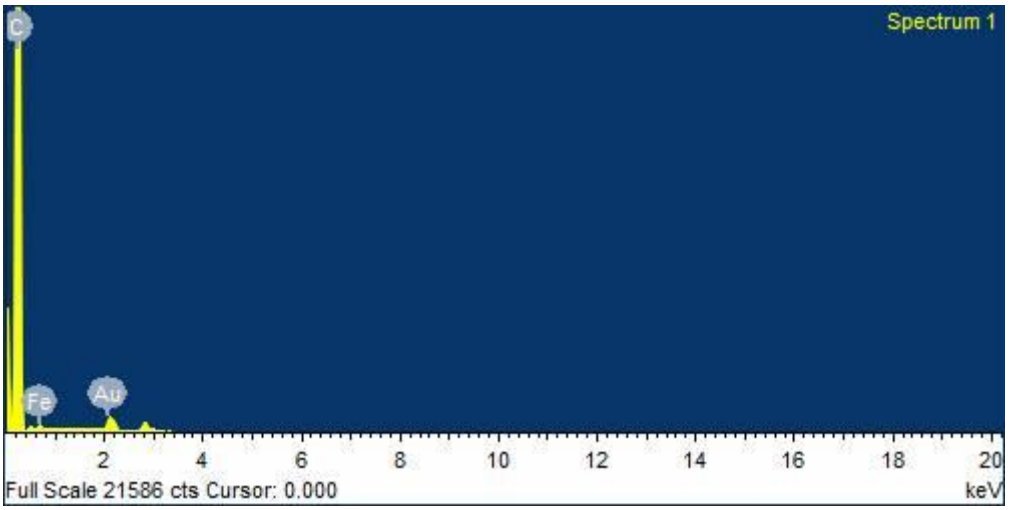
Energy dispersive x-ray spectroscopy (EDS) was used to investigate the element composition and purity of the CNTs. Both inorganic (e.g. metals) contaminants and organic components (e.g., carbon) that are in the as-produced CNTs, fCNTs and pCNTs were identified. In other words, it shows whether the impurities have been removed or not (Lui et al., 2007; Huang et al., 2003). Figure 4.5 shows the EDS spectra for the as-produced CNTs, fCNTs and the pCNTs.



(a) EDS spectrum for the as-produced CNTs



(b) EDS spectrum for the fCNTs



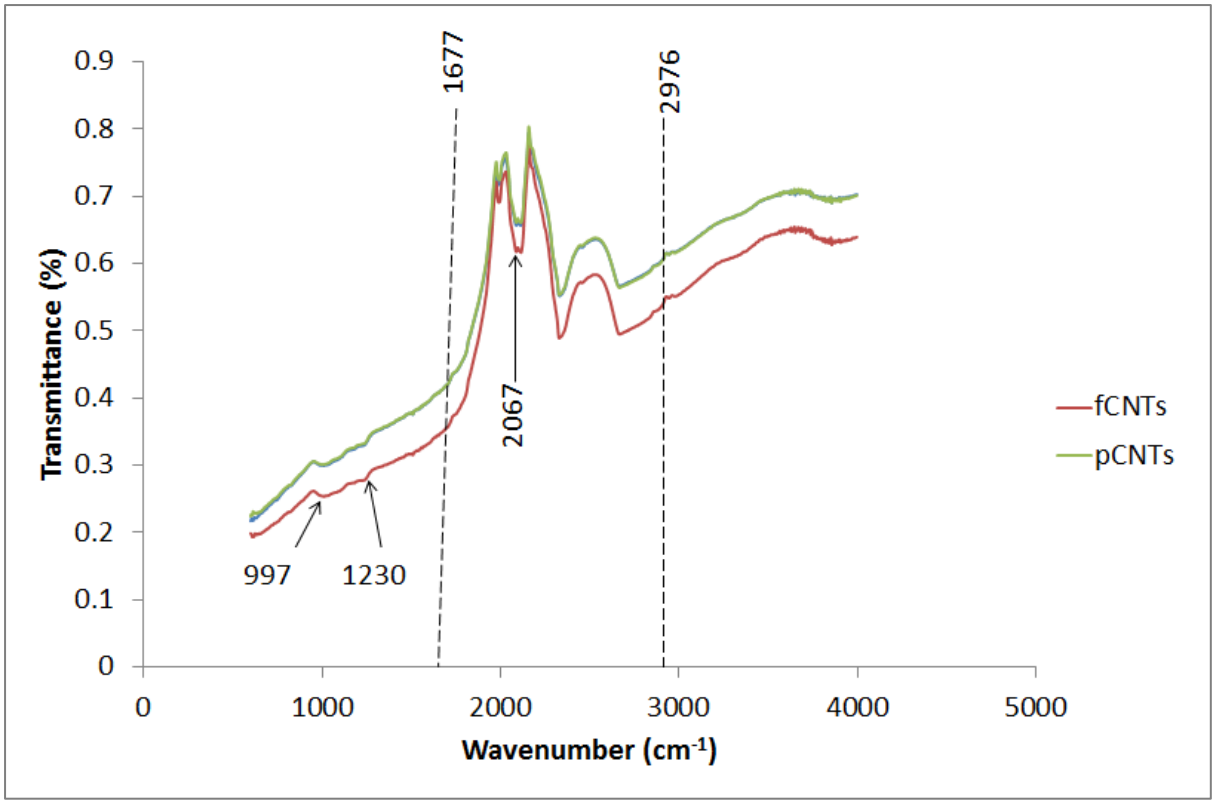
(c) EDS spectrum for the pCNTs

Figure 4.5: EDS spectra for the CNTs.

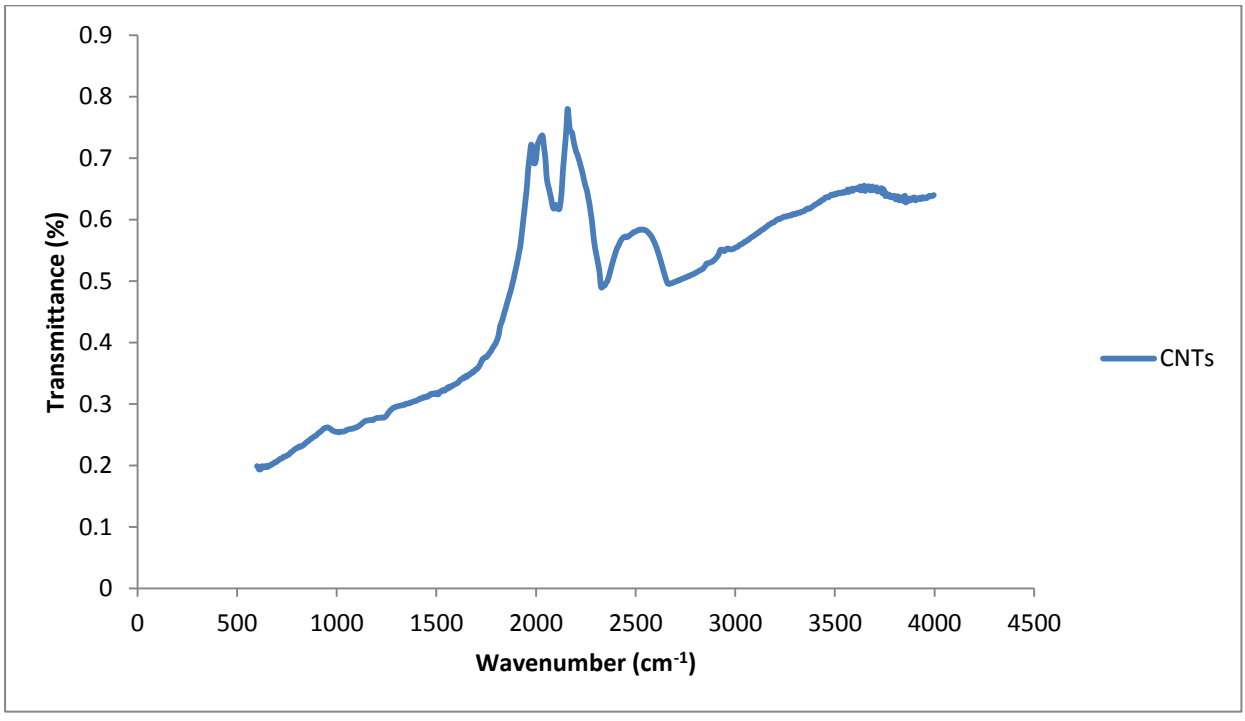
From figure 4.5(a), the following elements were identified in the as-produced CNTs: carbon (C) which made about 60% of weight, Iron (Fe), and gold (Au) which was used for sputter coating, there is also another unidentified element which shows a small peak between 2.8 and 3 keV which might have been either argon or nitrogen, all made the combined weight of about 40%. The CNTs after functionalization, in figure 4.5(b), were composed of; largely C which made 96% of mass, as well as Fe and Au (which made the combined 4% weight). The fCNTs were then purified in 4.5(c) as pCNTs and were found to contain C which made 99% of weight and others (Fe and Au) which made 1% of weight. Fe and C atoms in this case, came from ferrocene which was a source of carbon and a catalyst; Au was used as a sputter coater, either nitrogen or argon gases were the main gases during the synthesis of the CNTs. The Fe-containing catalyst as ferrocene was responsible for the black spots observed in the TEM images. Hence the main impurity that was not removed completely was the Fe. The acids used during functionalization were able to reduce the contaminants to at least 40% of the weight. This is confirmed by the removal of the Fe peak at the energy of about 6.4 keV and the reduction of another Fe peak at 0.6 keV in figure 4.5(b). In figure 4.5(c) shows that the impurities are still present in the CNTs, even after further treatment by the purifying acids. The impurity peaks, however, as indicated, have been reduced quiet to a smaller level as compared to the other two spectra. This presence indicates how resistant the impurities were to the acids. During functionalization and purification stages, the carbon peak has been growing, while the metal peaks were being reduced. This means that the CNTs were becoming more and more purified (becoming low defected and metal free) while their structure remained the same, i.e., the structure of the CNTs was not damaged by the use of the selected acids. This confirms the TGA as well as TEM and Raman spectroscopy results. These results are also comparable to the literature (Yao et al., 2008).

4.1.5 Fourier transform infrared (FTIR) spectroscopy analysis

Fourier Transform Infrared (FTIR) spectroscopy was used to analyse the functional groups and the functionalities in the CNTs. Figure 4.6 below shows infrared (IR) spectra for the fCNTs and the pCNTs in the same plane. Their individual spectra are in the appendix A. In figure 4.6(a), the CNT plot is not clearly visible since it is superimposed by the fCNTs plot; hence it was re-plotted in figure 4.6(b). Every functional group that is in figure 4.6(a), is also in 4.6(b) at the same position.



(a) IR spectra for the fCNTs and the pCNTs.



(b) IR spectrum for the as-produced CNTs

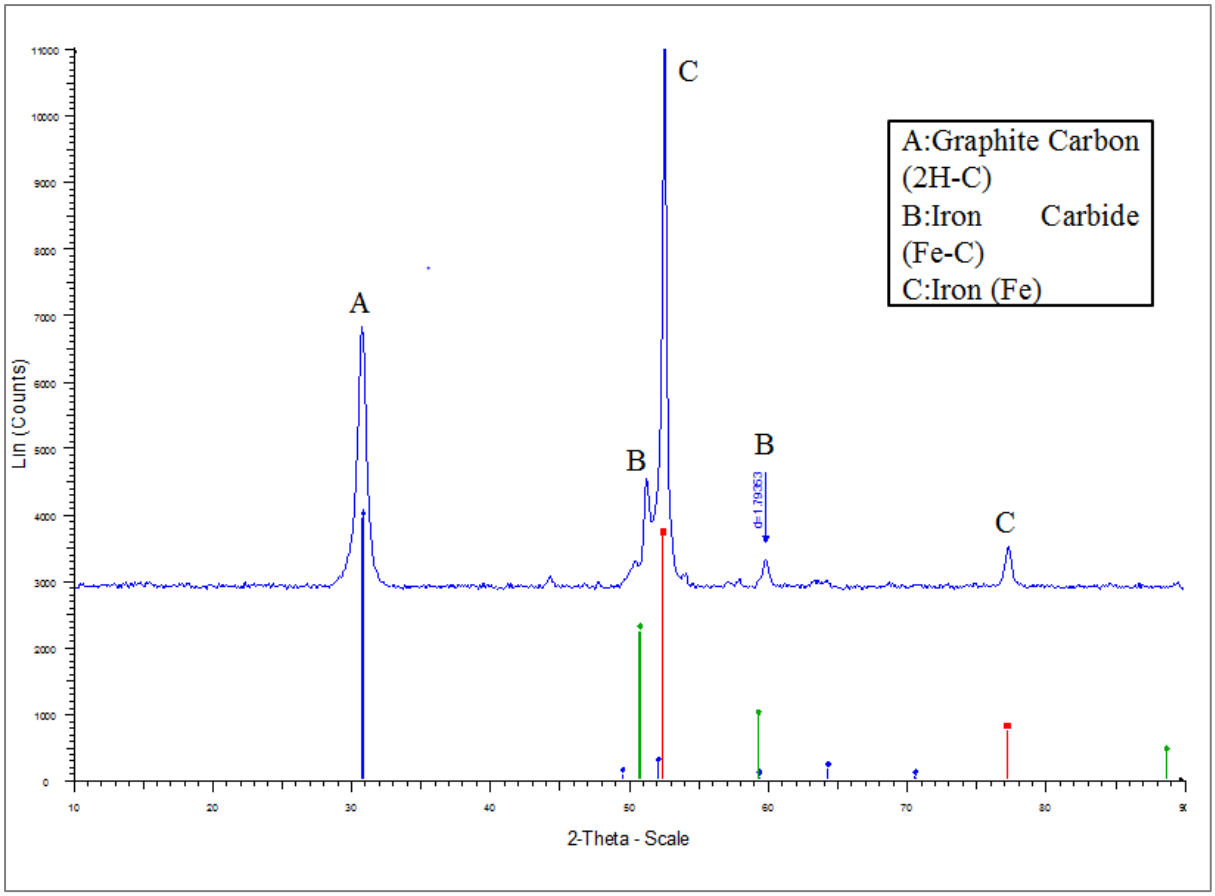
Figure 4.6: IR spectra for the (a) fCNTs with the pCNTs, and (b) as-produced CNTs

The spectra show five visible peaks between the wavenumbers of 997 and 2667 cm^{-1}. The use of acids during functionalization and purification processes did not introduce new functional groups on the spectra; the only effect done by the acids in this case is the shift of the intensity slightly down as it can be seen in figure 4.6(a). This might be due to the nature of these CNTs which contains very high level of defects and impurity particles that might have served as a protective shield and prevented the acids to the CNTs. This resulted to no functional groups being able to react and attach to the structure of the CNTs; hence those functional groups were washed away during acid neutralization with water.

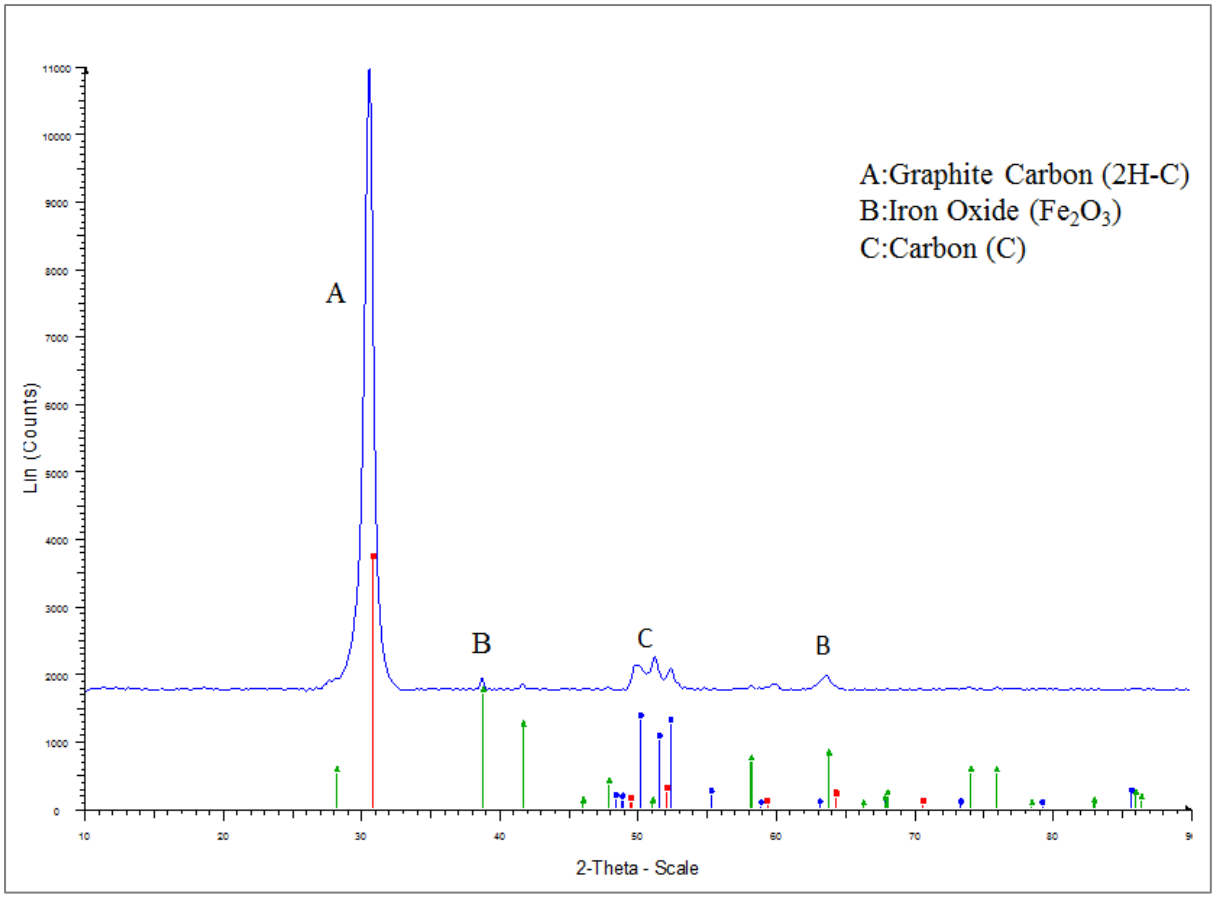
From figure 4.6(a), there is a weak peak at the wavenumber of ~997 cm^{-1} which corresponds to an sp^2 C-H bond bending in plane. This is due to the presence of aromatic rings in the ferrocene compound. A small visible peak at ~1230 cm^{-1} corresponds to a bending vibration of carbon to carbon (C-C) bond. This bond comes from the aromatic ring as well. An observable weak variable peak at ~1677 cm^{-1} corresponds to a vibrational stretch of a –C=C- bond in the ring. A strong peak at ~2067 cm^{-1} belongs to the vibrational asymmetric stretch of a –C=C- bond. This bond and the bond at 1677 cm^{-1} are different in such a way that one's mode is asymmetric while and the other is symmetric. This different vibration indicates the presence of defects in the graphitic MWCNTs. The peak at ~2976 cm^{-1} corresponds to the vibrational stretch of a sp^2 C-H bond. Furthermore, the anti-absorption peaks at ~1975, 2160 and 2160 cm^{-1} which have changed intensities, confirms the nature of the CNTs that they contain some disorders. These results agree with Raman spectroscopy results that indeed the produced MWCNTs are graphene CNTs. The graphene MWCNTs could provide good separation performance during the separation of the oil-containing wastewater (Jha et al., 2011).

4.1.6 XRD spectroscopy analysis

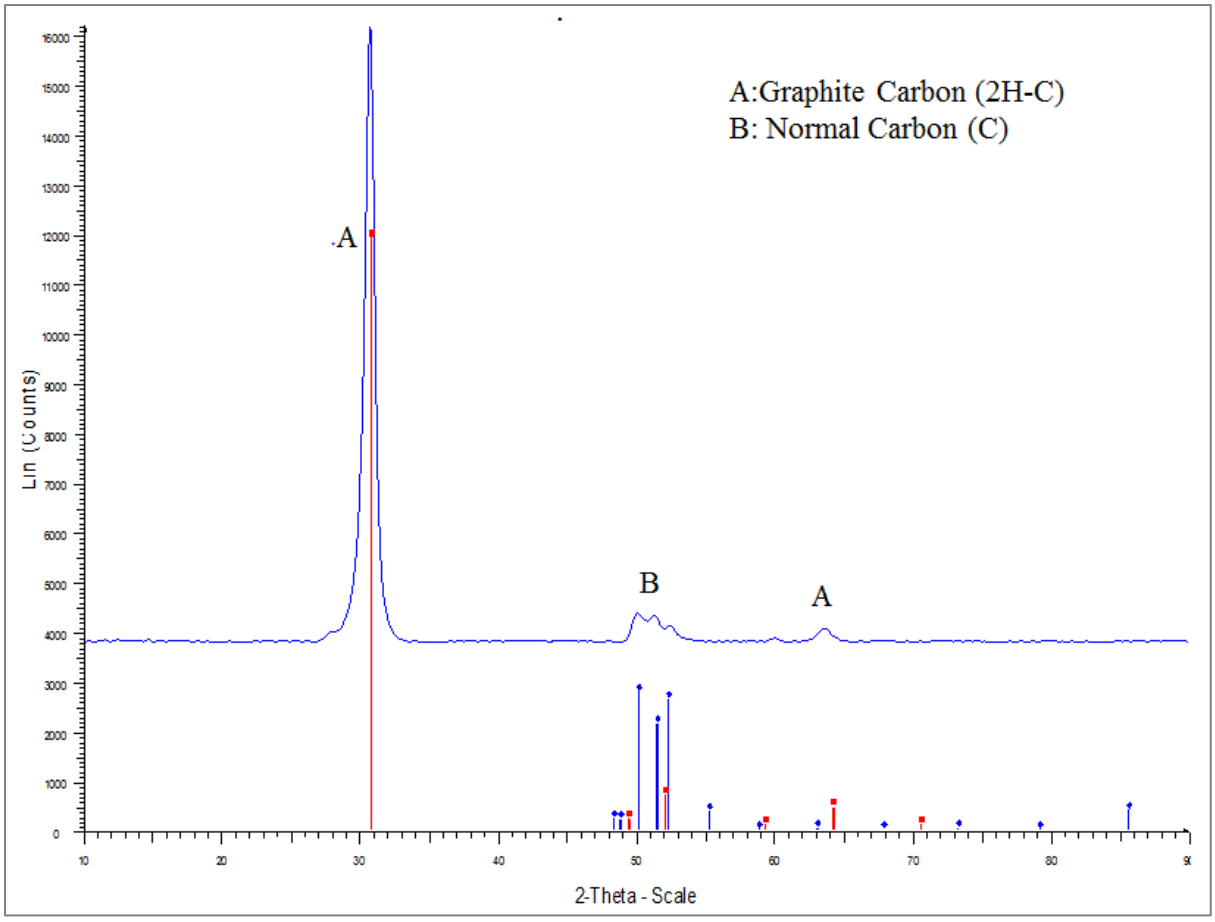
X-ray diffraction analysis (XRD) was used to identify the phase of the crystal arrangements and to give information on the dimension of the unit cell of the CNTs. Figure 4.7 shows the XRD spectra for the as-grown CNTs, fCNTs, and the pCNTs.



(a) XRD spectrum for the as-produced CNTs



(b) XRD spectrum for the fCNTs



c) XRD spectrum for the pCNTs

Figure 4.7: XRD spectra a) as-produced CNTs, b) fCNTs and c) pCNTs.

Figure 4.7(a) show four significant peaks at the 2-theta angles of ~30.9 (A), 52.5 (C), 59 (B) and 77º (C). All other peaks are similar to at least one of the mentioned three peaks as indicated in the diffractogram. The peak at 30.9º indicates that the CNTs are graphitic. The components in this material are arranged in a hexagonal crystal system represented by the primitive lattice. This is because two transition vectors (a = b = 2.47Å) are the same while the other, c = 6.72 Å, is different; their orientations are alpha (α) = beta (β) = 90º, and gamma (γ) = 120º. The inter-planer spacing (d) for this peak is ~2.14 Å, a common d-spacing for the CNTs. The multiple diffraction peaks at 52.5º appears to contain graphitic carbon, iron and iron carbide. The dominant line for this peak, as well as a peak at 77º contains the iron particles from the catalyst. These iron particles are arranged in a cubic system represented by a body centred lattice. This is shown by three equal sides (a_o = a = b = c = 2.87 Å) with α_o = α = β = γ = 90º. The d-spacing for this line is ~1.43 Å. A peak at ~59.4º corresponds to iron carbide (Fe-C) due to the catalyst. The Fe-C components are also arranged in a cubic system

represented by the face centred lattice. The d-spacing for this peak is 1.79 Å. In this case, there is no significant presence of the amorphous carbon observed because of the high crystal content indicated (Iyuke and Simate, 2011; Afolabi et al., 2007).

Figure 4.7(b) depicts four observable peaks at ~30.9 (A), 38.9 (B), 52.5 (C) and 64º (B). The graphite peak at 30.9º appears to have grown in size as compared to 4.7(a). This is due to the use of nitric and sulphuric acid. These acids decreased the iron content as indicated in 52.5, 59 and 77º. However, the use of these acids introduced the hematite iron oxide (Fe_2O_3) as shown at 38.9 and 64º. These iron oxide particles are arranged in a hexagonal crystal system represented by a primitive lattice. The axes for this system are: a = b = 5.04 Å and c = 13.7 Å, with $\alpha = \beta = 90^o$ and $\gamma = 120^o$. The d-spacing for this line is ~4.36 Å, which is also common spacing for the CNTs.

Three peaks at 30.9 (A), 52.5 (B) and 64º (A) are observed in figure 4.7(c). As it can be seen, iron oxide has been completely removed during purification process, the only remaining components are those containing graphite (A) and Fe-C catalyst particles (B). The intensity of the graphitic carbon has been increased and these materials contain over 91% of carbon particles and less than 9% of the catalyst particles. The particles are arranged in a hexagonal system represented by a primitive lattice with a = b = 2.52 Å, and c = 16.5Å. The d-spacing has a value of ~1.25 Å for this diffractogram. This means that the acids used during purification step decreased the amount of the catalyst particles but did not completely remove it as it still remains. These results are consistent with the TEM, TGA, Raman and other results already presented.

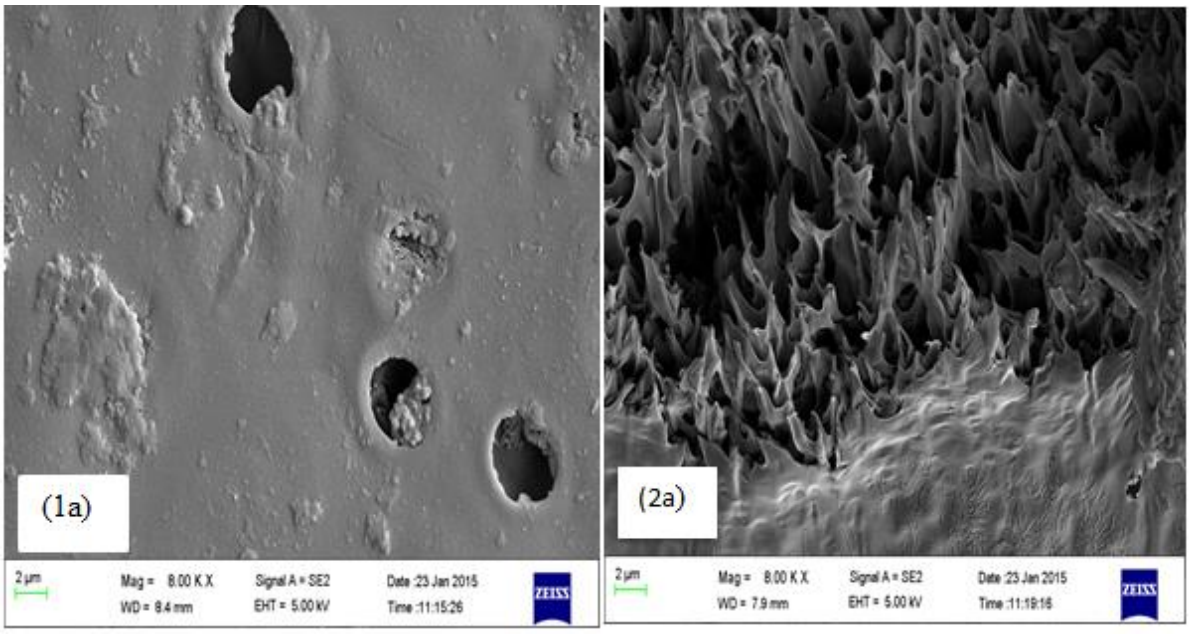
4.2 The PS membrane analysis: characterisation and assessment

Seven membranes were synthesized, two the CNTs [0 CNTs and 0 PVA (only contains the PVA layer), these are mainly for comparison purposes], one with the pCNTs (p7.5% CNTs), and the rest (2.5% CNTs, 5% CNTs, 7.5% CNTs and 10% CNTs) contains different amount of the concentration of CNTs.

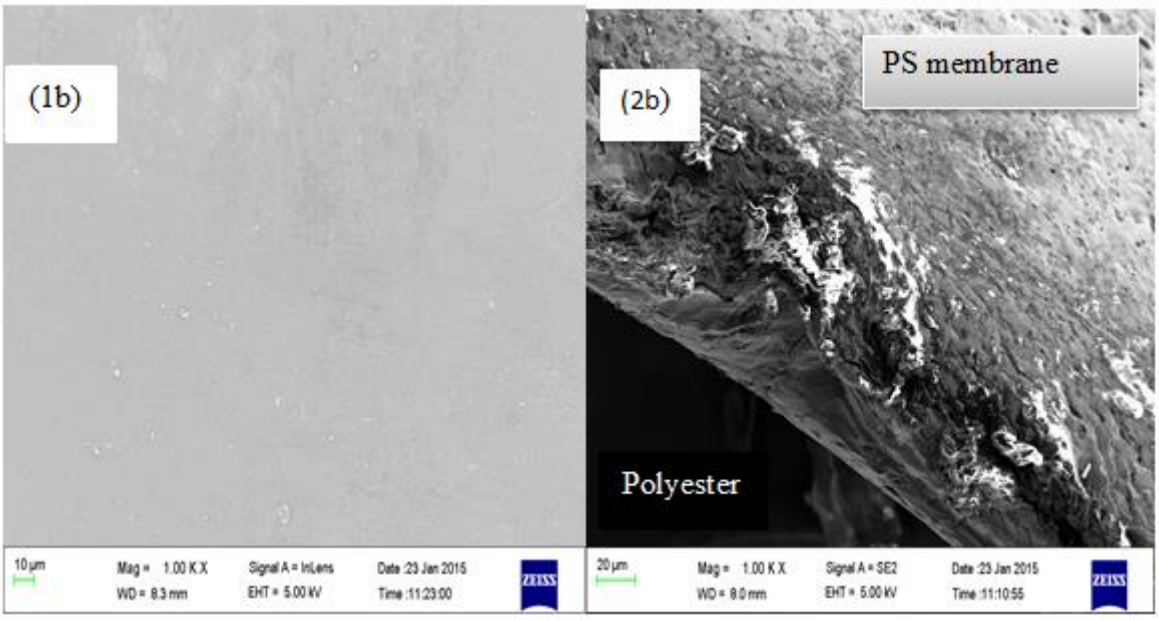
NB: *2.5% CNTs means the polysulfone (PS) membrane infused with 2.5% of the as-produced CNTs and this also applies to the other non-mentioned membranes. p7.5% CNTs means the PS membrane containing 7.5% of the pCNTs.*

4.2.1 SEM analysis of the PS membrane

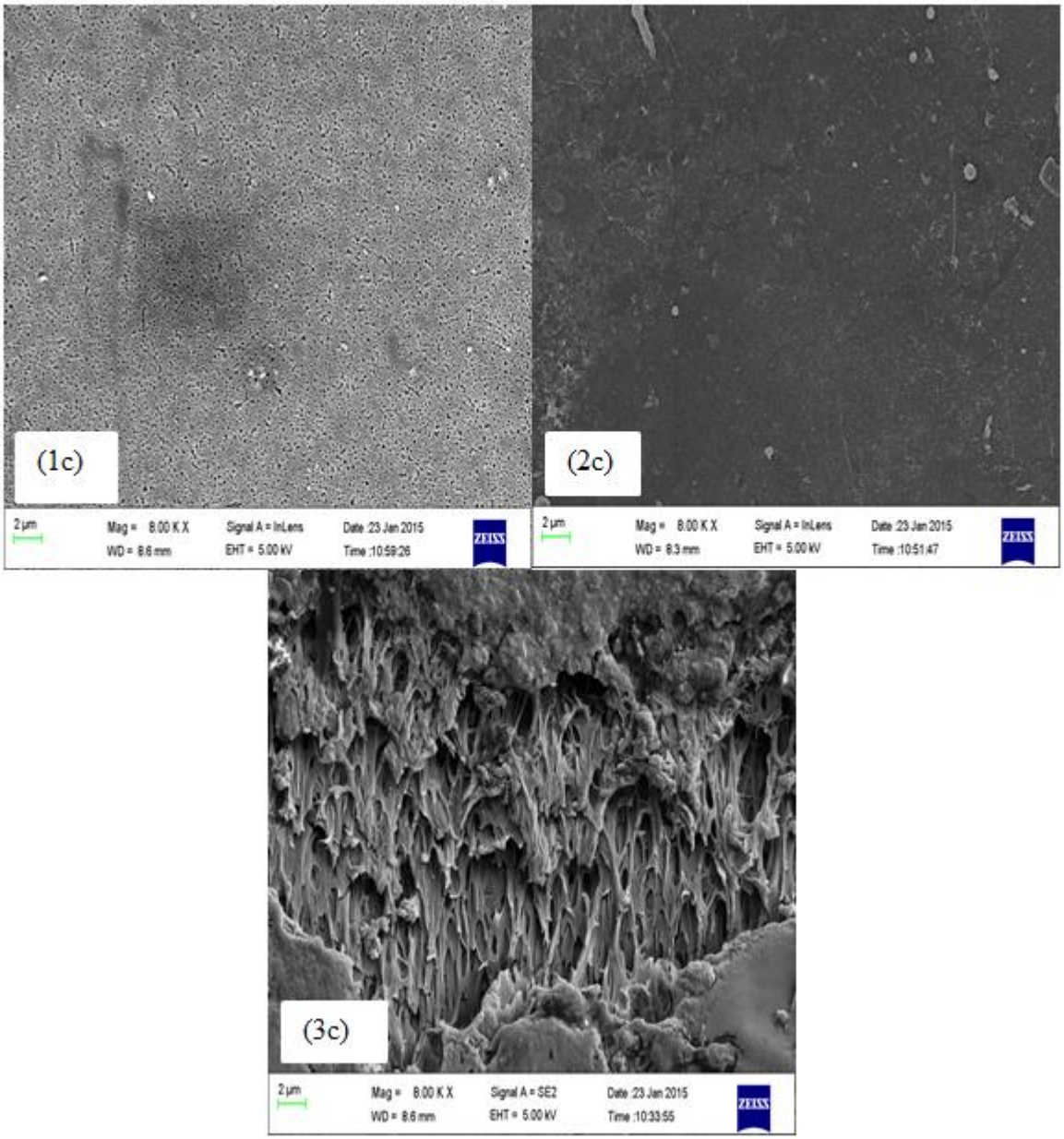
Scanning electron microscope (SEM) was used to observe the arrangement of the components making the PS membrane on the external surfaces and the cross section in 3D. The following results were obtained using the SEM equipment shown in figure 3.7, chapter 3. Figure 4.8 depicts the surfaces and the cross sections of the SEM images of 0 CNTs, 0 PVA, 2.5% CNTs, 5% CNTs, 7.5% CNTs, p7.5% CNTs and 10% CNTs PS membranes.



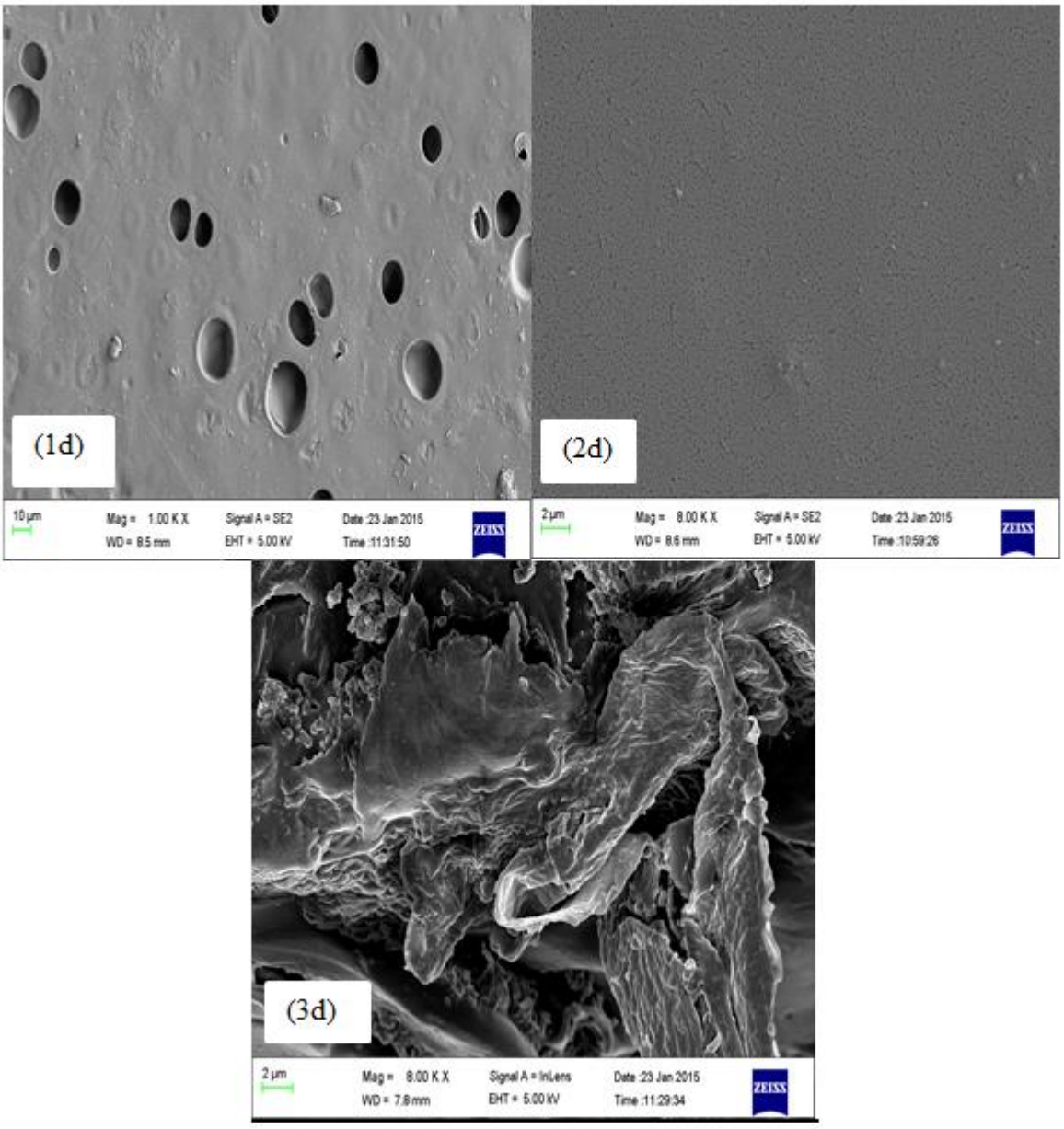
(a) SEM images for the 0 CNTs PS membrane; (1a) top surface layer and (2a) cross section.



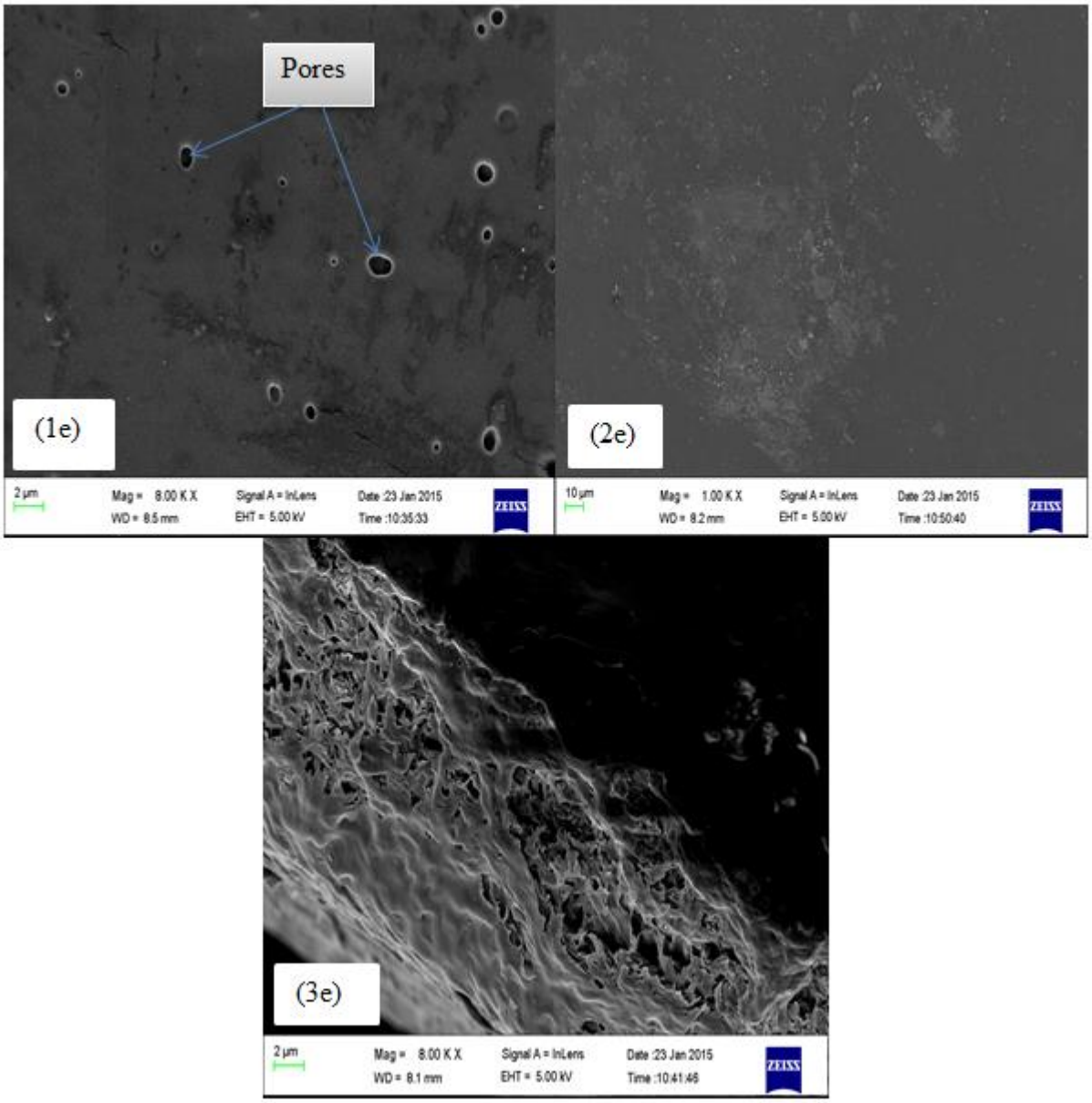
(b) SEM images for the 0 PVA PS membrane; (1b) top surface layer, and (2b) the cross section.



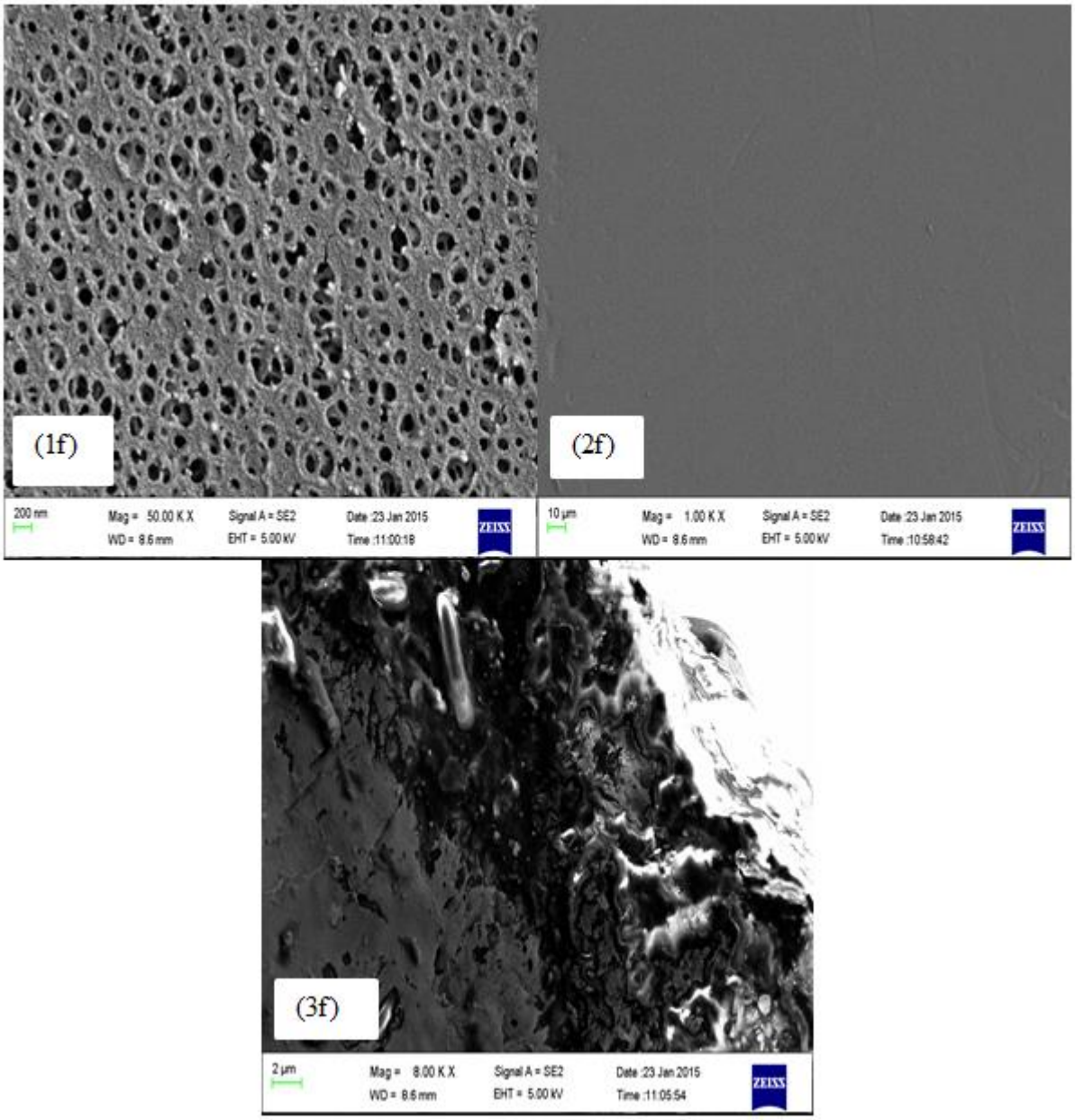
(c) SEM images for 2.5% CNTs PS membrane: (1c) top surface without PVA layer, (2c) top surface with PVA layer, and (3c) the cross section.



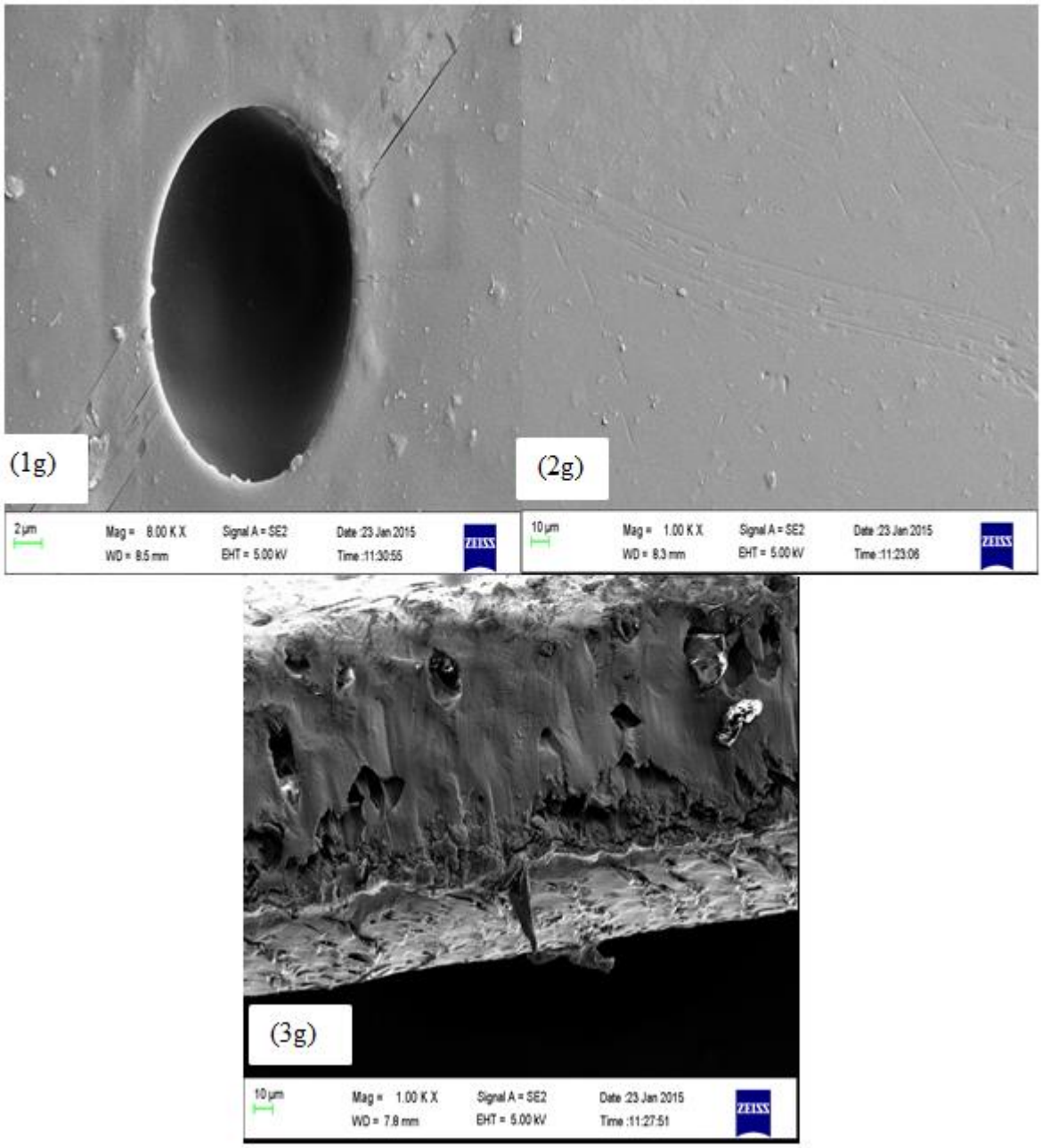
(d) SEM images for 5% CNTs PS membrane: (1d) top surface without PVA layer, (2d) top surface with PVA layer, and (3d) the cross section.



(e) SEM images for 7.5% CNTs PS membrane: (1e) top surface without PVA layer, (2e) top surface with PVA layer, and (3e) the cross section.



(f) SEM images for p7.5% CNTs PS membrane: (1f) top surface without PVA layer, (2f) top surface with PVA layer, and (3f) the cross section.



(g) SEM images for 10% CNTs PS membrane: (1g) top surface without PVA layer, (2g) top surface with PVA layer, and (3g) the cross section.

Figure 4.8: SEM images of the seven PS membranes.

Figure 4.8(a) depicts the SEM images for the 0 CNTs PS membrane (the membrane without the CNTs and the PVA layer). In this figure, (1a) indicates the pores on the surface layer of the membrane and (2a) shows the arrangement of the pores at the cross sectional area of this membrane. No CNTs are visible on any area of this membrane because the membrane itself

does not contain any. The arrangement of pores is uniform but their sizes are different. The average pore sizes are given in section 4.2.2.

The SEM images of the 0 PVA membrane are shown in figure 4.8(b). This membrane was also not blended with any amount of the CNTs, but it contains the PVA layer. The upper surface layer depicted in (1b) is covered with the PVA layer. At (2b) is the cross section area of this membrane. As it can be seen, there are no visible pores on either sides of this membrane. This is due to the hydrophilic PVA layer which covered both areas of this membrane, only the bottom side, which is not shown, was not covered by this layer. Thus the bottom side of the membrane is hydrophobic, while the upper surface is hydrophilic because of the PVA layer. This means that if the bottom side is to be used to separate oil-containing wastewater, wastewater will be rejected into the retentate and oil will be in the permeate. If the top side is used, the flow of fluids will be vice-versa.

In figure 4.8(c), the SEM images of the 2.5% CNTs PS membrane are shown. This membrane contains 2.5% concentration of the as-produced CNTs and is also covered with the PVA layer. Figure 4.8(1c) indicates the pores on the upper surface of 2.5% CNTs PS membrane with no PVA layer. (2c) is the same membrane covered with the PVA layer. The pores on this surface area are not visible because the membrane is covered with the PVA layer. Arrangements of the polymer material in a vertical position can be seen in the cross section of this membrane in (3c), CNTs are not observed because of the PVA layer which also covers the sides but not the bottom of the membrane.

Figure 4.8(d) shows the SEM images of the 5% CNTs PS membrane. A higher magnification of the top surface layer of the 5% CNTs PS membrane is depicted at (1d), where pores are clearly visible in this micrograph. (2d) Indicates the top surface layer of the same membrane with a PVA layer, in this case no pores are observed because of this layer. In (3d), no CNTs can be seen on the cross section of this membrane since the membrane is also covered with the PVA layer on the sides.

SEM micrographs of the 7.5% CNTs PS membrane are shown in figure 4.8(e). (1e) shows the upper surface cover of the 7.5% CNTs PS membrane at lower magnification. Pores are visible but not clearly. At (2e), the top layer of the same membrane with a PVA layer is shown. Position (3e) shows the cross section which is clearly covered with a PVA layer, including the sides.

In figure 4.8(f), SEM images of the p7.5% CNTs PS membrane are shown. This membrane is infused with 7.5% concentration of the pCNTs and it also contains the PVA layer. At (1f), the pores on the upper surface of the p7.5% CNTs PS membrane are clearly observable at the moderate magnification. Comparing the pores of this membrane with the already observed pores, it is clear that these membranes do not contain the same pore sizes. This was one of the very highly porous PS membranes synthesised in this project. A closer look shows that the pores on the surface of this membrane are not equal, i.e., they are asymmetric. This is a typical behaviour for the PS membranes synthesized using the phase inversion method (as indicated in section 2.8). Larger pores serve as pre-filters to the smaller ones. At (2f), the surface of p7.5% CNTs PS membrane covered with a PVA layer is shown. The cross section of this membrane is perfectly covered with the PVA layer; hence no CNTs or arrangements of pores are visible. The increased pores in these membranes are due to the increased hydrophilicity because of the pCNTs.

Figure 4.8(g) depicts the SEM images of the 10% CNTs PS membrane. Position (1g) shows one large pore on the upper surface of the 10% CNTs PS membrane without the PVA layer at high magnification. The pore filters to the top right hand ride of this image. At (2g) no pores are available due to the PVA layer. The cross section of this membrane is perfectly covered with the PVA layer at (3g), no CNTs or any pore arrangement can be seen. This is exactly how a membrane with the PVA layer and infused with the CNTs should look like.

The common information displayed by all these membranes on the SEM images is that the pore sizes on the top surface of each membrane are not equal. The larger one serves as a pre-filter to the smaller one. This is a typical of polysulfone membranes. Also all seven membranes do not have the same average pore sizes. There are no visible pores on the surface of a PS membrane that is covered with a PVA layer. BET provides the average pore sizes for each membrane is section 4.3.2 below. If a cross section of a membrane is perfectly covered with a PVA layer, there would be no pore arrangement or any CNT visible as it was indicated above. These results are consistent with the literature (Chuang et al., 2000; Maphutha et al,. 2013; Phao et al., 2013).

4.2.2 BET analysis

Brunauer-Emmett-Teller (BET) studies were used to examine the pore size, pore volume and the surface area of the PS membranes. The porosity was determined using equations (1) in chapter 3, section 3.3.7. Table 2 shows the summary of the average pore size, single point adsorption total pore volume, the porosity and the single point surface area of the six PS membranes indicated. The results were obtained using the BET equipment in section 3.3.6.1, more data is available in the appendix B.

Table 2: BET analysis showing the pore size, pore volume and the surface area of the PS membranes

PS membrane	Surface area (m^2/g)	Pore volume (cm^3/g)	Pore size (nm)	Porosity (%)
0 PVA	3.47	0.0193	24.39	39.7
2.5% CNTs	9.91	0.0276	11.61	44.0
5% CNTs	11.3	0.0353	12.95	45.6
7.5% CNTs	9.78	0.0302	12.88	46.0
p7.5% CNTs	8.86	0.0384	17.88	41.5
10% CNTs	10.5	0.0367	14.62	47.5

NB: See section 4.2 for the meaning of 0 PVA, 2.5% CNTs, etc.

From the table, it can be seen that the 5% CNTs PS membrane has the largest surface area for separation, whereas 0 PVA has the smallest. The surface area increases as the concentration of the CNTs increases. On the other hand, 5% CNTs and 7.5% CNTs indicates an opposite trend. This might due to the fact that the CNTs contained some defects as shown by the Raman spectroscopy and other characterisation methods in section 4.2 above. 0 PVA and p7.5% CNTs relates to each other since they have the lowest and the second lowest surface areas, respectively.

The p7.5% CNTs PS membrane has the highest pore volume compared to others. This is due to their pCNTs which are less defected, hence resulting in higher pore size, as well as lower surface area and porosity. These results are consistent with those in 0 PVA. For the as-produced CNT membranes, pore volume increases with an increase in CNT loading.

The 0 PVA membranes has the highest average pore size (because it does not contain the defected CNTs), this implies that it is capable of filtering particles or substances with diameters greater than 25 nm. The increased average pore size in this membrane is due to the fact that, this membrane does not contain the as-produced CNTs which are defected as indicated by the characterisation techniques discussed earlier (whereas others do) and it has only a PVA layer which improves its hydrophilicity (this is an advantage compared to those that contain the as-produced CNTs). The p7.5% CNTs membrane on the other hand, has the second highest pore size, this is because of the pCNTs used, which results in a stable and hydrophilic membrane, i.e., the pore size indicate that its separation performance will be better than the others and its life span has been prolonged because of the pCNTs. On the other hand, 2.5% CNTs has the lowest average pore size. Normally, the lower the size of the pore, the better is the performance of the membrane. Hence 20% PS solution was used instead of 10%, this was also influenced by the fact that when the synthetic oil-containing wastewater was used, 0 PVA membrane had the lowest average pore size and its performance was greater than the others. In this project it is expected that all membranes will produce the greatest performance since they all have reduced pores because of the use of 20% polysulfone solution (Huang & Yang, 2006). The mean average pore size in this case is 16.7 nm which went down from 26.1 nm when the synthetic oil-containing wastewater was used.

There is an increasing trend in porosity for the membranes-infused with the as-produced CNTs: 2.5% CNTs < 5% CNTs < 7.5% CNTs < 10% CNTs. This shows that the concentration of the CNTs increases as the porosity (which is proportional to the pore size for these membranes, the slight decrease for the 7.5% CNTs membrane are just experimental errors) of the PS membranes increases. This same trend (between the CNTs and the porosity) also applies for the 0 PVA and p7.5% CNTs PS membranes, i.e., as the CNTs are added, porosity of the membrane increases. However, the relationship is opposite when it comes to the pore size and the two membranes. Hence the pore size decreases as the pCNTs are loaded to the PS membrane. Since the increase in the pore size of the membrane is inversely proportional to the separation performance and directly proportional to the flux of the membrane, 0 PVA and p7.5% CNTs are expected to have a good separation performance during the separation process. The industrial oil containing wastewater has a single drop of size that ranges from 0.02 – 200μm (Chakrabarty et al., 2010; Steward and Arnold, 2008). Thus all these membranes are capable of separating this oil-containing wastewater. These

results are consistent with the literature (Huang and Young, 2006; Maphutha et al., 2013; Zhang et al., 2009).

4.2.3 Contact angle analysis

Contact angle was used to investigate the hydrophilicity of the membranes. If the angle is less than 90^{o}, then the membrane is hydrophilic. If the angle is greater than 90^{o}, it implies the membrane is hydrophobic. Six membranes were tested for hydrophilicity. Since these membranes contain both the hydrophobic and the hydrophilic sides, only the hydrophilic side was used for the investigations. The following results in Figure 4.9 were obtained using the contact angle calorimeter device on section 3.3.6.

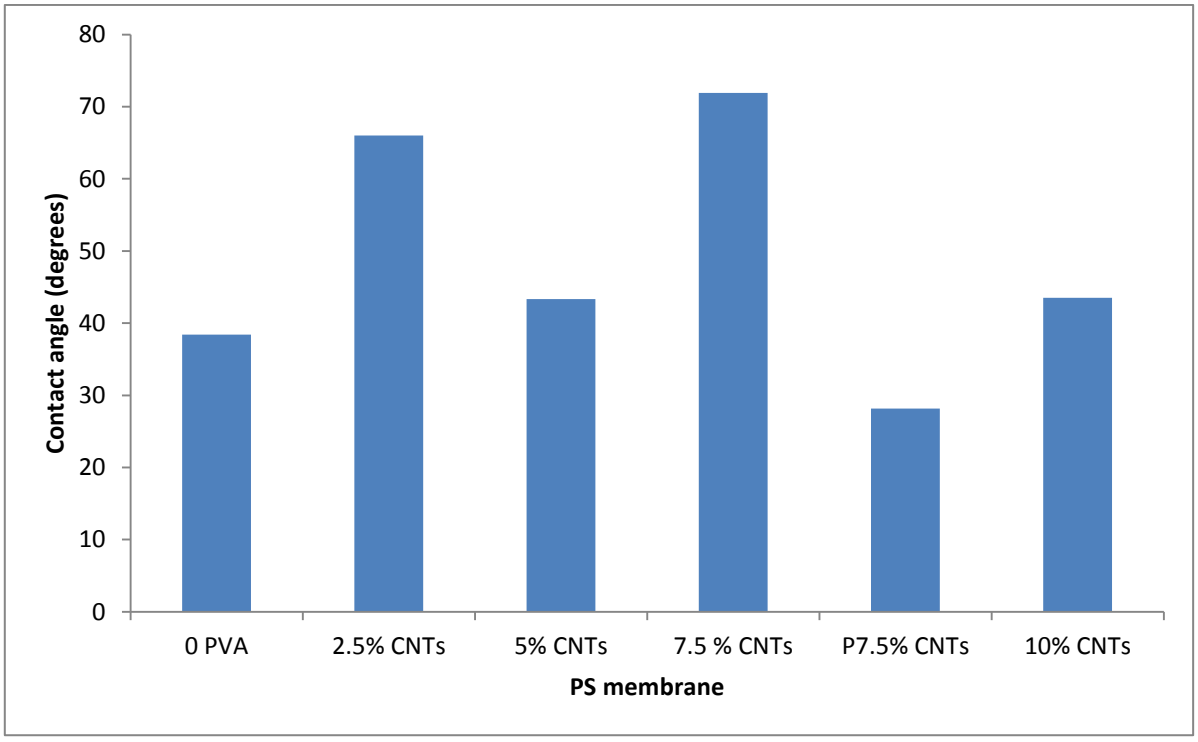


Figure 4.9: Contact angle plot for the PS membranes.

All angles are less than 90^{o}; this means that all membranes are hydrophilic. The plot in figure 4.9 indicates that p7.5 CNTs PS membrane has the lowest contact angle at 28.16^{o} whereas 7.5% CNTs has the highest at 71.92^{o}. This indicates that p7.5% PVA is the most hydrophilic membrane among all other five membranes. 0% CNTs PS membrane is not shown, of which it is expected to be less hydrophilic because it has no PVA layer which induces hydrophilicity. The lowest contact angle of p7.5% CNTs is due to the purified CNTs which

also prolonged the membrane's lifespan. There is an increasing trend between 0 PVA, 5 and 7.5% CNTs PS membrane, i.e., 0 PVA< 5% CNTs < 7.5% CNTs. This shows that 0 PVA is the most hydrophilic membrane among these three. The 5% CNTs PS membrane, on the other side, is the most hydrophilic membrane among the membrane infused with the as-produced CNTs. This implies that as the concentration of the as-produced CNTs is increasing, the hydrophilicity of the membrane decreases. This is because the as-produced CNTs contain the traces of the impurity ferrocene catalyst in their inner diameters in large amount. However, 2.5% and 10% CNTs PS membranes shows opposite relationship (as compared to the other membranes) between the as-produced CNTs and the hydrophilicity. This is due to the disorders that are in the as-produced CNTs as indicated by the Raman spectroscopy analysis.

4.2.4 FTIR analysis

Fourier Transform Infrared (FTIR) spectroscopy was used to analyse the functional groups and the functionalities in the PS membranes. The following results were obtained using the FTIR Bruker Tensor 27 equipment shown in figure 3.8. Figure 4.10 shows the infrared spectra of six PS membranes with different CNT concentrations (0, 2.5, 5, 7.5, 10 and p7.5%) without the PVA layer and the cross-linker MA. As it can be seen, the addition of these different concentrations of CNTs did not have much effect on the IR spectra as the spectra are similar [even similar to the ordinary PS membrane which contains no CNTs (0% CNTs)]. The only difference is their intensities; and when the CNTs were added and purified, the spectra contracted.

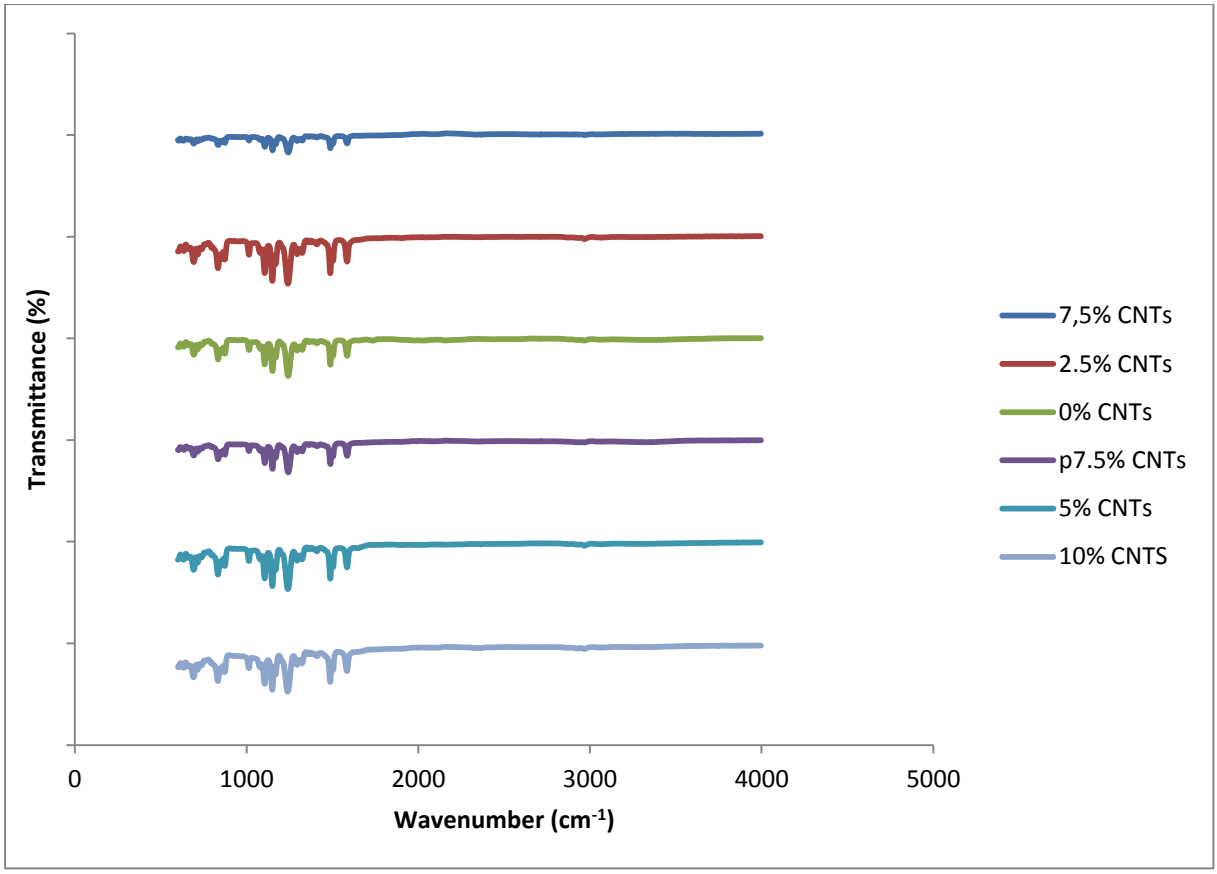


Figure 4.10: Infrared (IR) spectra for 6 PS membranes without PVA layer.

Figure 4.11 and 4.12 shows a clear view of the information in figure 4.10. There are 8 observable peaks in these figures (figures 4.10, 4.11 and 4.12); all due to polysulfone polymer. A peak at 835 cm^{-1} corresponds to a polymer C-H rock group. The peak at 1105 cm^{-1} belongs to a saturated C-C single bond. The 1151 cm^{-1} peak confirms the stretch of the symmetric C-SO_2-C group (Singh et al., 2006). There is a sharp and strong peak at 1242 cm^{-1} which indicates the presence of a stretching ether (C-O-C) group. A medium peak at 1488 cm^{-1} corresponds to the vibrational stretch of CH_3-C-CH_3 bond. Two peaks at 1506 cm^{-1} and 1587 cm^{-1} shows a stretch of C=C bond in the aromatic ring. A weak peak at 2976 cm^{-1} corresponds to the vibrational stretch of the sp^2 carbon-hydrogen (C-H) bond. This peak is due to the addition of CNTs in the membranes as it is also in the FTIR of the CNTs. There is no peak at 1680-1750 cm^{-1}, meaning there is no C=O group in the membrane.

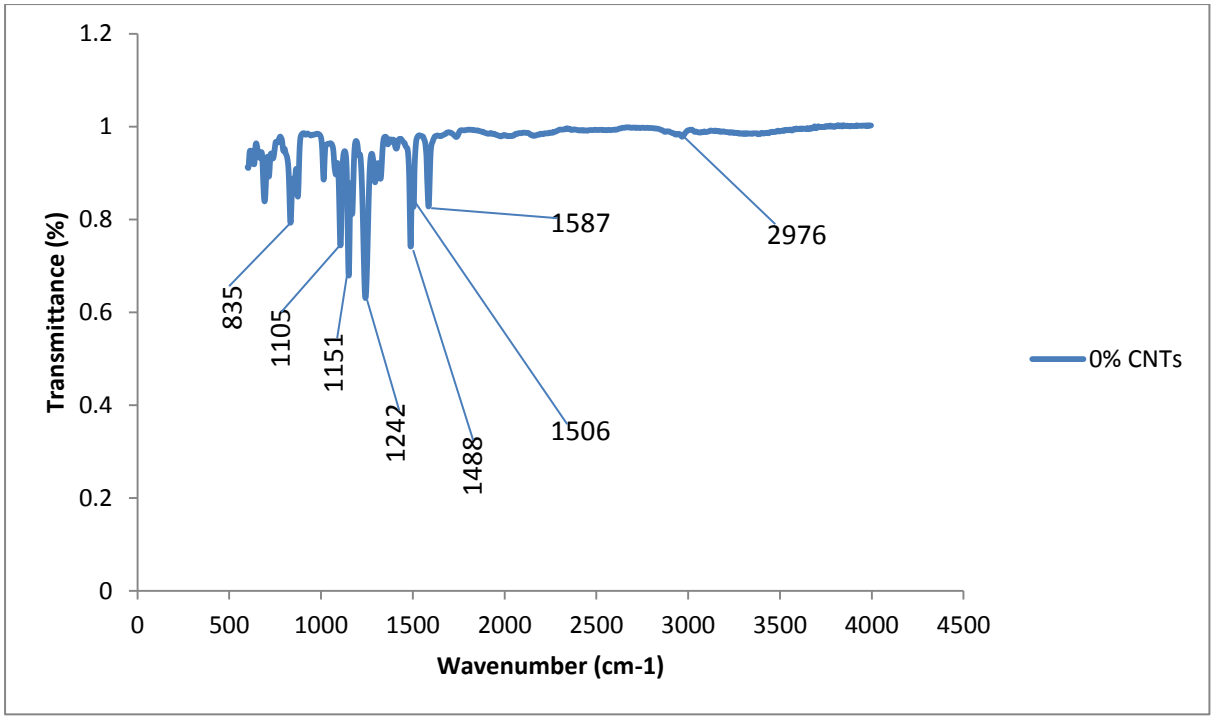


Figure 4.11: IR for the PS membrane with 0% CNTs.

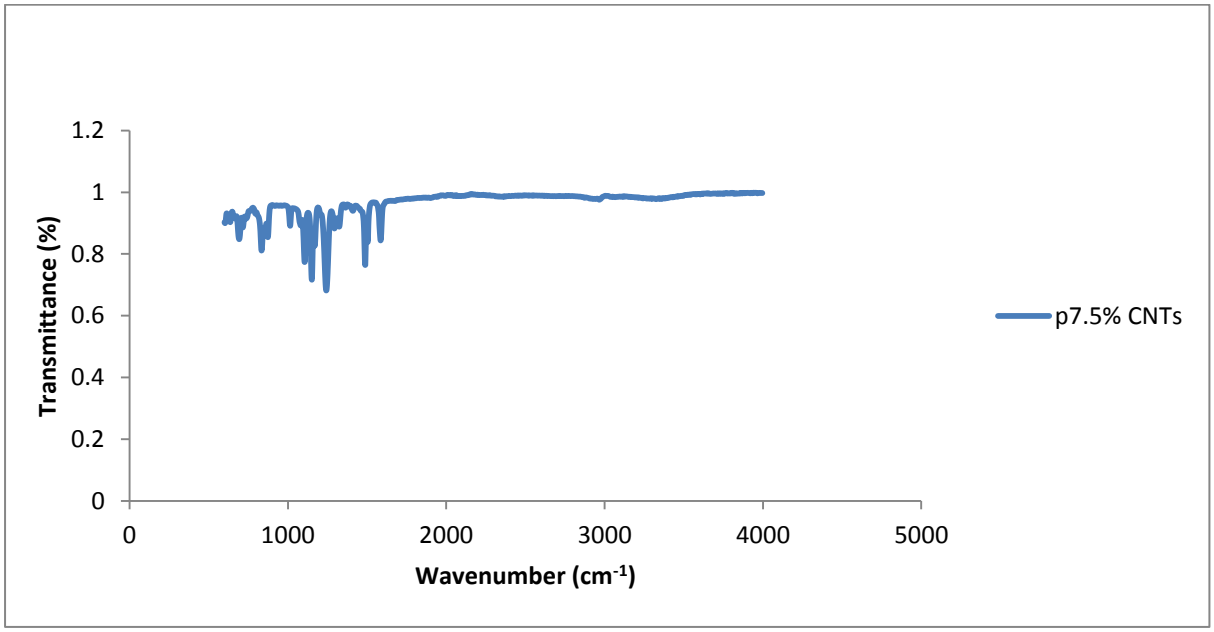


Figure 4.12: IR for the p7.5% CNTs (7.5 % of the pCNTs) PS membrane.

Figure 4.13 below depicts the IR for the PS membrane with p7.5 % CNTs and the PVA layer. All membranes which contain the PVA layer have the same spectra as shown in this figure

since only 1% of PVA was used to cover all membranes. Note that the only difference from this figure to figures 4.10, 4.11 and 4.12 is the additional peak at around 3330 cm^{-1}.

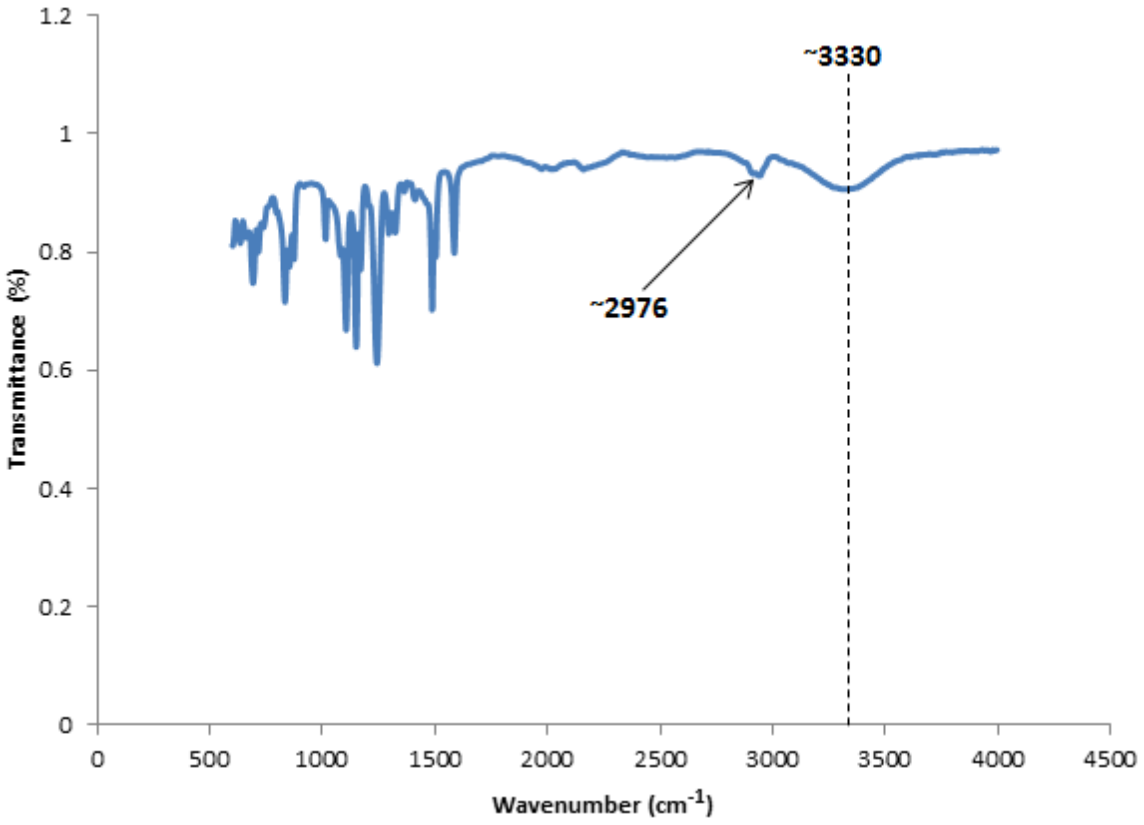


Figure 4.13: IR for p7.5% CNTs PS membrane with the PVA layer.

That broad peak at ~3330 cm^{-1} indicates the presence of an alcohol (O-H) group, because of the addition of PVA layer on the membrane. Surprisingly there is no observable peak between 1750-1650 cm^{-1} to indicate the presence of the C=O group from the addition of MA as a cross linker. These results confirm those in Raman and XRD spectroscopies. The results are also consistent with the literature (Singh et al., 2006; Gohil & Ray, 2009).

4.3 Application of the synthesised membranes for the treatment of oil-containing wastewater

The industrial oil wastewater emulsion used in this work was a metal working fluid (MWF) used to cool work pieces on a lathe provided by Oil skip / South Africa. Metal working fluid differs widely in its character but that it normally consists of water, oil, emulsifier,

antimicrobial additives and solid particles. The bulk of the oil used is typically mineral oil. However organic oil may also be present in small quantities since some of its components could assist in emulsification. The pH of this oil-containing wastewater was determined to be around 8-9, after the removal of the thick emulsion layer and some solids (which is a normal pH for the industrial oil-containing wastewater (Charkrabarty et al., 2010)). According to Charkrabarty et al. (2010) as well as Steward and Arnold (2008), the droplets of oil in this fluid range from 0.02-200 µm with the density around 1001 kg/m^3 (Charkrabarty et al. (2010). Fakhru'l-Razi et al. (2009) reported that the densities of the industrial oil-containing wastewater range from 1014-1140 kg/m^3. The industrial oil-containing wastewater was separated using the Schleicher and Schuell cross flow membrane filtration system (figure 3.12 in chapter 3, section 3.3.8).

4.3.1 Determination of the concentration of the permeate (Cp)

The calibration curve for the determination of the unknown concentration in the permeate (Cp) after the separation of the real industrial oil-containing wastewater, at the flow rates of 46.8, 50.4 and 52.2 L/h, is shown in Figure B.26 (in the appendix B). Cp is measured in order to know if the separated wastewater meets the acceptable discharge limits of 10-15 mg/L, as indicated in chapter one, before being disposed. The data for the curve was obtained using the UV-Vis spectrophotometer shown in figure 3.14. The data is available in the appendix B section.

The unknown oil concentrations in the permeate for all the seven membranes were determined by extrapolation lines corresponding to the known absorbance on the graph, as it can be seen on the figure. At the flow rate of 46.8 L/h, the permeate concentrations were found to be 21, 17, 20, 18, 21, 16 and 19 mg/L for the 0 CNTs (plane PS membrane with no blending of CNTs and PVA layer), 0 PVA (plane PS membrane with only PVA layer), 2.5% CNTs (PS membrane with 2.5% concentration of CNTs and the PVA layer), 5, 7.5, 10 and p7.5% CNTs PS membrane, respectively. Table B.11, in the appendix B, depicts all the Cp values obtained at the three different flow rates.

Figure 4.15 below depicts how Cp varies with the PS membranes containing different amount of CNT concentrations at the three flow rates. The permeate concentration ranges from 16-64

mg/L for all membranes at different flow rates. As the flow rates were increased, for e.g. from 46.8 to 52.2 L/h, the concentration of oil in the permeate also increased.

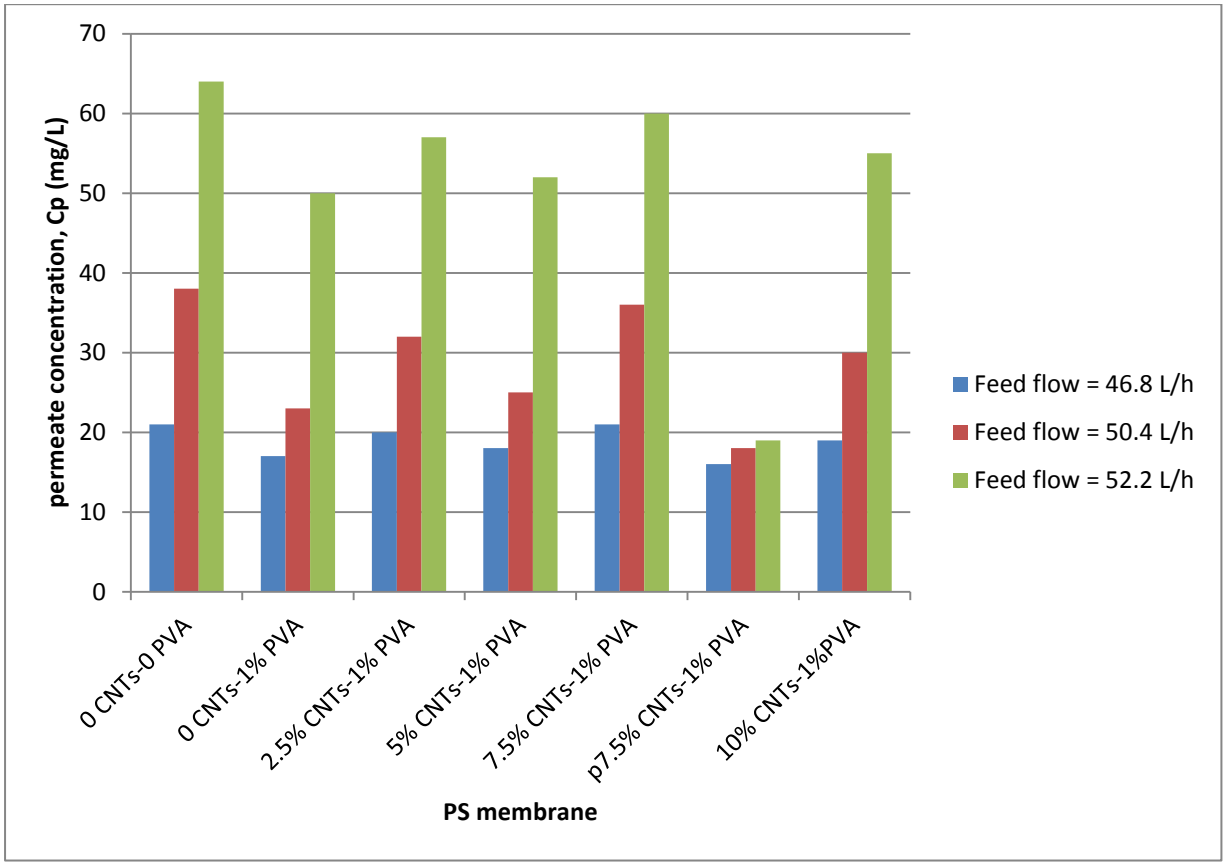


Figure 4.14: Variation of Cp of the PS membrane with different CNT concentrations at the flow rates of 46.8, 50.4 and 52.2 L/h.[2]

These results indicate that all seven membranes did not meet the minimum acceptable discharge limit of 10-15 mg/L. This might be due to the fact that relatively high flow rates were used during the separation since no permeate was achieved at lower flow rates. BET results shows that the pores of the membranes averages between 0.011 - 0.02µm, this might also had an effect on the concentration of oil in the permeate since the oil droplets of the industrial oil-containing wastewater have diameters of about 0.02 - 200µm at room temperature, so when they are heated they become narrower and just drops inside the pores of the membrane (Chakrabarty et al., 2010; Scott et al., 1994; Steward and Arnold, 2008). Oil-containing wastewater, was heated in this case to increase the flux of the permeate (and also

[2] All membranes contain 1% PVA layer, except 0 CNTs which is also not blended with the CNTs. Flow rates represents the rate at which the feed was flowing. **NB:** 0 CNTs-1% PVA = 0 PVA, 0 CNTs-0 PVA = 0 CNTs

to operate at the same industrial working conditions). The Cp concentration of p7.5% CNTs PS membrane, which is the lowest among the PS membrane with different CNT concentration at all flow rates, indicates the improved hydrophilicity of the PS membrane by the pCNTs. 0 PVA, which has the lowest concentration of the permeate; and the 0 CNTs which has the highest concentration in overall, were used for the comparison reasons.

4.3.2 The percentage of the removed oil concentration (R%)

The percentage of the oil concentration removed (R%) was calculated using equation (4) in section 3.3.8, together with the Cp results from section 4.3.1 above. The concentration of oil in the oil-containing wastewater was 372 mg/L. At the flow rate of 46.8 L/h, the rejected concentration of oil was about 94.0, 95.4, 94.6, 95.2, 94.4, 95.7 and 94.9 % for the 0 CNTs, 0 PVA, 2.5% CNTs, 5, 7.5, 10 and p7.5% CNTs PS membrane; respectively (See table B.12 in the appendix for the rejection values at 50.4 and 52.2 L/h). Figure 4.16 shows how the membranes rejected the concentration of oil.

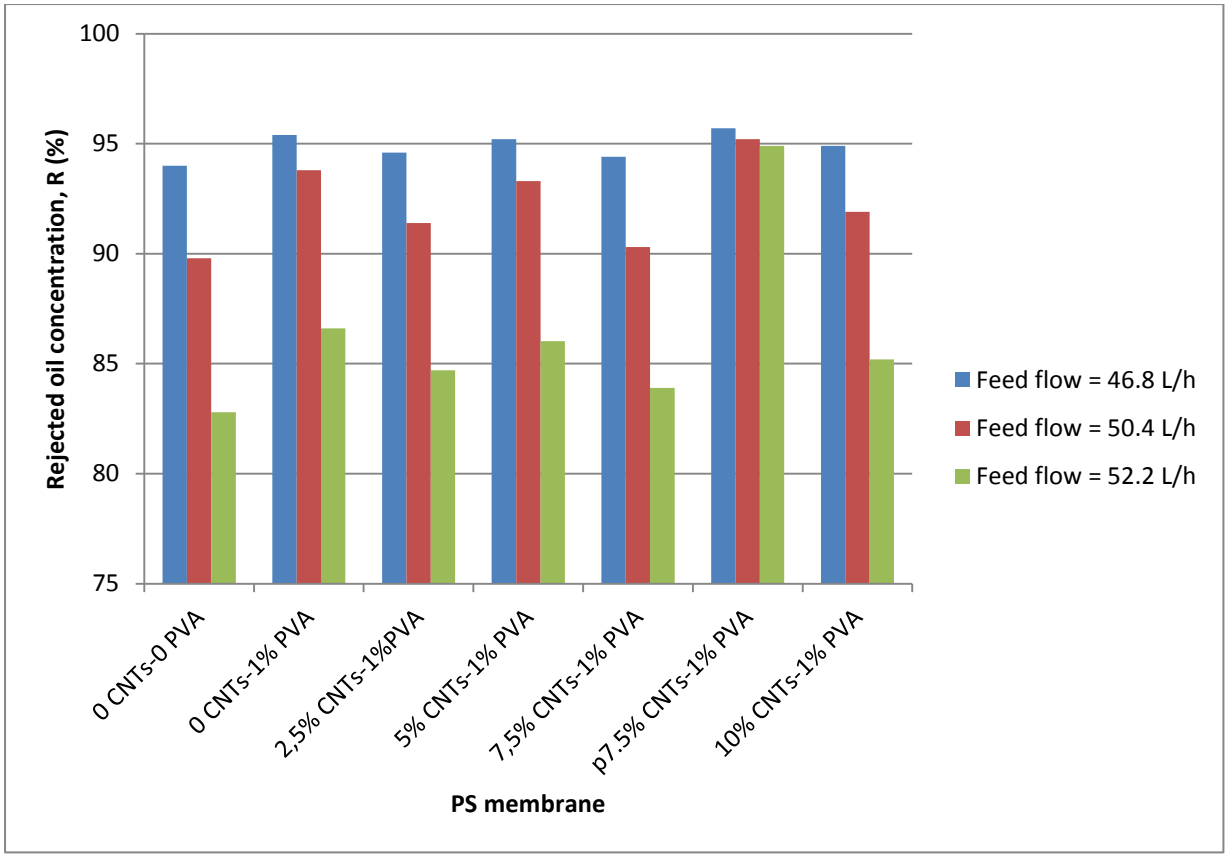


Figure 4.15: The rejected concentration of oil in the retentate, R (%), by the PS membrane with different CNT concentrations.[3]

From the figure, the rejection of oil ranges from 82-95.7% for all PS membranes. P7.5% CNTs, rejected most of the oil with the average of 95.2 % at all flow rates, with the highest rejection of 95.7% being achieved at 46.8 L/h. This is due to the hydrophilic PVA layer that all membranes possess, except the 0 CNTs which rejected the least. This layer only permits water to cross to the permeate and repels the oil. Oil only enters the pores when the feed exerts a force much greater than the opposing capillary force on the surface of the membrane (Chakrabarty et al., 2010), i.e., this only happens when the flow rates or temperature of the feed is increased. The fact that p7.5% CNTs rejected the most (even more than 0 PVA because usually 0 PVA rejects the most (Maphutha et al., 2013), is because it also contains the pCNTs which enhanced the hydrophilicity even further. These results are supported by the contact angle results in which p7.5% CNTs indicated to be the most hydrophilic PS membrane. The results also indicate that, as the flow rate was increased, the rejection of oil

[3] All membranes contain 1% PVA layer, except 0 CNTs which is also not blended with the CNTs. Flow rates represent the rate at which the feed was flowing.

decreased and the Cp increased. Hence the membranes cannot be operated at higher flow rates (pressures). The rejected oil concentration, increases with a decrease of the permeate concentration as it can be seen from both figure 4.15 and 4.16. R (%) also is not proportional to the addition of different CNTs concentration, as it can be seen on these figures, i.e., the percentage rejection increases as follows: 0 CNTs < 7.5% CNTs < 2.5% CNTs < 10 % CNTs < 5% CNTs < 0 PVA < p7.5% CNTs. Hence it is only proportional to and depends on the hydrophilicity of the membrane. In other words, the rejection of oil is inversely proportional to the increasing concentration of CNTs in the PS membranes. The rejection of the concentration of oil is comparable to when the synthetic oil-containing wastewater was used (Maphutha et al., 2013; Chakrabarty et al., 2010).

4.3.3 Membrane flux (MF)

Equation (5) in section 3.3.8 was used to calculate the membrane flux (MF) in order to evaluate the separation performance of the PS membranes. The total effective area of the membrane was 24 cm^2. The flux through the membrane was 50.02, 70.03 and 120.05 $Lh^{-1}m^{-2}$ for the 0 CNTs at the flow rates of 46.8, 50.4 and 52.2 L/h; respectively. Figure 4.17 shows how the flux through the membrane, MF, varies with the flow rates. This plot was used to investigate how the hydrophilicity as well as the porosity affected the separation performance of the membrane. The PS membrane with the lowest MF indicates resistance to fouling as well as good separation performance of that membrane.

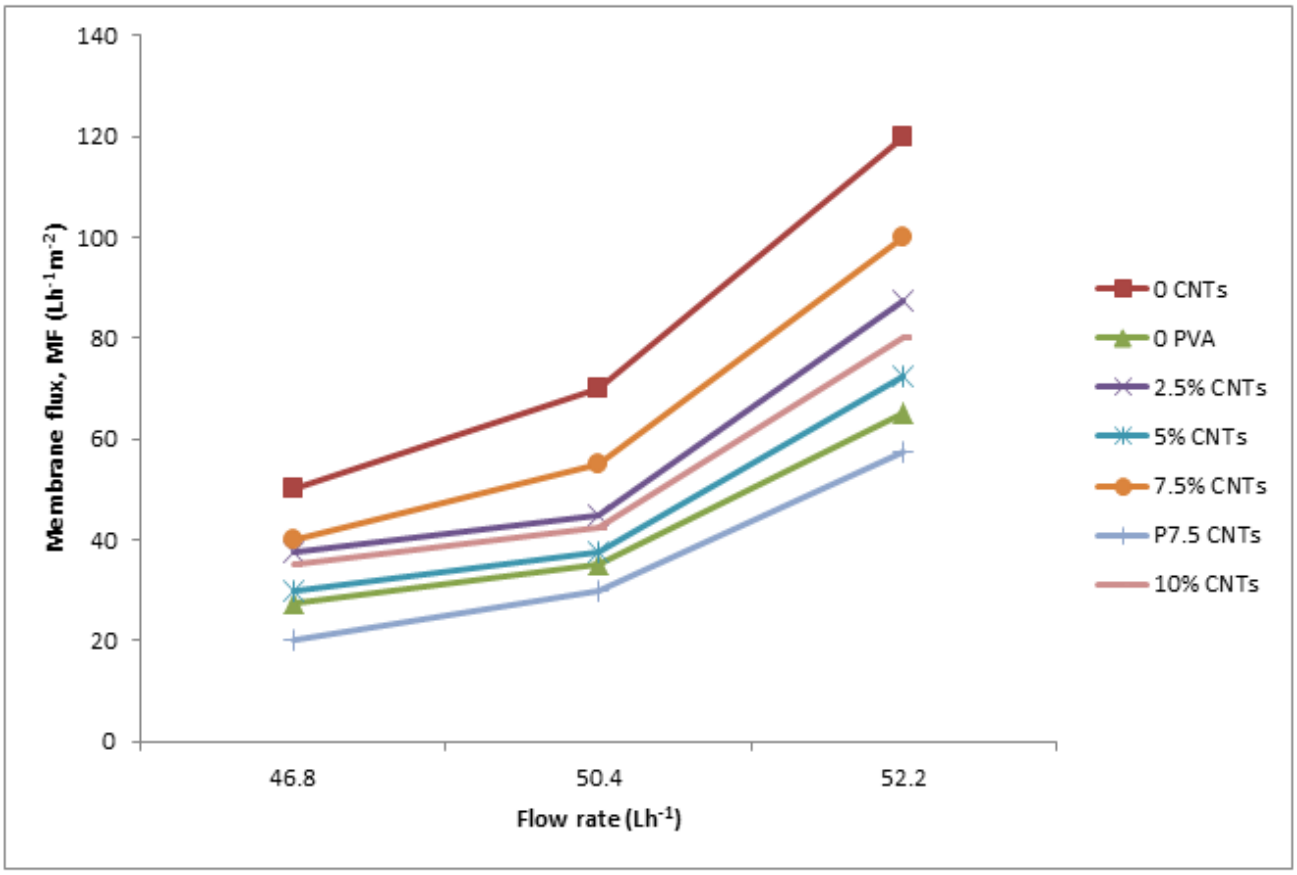


Figure 4.16: Variation of the membrane flux changes with the flow rates and membranes with different concentrations of the CNTs.

As shown in the figure, the membrane's flux increases as the flow rate increases, for all membranes. The values of the membrane's flux ranges between 20.01 and 120.05 $Lh^{-1}m^{-2}$. 0 CNTs and 7.5% CNTs shows very high fluxes, whereas 0 PVA and p7.5% CNTs indicates the lowest fluxes.

The flux through the membrane is affected by the porosity and the hydrophilicity of the membrane (Chakrabarty et al., 2010; Wu et al., 2010). 0 CNTs has the highest fluxes at all flow rates. This implies that the hydrophilicity also increases the membrane's flux but at lower rate since all membranes with the PVA layer (the hydrophilic layer) have lower fluxes, compared to 0 CNTs. The lowest fluxes in 0 PVA and p7.5% further supports this evidence. This is because these two membranes have the lowest contact angles (see figure 4.9) since they are not infused with the highly defected as-produced CNTs. These findings support the fact that the hydrophilicity increases as the flux through the membrane increases.

The addition of different amount of the CNTs also influenced the structure of the membrane (see the SEM images), this affected the membrane flux. BET analysis indicates that the porosity increases with an increase of the amount of the CNTs (see table 2), of which the pCNTs-infused membrane shows low porosity (this is consistent with the hydrophilicity results). 0 PVA membrane indicates the second lowest membrane fluxes at all flow rates. This shows that the addition of the as-produced CNTs further increases the membrane's flux. This implies that the porosity of the membrane increases the membrane's flux. This is achieved because the as-produced CNTs (due to their graphitic and defected nature, see the Taman spectroscopy analysis) increases the porosity of the membranes thereby permitting the oil concentration to easily pass through the pores without any or with minimum hindrance (Maphutha et al., 2013). The rejected oil concentration showed to increase with an increase in the addition of pCNTs, and decrease with an increase in the concentration of the permeate, the amount of the as-produced CNTs. This means that the rejected oil concentration is inversely proportional the porosity of the membrane. Hence the flux through the membrane increases with an increase concentration of the permeate and a decrease in the concentration of the rejected oil. The p7.5% CNTs PS membrane has the lowest membrane flux because it had the highest rejections due to its increased hydrophilicity and lower porosity. These fluxes are much lower compared to when the synthetic oil-containing wastewater was used due to the reduced pores of the membranes and the nature of the real industrial oil-containing wastewater (Maphutha et al., 2013). These results are comparable to the literature (Celik et al., 2011; Mondal and Wickramasinghe, 2008; Okiel et al., 2015).

Figure 4.18 shows how the membrane's flux behaves as time increases at a flow rate of 52.2 Lh^{-1}. The seven PS membranes used are shown in the figure.

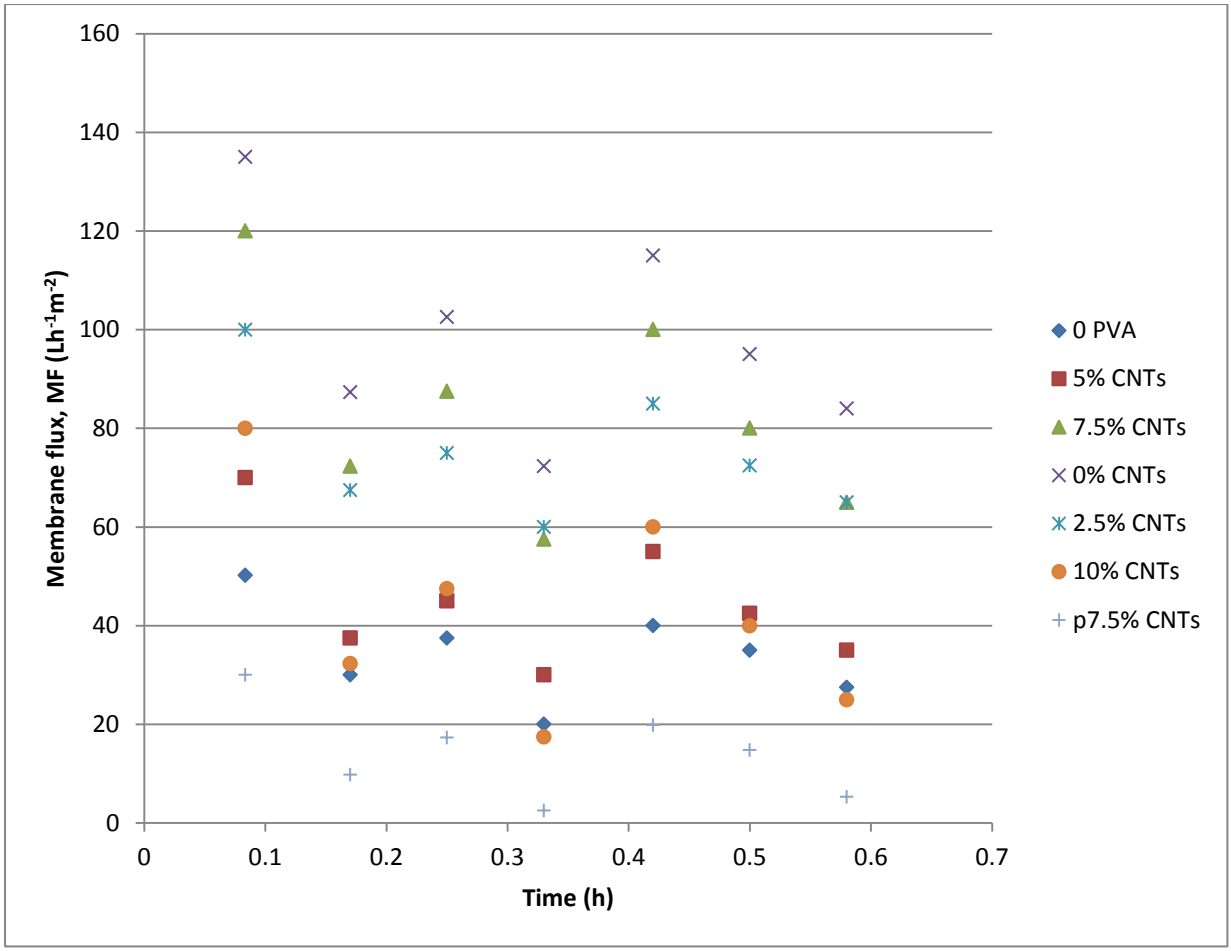


Figure 4.17: The flux of the membrane as a function of time.

From the figure, it can be seen that as time increases, the membrane flux decreases for all membranes. 0% CNTs and 7.5% shows the highest membrane flux over time, whereas 0 PVA and p7.5% CNTs indicates the least. This difference is due to their porosity (Table 1) and hydrophilicity (Figure 4.9), i.e., the lower the porosity, the higher the hydrophilicity and hence the lower the membrane's flux overtime. The additives in the CNTs also have an effect on the membrane's flux (Chakrabarty et al., 2010). Hence the decrease in the MF is also due to a decrease in concentration of the as-produced CNT (which had very high level of defects, figure 4.1) loading. This is supported by the lowest MF in p7.5% membrane and the 0 PVA, as well as fouling and concentration polarisation at higher flow rates (Chakrabarty et al., 2008), of which in this case are minimised, but not completely removed, since MF increased as the flow rates were increasing (Figure 4.17). The higher concentration of oil in the retentate also indicates the minimised fouling and concentration polarisation. Hence the membrane's flux decreases as time increases. These results are consistent with the previous findings in the literature (Maphutha, 2014; Phao et al., 2013; Chakrabarty et al., 2010).

4.3.4 The relative flux

Figure 4.19 shows the relative flux (RF), as a function of time, the PS membranes used are shown in the figure. The values were calculated using equation (6) in section 3.3.8, of which the S_F was the MF value for the 0 CNTs PS membranes at all flow rates. This plot measures whether the PS membranes that were used were resistant to fouling and concentration polarisation or not.

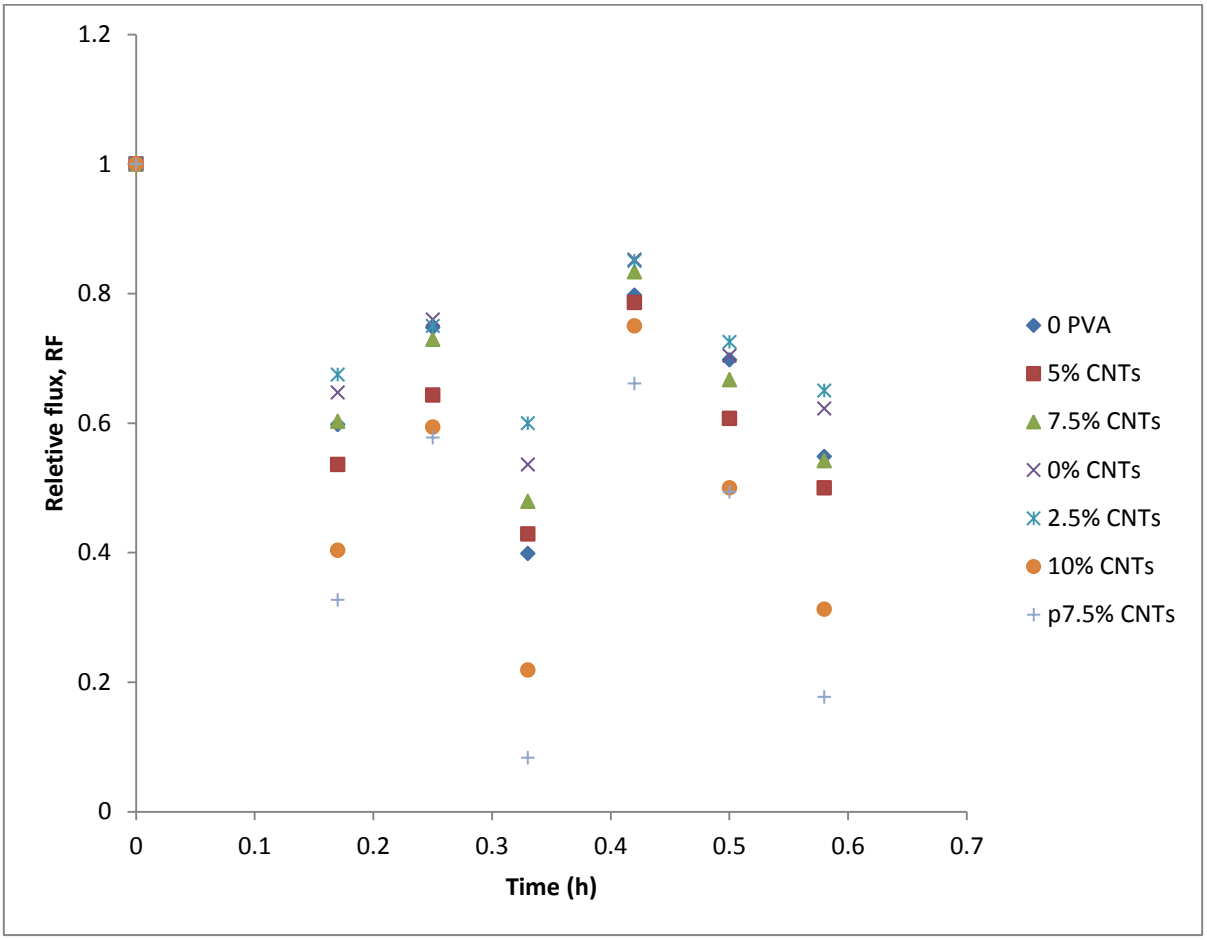


Figure 4.18: Relative flux as a function of time.

As it can be seen from the figure, the general trend is that RF decreases as the time is increased. This behaviour is similar to the flux of the membrane in figure 4.18. Hence RF is proportional to the MF and inversely proportional to the rejected concentration of oil in the retentate. On the other hand, RF is decreases as the flow rate increases. This decrease in RF is due to the membranes starting to show indication of accumulating fouling and concentration polarisation at higher flow rates (Chakrabarty et al., 2010), i.e., the pores of the membranes were starting to be blocked a little. As it can be seen, there is no significant accumulation of

fouling and concentration polarisation. This is because all the membranes contained a hydrophilic layer which minimised this. The fact that p7.5% CNTs membrane has the smallest RF shows that the membrane was the smallest to be affected by fouling. High oil rejections showed by these membranes indicates that fouling was successfully controlled. 0 CNTs membrane has the highest RF since it has no PVA layer or any amount of CNTs. RF is directly proportional to the increasing concentration of the CNTs. Hence 7.5% CNT membrane did not perform to expectations. This indicates that the membranes with non-purified or functionalised CNTs could easily be affected by fouling. In this case fouling was minimised for those membranes without pCNTs or fCNTs, because they contained the hydrophilic layer. These findings are consistent with those in the literature (Ebrahimi et al., 2009; Chakrabarty et al., 2010; Koltuniewicz, 1992).

4.3.5 The decrease in flux, DF (The flux decline)

Figure 4.20 shows the variation of the decrease in flux, DF, with the change in the concentration of the PS membranes, the DF values were obtained using equation (7) in section 3.3.8 with 0 CNTs as initial conditions. The higher the DF value, the greater the performance of the membrane.

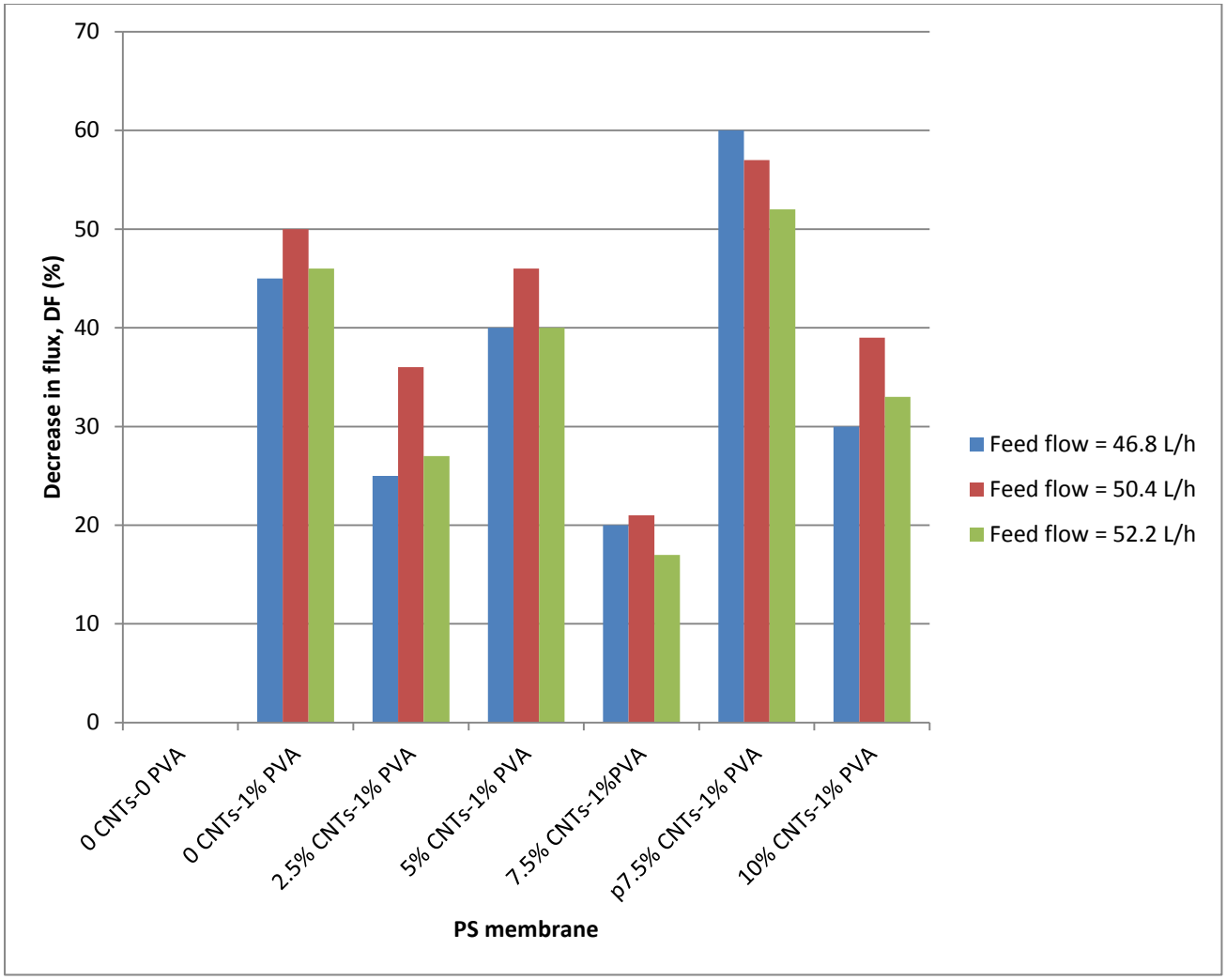


Figure 4.19: Variation of DF with PS membranes containing different concentration of CNTs.

The PS membrane that showed the highest decrease in flux was p7.5% CNTs with the greatest decline at 46.8 L/h**.** The flux through the membrane increased as the flow rates increased. This confirms the hydrophilicity of this membrane and shows how it was resistant to fouling. The flux through the 0 CNTs PS membrane also followed the same pattern. This is due to that this membrane is the second highest performing membrane with the greater oil rejection. The least performing membrane which contains CNTs is the 7.5% CNTs. The performance shown by this membrane is different as it was one of the second best performing CNT infused membrane when the synthetic oil was used. The best performing membrane containing the as-produced CNTs is 5% CNTs as it showed the third highest decrease in flux for all flow rates. These results are comparable to the literature (Chakrabarty et al., 2008; Koltuniewicz et al., 1995).

In summary, the separation performance of these membranes is consistent to the separation performance those membranes when the synthetic oil-containing wastewater that was used earlier (Maphutha et al., 2013). In this case the increasing trend (from the least performing to the best) is as follows: 0 CNTs < 7.5% CNTs < 2.5% CNTs < 10 % CNTs < 5% CNTs < 0 PVA < p7.5% CNTs, that is, p7.5% CNTs is the best performing membrane in this case. The 5% CNTs membrane was the best performing membrane for the membranes without the pCNTs. In case of the synthetic oil-containing wastewater, the increasing trend was as follows: 10% CNTs < 7.5% CNTs < 5% CNTs < 0 PVA. The overall best membrane was 0 PVA. The CNTs were not purified when the synthetic oil-containing wastewater was used. The best membrane in terms of concentration of CNTs was also 5% in this case. The separation performance increases as the CNT concentration is decreased. This confirms once again that the separation performance of the membrane is inversely proportional to the increasing concentration of the CNTs. The rejection of the concentration of oil was almost the same. The only major difference is that, in this case, the concentration of oil in the permeate is above the acceptable discharge limit of 10-15 mg/L, of which after some little modifications, these membranes will be able to reach the discharge limit. These results suggests that, a composite PS membrane with the PVA layer and the pCNT has a potential to produce a great separation performance only if the PS solution is reduced to lower concentrations in order to increase the pore size which will maximise the flux. The fact that the acceptable discharged limit was not met is because of the nature of the industrial oil-containing wastewater (the size of the droplet and the value of pH, (Chakrabarty et al., 2010)), however, with some little modification this will be met in future. The membranes continue to show good rejection performance, which is owed to the hydrophilic layer as well as the pCNTs for the p7.5% CNTs membrane. At the moment the best recommended PS membrane is the p7.5% CNTs.

CHAPTER 5: CONCLUSIONS AND RECOMMENDATIONS

5.1Conclusions

The aim of this project was to optimise the synthesis and the separation performance of nanotube-infused polysulfone membrane with a polyvinyl alcohol layer to separate oil-containing wastewater. The phase inversion immersion method was used to synthesize all the membranes involved in this project. Seven membranes were produced; the first four contained both the as-produced CNTs and the polyvinyl layer in different concentration, the fifth membrane was composed of the pCNTs and the polyvinyl alcohol layer, the sixth did not contain any CNT or polyvinyl alcohol layer and seventh membrane contain the polyvinyl alcohol layer but no CNTs. Thus from the characterisations of the CNTs and the membranes as well as the separation performances, it can be concluded that:

- Ferrocene can be used as both the source of carbon and the catalyst for the synthesis of CNTs when using argon as the carrier gas and nitrogen gas as the contaminant remover.
- Ferrocene as a catalyst produces MWCNTs with length of about 600-950 nm at 850^{o}C using a vertical-swirled chemical vapour deposition method.
- The mixture of nitric acid and the sulphuric acid in a ratio 1:3 is effective for the functionalization of the CNTs; it has removed about 59% of the contaminated particles.
- Hydrofluoric acid, together with distilled water, hydrochloric acid and metal oxidation process can be used to remove about 90% of the catalyst particles. This is indicated quantitatively by the TGA, EDS (both more than 99% of the catalyst particles impurities removed) and XRD (more than 91% removed).
- The use of 20% polysulfone/solvent solution reduces the pore sizes of the membranes and improves the quality of the membrane; the inclusion of the CNTs decreases the pore sizes.
- The concentration of oil in the permeate during the separation of oil-containing wastewater increases with an increase in the feed flow rate.
- The rejected concentration of oil in the retentate is proportional to the increase of the amount of CNTs (both purified and as-grown), but inversely proportional to the increase in feed flow rate and the concentration of oil in the permeate.

- The flux of the membrane increases with an increase in feed flow rate but high flux decreases the separation performance of the membrane (rejection%).
- Hydrophilicity of the membrane improves the separation performance of the membrane, by rejecting very high concentration of oil in the wastewater. All membranes rejected oil of more than 82% at all flow rates. Hydrophilicity is also inversely proportional to the concentration of the as-produced CNTs. 5 % CNTs PS membrane was more hydrophilic than 7.5% CNTs PS membrane, with the contact angles of 43.34 and 71.92º, respectively.
- The rejection capacity of these membranes on industrial oil-containing wastewater is similar to results when synthetic oil was used (Maphuta et al., 2013).
- 5% CNTs PS membrane is the best performing membrane containing the as-produced CNTs amongst the PS membranes. Thus these results also confirm those indicated by Maphutha et al. (2013) when synthetic oil containing wastewater was used. It was found that 5% CNTs PS membrane produces high throughput and oil rejection of more than 95% at the flow rate of 46.8 L/h and more than 86% at the flow rate of 52.2 L/h during the separation of the real industrial oil-containing wastewater. This membrane was also the best performing membrane during the separation of the synthetic oil-containing wastewater. It is also the second overall best performing membrane in this project for the membranes which are infused with CNTs.
- The p7.5% CNTs is by far the best overall performing PS membrane in this project than any other membrane, including 0 PVA membranes (which were used only for the comparison purposes). It has rejected more than 95% at the flow rate of 46.8 L/h and more than 94% at higher flow rate of 52.2 L/h, using the industrial oil-containing wastewater. Thus the more the hydrophilic the membrane is, the greater is its performance.
- High rejections of oil concentration do not always imply that the minimum discharge limits are met. The concentration of oil in the permeate for all these membranes did not meet the minimum discharge limit of 10-15 mg/L, only the closest PS membrane was p7.5% at 16 mg/L. This was mainly due to the nature of the industrial oil-containing wastewater with higher pH (8-9) and very small droplets.
- To answer the raised questions in section 1.3, it can be concluded that:
  - The use of 20% PS solution improves the quality of the membrane but reduces the porosity which in turn reduces the membrane's flux but maintains the separation

performance of the membrane since all membranes have rejected the concentration of oil in the retentate of over 82%.

- The utilisation of the purified CNTs increases the hydrophilicity which in turn improves the fouling resistance and enhances the mechanical stability of the membrane.
- Thus the separation performance of the PS membrane with the PVA layer and the pCNTs is greater than that with the infused as-produced CNTs.

5.2Recommendations

- Further modifications are needed in order for the membrane to meet the minimum discharge limits.
- Alternative ways of producing completely pCNTs is required in order to avoid the use of acids. Afolabi et al. (2007) has indicated that pure CNTs could be synthesised at the temperature range of 1000 or 1050^{o}C. An assessment of the cost analysis between the methods presented in this work and the Afolabi et al. (2007) methods may be required. Otherwise the use of a strong acid which will not damage the structure of the CNTs is also recommended.
- The concentration of polysulfone/solvent solution should remain at 10% (in case polyether glycol is used) as it has shown that those membranes contained higher pore sizes which maximised the flux, but a polymer such as polyether glycol or polyvinyl pyrolidone should be used as an additive in the water bath in order to increase the pore sizes in the membranes when using use 20% polysulfone solution.
- SEM images show the arrangement of components in the cross section of the PS membranes for the non-PVA layered membranes.
- The CNTs, which could not be seen in those images, were blended by first being dissolved in the solvent and stirred with the magnetic stirrer equipped with a magnetic bar until the solution was homogeneous when the PS pellets were added. For further modifications, dissolve the PS solution until is homogeneous and then use the ultra-sonication to disperse the CNTs.
- Curing temperature (membranes should be dried at room temperature), water-soluble layer other than PVA (such as, for e.g., Polyhydroxyalky acrylates) and a type of

solvent other than dimethylformamide, DMF (e.g., 1-Methyl-2-pyrrolidinone, NMP) – which was used to prepare the polysulfone solution, should be investigated.

- Separation performance of the membrane is also affected by operating conditions at which the separation is conducted. Further investigation of the operating variables such as temperature, feed flow rate, upstream pressure is essential.
- The FTIR spectra does not show the introduction of any new functional group present in both the fCNTs and the pCNTs, because of the defected and graphitic nature of the CNTS and that functionalization was performed before purification. Hence is advisable that, functionalization be performed after purification in future in order to be able to obtain functional groups on the structure of the CNTs.
- Moderate fluxes were due to the reduced pores of the membranes because of the use of higher concentration of PS solution, this need to be modified in the near future.

REFERENCES

1. Abadi, S. R., Sebzari, M. R., Rekabdar, M. H. & Mohammadi, T. (2011). Ceramic membrane performance in microfiltration of oily wastewater. Desalination, 265, pp. 22–228.

2. Afolabi, A.S., Abdulkareem, A.S., Iyuke, S.E. (2007). Synthesis of carbon nanotubes and nanoballs by swirled floating catalyst chemical vapour deposition method. Journal of Experimental Nanoscience, 2, pp. 269-277.

3. Afolabi, A.S., Abdulkareem, A.S., Mhlanga, S.D., Iyuke, S.E. (2011). Synthesis and purification of bimetallic catalysed carbon nanotubes in a horizontal CVD reactor. Journal on Experimental nanoscience, 6, pp. 248-262.

4. Agboola, A. E., Pike, R. W., Hertwig, T. A. & Lou, H. H. (2007). Conceptual design of carbon nanotube processes. Clean Technologies and Environmental Policy, 9, pp. 289-311.

5. Ahmed, F.E., Lalia, B.S., Hashaikeh, R. (2015). A review on electrospinning for membrane fabrication: Challenges and applications. Desalination, 356, pp. 15–30.

6. Al-Amoudi, A. & Lovitt, R. W. (2007). Fouling strategies and the cleaning system of NF membranes and factors affecting cleaning efficiency. J. Membrane Sci., 303, pp. 6–28

7. Al-Jeshi, S., Neville, A. (2008). An experimental evaluation of reverse osmosis membrane performance in oily water. Desalination, 223, pp. 287-294.

8. Alibaba. (retrieved 2015). Oil water separator prices. www.Alibaba.com/trade

9. Alpatova, A., Meshref, M., McPhedran, K.N., El-din, M.G. (2015). Composite polyvinylidene fluoride (PVDF) membrane impregnated with Fe_2O_3 nanoparticles and multiwalled carbon nanotubes for catalytic degradation of organic contaminants. Journal of membrane science, 490, pp. 227-235.

10. Alsawat, A., Altalhi, T., Kumeria, T., Santos, A., Losic, D. (2015). Carbon nanotube-nanoporous anodic alumina composite membranes with controllable inner diameters and surface chemistry: Influence on molecular transport and chemical selectivity. Carbon, doi: http://dx.doi.org/10.1016/jcarbon.2015.05.090.

11. AMI membranes. (retrieved 2015). Reverse osmosis RO membranes, water anywhere. http://www.wateranywhere.com/index.php?cPath=22_29_225&_ga=1.167464126.1005634027.1440877021

12. Aoustin, E., Schafer, A.I., Fane, A. G. and Waite, T. D. (2001). Ultrafiltration of natural organic matter. Separation and Purification Technology, pp. 22-23, pp.63-78.

13. Apel, P. (2001). Tracketching technique in membrane technology. Radiation Measurements 34, pp. 559–566.

14. API (American Petroleum Institute). (1969). Manual on disposal of refinery wastes. American Petroleum Institute, Washington, DC.

15. API (American Petroleum Institute). (1990). Design and Operation of Oil-Water Separators. American Petroleum Institute, Washington, D.C. Publication 421.

16. Arthur, J.D., Langhus, B.G., Patel, C. (2005). Technical summary of oil and gas produced water treatment technologies. All consulting, LCC, Tulsa USA.

17. Baek, Y., Kim., C., Seo., D.K., Kim, T., Lee, J.S., Kim, Y.H., Ahn, K.H., Bae, S.S., Lee, S.C., Lim, J., Lee, K., Yoon, J. (2014). High performance and antifouling vertically aligned carbon nanotube membrane for water purification. Journal of membrane science, 460, pp. 171-177.

18. Baker, J.S.; Dudley, L.Y. 1998. Biofouling in membrane systems — A review. Desalination, 118, pp. 81–89.

19. Baker, L.A.; Martin, Choi (2006). Current Nanoscience. Nanomedicine: Nanotechnology, Biology and Medicine, 2, pp. 243–255.

20. Baker, R. (2012). Microfiltration, in Membrane Technology and Applications. John Wiley & Sons Ltd, 3rd edn, California. pp. 303.

21. Baker, R.W. (2004). Membrane Technology and Applications, England: John Wiley & Sons Ltd.

22. Barreiro, A., Hampel, S., Rummeli, M.H., Kramberger, C., Gruneis, A. (2006). Thermal decomposition of ferrocene as a method for production of single-walled carbon nanotubes without additional carbon sources. Journal of Physical Chemistry B, 110, pp. 20973-20977.

23. Bertera R, Steven H, Metcalfe M. (1984). Development Studies of cross-flow filtration. The Chemical Engineer, 401, pp. 10.

24. Bevis, A. (1992). The treatment of oily water by coalescing. Filt. Sep., pp. 295–301.

25. Beychok, Milton R. (1967). Aqueous Wastes from Petroleum and Petrochemical Plants (1st ed.). John Wiley & Sons.

26. Bom, D., Andrews, R., Jacques, D., Anthony, J., Chen, B., Meier, M.S., Selegue, J.P. (2002). Thermogravimetric Analysis of the Oxidation of Multiwalled Carbon Nanotubes: Evidence for the Role of Defect Sites in Carbon Nanotube Chemistry. Nano letters, 2 (6), pp. 615-619.

27. Boncel, S., Pattison, W.S., Geiser, V., Shaffer, M.S.P., Koziol, K.K.K. (2014). En route to controlled catalytic CVD synthesis of densely packed and vertically aligned nitrogen-doped carbon nanotube arrays. Beilstein Journal of Nanotechnology, 5, pp. 219-233.

28. Borup, R., Meyers, J., Pivovar, B., Kim, Y.S., Mukundan, R., Garland, N., Myers, D., Wilson, M., Garzon, F., Wood, D., Zelenay, P., More, K., Stroh, K., Zawodzinski, T., Boncella, J., McGrath, J.E., Inaba, M., Miyatake, K., Hor,i M., Ota, K., Ogumi, Z., Miyata, S., Nishikata, A., Siroma, Z., Uchimoto, Y., Yasuda, K., Kimijima, K., Iwashita, N. (2007). Scientific aspects of polymer electrolyte fuel cell durability and degradation. Chemical Reviews, 107 (10), pp. 3904–3951

29. Brunauer, Emmett, P.H., Teller, E. (1938). Adsorption of Gases in Multimolecular Layers. J. Am. Chem. Soc., 60 (2), pp.309–319.

30. Cao, Q., Rogers, J. A. (2009). Ultrathin Films of Single-Walled Carbon Nanotubes for Electronics and Sensors: A Review of Fundamental and Applied Aspects. Adv. Mater., 21, pp. 29– 53.

31. Calvero (2006, retrieved 2014). A polysulfone repeating unit. http://commons.wikimedia.org/wiki/File:Polysulfone_repeating_unit.png

32. Casellas-Salha, C., Acobas, F., Bontoux, J., Moreaud, H. (1981). Testing the flocculation/coagulation of wastewater by granulometric analysis of suspended solids in the water using laser diffraction meter. Water Research, Volume 15, Issue 8, pp. 969-975.

33. Celik, E., Park, H., Choi, H., Choi, H. (2011). Carbon nanotube blended polyethersulfone membranes for fouling control in water treatment. Water Research, 45, pp. 274-282.

34. Chakrabarty, B., Ghoshal, A. K. & Purkait, M. K. (2010). Cross-flow ultrafiltration of stable oil-in-water emulsion. Chem. Eng. J. 165, pp. 447–456.

35. Chakrabarty, B., Ghoshal, A. K. & Purkait, M. K. (2008). Ultrafiltration of stable oil-in-water emulsion by polysulfone membrane. J. Membrane Sci., 325, pp. 427–437.

36. Chen, X., Hong, L., Xu, Y., Ong, Z.W. (2012). Ceramic Pore Channels with Inducted Carbon Nanotubes for Removing Oil from Water. ACS Appl. Mater. Interfaces, 4 (4), pp. 1909–1918.

37. Cheryan, M. (1998). Fouling and Cleaning in Ultrafiltration and Microfiltration Handbook. 2nd edn., CRC Press, Florida, pp. 1-9.

38. Chiang, I.W., Brinson, B.E., Smalley, R.E., Margrave, J.L., Hauge, R.H. (2001.). Purification and characterization of single-walled carbon nanotubes. Journal of Physical Chemistry B,105, pp. 1157-1161.

39. Choi, H., Zhang, K., Dionysiou, D.D.,Oerther, D.B.& Sorial, G.A. (2005) Effect of permeate flux and tangential flow on membrane fouling for wastewater treatment. J. Separation and Purification Technology, 45, pp.68-78.

40. Chuang, W.Y., Young, T.H., Chiu, W.Y., Lin, C.Y. (2000). The effect of polymeric additives on the structure and permeability of poly(vinyl alcohol) asymmetric membranes. Polymer, 41, pp. 5633–5641.

41. Chung, C.V., Buu, N.Q., Chau, N.H. (2005). Influence of surface charge and solution pH on the performance characteristics of a nanofiltration membrane. Science and technology of advanced materials, 6, pp. 246-250.

42. Clever, M.; Jordt, F., Knauf, R.; Räbiger, N., Rüdebusch, M., Hilker-Scheibel, R. (2000). Process water production from river water by ultrafiltration and reverse osmosis. Desalination ,131 (1-3), pp.325–336.

43. Colic, M., Morse, D.E., Morse, W.O., Matherly, T.G., Carty, S., Miller, J.D. (2001). From air-sparged hydrocyclone to bubble accelerated floatation.

44. CPO, Centrifugal-Pump.Org. (2015). Horizontal vs vertical design. centrifugal-pump.org/pump_horizontal_vertical, retrieved 2015.

45. Crittenden, J, Trussell, R, Hand, D, Howe, K & Tchobanoglous, G. (2012). Principles of Water Treatment. John Wiley and Sons, New Jersey., 2nd edn., 8.1

46. Daraei, P., Madaeni, S.S., Ghaemi, N., Khadivhi, M.A., Astinchap, B., Moradian, R. (2013). Enhancing antifouling capacity of PES membrane via mixing with various types of polymer modified multi-walled carbon nanotubes. Journal of membrane science, 444, pp. 184-191.

47. De Volver, M.F.L., Tawfick, S.H., Baughman, R.H., Hart, A.J. (2013). Carbon nanotubes: Present and future commercial applications. Science, 339, pp. 535-539.

48. Doménech-Carbó, M.T., Aura-Castro, E. (1999). Evaluation of the phase inversion process as an application method for synthetic polymers in conservation work. Studies in Conservation, 44, pp. 19-28.

49. Dumee, L., Campbell, J.L., Sears, K., Schultz, J., Finn, N., Duke, M., Gray, S. (2011). The impact of hydrophobic coating on the performance of carbon nanotube bucky paper membranes in membrane distillation. Desalination, 283, pp. 64-67.

50. Ebrahimi, M., K. Shams Ashaghi, L. Engel, D. Willershausen, P. Mund, P. Bolduan, P. Czermak. (2009). Characterization and application of different ceramic membranes for the oil-field produced water treatment. Desalination, 245, pp.533–540

51. Edzwald, J. (1995). Principles and applications of dissolved air floatation. Water Science and Technology, 31 (3), pp 1-23,

52. Environmental Protection Agency (EPA). Cruise ship discharge assessment report. (December 28, 2008-retrived 2014). Section 4: Oily Bilge Water. http://www.epa.gov/owow/oceans/cruise_ships/disch_assess.html.

53. Environmental technology centre. (retrieved 2015). Membrane filtration http://www.nottingham.ac.uk/etc/sol_m_membranefiltration.php

54. Everett, D.H. (1988). Characterization of Porous Solids. Editors: Unger, K.K., Rouquerol, J., Sing, K.S.W and Kral, H. Elsevier, Amsterdam, pp. 1-21.

55. Fakhru'l-Razi, A., Pendashteh, A., Abdullah, L.C., Biak, D.R.A, Madaeni, S.S., Abidin, Z.Z (2009). Review of technologies for oil and gas produced water treatment. Journal of Hazardous Materials, 170, pp. 530-551.

56. Farahbakhsh, K., Adham, S. S., Smith, D. W. (June 2003). Monitoring the Integrity of Low-Pressure Membranes. Journal AWWA, pp. 95–107.

57. Feng, C., Khulbe, K.C., Matsuura, T. (2010). Recent Progress in the Preparation, Characterization, and Applications of Nanofibers and Nanofiber Membranes via Electrospinning/Interfacial Polymerization. Journal of Applied Polymer Science, 115, pp.756–776.

58. Flemming, H.C., Schaule, G., Griebe, T., Schmitt, J., Tamachkiarowa, A. (1997). Biofouling—the Achilles heel of membrane processes. Desalination, 113, pp.215–225.

59. Flottweg Separation technology. (Retrieved 2014). http://www.sgconsulting.co.za/industrial-equipment/flottweg/flottweg-sx-crud-treatment.

60. Frankiewicz, T. (2001). Understanding the fundamentals of water treatment, the dirty dozen-12 common causes of poor quality water. Presented at the 11th produced water seminar, Houston, TX, January 17-19.

61. Gekas, V. & Hallstrom, B. (1990). Microfiltration membranes, cross-flow transport mechanisms and fouling studies. Desalination 77, pp.195–218.

62. Gitis, V., I. Rubinstein, M. Livshits, G. Ziskind. (2010). Deep-bed filtration model with multistage deposition kinetics. Chem. Eng. J., 163, pp. 78–85.

63. Gohil, J. M. & Ray, P. (2009). Polyvinyl alcohol as the barrier layer in thin film composite nanofiltration membranes: Preparation, characterization, and performance evaluation. J. Colloid Interface Sci. 338, pp.121–127.

64. Gu, J., Xiao, P., Chen, J., Zhang, J., Huang, Y., Chen, T. (2014). Janus polymer/carbon nanotube hybrid membranes for oil/water separation. ACS Applied materials and interfaces, 6(18), pp. 16204-16209.

65. Gu, J., Xiao, P., Huang, Y., Zhang, J., Chen, T. (2015). Controlled functionalization of carbon nanotubes as super hydrophobic metals for adjustable oil/water separation. Journal of material chemistry A, 3, pp. 4124 – 4128.

66. Gulino, G., Vieira, R., Amadou, J., Nguyen, P., Ledoux, M.J., Galvagno, S., Centi, G., Pham-Huu. (2005). C_2H_6 as an active carbon source for a large scale synthesis of carbon nanotubes by chemical vapour deposition. Applied Catalysis A, 279, pp. 89-97.

67. Gullapalli, S.; Wong, M.S. (2011). Nanotechnology: A Guide to Nano-Objects. Chemical Engineering Progress 107 (5), pp. 28–32.

68. Hamlyn, C. (1990). A Science of Impurity. Water Analysis in Nineteenth Century Britain. University of California Press, Berkeley, CA.

69. Han, Y., Jiang, Y., Gao, C. (2015). High-flux graphene oxide nanofiltration membrane intercalated by carbon nanotube. ACS Appl. Mater. Interfaces, 7(15), pp. 8147-55.

70. Haweel, C.K., Ammar, S.H (2008). Preparation of Polyvinyl Alcohol from Local Raw Material. Iraqi Journal of Chemical and Petroleum Engineering, 9(1), pp. 15-21.

71. Haynie, D. T. (2001). Biological Thermodynamics. Cambridge: Cambridge University Press. pp. 130–136.

72. Hickner, M.A., Ghassemi, H., Kim, Y.S., Einsla, B.R., McGrath, J.E. (2004). Alternative Polymer Systems for Proton Exchange Membranes (PEMs). Chem. Rev., 104, pp. 4587-4612.

73. Hinds, W. C. (1998). Aerosol Technology, 2nd edition. Wiley-Interscience, New York.
74.

75. Hong, S., Elimelech, M. (1997). Chemical and physical aspects of natural organic matter (NOM) fouling of NF membranes. Journal of Membrane Science, 132, pp.159-181.

76. Hu, L. B., Hecht, D. S., Grüner, G. (2010). Carbon Nanotube Thin Films: Fabrication, Properties, and Applications. Chem. Rev., 110, pp.5790– 5844.

77. Hu, L., Gao, S., Ding, X., Wang, D., Jiang, J., Jin, J., Jiang, L. (2015). Photochemical-responsive single walled carbon nanotube-based ultrathin membranes for on/off switchable separation of oil-in-water nano-emulsions. ACS Nano, 9(5), pp. 4835-4842.

78. Huang, H, Yang, S. (2006). Filtration characteristics of polysulfone membrane filters. Aerosol Science, 37, pp. 1198 – 1208.

79. Huang, W., Wang, Y., Luo, G., Wei, F. (2003). 99.9% purity multi-walled carbon nanotubes by vacuum high temperature anneling. Carbon, vol. 41, pp. 205-2590.

80. Hummer, G., Rasaiah, J. C., Noworyta, J. P. (2001). Water conduction through the hydrophobic channel of a carbon nanotube. 414 (6860), pp. 188–90.

81. Igunnu, E.T., Chen, G.Z. (2012). Produced water treatment technologies. International Journal of Low-Carbon Technologies , 0, pp. 1-21.

82. Iijima, S. (1991). Helical microtubules of graphitic carbon. Nature, 354, pp.56–58.

83. Iritani, E., Mukai, Y., Tanaka, Y. and Murase, T. (1995). Flux decline behaviour in deadend microfiltration of protein solutions. Journal of Membrane Science, 103, pp.181-191.

84. Ital traco. (2015). Oil in water separation from state of art technology to zeroil technology. www.etna-usa.com/zertech.pdf

85. Iyuke, S.E., Mamvura, T.A., Liu, K., Sibanda, V., Meyyapan, M. (2009). Process synthesis and optimization for the production of carbon nanostructures. Nanotechnology, 20, pp 375602.

86. Iyuke, S.E., Simate, G.S. (2011). Synthesis of Carbon Nanomaterials in a Swirled Floating Catalytic Chemical Vapour Deposition Reactor for Continuous and Large Scale Production, Carbon nanotubes-Growth and Applications, Dr. Mohammad Naraghi (Ed.), ISBN: 978-953-307-566-2.

87. Janas, D., Kreft, S.K., Koziol, K.K.K. (2014). Steam reforming on reactive carbon nanotube membranes. Journal of industrial and engineering chemistry, 25, pp. 222- 228.

88. Jia, Y. Wei, J.Q., Shu, Q.K., Chand, J.G., Wang, K.L., Wang, K.Q., Luo., J.B., Lui, W.J., Zheng, M.X., Wy.D.H. (2007). Spread of double-walled carbon nanotube membrane. Chinese Science Bulletin, 52(7), pp.997-1000.

89. Jha, N., Jafri, R.I, Rajalakshmi, N., Ramaprabhu, S. (2011). Graphene-multi walled carbon nanotube hybrid electrocatalyst support material for direct methanol fuel cell. International Journal of Hydrogen Energy. Volume 36, Issue 12, pp. 7284–7290.

90. Javiya, S., Yogesh, Gupta, S., Singh, K., Bhattacharya, A. (2008). Porometry studies of the polysulfone membranes on addition of poly(ethylene glycol) in gelation bath during preparation. J. Mex. Chem. Soc., 52(2), pp.140-144.

91. Journet, C., Bernier, P. (1998). Production of carbon nanotubes, Applied Physics A, 67, pp. 1-9.

92. Journet, C., Maser, W. K., Bernier, P., Loiseau, A., Lamy de la Chapelle, M., Lefrant, S., Denlard, P., Lee, R. & Fischer, J. E. (1997). Large-scale production of single-walled carbon nanotubes by the electric arc discharge, Nature 388, pp. 756-758.

93. Kar, S., Subramanian, M., Pal., A., Ghosh, A.K., Bindal, R.C., Prabhakar, S., Nuwad, J., Pillai, C. G.S., Chattopadhyay, S. Tewani, P.K. (2013). Preparation, characterization and

peformance evaluation of anti-biofouling property of carbon nanotube-polysulfone composite membrane. AIP Conf. Proc., 1538 (1), pp. 181.

94. Kausar, A. (2014). Novel water purification membranes of polystyrene/multi-walled carbon nanotube-grafted-graphene oxide hybrids. American journal of polymer science, 4(3), pp. 63-72.

95. Kenna, E., Zander, A. (2000). Current Management of Membrane Plant Concentrate. American Water-works Association, Denver., p.14

96. Kesting, R.E. (1972). Synthetic Polymer Membranes. McGraw Hill, New York.

97. Khan, M.M., Filiz,V., Bengtson, G., Shishatskiy, S., Rahman, M., Abetz, V. (2011). Functionalized carbon nanotubes mixed matrix membranes of polymers of intrindic microporosity for gas separation. Nanoscale Research Letters, 2014(9), pp. 698.

98. Kim, E.S., Liu, Y., El-din, M.G. (2013). An in-situ integrated system of carbon nanotubes nanocomposite membrane for oil sands process-affected water treatment. Journal of membrane science, 429, pp. 418-427.

99. Kim, H.J., Tyagi, R.K., Fouda, A.E., Jonasson, K. (1996). The kinetic study for asymmetric membrane formation via phase-inversion process, Journal of Applied Polymer Science, 62, pp.621–629.

100. Kim, S.J., Ko, S.H., Kang, K.H., Han, J. (2010). Direct seawater desalination by ion concentration Polarization. Nature Nanotechnology, 5, pp.297-301.

101. Kiuru, H.; Vahala, R. (2000). Dissolved air flotation in water and waste water treatment. 4th international conference on DAF in water and waste water treatment, Helsinki, Finland. IWA Publishing, London, pp. 210.

102. Klein Wolterink, J.W., Hess, M., Schoof, L.A.A., Wijnen, J.W. (2004). Optimum solutions for collecting, treatment and disposal of relevant ship-generated solid and liquid wastes. Tebodin consultants and engineers, PROJECT MED.B4.4100.97.0415.8.

103. Koltuniewicz, A. (1992). Predicting permeate flux in ultrafiltration on the basis of surface renewal concept. Journal of membrane science, 68, pp. 107-118.

104. Koltuniewicz, A.B., Field, R.W., Arnot, T.C. (1995). Cross-flow and dead-end microfiltration of oily-water emulsion. Part I: Experimental study and analysis of flux decline. Journal of Membrane Science, 102, pp. 193-207.

105. Koros, W.J., Ma, Y.H., Shimidzu, T. (June 1996). Terminology for membranes and membrane processes (IUPAC). Pure & Applied Chemistry, 86, pp.1479–1489.

106. Kusworo, T.D., Ismail, A.F., Budiyono, Widiasa, I.N., Johari, S, Sunarso. (2012). The uses of carbon nanotubes mixed matrix membranes (MMM) for biogas purification. Internat. J. of waste resources, 2, pp. 5-10.

107. Lafreniere, L.Y., Talbot, F.D.F., Matsuura, T., Sourirajan, S. (1987). Effect of polyvinylpyrrolidone additive on the performance of polyethersulfone ultrafiltration membranes. Ind. Eng. Chem. Res, 26, pp. 2385–2389.

108. Lalia, B.S., Kochkodan, V., Hashaikeh, R., Hilal, N. (2013). A review on membrane fabrication: Structure, properties and performance relationship. Desalination, 326, pp.77-95.

109. Larry. (2011). Modern technology today, retrieved 2015. http://moderntechnologyoftoday.blogspot.com/2011/06/advantages-and-disadvantages-of-reverse.html

110. Lee, K. P., Arnot, T. C. & Mattia, D. (2011).A review of reverse osmosis membrane materials for desalination–development to date and future potential. J. Membrane Sci. 370, pp.1–22.

111. Lee, R. (2000). Coagulation and flocculation in wastewater treatment. 141, pp.29-32.

112. Lee, S., Cho, J. and Elimelech, M. (2005). Combined influence of natural organic matter (NOM) and colloidal particles on nanofiltration membrane fouling. Journal of Membrane Science, 262, pp.27-41.

113. Lee, S. J., Baik, H. K., Yoo, J. & Han, J. H. (2002). Large scale synthesis of carbon nanotubes by plasma rotating arc discharge technique, Diamond and Related Materials 11, pp.914-917.

114. Letterman, R. D. (1999). Water Quality and Treatment. New York: American Water Works Association and McGraw-Hill, 5th edition.

115. Li, H., Zou, L. (2011). Ion-exchange membrane capacitive deionization: A new strategy for brackish water desalination. Desalination, 275(1-3), pp. 62-66.

116. Lin, Z. S., Wen, W. (2003). Study on the technology of treating oily wastewater by coagulation and adsorption. Mar. Environmental Science. 22, pp. 15-19.

117. Liu, Q., Z.G. Chen, B. Liu, W. Ren, F. Li, H. Cong and H.M. Cheng. (2008). Synthesis of different magnetic carbon nanostructures by the pyrolysis of ferrocene at different sublimation temperatures. Carbon, 46, pp. 1892-1902.

118. Liu, T-Y.L., Tong, Y., Liu, Z-H., Lin, H-H., Lin, Y-K., Van der Bruggen, B. (2015). Extracellular polymeric substances removal of dual-layer (PES/PVDF) hollow fiber UF membrane comprising multi-walled carbon nanotubes for preventing RO biofouling. Separation and purification technology, 148, pp. 57-67.

119. Lou, Z., Chen, Q., Wang, W., Zhang, Y. (2003). Synthesis of carbon nanotubes by reduction of carbon dioxide with metallic lithium. Carbon, 41, pp. 3036-3074.

120. Lui, Y., Gao, L., Sun, J., Zheng, S., Jiang, L., Wang, Y., Kajiura, H., Li, Y., Noda, K. (2007). A multi-step stratergy for cutting and purification of single-walled carbon nanotube. Carbon, 45, pp. 1972-1978.

121. Luthy, R.C. (1978). Removal of Emulsified Oil with Organic Coagulants and Dissolved Air Flotation, Journal Water Pollution Control Federation, pp.331-346.

122. Majumder, M., Chopra, N., Andrews, R., Hinds, B. J. (2005). Nanoscale hydrodynamics: Enhanced flow in carbon nanotubes. Nature, 438 (7064), pp. 44.

123. Makdissy, G., Croue , J.P., Buisson, H., Amy, G., and Legube, B. (2003). Organic matter fouling of ultrafiltration membranes. Water Science and Technology Water Supply, 3(5-6), 1, pp.75-182.

124. Malki, M. (2008). Optimizing scale inhibition costs in reverse osmosis desalination plants. International Desalination and Water Reuse Quarterly, 17(4), pp.28–29.

125. Maphutha, S., Moothi, K., Meyyappan, M., Iyuke S. E. (2013) A carbon nanotube-infused polysulfone membrane with polyvinyl alcohol layer for treating oil-containing waste water. Sci. Rep. 3, pp 1509.

126. Marthinussen, S.A. (2011). The Effect of Fluid Viscosity on Hydrocyclone Performance: Design and Commissioning of an Experimental Rig and Results. Master Thesis Process Technology, University of Bergen.

127. Marulanda, J.S. (2010). Carbon nanotubes. In-tech. ISBN 978-953-307-054-4

128. McNaught, A.D., Wilkinson, A. (1997). IUPAC. Compendium of chemical terminology, 2nd edition (the "Goldbook"). Blackwell Scientific Publications, Oxford.

129. Mercer International Inc. (2012). Innovation in oil water separation; API oil/water separators: Simple but costly. www.oil-water-separators.com.

130. Mhlanga, S.D. and Coville, N.J. (2008) Iron–cobalt catalysts synthesized by a reverse micelle impregnation method for controlled growth of carbon nanotubes. Diamond & Related Materials. 17, pp 1489–1493.

131. Mionic, M., Alexander, D.T.L., Ferró, L., Magrez, A. (2008). Influence of the catalyst drying process and catalyst support particle on the carbon nanotubes produced by CCVD. Phys. Status Solidi B, 245, pp.1915.

132. Miranda, C.A. (2013). Methods to clean produced water. Petroleum Production Specialization Project, Norwegian university of Science and Technology.

133. Mo, L., Huanga, X. (2003). Fouling characteristics and cleaning strategies in coagulation micro filtration combination process for water purification. Desalination, 159, pp.1-9.

134. Modise, C.M., Shan, H.F., Neufeld, R.D., Vidic, R.D. (2005). Evaluation of Permeate Flux Rate and Membrane Fouling in Dead-End Microfiltration of Primary Sewage Effluent. Environmental Engineering Science, 22(4), pp.427-439.

135. Mondal, S. & Wickramasinghe, S. R. (2008). Produced water treatment by nanofiltration and reverse osmosis membranes. Journal of Membrane Science, 322, pp.162–170.

136. Moothi, K. (2009). Carbon nanotube production from greenhouse gases during syngas synthesis. M.Sc. (Eng.) thesis, University of the Witwatersrand.

137. Morgan, P. W., Kwolek, Stephanie L. (1959). Interfacial Polycondensation. II. Fundamentalsof Polymer Formation at Liquid Interfaces. Journal of Polymer Science 40 (137), pp. 299–327.

138. Motchelaho, M.A.M., Xiong, H., Moyo, M., Jewel, L.L., Coville, N.J. (2011). Effect of acid treatment on the surface of multiwalled carbon nanotubes prepared from Fe–Co supported on $CaCO_3$: Correlation with Fischer–Tropsch catalyst activity. Journal of Molecular Catalysis A: Chemical. Volume, 335(1–2), pp.189–198.

139. Naes, B.E. (2009). Elemental Analysis of Glass and Ink by Laser Ablation Inductively Coupled Plasma Mass Spectrometry (LA-ICP-MS) and Laser Induced Breakdown

Spectroscopy (LIBS). FIU electronic theses and dissertations, Florida international university.

140. New logic (retrieved 2015). Using vibrating membranes to treat oily wastewater from a waste hauling facility. New logic research, Emeryville CA , USA, http://www.vsep.com/pdf/OilyWastewater.pdf

141. Ngoy, J.M. (2010). Polymer and carbon nanotube bound folic acid and methotrexate for cancer therapy. MSc(Eng) Thesis, University of the Witwatersrand, Johannesburg, South Africa.

142. Odian, G. (2004). Principles of Polymerization. Wiley-Interscience. 4th edition, pp. 90–92.

143. Okiel, K., El-Aassar, A.H., Temraz, T., El-Etriby, S., Shawky, H.A. (2015). Vacuum enhanced direct contact membrane distillation for oilfield produced water desalination: specific energy consumption and energy efficiency. Desalination and water treatment, DOI: 10.1080/19443994.2015.1048305

144. Orecki, A., Tomaszewska, M. (2007). The oily wastewater treatment using the nanofiltration process. Polish Journal of Chemical Technology, 9, 4, pp. 40 – 42.

145. Paradise, M. & Goswami, T. (2007). Carbon nanotubes – Production and industrial applications, Materials and Design 28, pp.1477-1489.

146. Parker, S.P. (2003). Dictionary of Scientific & Technical Terms. McGraw-Hill, 6th edition.

147. Parker, W.J., Monteith, H.D. (1996). Stripping of Voc's from dissolved air floatation. Environmental progress, 15(2), pp. 73-81.

148. Perry, R.H., Green, D.W. (2007). Perry's Chemical Engineers' Handbook. McGraw-Hill Professional, New York, 8th Edn, pp. 2072-2100.

149. Phao, N., Nxumalo, E. N., Mamba, B. B., Mhlanga, S. D. (2013). A nitrogen-doped carbon nanotube enhanced polyethersulfone membrane system for water treatment. Physics and Chemistry of the Earth, 66, pp.148–156.

150. Pieralisi group. (retrieved 2014). Centrifugal separators for industrial use. Gruppo Pieralisi, dedicated innovators. http://www.waterforum.net/images/stories/bedrijfspreentatie/pieralisi-benelux-bv/Separators_EN.pdf

151. Pietrzak, W.S., Verstynen, M.L., Sarver, D.R. (1997). Bioabsorbable polymer science for the practicing surgeon. The Journal of craniofacial surgeory, 8 (2), pp. 87 – 91.

152. Pinnau, I., Freeman, B.D. (2000). Formation and modification of polymeric membranes: Overview. Membrane Formation and Modification. 744, pp. 1–22.

153. Probstein, R.F. (1994). Physicochemical Hydrodynamics, Wiley, NY.

154. Purchase advantage. (2015). Filmtec NF membranes. http://www.thepurchaseadvantage.com/page/TPA/CTGY/filmtec_nf_membranes

155. Rahimpour, A., Rajaeian, B., Hoseinzadeh, A., Madaeni, S.S., Ghoreishi, F. (2011). Treatment of oily wastewater produced by washing of gasoline reserving tanks using self-made and commercial nanofiltration membranes. Desalination, 265, pp.190-198.

156. Rahimpour, A; Jahnshahi, M., Mortazavian, N., Madaeni, S.S. (2010). Preparation and Characterisation of Asymmetric Polyethersulfone and Thin-Film Composite Polyamide Nanofiltration Membranes for Water Softening. Applied Surface Science, 256 (6), pp. 1657–1663.

157. Ramli, N.H., Lord, A., Powell, L., Williams, P.M. (2012). Experimental study of the ultrafiltration for bi-disperse silica systems. *Desalination Publications,* 42, pp. 1-7.

158. Records, A., Sutherland, K. (2001). Decanter centrifuge handbook, first edition. Elsevier Science Ltd, United Kingdom.

159. Robertson, J. (2004). Realistic applications of CNTs. Materials Today, 7, pp.46-52.

160. Rubinstein, I., Zaltzman, B. (2000). Electro-osmotically induced convection at a permselective Membrane. Physical Review E., 62, pp.2238.

161. Sammons, J.K., Fox Jr, C.H. (1979). Centrifugal water oil separator. Continental oil company, 937 (391). United States Patent 4,175,040.

162. Saffar, A., Carreau, P.J., Abdellah Ajji, A., Kamal, M.R. (2014). Influence of Stretching on the Performance of Polypropylene-Based Microporous Membranes. Ind. Eng. Chem. Res., 53, pp.14014−14021.

163. Sauvetgoichon, B (2007). Ashkelon desalination plant — A successful challenge. Desalination, 203, pp.75–81.

164. Schafer, A.I. (2005). Nanofiltration Principles and Applications. Oxford: Elsevier.

165. Schwan, J., Ulrich, S., Batori, V., Ehrhardt, H. (1996). Raman spectroscopy on amorphous carbon films. J. Appl. Phys., 80, pp. 440-447.

166. Schnorr, J. M., Swager, T. M. (2011). Emerging Applications of Carbon Nanotubes. Chem. Mater, 23, pp.646– 657

167. Scott, K., Adhamy, A., Atteck, W., Davidson, C. (1994). Crossflow microfiltration of organic/water suspensions. Water Res., 28, pp.137–145.

168. Seadler ,J & Henley, E. (2006). Separation Process Principles. John Wiley & Sons Inc., New Jersey, 2nd Edn. p.501.

169. Shah, P., Murthy, C.N. (2013). Studies on the porosity control of MWCNT/Polysulfone composite membrane and its effect on metal removal. Journal of Membrane Science, 437, 90-98.

170. Shakaib, M. (2008). Pressure and concentration gradients in membrane feed channels: Numerical and experimental investigations. Ned University of Engineering and Technology, Karachi.

171. Shammas, N. K., Bennett, G. F. (2010). Principles of Air Flotation Technology. In Wang, L. K., Shammas, S., William, A. et al. Flotation Technology. Handbook of Environmental Engineering, New York: Humana Press. pp. 29–32.

172. Shen, C., Brozena, A.H., Wang, Y. (2011). Double-walled carbon nanotubes: Challenges and opportunities. Nanoscale, 2011, 3, pp.503-505.

173. Shen, Y., Xia, Z., Wang, Y., Poh, C.K., Lin, J. (2014). Pt coated vertically aligned carbon nanotubes as electrodes for proton exchange membrane fuel cells. Procedia engineering, 93, pp. 34-42.

174. Shi, Z., Zhang, W., Zhang, F., Liu, X., Wang, D., Jin, J., Jiang, L. (2013). Ultrafast separation of emulsified oil/water mixtures by ultrathin free-standing single-walled carbon nanotubes network films. Advanced materials, 25 (17), pp. 2422-2427.

175. Shie, S. (2011). Carbon Nanotube Usage for Desalination. COSMOS, Cluster 8.

176. Sholl, D. S., Johnson, J.K. (2006). Making High-Flux Membranes with Carbon Nanotubes. Science, 312 (5776), pp. 1003–4.

177. Singh, P.S., Joshi, S.V., Trivedi, J.J., Devmurari, C.V., Rao, A.P., Ghosh, P.K. (2006). Probing the structural variations of thin film composite RO membranes obtained by coating polyamide over polysulfone membranes of different pore dimensions. Journal of Membrane Science, 278, 19–25.

178. Siriverdin, T., Dallbauman, L. (2004). Organic matrix in produced water from the osage-skiatook petroleum environmental research site. Chemosphere, 57, pp. 463–469.

179. Steward, M., Arnold, K. (2008). Emulsions and Oil Treating Equipment: Selection, Sizing and Troubleshooting; Chapter 3 Produced Water Treating Systems.

180. Strathmann, H.,Kock, K.,Amar, P., Baker, R.W. (1975). Formation mechanism of asymmetric Membranes. Desalination, 16, pp.179–203.

181. Sun, L., Crooks, R.M. (2000). Single Carbon Nanotube Membranes: A Well-Defined Model for Studying Mass Transport through Nanoporous Materials. J. Am. Chem. Soc., 122 (49), pp. 12340-12345.

182. Supercritical group. (retrieved 2014). Polymer synthesis and processing: http://www2.dq.fct.unl.pt/scf/research.htm

183. Sutherland, K. (2007). Filters and filtration handbook, 5th edition. Elsevier Ltd. Swift, G. (1994). Water-soluble polymers. Polymer Degradation and Stability, 45, pp.215-231.

184. Tam, N.T.T., Nghia, N.X., Quynh, N.T., Khoi, P.H., Minh, P.N. (2008). Analyzing the purity of carbon nanotubes by using different methods. Journal of the Korean Physical Society, 52 (5), pp. 1382-1385.

185. Tsai, P., Kuo, H., Chui, W., Wu, J. (2013). Purification and Functionalization of Single-Walled Carbon Nanotubes through Different Treatment Procedures. Journal of Nanomaterials, Hindawi Publishing Corporation.

186. Tuinstra, F., Koenig, J.L. (1970). Raman spectrum of graphite. J. Chem. Phys., 53, pp.1126–1130.

187. Ullrich, R; Lorber, C; Röder, G; Urak, G; Faryniak, B; Sladen, RN; Germann, P (1999). Controlled airway pressure therapy, nitric oxide inhalation, prone position, and extracorporeal membrane oxygenation (ECMO) as components of an integrated approach to ARDS. Anesthesiology, 91 (6), pp.1577–86.

188. Van der Bruggen, B., Manttari, M. & Nystromb, M. (2008). Drawbacks of applying nanofiltration and how to avoid them: a review. Sep. Purif. Technol. 63, pp. 251–263.

189. Wakeman, R. J., Williams, C. J. (2002). Additional techniques to improve microfiltration. Sep. Purif. Technol. 26, pp.3–18.

190. Wang F.X., Gao, X.P., Lu, Z.W., Ye, S.H., Qu, J.Q., Wu, F., Yuan, H.T., Song, D.Y. (2004a). Electrochemical properties of Mg-based alloys containing carbon nanotubes. Journal of alloys and compounds, 370, pp. 326-330.

191. Wang, J., Kim, S.C., Pui, D.Y.H. (2008). Figure of merit composite filters with micrometer and nanometer fibers. Aerosol science and technology, 42, pp. 722-728.

192. Wang, L.K., Hung, Y.T., Lo, H.H., Yapijakis, C. (2004). Handbook of Industrial and Hazardous Wastes Treatment (2nd ed.). CRC Press.

193. Wang, T. (2007). Improve the efficiency of the sewage settling tank degreasing with flotation. Oil-Gasfield Surface Engineering, 26, pp. 26-27.

194. Webster, M. (retrieved 2015). Centrifugal force. An encyclopaedia Britanicca company, http://www.merriam-webster.com/dictionary/centrifugal%20force.

195. Weisner, M. R., Clarke, M. M., Jacanglo, J.G., Lykins, B.W., Marinas, B. J., O'Mellia, C.R., Ritmann, B.E., and Semmens, M.J. (1992). Committee report: Membrane processes in portable water treatment. Journal of the American Water Works Association, 84(1), pp.59-67.

196. Wijmans, H. Membrane Technology and Research. (2000). Academic Press. Menlo Park, CA, USA.

197. Wu, C., Li, A., Li, L., Zhang, L., Wang, H., Qi, X., Zhang, Q. (2008). Treatment of oily water by a poly(vinyl alcohol) ultrafiltration membrane. Desalination, 225, pp.312-321.

198. Wu, H., Tang, B., Wu, P. (2010). Novel ultrafiltration membranes prepared from a multi-walled carbon nanotubes polymer composite. Journal of membrane science, 362, pp. 374-383.

199. Yah, C.S., Iyuke, S.E., Simate, G.S. (2011b). Continuous synthesis of multiwalled carbon nanotubes from xylene using the swirled floating catalyst chemical vapour deposition technique. J. Mater. Res., Vol. 26, No. 0, pp.1-5.

200. Yah, C. S., Simate, G. S., Moothi, K., Maphutha, K. S. & Iyuke, S. E. (2011). Synthesis of large carbon nanotubes from ferrocene: the chemical vapour deposition technique. Trends Appl. Sci. 6, pp.1270–1279.

201. Yao, Y.; Zhang, S.; Yang, Y. (2008). CVD synthesis and purification of multi-walled carbon nanotubes. Nanoelectronics conference, 2nd IEEE international, pp.562,565.

202. Yesil, S., Bayram, G. (2011). Effect of carbon nanotube purification on the electrical and mechanical properties of poly(ethylene terephthalate) composites with carbon nanotubes in low concentration. Journal of Applied Polymer Science, 119(6), pp.3360 - 3371.

203. Yu, S.L., Lu, Y., Chai, B.X. (2006). Treatment of oily wastewater by organic–inorganic composite tubular ultrafiltration (UF) membranes. Desalination, 196, 7, pp.6-83.

204. Zhang, B., Lui, L., Xie, S., Shen, F., Yan, H., Wu, H., Wan. Y., Yu, M., Ma, H., Li, L., Li, J. (2014). Built-up superhydrophobic composite membrane with carbon nanotubes for water desalination. RSC advances, 4, pp. 16561-16566.

205. Zhang, J., Sun, Y.R., Huang, Z.F., Lui, X.Q., Meng G.Y. (2006). Treatment of phosphate-containing oily wastewater by coagulation and microfiltration. Journal of environmental sciences, 18 (4), pp. 629-633.

206. Zhang, Y., Cui, P., Du, T., Shan, L., Wang, Y. (2009). Development of a sulfated Y-doped nonstoichiometric zirconia/polysulfone composite membrane for treatment of wastewater containing oil. Separation and purification technology, 70, pp.153-159

207. Zheng, Q.Z., Wang, P., Yang, Y.N., Cui, D.J. (2006). The relationship between porosity and kinetics parameter of membrane formation in PSF ultrafiltration membrane. Journal of Membrane Science. 286, pp.7–11.

208. Zheng, Z., Li, Y., Lui, J. (2002). CVD synthesis and purification of single-walled carbon nanotubes on aerogel-supported catalyst. Applied Physics A: Materials Science and Processing, 74, pp. 345-348

209. Zhu, D. H., Zhang, Z. H. (2002). Environmental Protection Petrochem. Ind. 25. pp. 16-18.

APPENDIX A

This section contains the missing information from chapter four that has to deal with the CNTs is included in this section. Explanation of the meaning of the information presented in this section is in chapter 4.

A.1 Raman spectroscopy data

These results were obtained using the device in chapter 3, section 3.3.4. Figure A.40 depicts the Raman spectrum/shift for the CNTs synthesized at the temperature of 850^{o}C. All the CNTs were synthesized at 850^{o}C. Figure A.1 below shows the Raman spectrum for the as-produced CNTs.

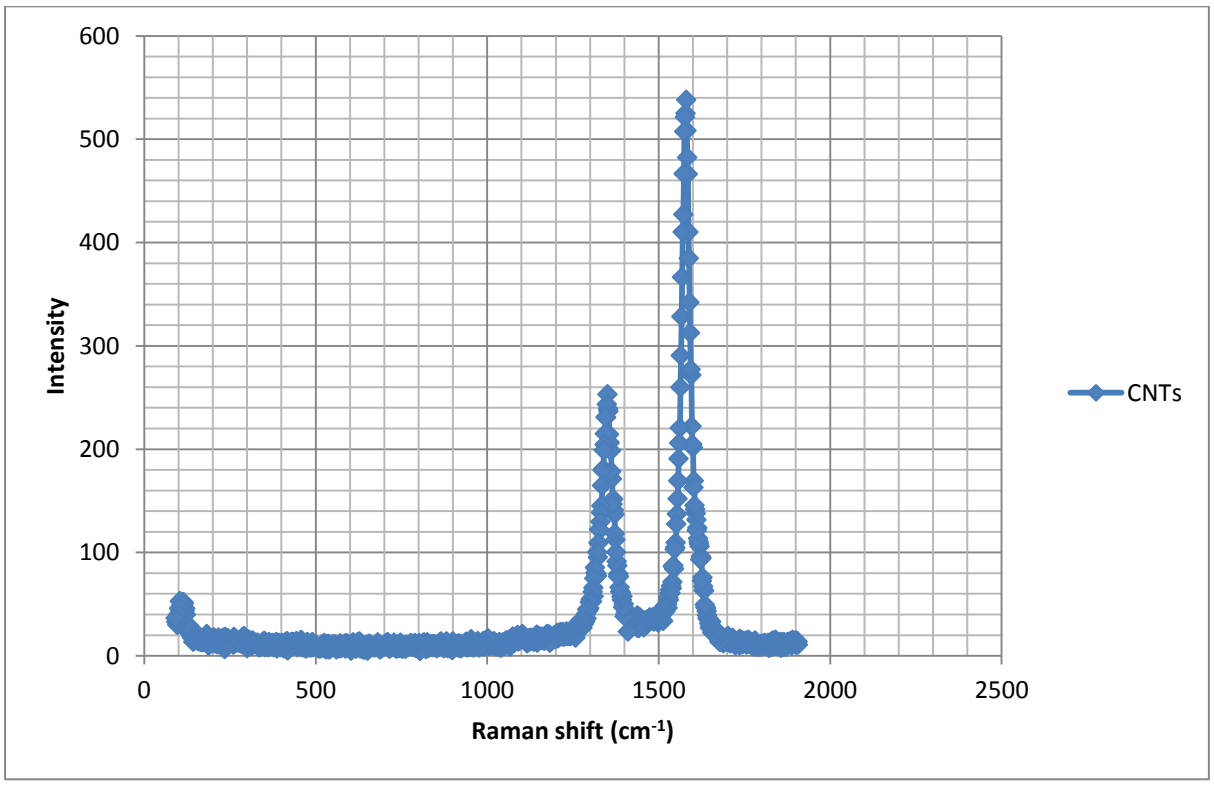


Figure A.1: Raman Shift of the CNTs at 850^{o}C.

Figure A.2 shows the Raman spectrum for the fCNTs.

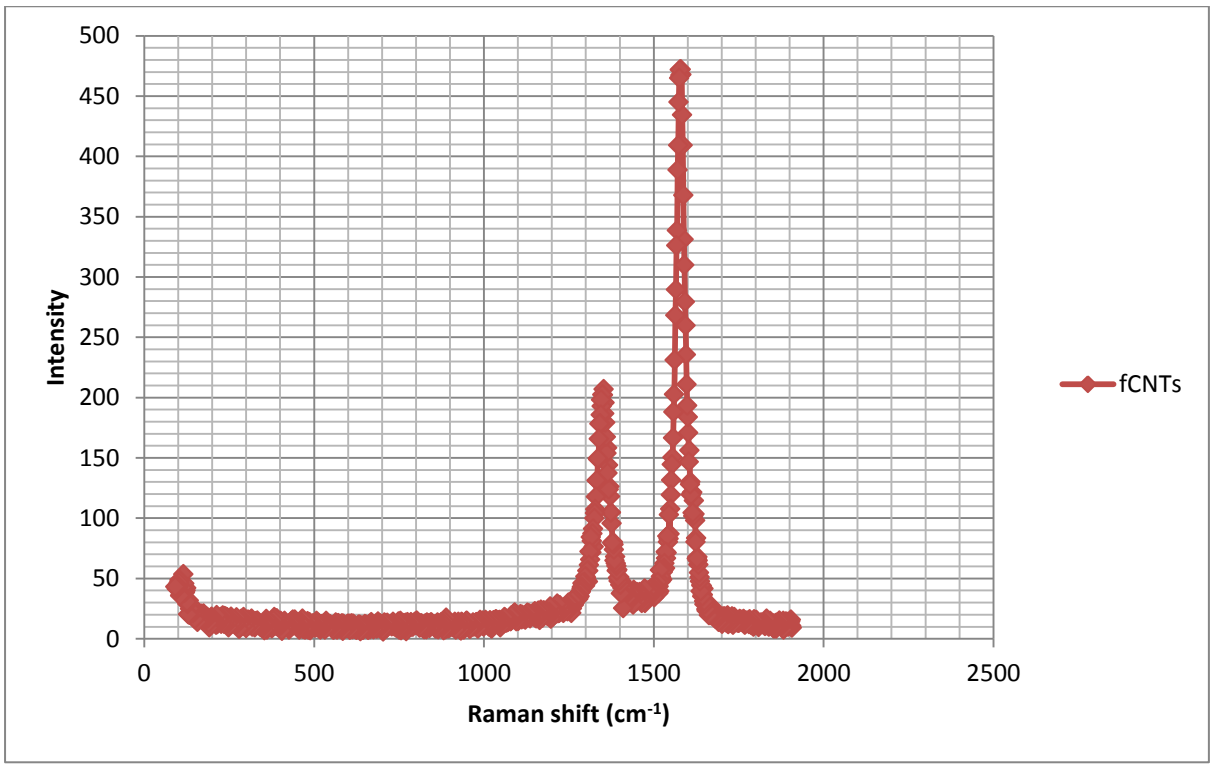


Figure A.2: Raman shift of the fCNTs at 850^{o}C.

Figure A.3 indicates the Raman spectrum for the pCNTs.

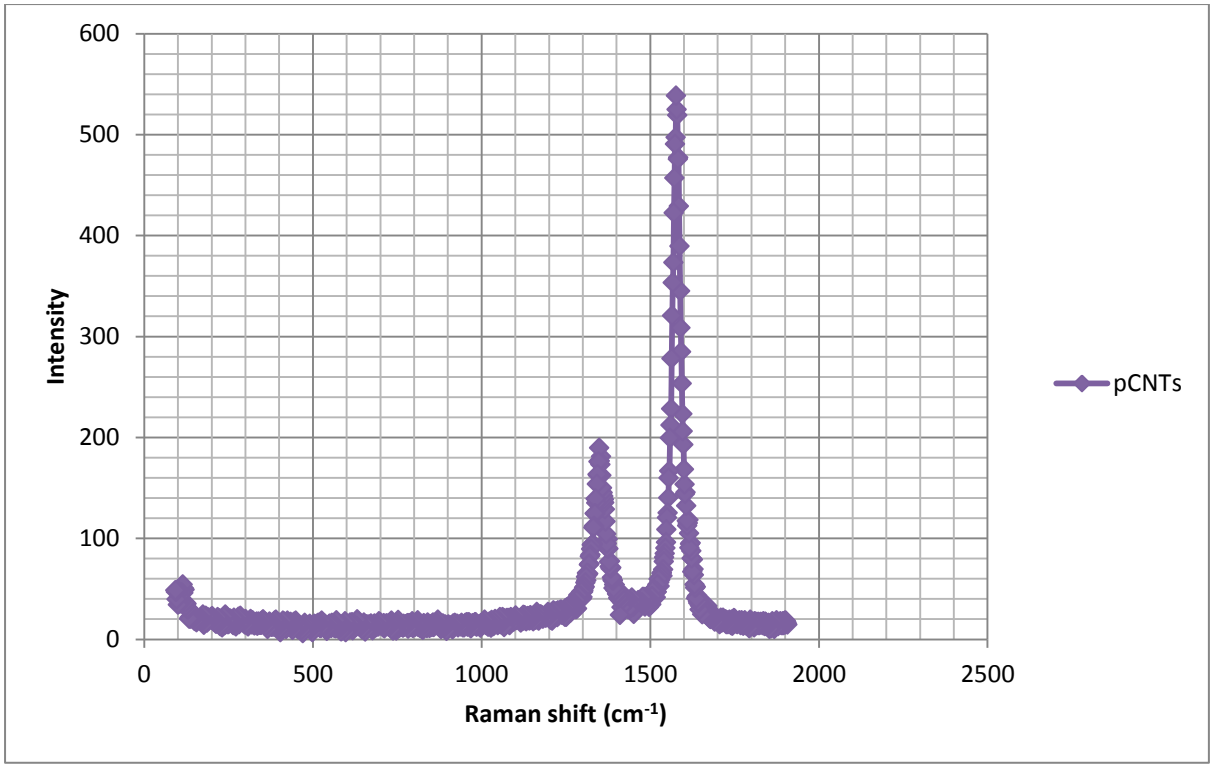


Figure A.3: Raman shift of the pCNTs at 850^{o}C.

Figure A.4 depicts the Raman spectra for the CNTs, fCNTs and the pCNTs.

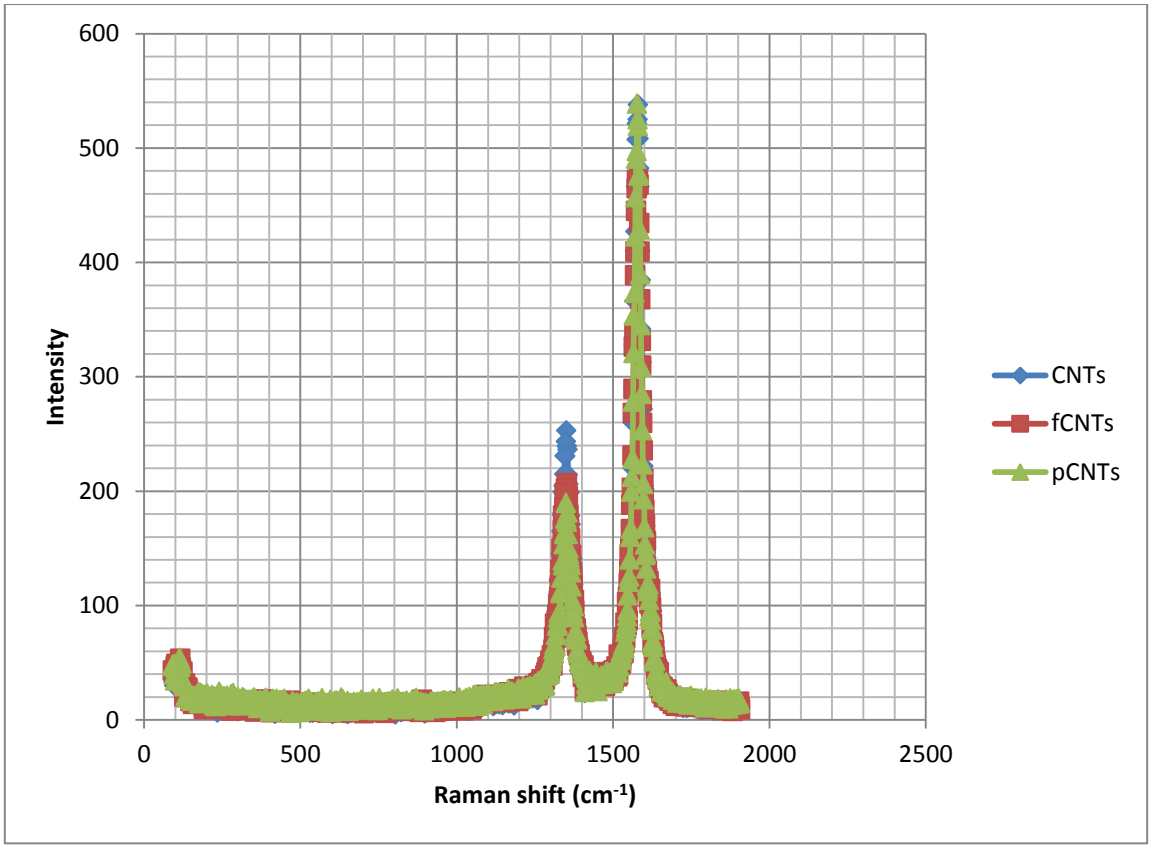


Figure A.4: Raman shift for the CNTs, fCNTs and pCNTs.

A.2 Fourier transform infrared (FTIR) spectroscopy for the CNTss

Figure A.5 shows the infrared (IR) spectrum for the CNTs.

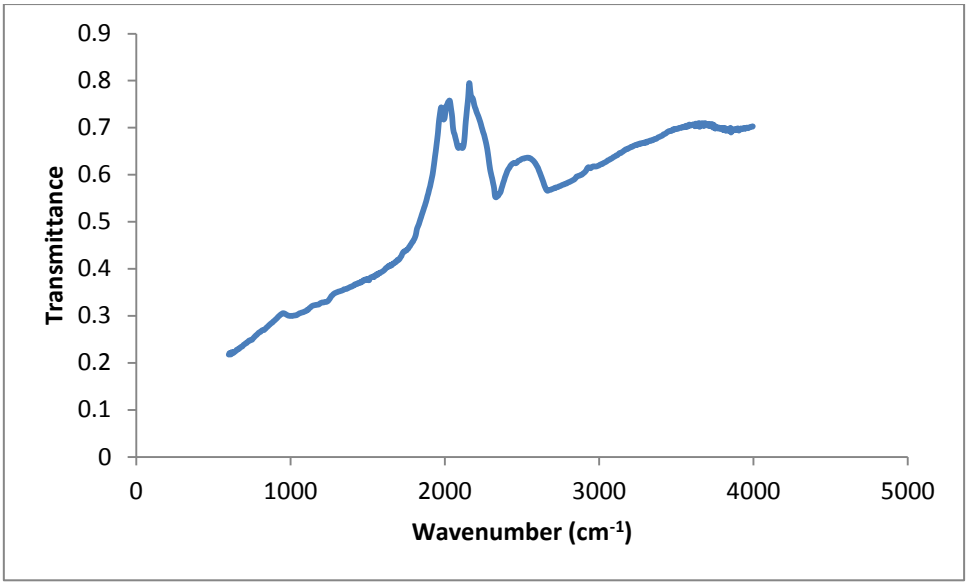


Figure A.5: IR spectrum for the CNTs.

Figure A.45 depicts the IR spectrum for the fCNTs.

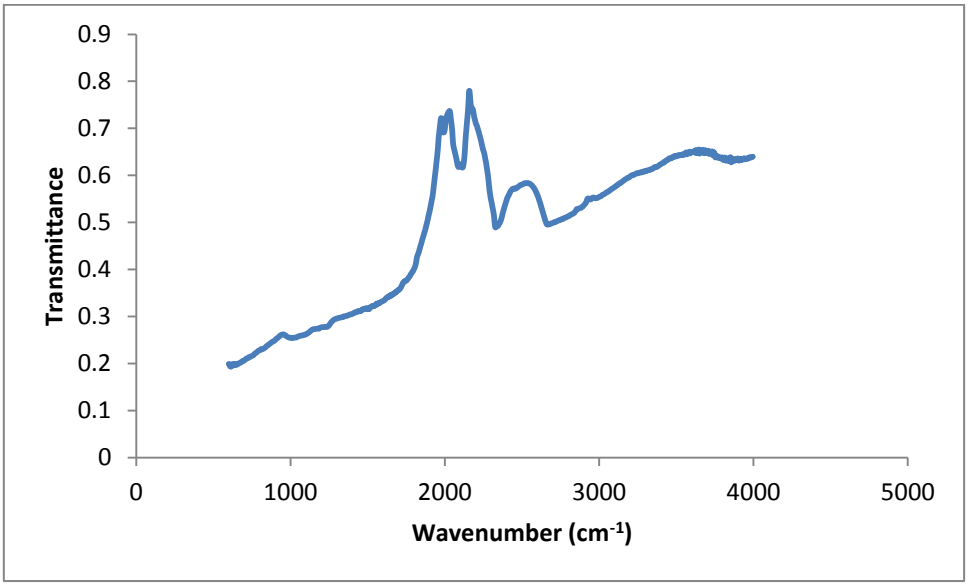


Figure A.6: IR spectrum for the fCNTs.

Figure A.7 indicates the IR spectrum for the pCNTs.

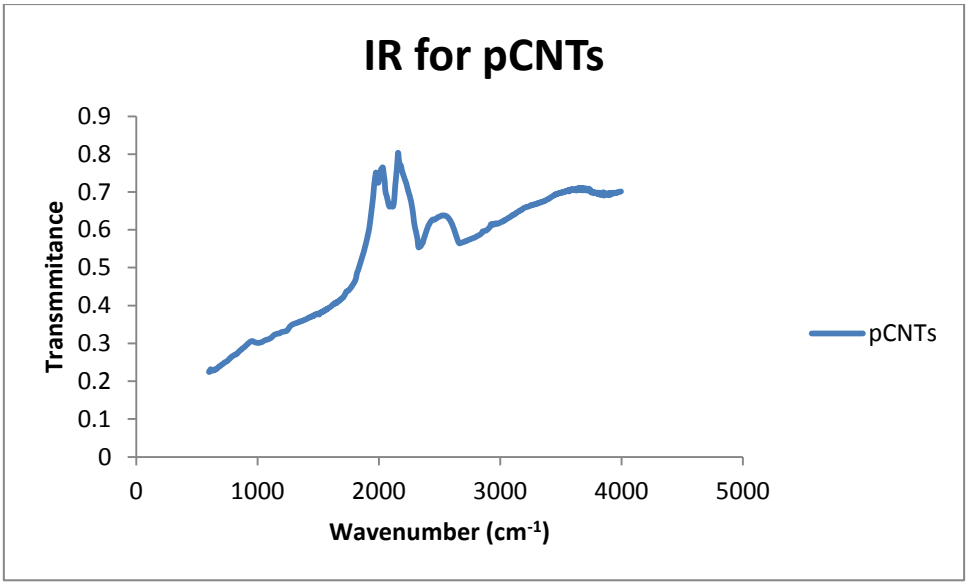


Figure A.7: IR for the pCNTs.

Figure A.8 shows the IR spectra for the CNTs, fCNTs and the pCNTs.

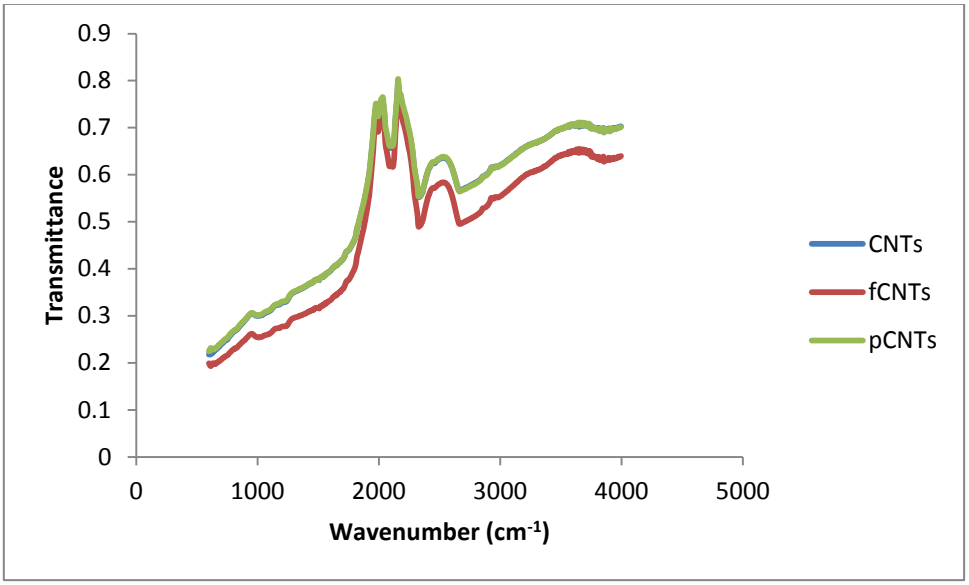


Figure A.8: The IR spectra for the CNTs, fCNTs and the pCNTs.

A.3 X-ray diffraction (XRD) analysis

The results below were obtained using the XRD Bruker D2 Phaser equipment in figure 3.9, section 3.3.4.6, chapter 3. X-ray diffraction.

Figure A.9. below shows the XRD spectrum for the as-produced CNTs.

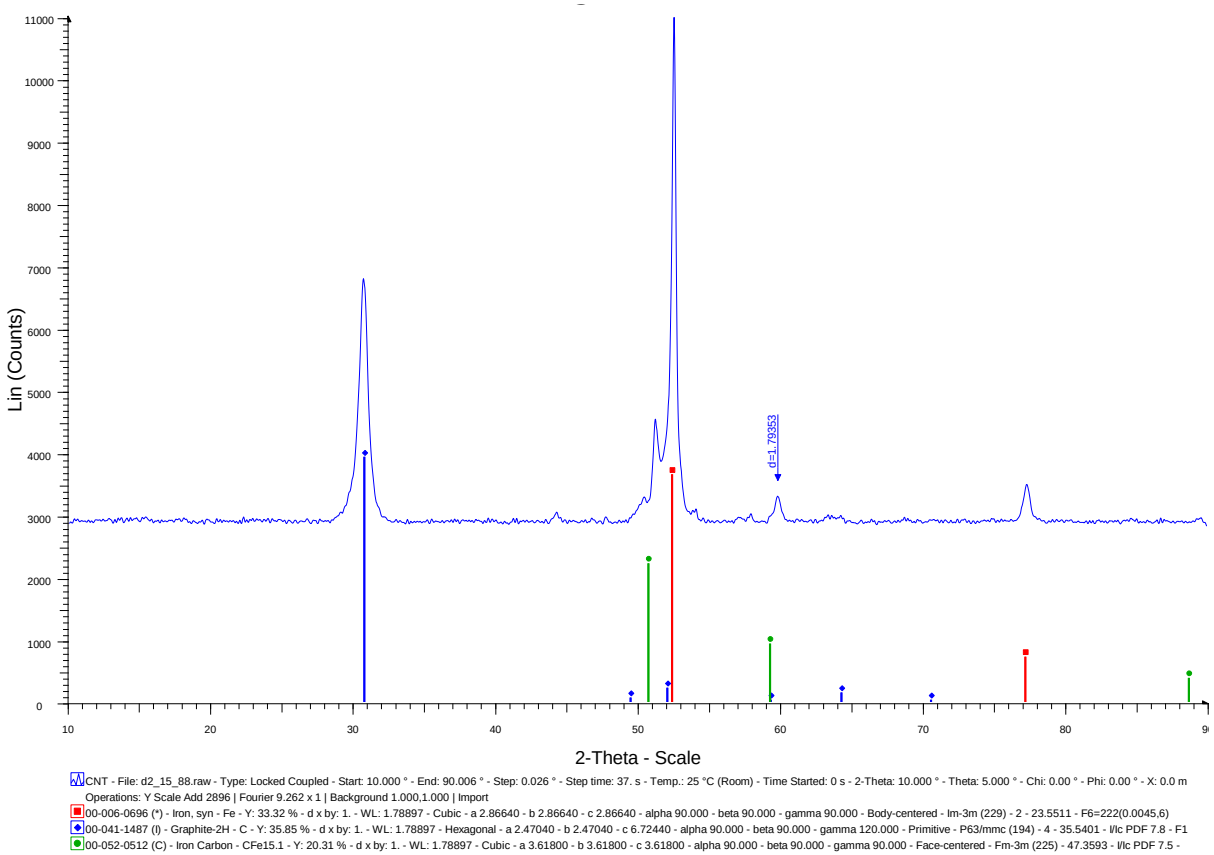


Figure A.9: XRD Spectrum for the as-produced CNTs.

Figure A.10 below shows the XRD spectra for the fCNTs.

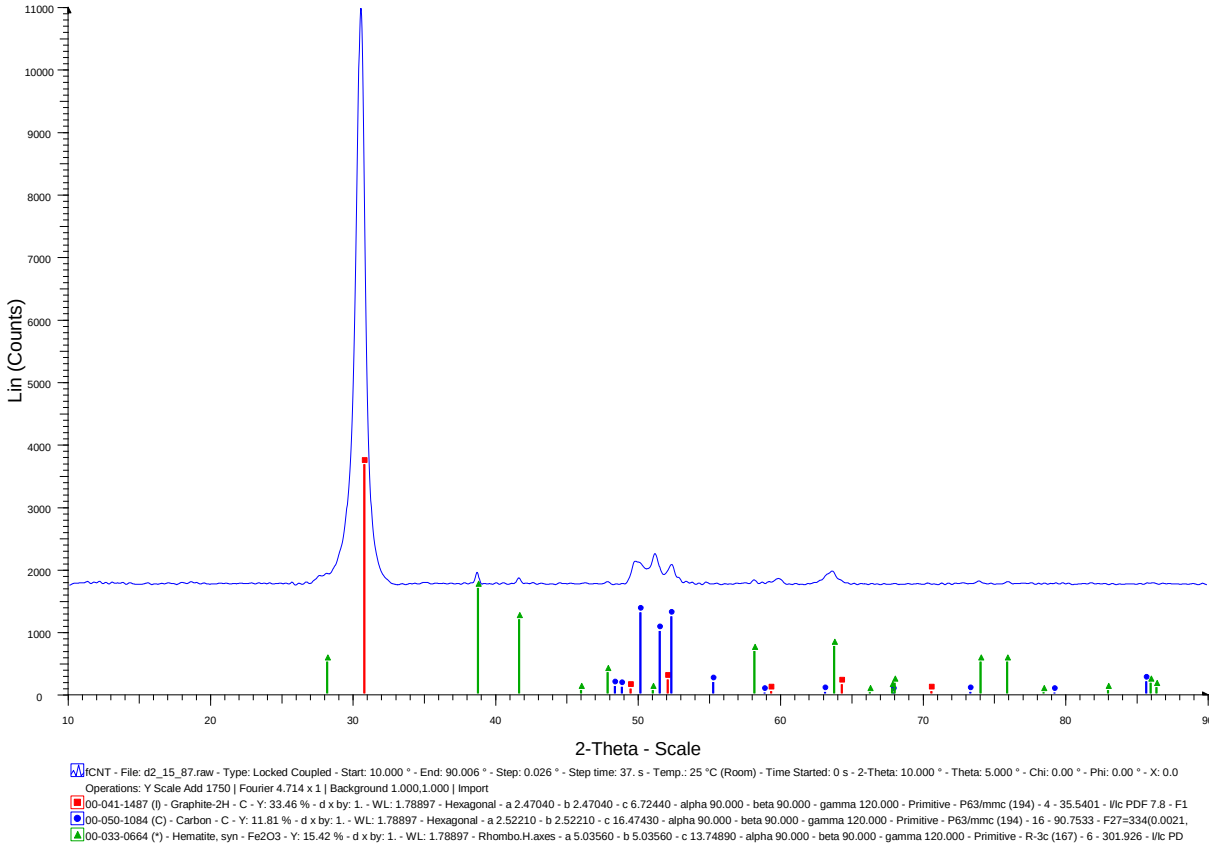


Figure A.10: XRD spectrum for the fCNTs.

Figure A.11 below shows the XRD spectra for the pCNTs.

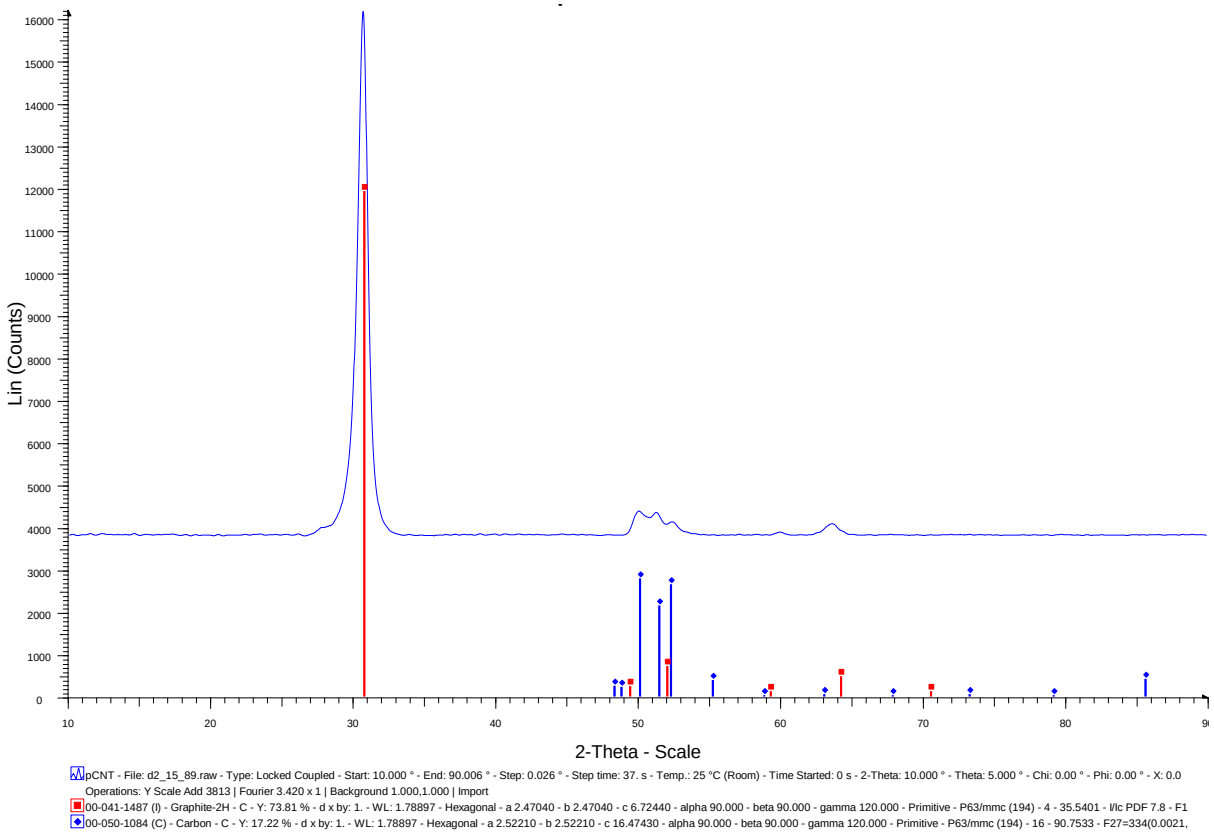


Figure A.11: XRD spectrum for the pCNTs.

A.4 CNTs functionalization equipment

The schematic setup diagram of this experiment is shown Figure A.13.

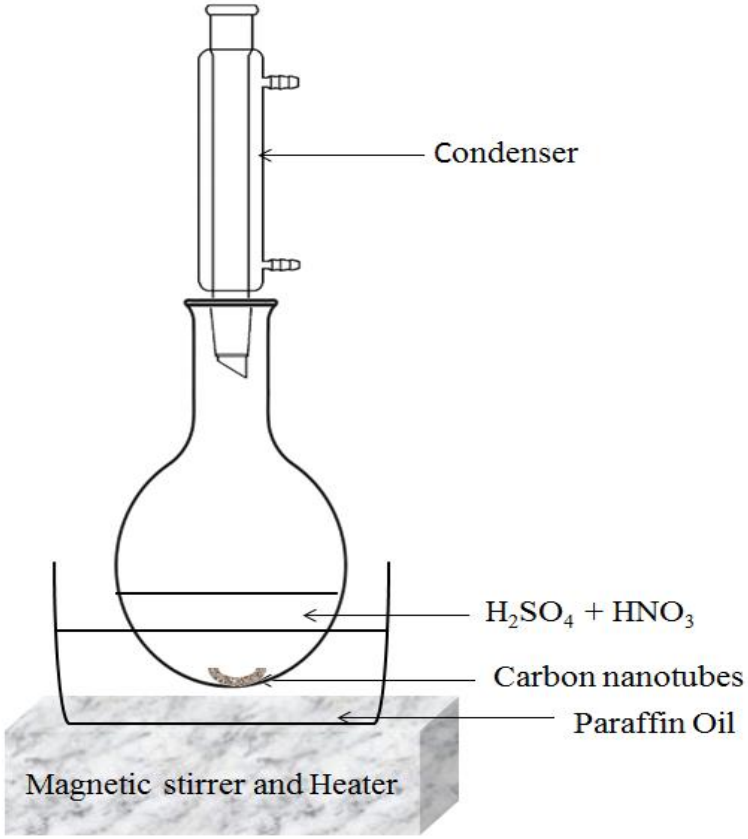


Figure A.112: Schematic setup drawing of the functionalization of the CNTs.

APPENDIX B

All the missing information from section for that has to deal with the PS membrane is included in this section.

B.1 Brunauer-emmet-teller (BET) data

This subsection contains the BET data for the 0 PVA, 2.5% CNTs, 5% CNTs, 7.5% CNTs, p7.5% CNTs and 10% CNTs PS membranes. The following BET information was obtained using the BET Micromeritics Tristar 3000 equipment shown in section 3.3.6.1.

B.1.1 BET data for the 0 PVA PS membrane

Table B3: Isotherm linear report for the adsorption of 0 PVA PS membrane.

Relative Pressure (P/Po)	Quantity Adsorbed (cm^3/g STP)
0.052279	0.896216
0.124044	1.023588
0.199473	1.074214
0.274365	1.098162
0.348876	1.111801
0.988652	12.44544

where Po represents the initial pressure, of the adsorbed material, in mmHg.

Figure B.1 shows the isotherm linear plot for the adsorption of 0 PVA PS membrane

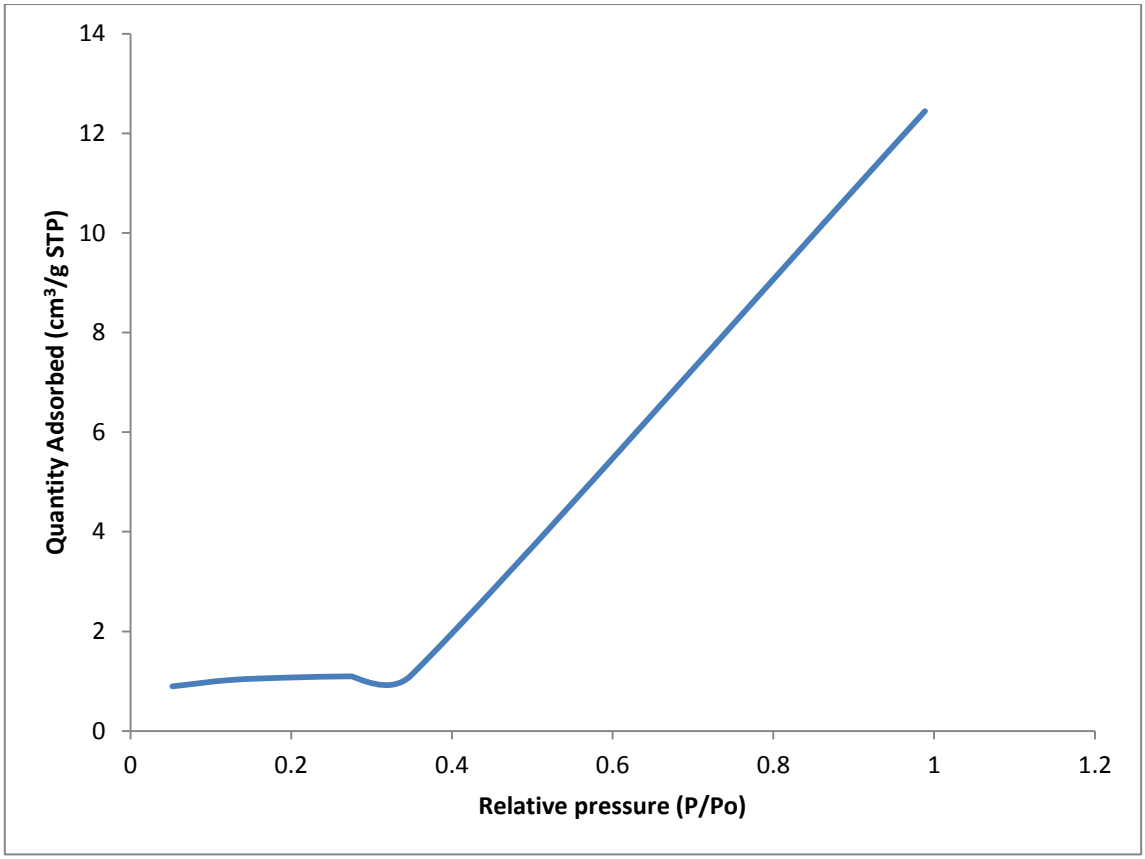


Figure B.1: The BET Isotherm linear plot for the adsorption of 0PVA PS membrane.

Table B.5 below shows the BET surface area report data.

Table B.4: BET surface area report data

Relative Pressure (P/Po)	1/[Q(Po/P - 1)]
0.052279	0.061551
0.124044	0.138347
0.199473	0.231962
0.274365	0.344306
0.348876	0.481927

Where Q is the quantity of the membrane adsorbed, in cm^3/g STP

Figure B.2 shows the BET surface area plot for the 0 PVA PS membrane

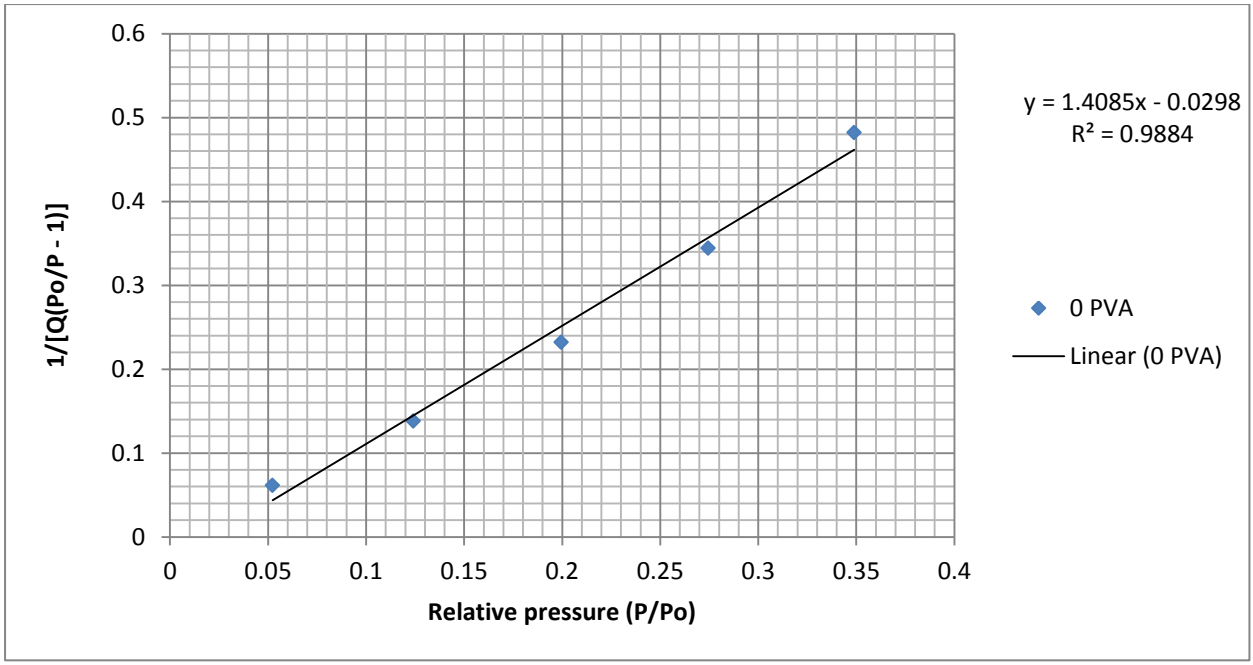


Figure B.2: BET surface area plot for the 0 PVA PS membrane.

Table B.6 below shows the Langmuir surface area report data.

Table B.5: Langmuir surface area report data

Pressure (mmHg)	P/Q (mmHg·g/cm³ STP)
32.11134	35.82991
76.19193	74.43616
122.5224	114.0577
168.5239	153.4599
214.2908	192.742

Figure B.3 shows the Langmuir surface area plot

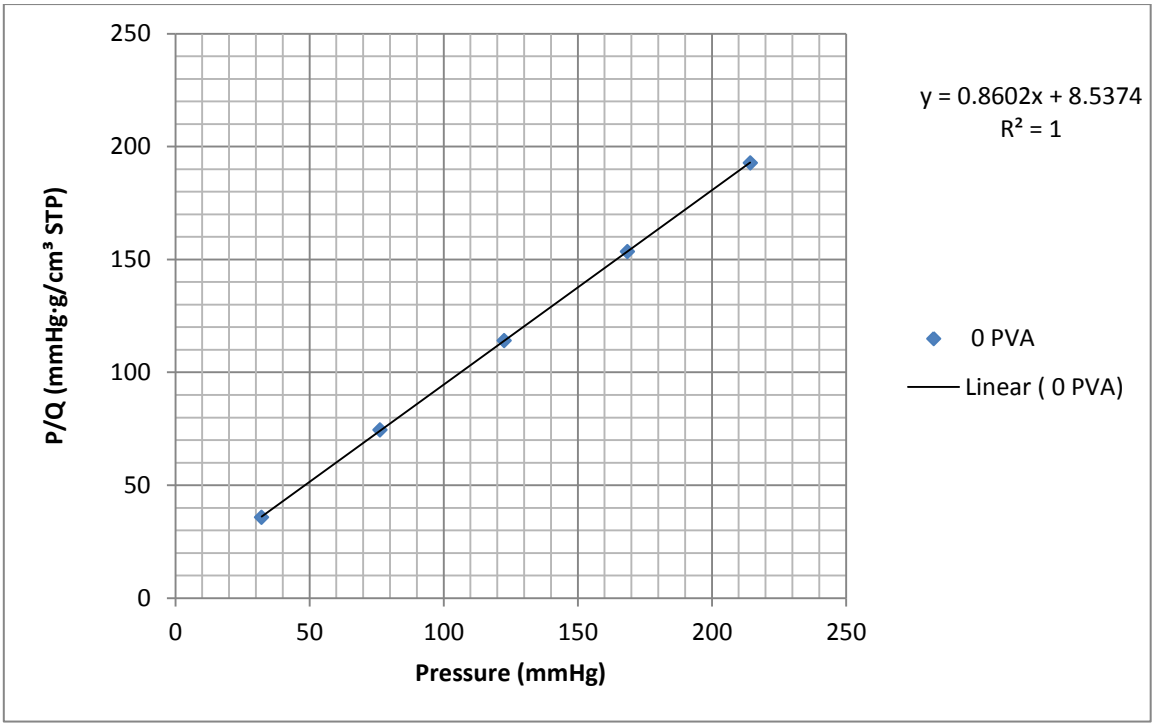


Figure B.3: The Langmuir surface area plot for the 0 PVA membrane.

B.1.2 BET data for the 5% PS membrane

BET Surface area report

BET Surface Area:	10.9198 ± 0.4002 m²/g
Slope:	0.400553 ± 0.014250 g/cm³ STP
Y-Intercept:	-0.001900 ± 0.003218 g/cm³ STP
C:	-209.809296
Qm:	2.5084 cm³/g STP
Correlation Coefficient:	0.9981069
Molecular Cross-Sectional Area:	0.1620 nm²

Table B.6: BET surface area report data

Relative Pressure (P/Po)	Quantity Adsorbed (cm^3/g STP)	1/[Q(Po/P - 1)]
0.051904101	2.5305	0.021634
0.122450296	3.0109	0.046344
0.199235219	3.3273	0.074778
0.274436882	3.5736	0.105844
0.349699172	3.7993	0.141541

Figure B.4 shows the surface area plot for the 5% CNTs PS membrane

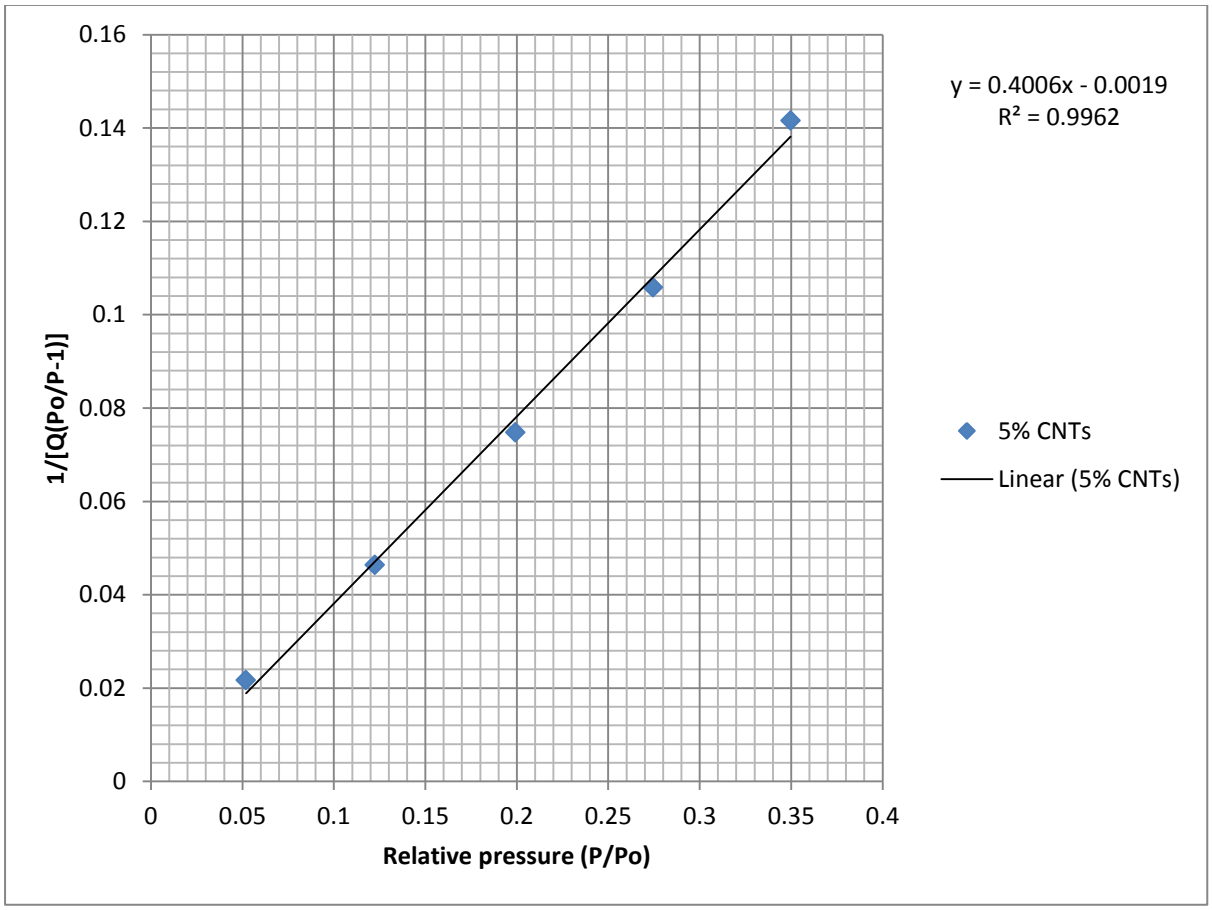


Figure B.4: BET surface area plot for PS membrane with 5% CNTs

Data for BET Isotherm linear report

Table B.7: BET linear isotherm report data

Relative Pressure (P/Po)	5% CNTs Adsorbed (cm^3/g STP)
0.051904	2.530495
0.12245	3.010861
0.199235	3.327253
0.274437	3.573555
0.349699	3.799257
0.988293	22.85033

Figure B.5 shows the BET linear isotherm plot for the adsorption of 5% CNTs PS membrane

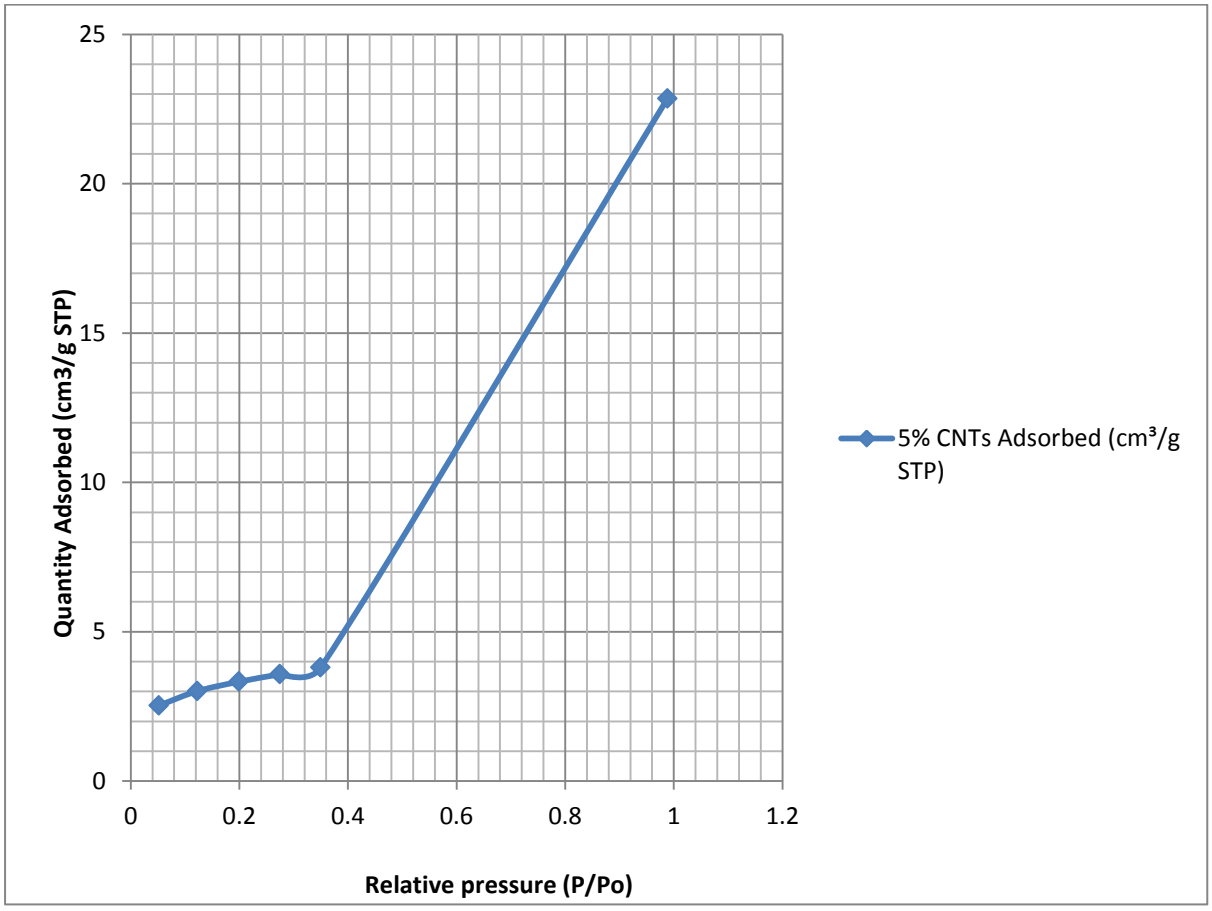


Figure B.5: BET linear isotherm plot for the adsorption of 5% CNTs PS membrane.

Langmuir Surface Area Report

Langmuir Surface Area:	18.1725 ± 0.6944 m^2/g
	0.239548 ± 0.009153 g/cm^3
Slope:	STP
	6.252646 ± 1.269660
Y-Intercept:	$mmHg \cdot g/cm^3$ STP
b:	0.038311 1/mmHg
Qm:	4.1745 cm^3/g STP
Correlation Coefficient:	0.997817
Molecular Cross-Sectional Area:	0.1620 nm^2

Table B.8: Langmuir Surface Area Report data

Pressure (mmHg)	Quantity Adsorbed (cm^3/g STP)	P/Q ($mmHg \cdot g/cm^3$ STP)
31.88113	2.5305	12.599
75.21283	3.0109	24.981
122.37655	3.3273	36.780
168.56778	3.5736	47.171
214.79625	3.7993	56.536

Langmuir surface area plot

Table B.9: Langmuir surface area report data

Pressure (mmHg)	P/Q ($mmHg \cdot g/cm^3$ STP)
31.88113	12.59877
75.21283	24.98051
122.3765	36.78006
168.5678	47.1709
214.7962	56.53639

Figure B.6 shows the Langmuir surface area plot

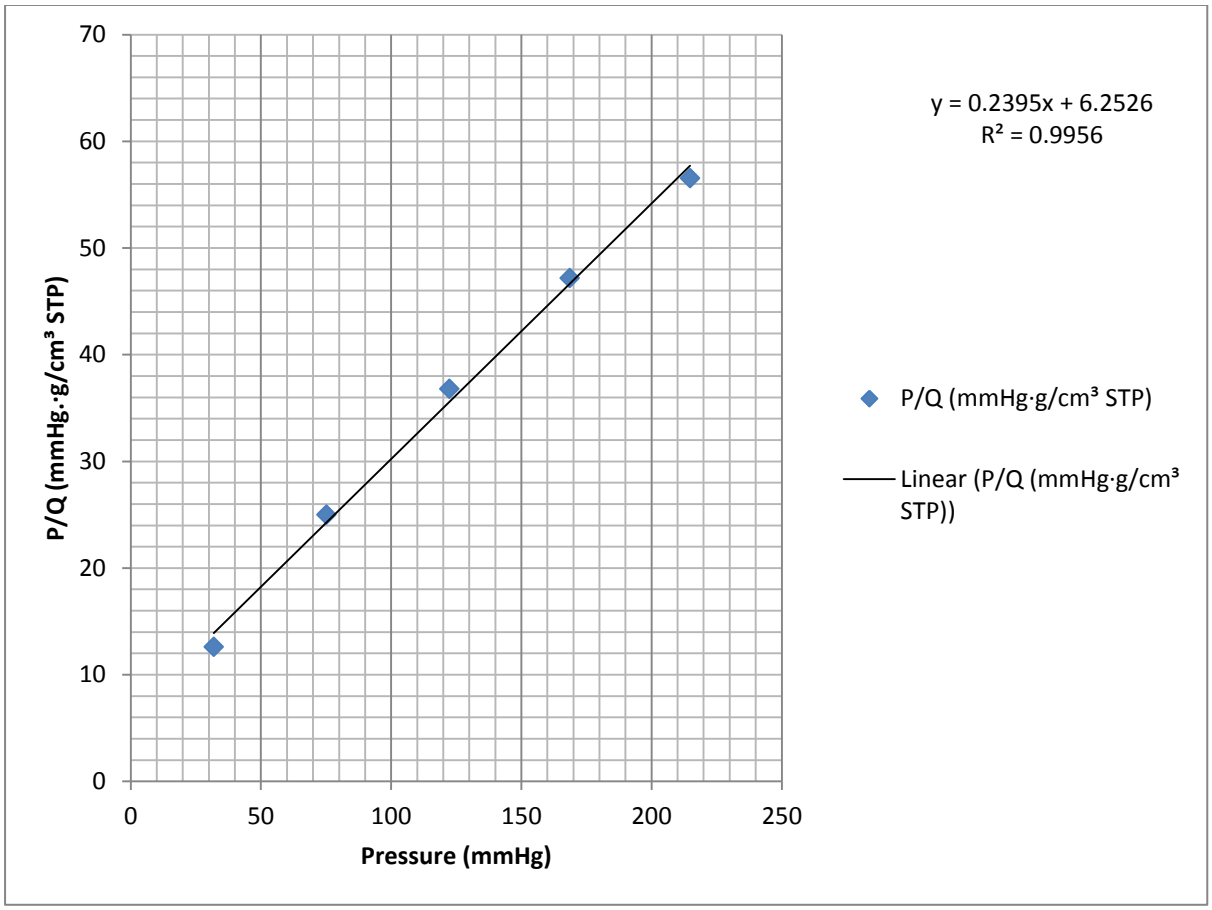


Figure B.6: The Langmuir surface area plot for the 5% CNTs PS membrane.

B.1.3 BET data for 2.5% CNTs PS membrane

Table B.10: BET linear isotherm data for the adsorption of 2.5% CNTs PS membrane

Relative Pressure (P/Po)	Quantity Adsorbed (cm^3/g STP)
0.056221	2.288247
0.123247	2.668116
0.199358	2.93183
0.274387	3.136267
0.349477	3.319959
0.986913	17.85581

Figure B.7 below shows the BET linear isotherm plot for the adsorption of 2.5% CNTs PS membrane.

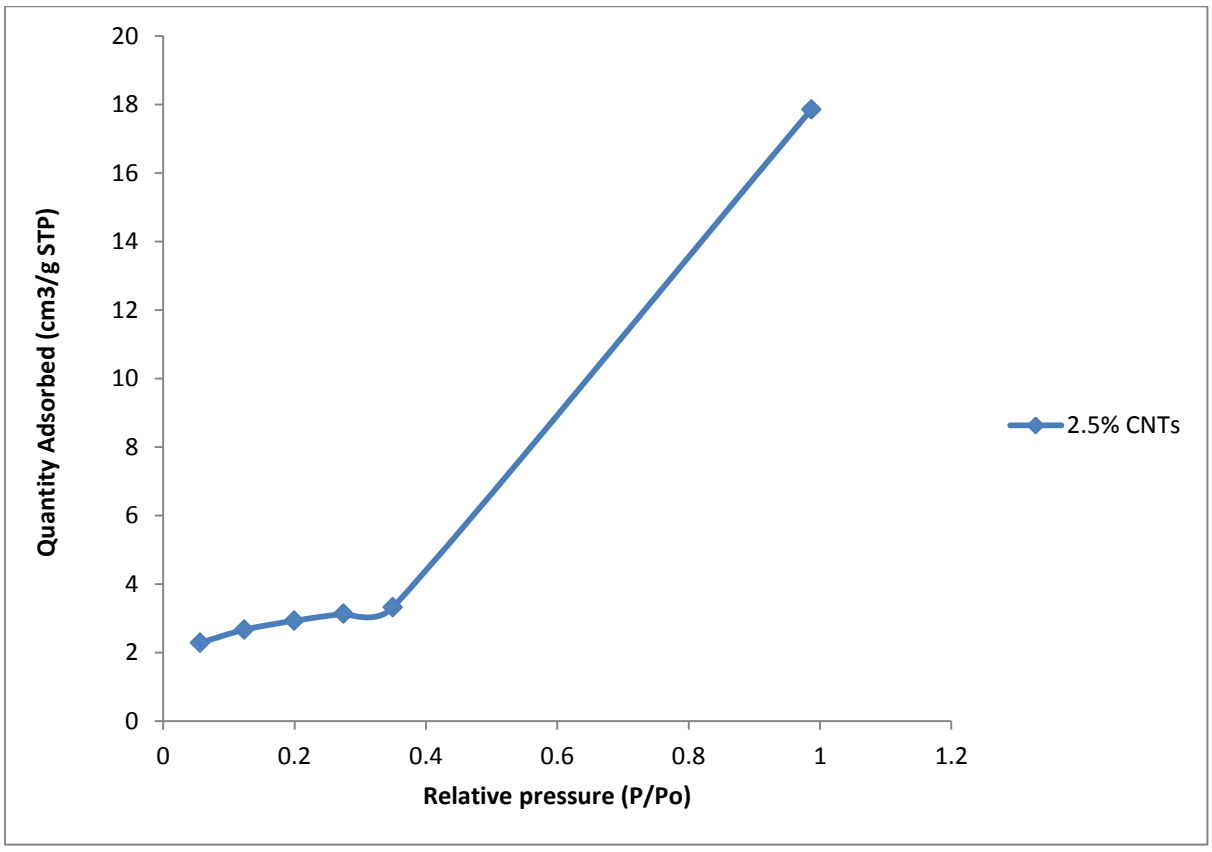


Figure B.7: BET linear isotherm plot for the adsorption of 2.5% CNTs PS membrane.

Table B.12 below shows the BET surface area data for 2.5% CNTs PS membrane.

Table B.11: BET surface area data for 2.5% CNTs PS membrane.

Relative Pressure (P/Po)	1/[Q(Po/P - 1)]
0.056221	0.026033
0.123247	0.052686
0.199358	0.084929
0.274387	0.120572
0.349477	0.161816

Figure B.8 below shows the BET surface area plot for 2.5% CNTs PS membrane.

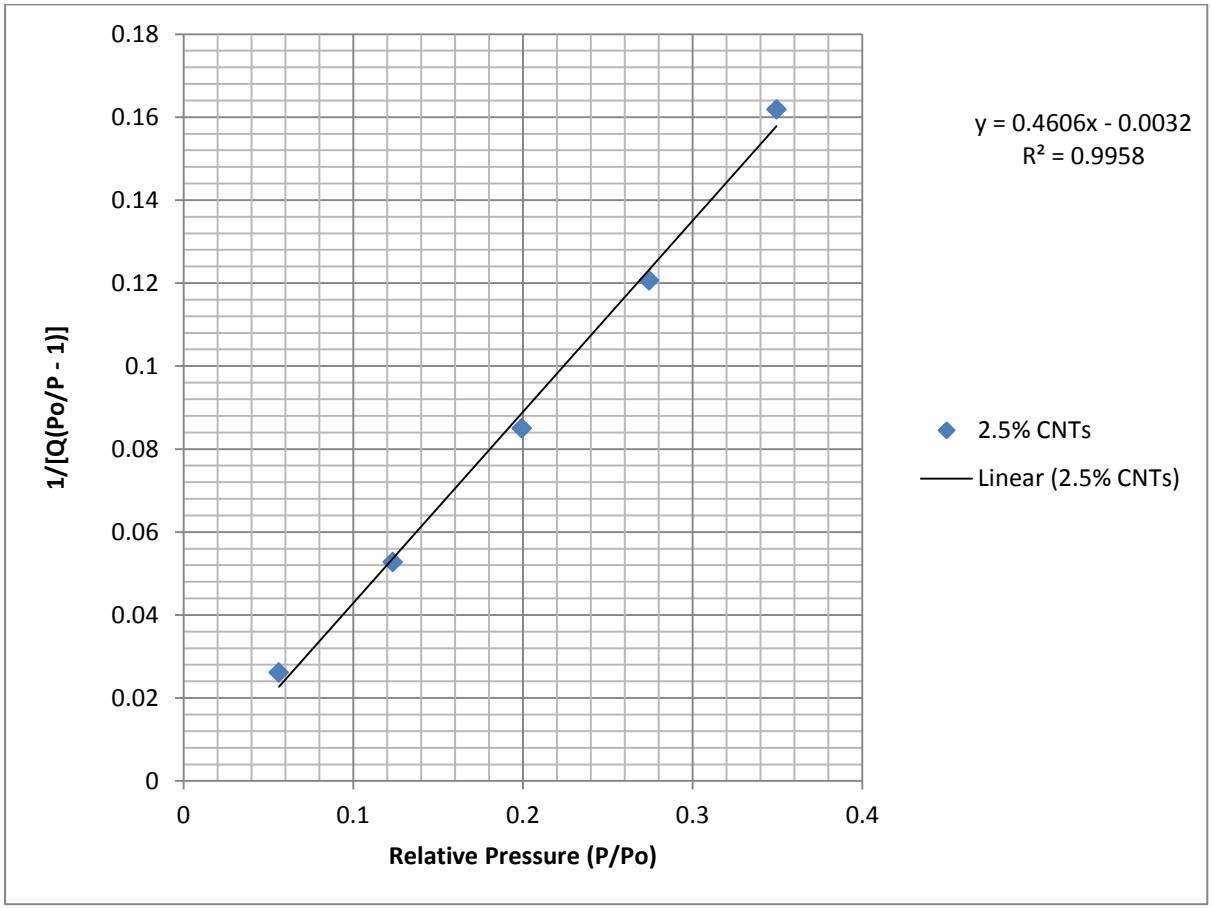


Figure B.8: BET surface area plot for 2.5% CNTs PS membrane.

Table B.13 below shows the Langmuir surface area data for 2.5% CNTs PS membrane.

Table B.12: Langmuir surface area data for 2.5% CNTs PS membrane.

Pressure (mmHg)	P/Q (mmHg·g/cm³ STP)
34.53289	15.09142
75.70245	28.373
122.4521	41.76643
168.5372	53.73815
214.6595	64.65726

Figure B.9 below shows the Langmuir surface area plot for 2.5% CNTs PS membrane.

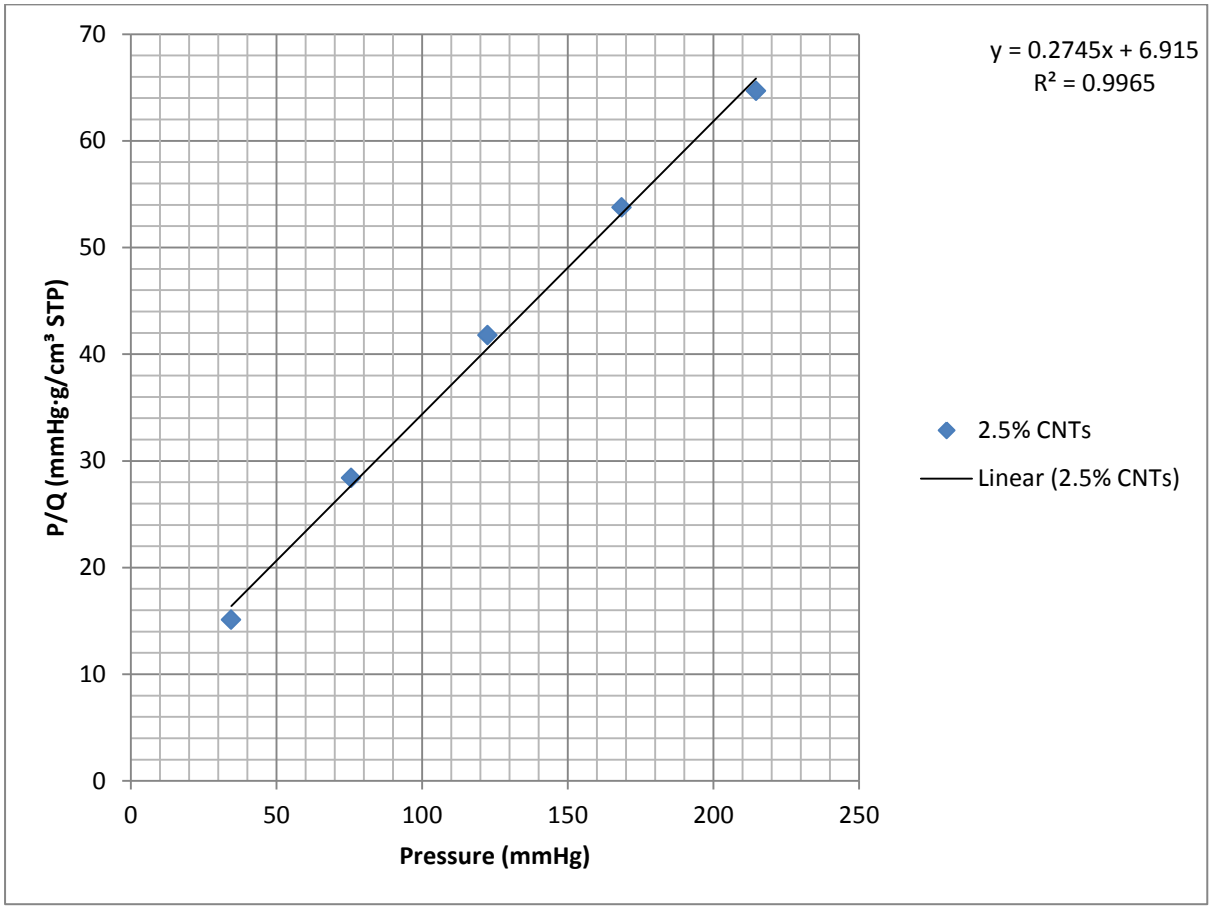


Figure B.9: Langmuir surface area plot for 2.5% CNTs PS membrane.

B.1.4 BET data for 7.5% CNTs PS membrane

Table B.14 below shows the BET linear isotherm data for the adsorption of 7.5% CNTs PS membrane.

Table B.13: BET linear isotherm data for the adsorption of 7.5% CNTs PS membrane.

Relative Pressure (P/Po)	Quantity Adsorbed (cm^3/g STP)
0.049697	2.210784
0.140365	2.716219
0.199177	2.902638
0.274035	3.093183
0.348758	3.266655
0.987375	19.52894

Figure B.10 below shows the BET linear isotherm plot for the adsorption of 7.5% CNTs PS membrane.

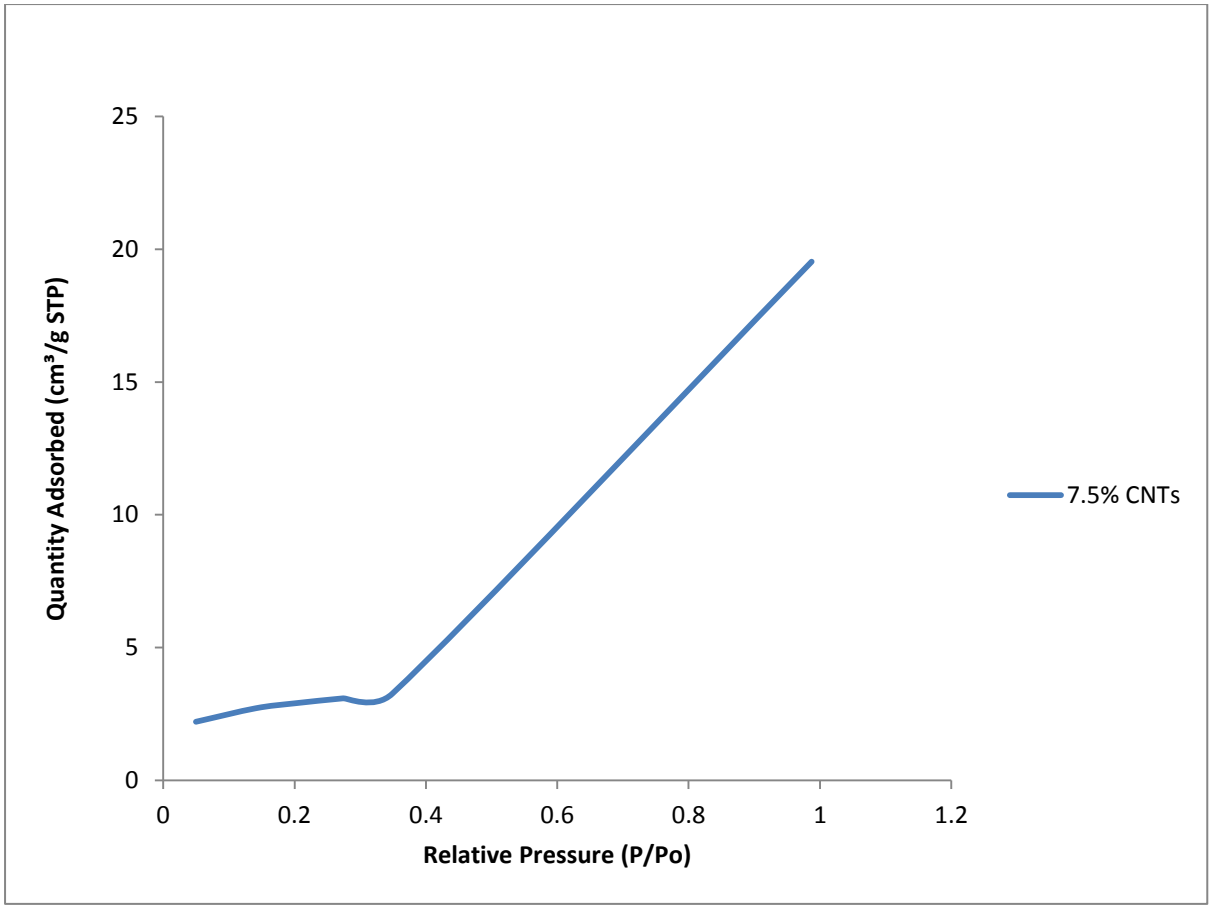


Figure B.10: BET linear isotherm plot for the adsorption of 7.5% CNTs PS membrane.

Table B.15 below shows the BET surface area data for 7.5% CNTs PS membrane.

Table B.14: BET surface area data for 7.5% CNTs PS membrane.

Relative Pressure (P/Po)	1/[Q(Po/P - 1)]
0.049697	0.023655
0.140365	0.060114
0.199177	0.085686
0.274035	0.122035
0.348758	0.163938

Figure B.11 below shows the BET surface area plot for 7.5% CNTs PS membrane.

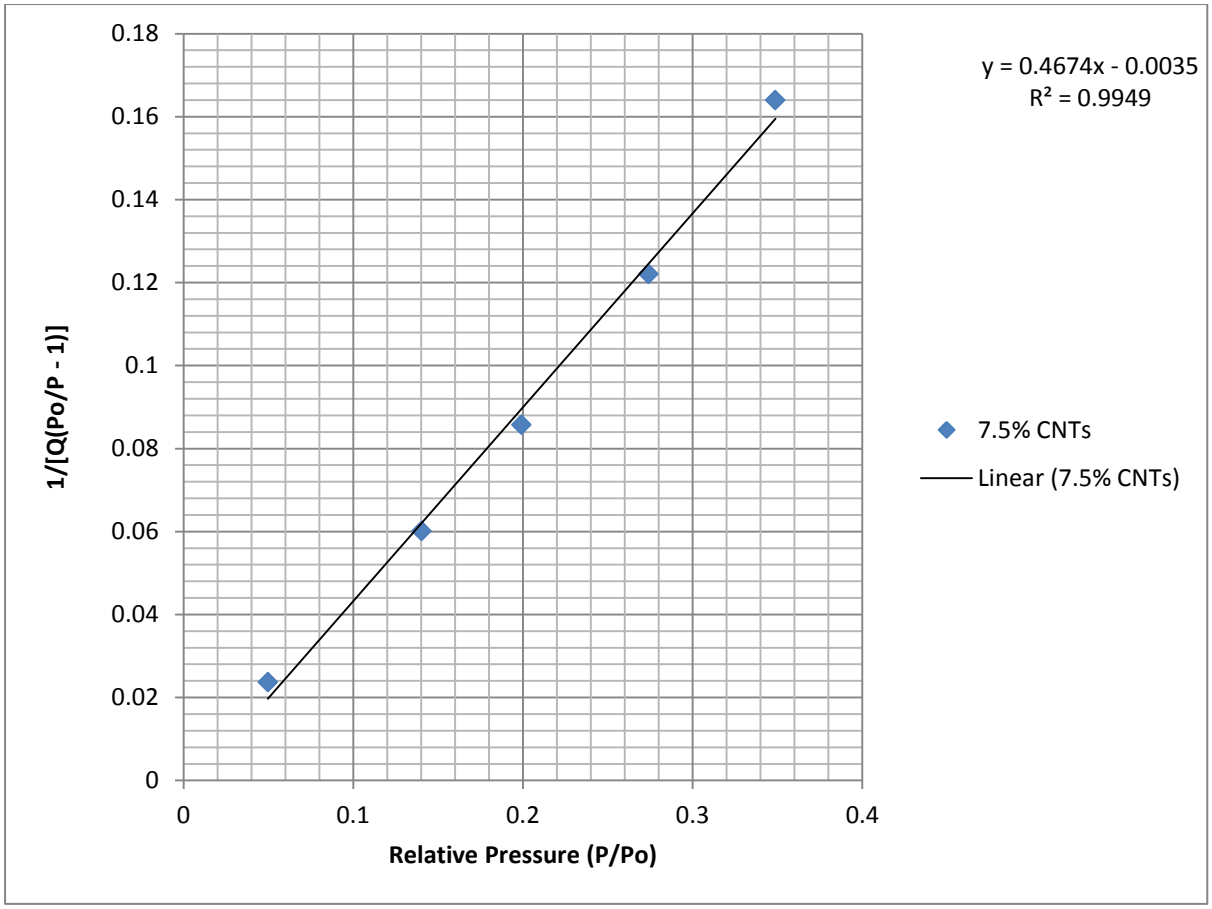


Figure B.11: BET surface area plot for 7.5% CNTs PS membrane.

Table B.16 below shows the Langmuir surface area data for 7.5% CNTs PS membrane.

Table B.15: Langmuir surface area data for 7.5% CNTs PS membrane.

Pressure (mmHg)	P/Q (mmHg·g/cm³ STP)
30.47025	13.78255
86.06026	31.68385
122.1195	42.07192
168.0161	54.3182
213.8305	65.45854

Figure B.12 below shows the Langmuir surface area plot for 7.5% CNTs PS membrane.

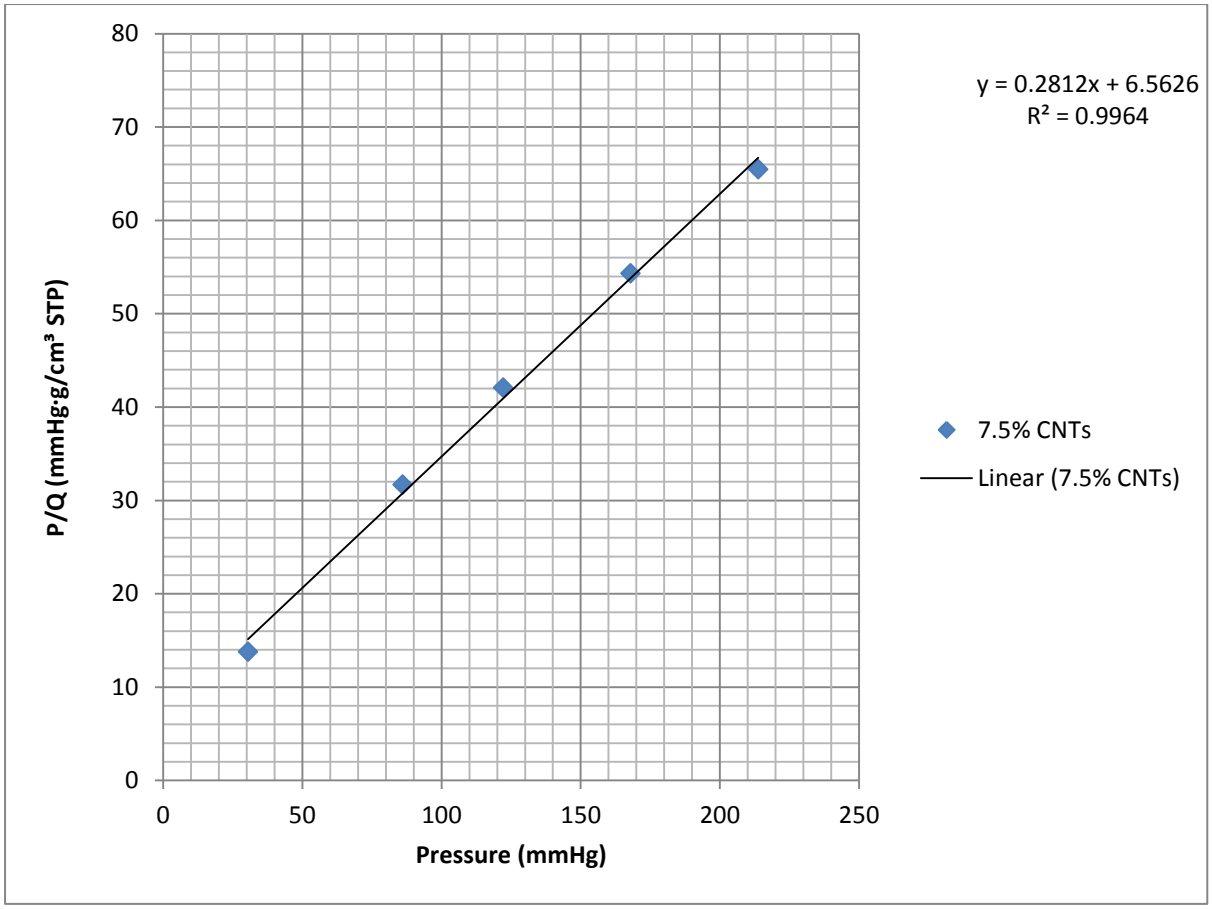


Figure B.12: Langmuir surface area plot for 7.5% CNTs PS membrane.

B.1.5 BET data for p7.5% CNTs PS membrane

Table B.17 below shows the BET linear isotherm data for the adsorption of p7.5% CNTs PS membrane.

Table B.16: BET linear isotherm data for the adsorption of p7.5% CNTs PS membrane.

Relative Pressure (P/Po)	Quantity Adsorbed (cm³/g STP)
0.054914	1.947384
0.123429	2.357897
0.199208	2.614614
0.274106	2.803385
0.34901	2.976008
0.992116	24.81561

Figure B.13 below shows the BET linear isotherm plot for the adsorption of p7.5% CNTs PS membrane.

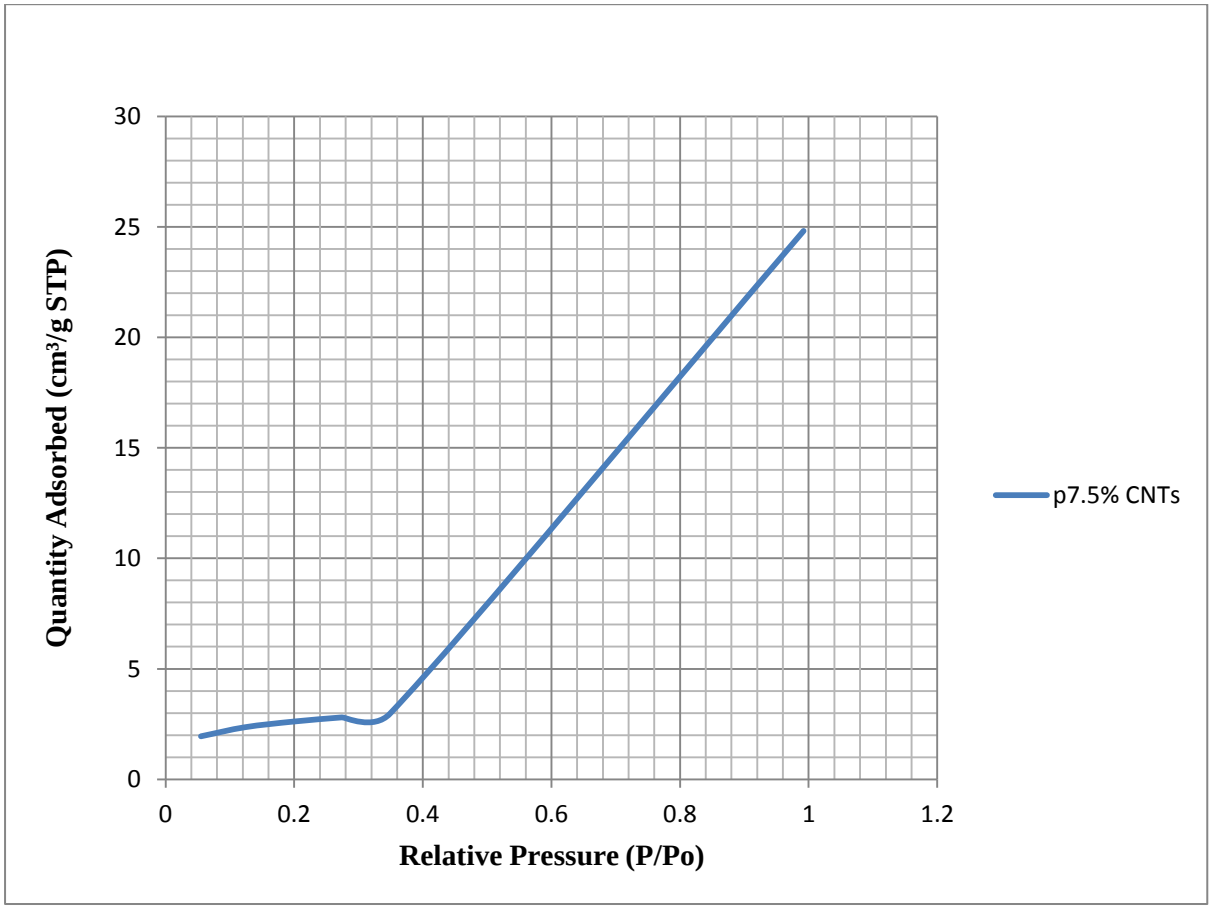


Figure B.13: BET linear isotherm plot for the adsorption of p7.5% CNTs PS membrane.

Table B.18 below shows the BET surface area data for p7.5% CNTs PS membrane.

Table B.17: BET surface area data for p7.5% CNTs PS membrane.

Relative Pressure (P/Po)	1/[Q(Po/P - 1)]
0.054914	0.029837
0.123429	0.059718
0.199208	0.095144
0.274106	0.134698
0.34901	0.180148

Figure B.14 below shows the BET surface area plot for p7.5% CNTs PS membrane.

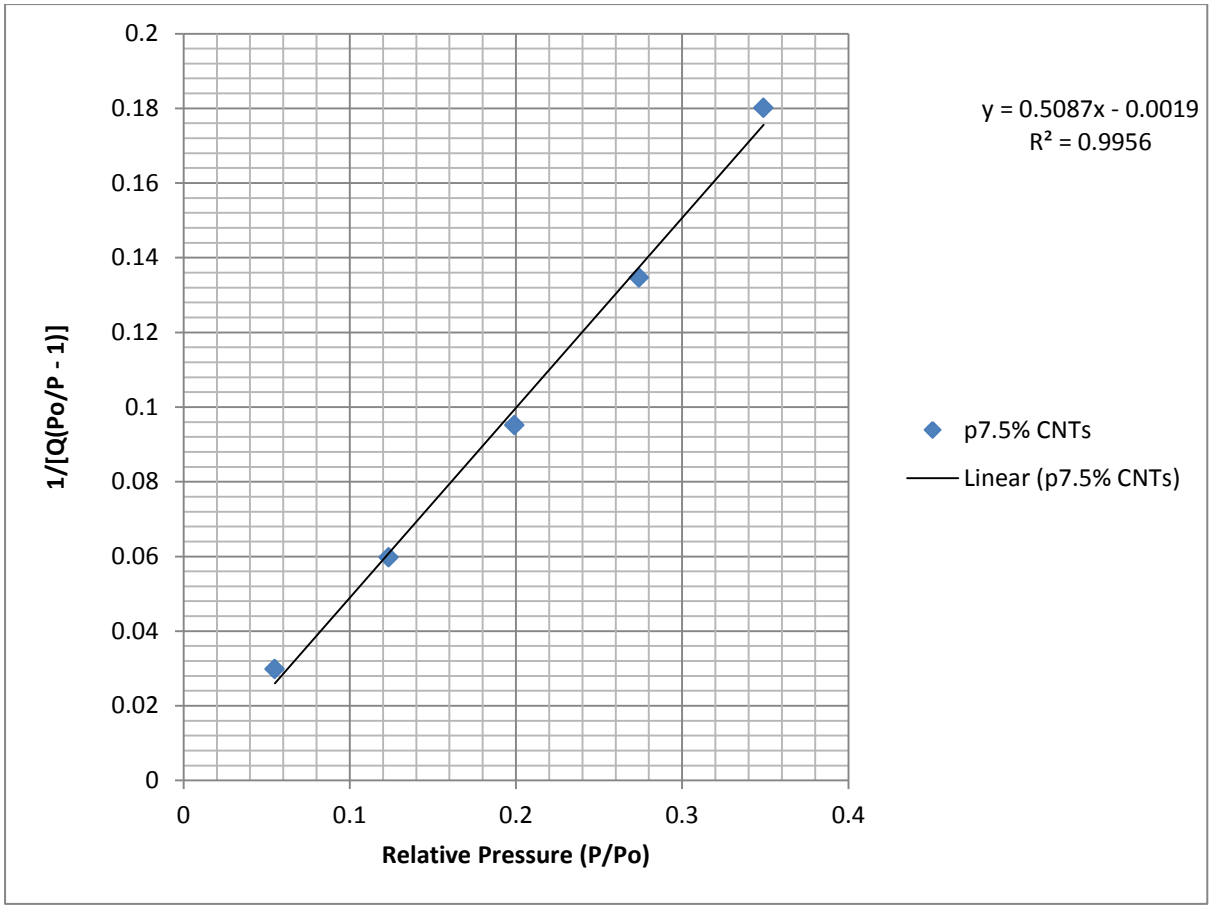


Figure B.14: BET surface area plot for p7.5% CNTs PS membrane.

Table B.19 below shows the Langmuir surface area data for p7.5% CNTs PS membrane.

Table B.18: Langmuir surface area data for p7.5% CNTs PS membrane.

Pressure (mmHg)	P/Q (mmHg·g/cm³ STP)
33.66887	17.28928
75.67651	32.09492
122.1384	46.71375
168.0595	59.94877
213.9847	71.90326

Figure B.15 below shows the Langmuir surface area plot for p7.5% CNTs PS membrane.

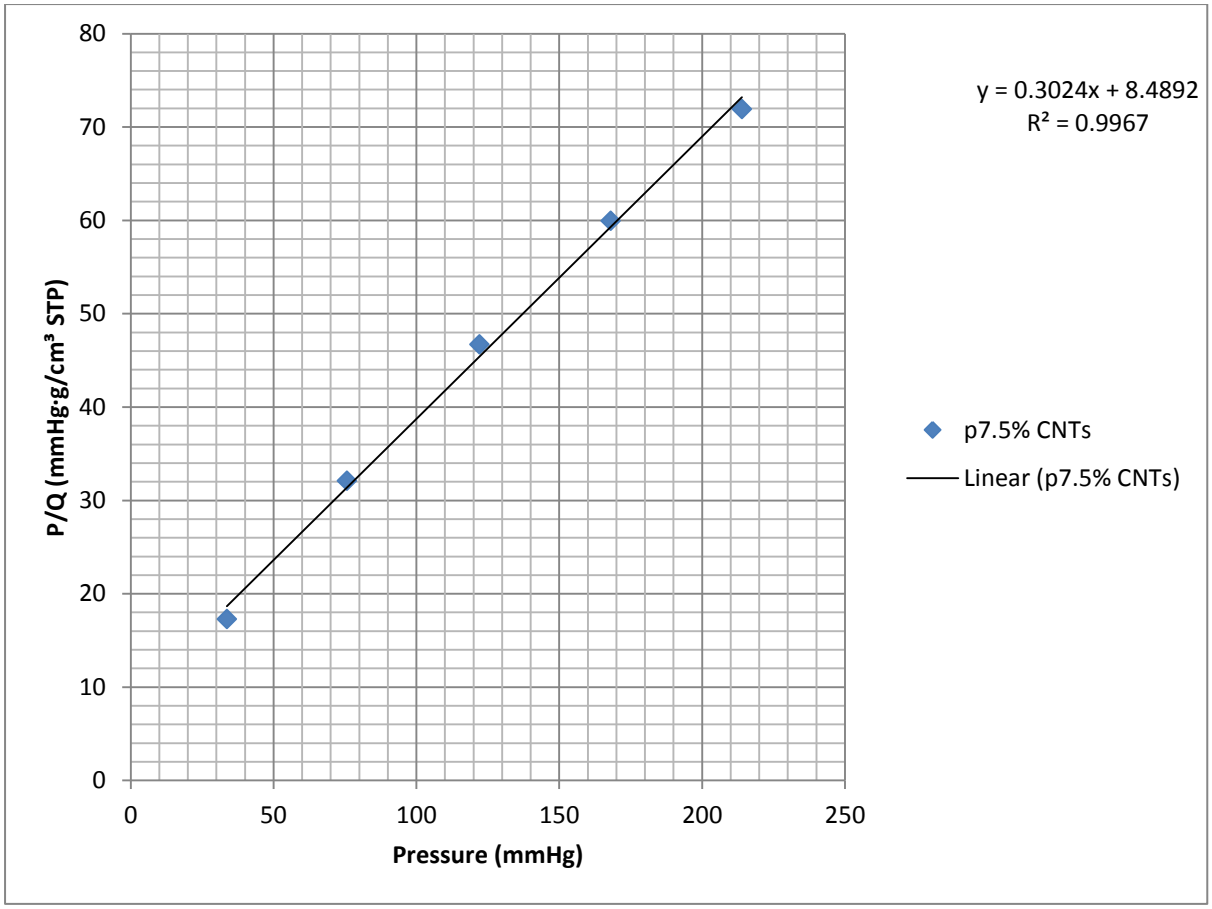


Figure B.15: Langmuir surface area plot for p7.5% CNTs PS membrane.

B.1.6 BET data for 10% CNTs PS membrane

Table B.20 below shows the BET linear isotherm data for the adsorption of 10% CNTs PS membrane.

Table B.19: BET linear isotherm data for the adsorption of 10% CNTs PS membrane.

Relative Pressure (P/Po)	Quantity Adsorbed (cm^3/g STP)
0.055961	2.431391
0.123156	2.830931
0.199237	3.102424
0.274258	3.313972
0.34926	3.502484
0.988957	23.70554

Figure B.16 below shows the BET linear isotherm plot for the adsorption of 10% CNTs PS membrane

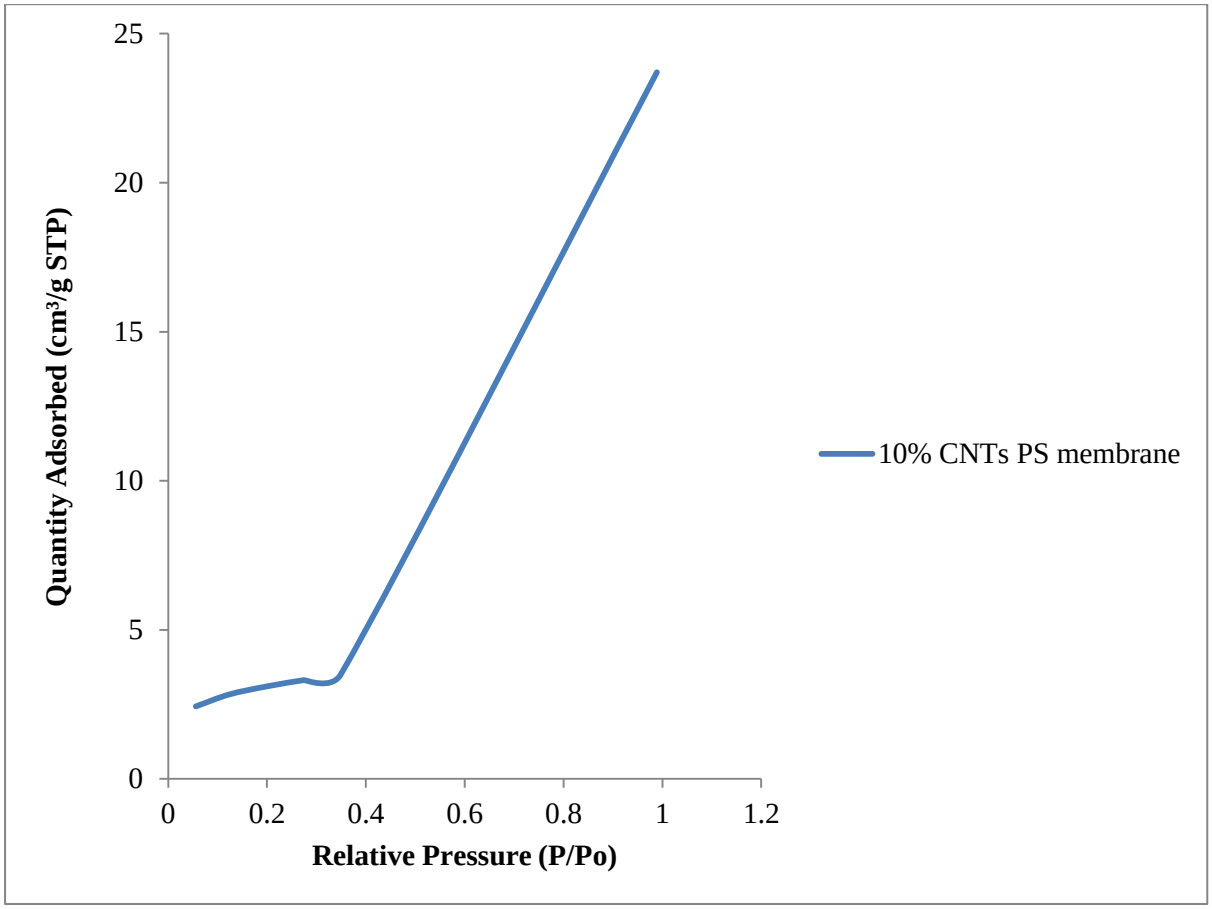


Figure B.16: BET linear isotherm plot for the adsorption of 10% CNTs PS membrane.

Table B.21 below shows the BET surface area data for 10% CNTs PS membrane.

Table B.20: BET surface area data for 10% CNTs PS membrane.

Relative Pressure (P/Po)	1/[Q(Po/P - 1)]
0.055961	0.02438
0.123156	0.049614
0.199237	0.080198
0.274258	0.114033
0.34926	0.153237

Figure B.17 below shows the BET surface area plot for 10% CNTs PS membrane

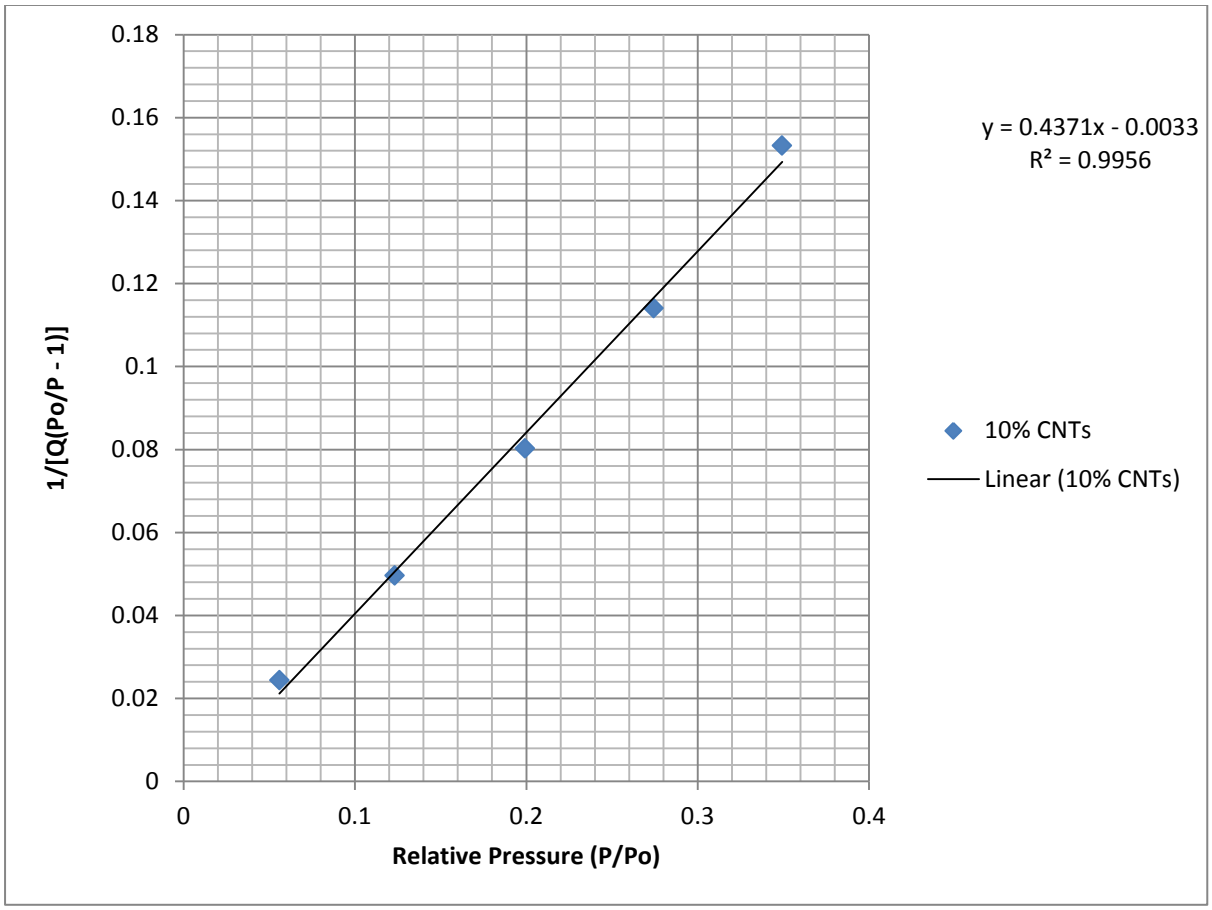


Figure B.17: BET surface area plot for 10% CNTs PS membrane.

Table B.22 below shows the Langmuir surface area data for 10% CNTs PS membrane.

Table B.21: Langmuir surface area data for 10% CNTs PS membrane.

Pressure (mmHg)	P/Q (mmHg·g/cm³ STP)
34.3107	14.11155
75.50919	26.67292
122.1559	39.37432
168.153	50.74063
214.1378	61.13883

Figure B.18 below shows the Langmuir surface area plot for 10% CNTs PS membrane.

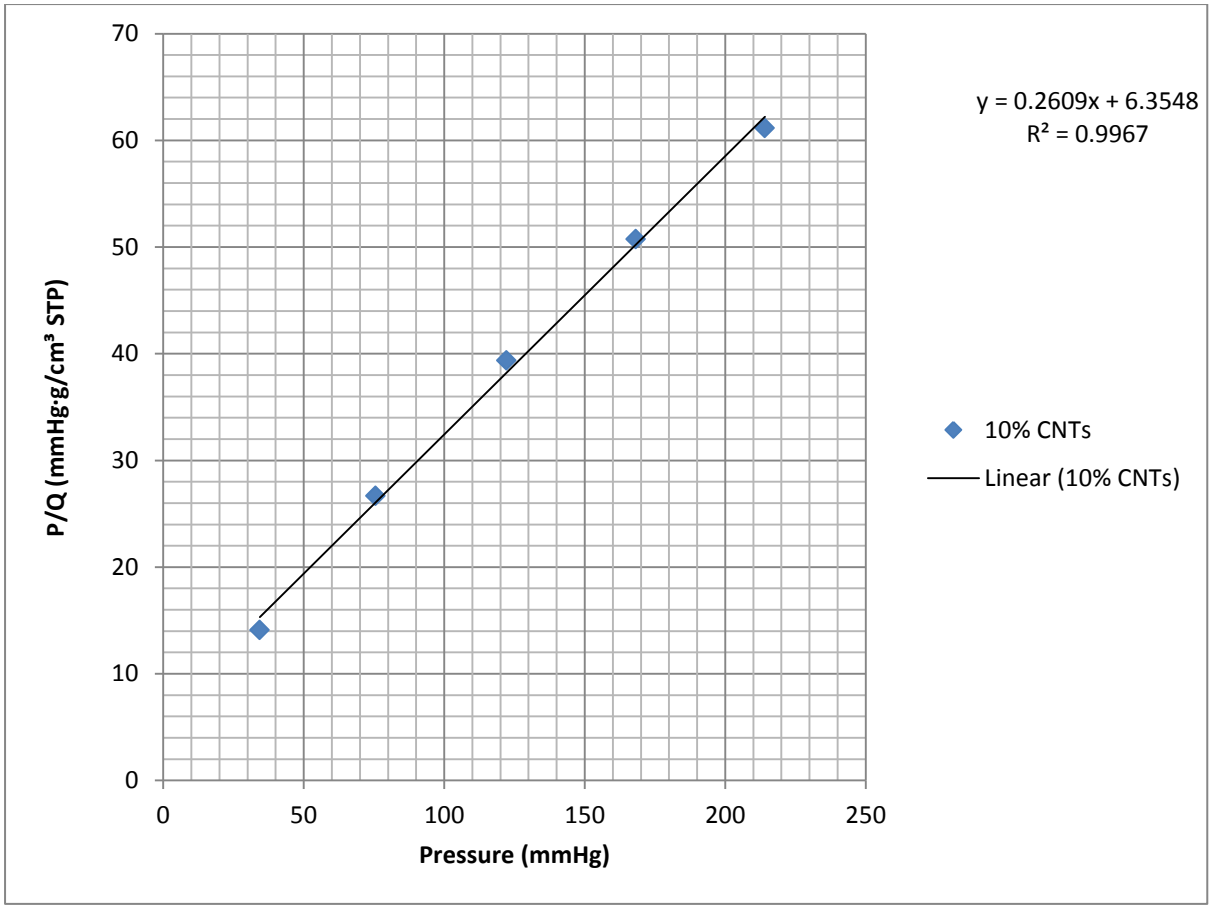


Figure B.18: Langmuir surface area plot for 10% CNTs PS membrane.

B.2 FTIR data for the PS membranes

These data was obtained using the FTIR equipment in section 3.3.4.6. Figure B.19 shows the IR spectrum for the 0 CNTs PS membrane.

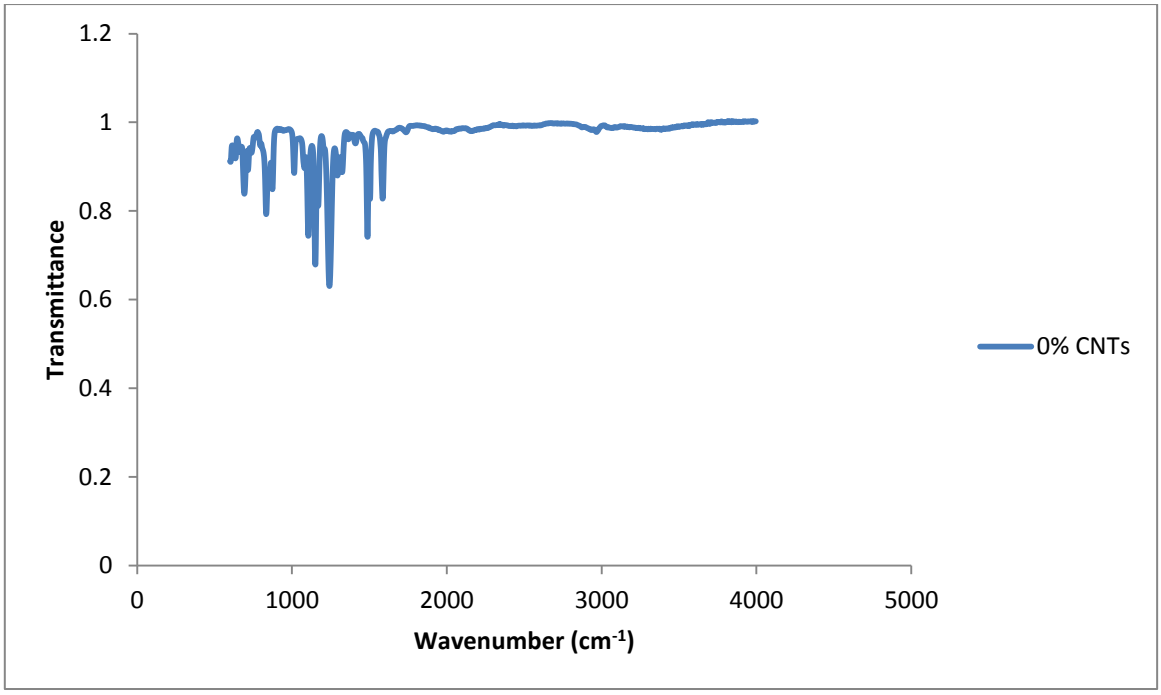


Figure B.19: The IR spectrum for the 0% CNTs PS membrane.

Figure B.20 shows the IR spectrum for the 5% CNTs PS membrane.

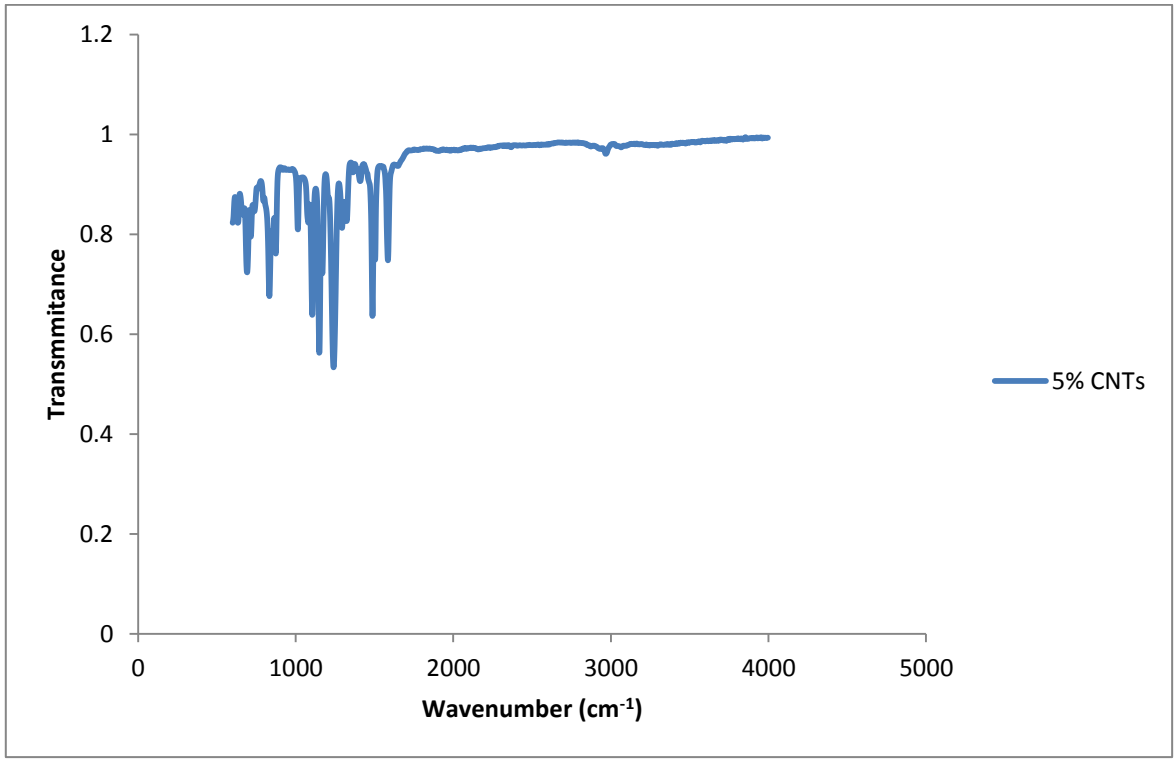


Figure B.20: The IR spectrum for the 5% CNTs PS membrane

Figure B.21 shows the IR spectrum for the 2.5% CNTs PS membrane.

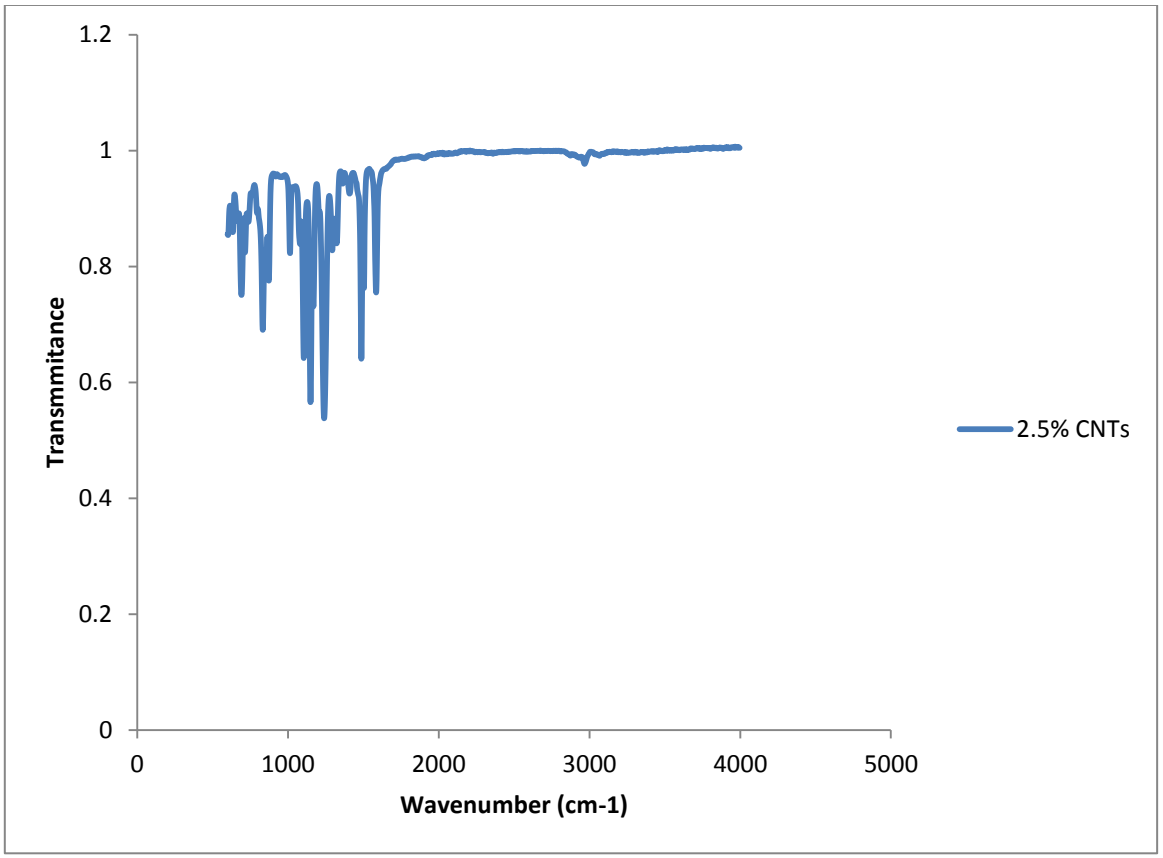


Figure B.21: The IR spectrum for the 2.5% CNTs PS membrane

Figure B.22 shows the IR spectrum for the 7.5% CNTs PS membrane.

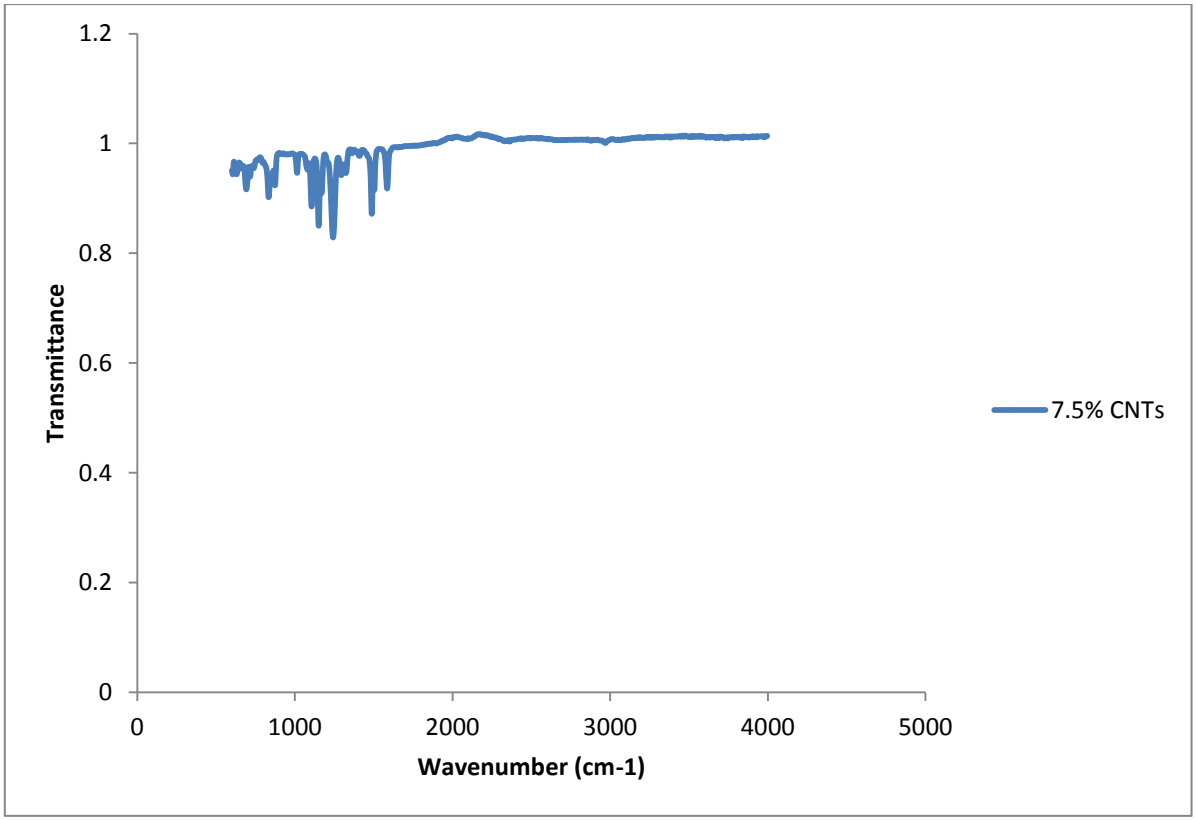


Figure B.22: The IR spectrum for the 7.5% CNTs PS membrane

Figure B.23 shows the IR spectrum for the 10% CNTs PS membrane.

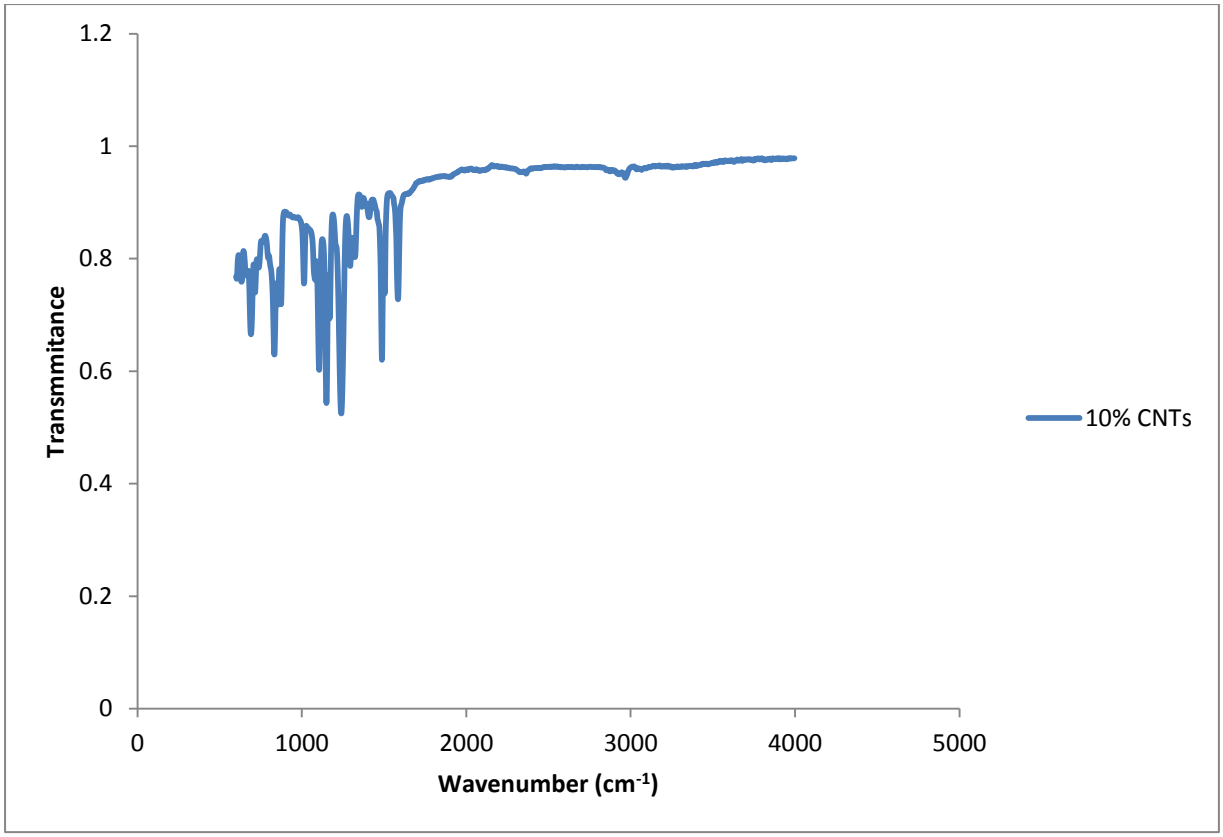


Figure B.23: The IR spectrum for the 10% CNTs PS membrane.

Figure B.24 shows the IR spectrum for the 7.5% CNTs PS membrane.

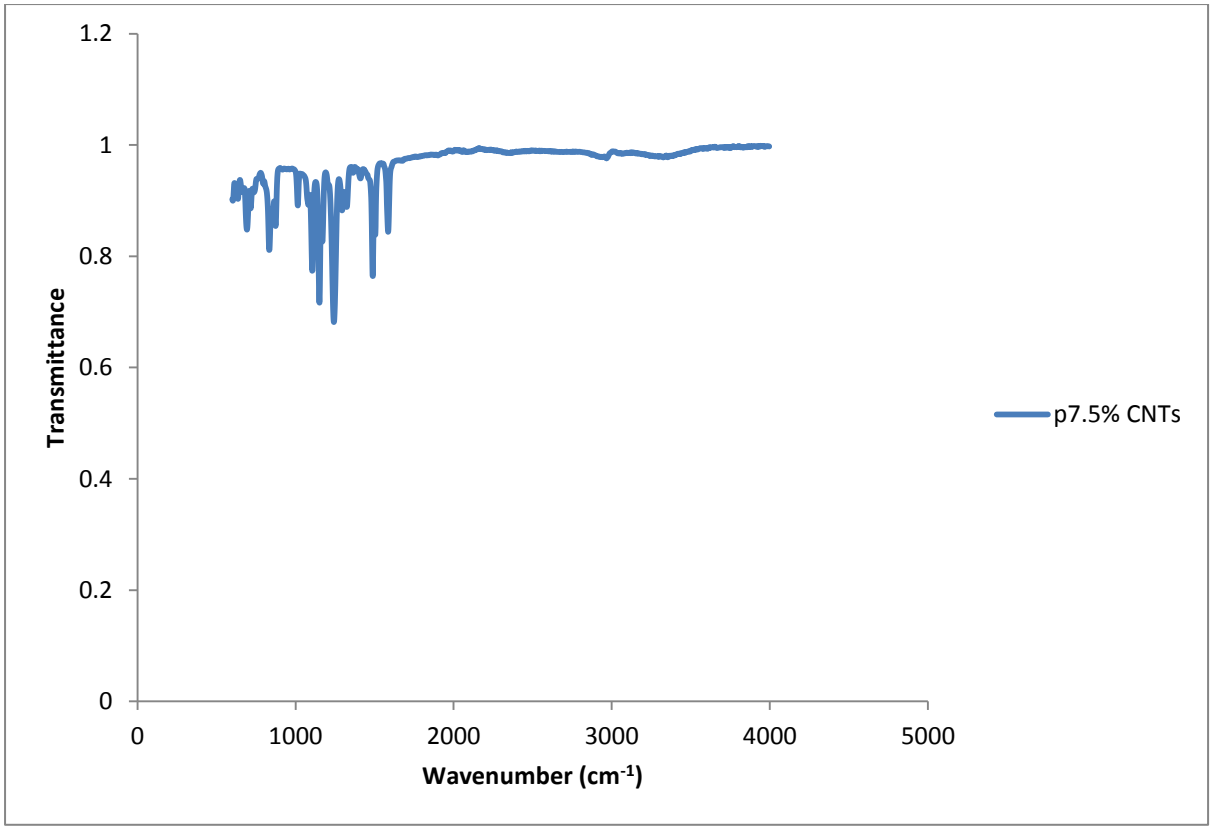


Figure B.24: The IR spectrum for the p7.5% CNTs PS membrane.

Figure B.25 shows the IR spectra of all the PS membrane in the same plane

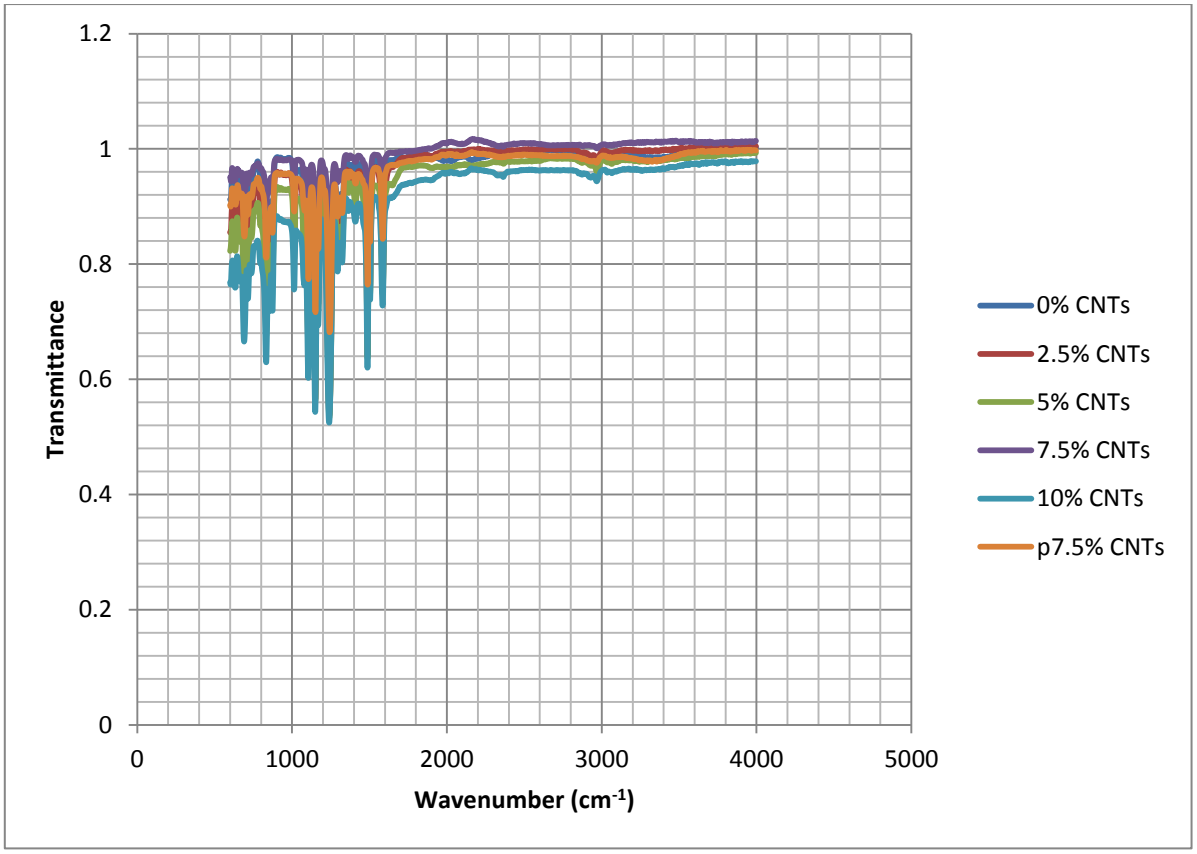


Figure B.25: The IR spectra of all the PS membranes.

B.3 Separation performance data

Figure B.26 shows the calibration curve for the determination of permeate concentrations of oil.

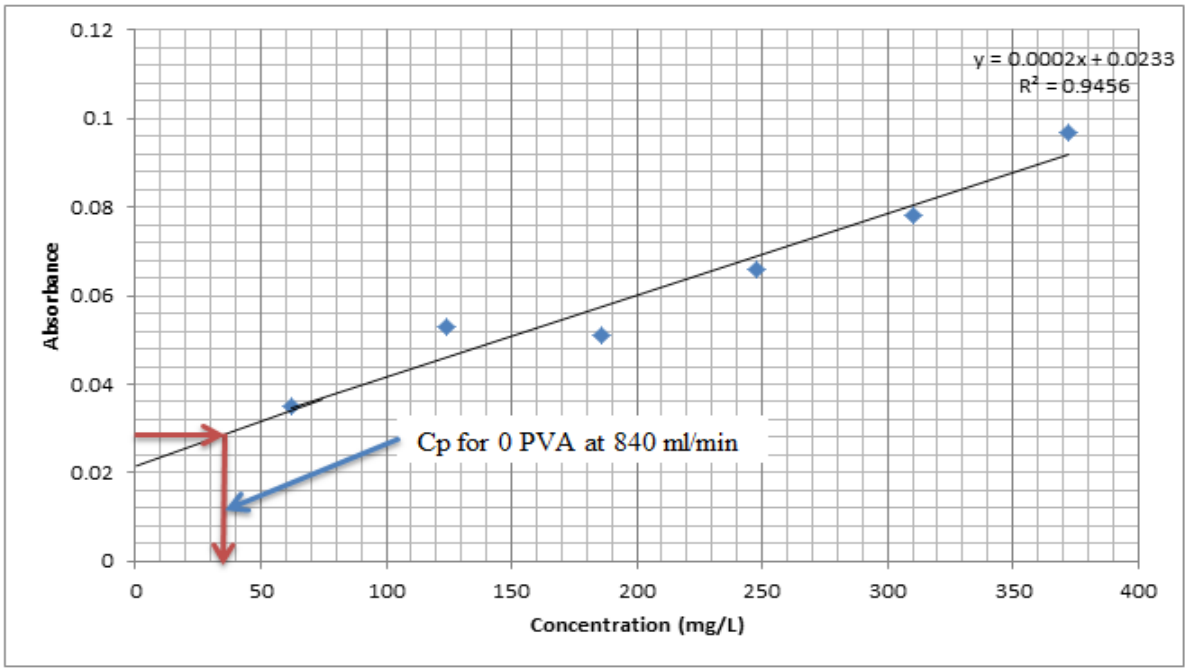


Figure B.26: A calibration curve for the determination of the unknown concentration of the oil-containing wastewater permeates (Cp), at the flow rates of 46.8, 50.4 (840 ml/min) and 52.2 L/h.

Table B.22: Concentration of oil in the permeate (Cp), in mg/L; at the flow rates of 46.8, 50.4 and 52.2 L/h.

PS membrane	46.8 L/h	50.4 L/h	52.2 L/h
0 CNTs	21 mg/L	38 mg/L	64 mg/L
0 PVA	17 mg/L	23 mg/L	50 mg/L
2.5 % CNTs	20 mg/L	32 mg/L	57 mg/L
5% CNTs	18 mg/L	25 mg/L	52 mg/L
.7.5% CNTs	21 mg/L	36 mg/L	60 mg/L
P7.5% CNTs	16 mg/L	18 mg/L	19 mg/L
10% CNTs	19 mg/L	30 mg/L	55 mg/L

Note: 0 CNTs is the plane PS membrane with no blending of CNTs and PVA layer), 0 PVA is the plane PS membrane with only PVA layer, 2.5% CNTs is the PS membrane with 2.5% concentration of CNTs, p in p7.5% CNTs means the pCNTs.

Table B.23: Rejection of oil concentration, R (%) in the retentate data

PS membrane	46.8 L/h	50.4 L/h	52.2 L/h
0 CNTs	94.0%	89.8%	82.8%
0 PVA	95.4%	93.8%	86.6%
2,5% CNTs	94.6%	91.4%	84.7%
5% CNTs	95.2%	93.3%	86.0%
7,5% CNTs	94.4%	90.3%	83.9%
p7.5% CNTs	95.7%	95.2%	94.9%
10% CNTs	94.9%	91.9%	85.2%

All the parameters are as explained in table B.23 above.

Table B.24: Data for the separation performance.

At the flow rate of 46.8 L/h

PS membrane	Time (min)	Time (hours)	Volume (ml)	Membrane flux ($Lh^{-1}m^{-2}$)	Relative flux (MF)	Decrease in flux, DF (%)
0 CNTs	5	0.083	10	50.02	1.00	0.0
0 PVA	25	0.420	5.5	27.51	0.55	45
2.5% CNTs	15	0.250	7.5	37.52	0.75	25
5% CNTs	30	0.500	6.0	30.01	0.60	40
7.5% CNTs	10	0.170	8.0	40.02	0.80	20
p7.5% CNTs	35	0.580	4.0	20.01	0.40	60
10% CNTs	20	0.330	7.0	35.01	0.70	30

At the flow rate of 50.4 L/h

PS membrane	Time (min)	Time (hours)	Volume (ml)	Membrane flux ($Lh^{-1}m^{-2}$)	Relative flux (MF)	Decrease in flux, DF (%)
0 CNTs	5	0.083	14	70.03	1.00	0.0
0 PVA	25	0.420	7.0	35.01	0.50	50
2.5% CNTs	15	0.250	9.0	45.02	0.64	36
5% CNTs	30	0.500	7.5	37.52	0.54	46
7.5% CNTs	10	0.170	11	55.02	0.79	21
p7.5% CNTs	35	0.580	6.0	30.01	0.43	57
10% CNTs	20	0.330	8.5	42.52	0.61	39

At the flow rate of 52.2 L/h:

(a) Relative Flux (RF) data

time (h)	0 PVA	5% CNTs	7.5% CNTs	0% CNTs	2.5% CNTs	10% CNTs	p7.5% CNTs	Volume (ml)
0	1	1	1	1	1	1	1	24.0
0.42	0.797211	0.785663	0.833319	0.852148	0.8499	0.749875	0.660667	13.0
0.25	0.74741	0.642867	0.729196	0.75963	0.7499	0.593625	0.577333	17.5
0.5	0.69741	0.607168	0.666639	0.703926	0.7249	0.49975	0.493667	14.5
0.17	0.597809	0.53577	0.602499	0.646889	0.6749	0.4035	0.327	20.0
0.58	0.548008	0.499929	0.541691	0.622222	0.6498	0.31225	0.177	11.5
0.33	0.398606	0.428531	0.479134	0.535778	0.5998	0.218375	0.083333	16.0

(b) Membrane flux in $Lh^{-1}m^{-2}$

Time (h)	0 PVA	5% CNTs	7.5% CNTs	0% CNTs	2.5% CNTs	10% CNTs	p7.5% CNTs	Volume (ml)
0.0833	50.2	70.03	120.05	135	100	80	30	24.0
0.42	40.02	55.02	100.04	115.04	84.99	59.99	19.82	13.0
0.25	37.52	45.02	87.54	102.55	74.99	47.49	17.32	17.5
0.5	35.01	42.52	80.03	95.03	72.49	39.98	14.81	14.5
0.17	30.01	37.52	72.33	87.33	67.49	32.28	9.81	20.0
0.58	27.51	35.01	65.03	84	64.98	24.98	5.31	11.5
0.33	20.01	30.01	57.52	72.33	59.98	17.47	2.5	16.0

(c) Decrease in flux, DF (%)

Time (h)	0 PVA	5% CNTs	7.5% CNTs	0% CNTs	2.5% CNTs	10% CNTs	p7.5% CNTs	Volume (ml)
0.0833	0	0	0	0	0	0	0	24.0
0.42	20.27888	21.43367	16.66805	14.78519	15.01	25.0125	33.93333	13.0
0.25	25.25896	35.71327	27.08038	24.03704	25.01	40.6375	42.26667	17.5
0.5	30.25896	39.28316	33.33611	29.60741	27.51	50.025	50.63333	14.5
0.17	40.21912	46.42296	39.7501	35.31111	32.51	59.65	67.3	20.0
0.58	45.1992	50.00714	45.8309	37.77778	35.02	68.775	82.3	11.5
0.33	60.13944	57.14694	52.08663	46.42222	40.02	78.1625	91.66667	16.0